REPORT DOCUMENTATION PAGE

Form Approved
OMB No. 0704-0188

1. AGENCY USE ONLY (*Leave Blank*)	2. REPORT DATE	3. REPORT TYPE AND DATES COVERED
	23 Sept. 1996	Interim, July 1994 - July 1996

4. TITLE AND SUBTITLE
Effects of Elevated Driver-Tube Temperature on the Extent of Quiet Flow in the Purdue Ludwieg Tube

5. FUNDING NUMBERS
F49620-94-1-0067
F49620-94-1-0326

6. AUTHOR(S)
Scott Edward Munro

7. PERFORMING ORGANIZATION NAME(S) AND ADDRESS(ES)
Aerospace Sciences Laboratory
Purdue University Airport, Hangar 3
West Lafayette, IN 47906-3371

9. SPONSORING/MONITORING AGENCY NAME(S) AND ADDRESS(ES)
Air Force Office of Scientific Research/NA
110 Duncan Ave, Suite B115
Bolling AFB, Washington DC, 20332

10. SPONSORING/MONITORING AGENCY REPORT NUMBER

11. SUPPLEMENTARY NOTES
A School of Aeronautics and Astronautics M.S. Thesis giving detailed documentation for work in the Purdue University Quiet-Flow Ludwieg Tube. Abstract prepared by the supervising Prof., S.P. Schneider.

12a. DISTRIBUTION/AVAILABILITY STATEMENT
Approved for public release; distribution unlimited.

12b. DISTRIBUTION CODE

13. ABSTRACT (*Maximum 200 words*)

Heated driver-tube air will be needed when the existing Mach-4 test section of the Purdue Quiet-flow Ludwieg tube is replaced with a Mach-6 test section. Thus, a system was developed to heat the air in the driver tube. The air was successfully heated without dramatic adverse effects on the quiet-flow performance. Measurements of the mean and fluctuating pressure were made with a Kulite pressure transducer about 10 cm downstream of the onset of uniform flow. Temperature measurements were made with thermocouples and a cold wire. In agreement with previous results, the cold-driver quiet Reynolds number was about 400,000. The quiet-length Reynolds number decreased with increasing driver-tube temperature, dropping to 380,000 at 90C and 340,000 at 140C. Thus, a nozzle wall that is colder than the gas moves transition forward on the nozzle wall. This trend agrees with Harvey's 1975 observation that a heated nozzle wall delays transition. Problems with nozzle cleanliness were encountered during the heating; there were also problems with maintaining a uniform driver-tube temperature due to heat transfer to the nozzle and to the unheated upstream section of the driver tube.

14. SUBJECT TERMS
Supersonic laminar-turbulent transition, boundary layers, low-disturbance wind tunnels

15. NUMBER OF PAGES
242

16. PRICE CODE

17. SECURITY CLASSIFICATION OF REPORT	18. SECURITY CLASSIFICATION OF THIS PAGE	19. SECURITY CLASSIFICATION OF ABSTRACT	20. LIMITATION OF ABSTRACT
UNCLASSIFIED	UNCLASSIFIED	UNCLASSIFIED	UNLIMITED

Graduate School Form 9
(Revised 7/94)

PURDUE UNIVERSITY
GRADUATE SCHOOL
Thesis Acceptance

This is to certify that the thesis prepared

By Scott Edward Munro

Entitled

Effects Of Elevated Driver-Tube Temperature On The
Extent Of Quiet Flow In The Purdue Ludwieg Tube

Complies with University regulations and meets the standards of the Graduate School for originality and quality

For the degree of Master of Science in Aeronautics and Astronautics

Signed by the final examining committee:

_____, chair

_____

_____

_____

Approved by: _____ 9/23/96
Department Head Date

This thesis ☐ is ☒ is not to be regarded as confidential.

_____
Major Professor

Format Approved by:

_____ or _____
Chair, Final Examining Committee Thesis Format Adviser

EFFECTS OF ELEVATED DRIVER-TUBE TEMPERATURES ON THE EXTENT OF QUIET FLOW IN THE PURDUE LUDWIEG TUBE

A Thesis

Submitted to the Faculty

of

Purdue University

by

Scott Edward Munro

In Partial Fulfillment of the

Requirements for the Degree

of

Master of Science in Aeronautics and Astronautics

December 1996

ACKNOWLEDGMENTS

This project is funded by the Air Force Office of Scientific Research under grants F49620-94-1-0067 and F49620-94-1-0326 monitored by Dr. L. Sakell. Matching funds for facility construction were provided by a gift from the Boeing Company and in a gift in memory of K. H. Hobbie. Heater wire for the experimental apparatus was provided by a gift from Magnet Wire, Essex Group Inc. I would like to personally think my co-workers who made themselves available when I needed an extra hand. I also need to thank Dale Ladoon specifically, because he provided the basic Ludwieg tube drawings which I used over and over again in my schematics. J.D. Schmisseur has been particularly helpful on several occasions on a variety of subjects. I would also like to thank the ASL Machine shop, they always made time to grind, cut, thread, or machine when I needed it. And finally, I would like to thank my advisor Dr. Steven Schneider whose guidance and instruction was invaluable. I also thank Dr. John Sullivan and Dr. T. N. Farris for their willingness to participate on my advisory committee.

TABLE OF CONTENTS

Page

LIST OF TABLES

LIST OF FIGURES

Figure

ABSTRACT

Munro, Scott Edward. M.S., Purdue University, December 1996. Effects of Elevated Driver-Tube Temperature on the Extent of Quiet Flow in the Purdue Ludwieg Tube. Major Professor: Steven P. Schneider.

The purpose of the present research was to develop a system to heat the driver air in the Purdue quiet-flow Ludwieg tube. This system needed to effectively heat the air while not producing any disturbances that could adversely affect the quiet-flow performance. A study was performed to determine the heating system effectiveness and to investigate the effects on the quiet-flow region. A study of the baseline tunnel configuration was also performed. The baseline quiet-flow Reynolds number was determined to be 400,000. This agrees with previous results. The driver air was heated to 4 different desired temperatures, 100 C, 125 C, 150 C, and 180 C. Measurements were made approximately 10 cm downstream of the onset of uniform flow. The quiet length Reynolds number was found to decrease with increasing temperature. The quiet length Reynolds number dropped to 380,000 and 340,000 at driver air temperatures of 90 C, 140 C, respectively. The heating system was able to heat the driver air uniformly, at least for the first second of flow. Thermocouples used to monitor the driver tube temperature were typically 25 C higher than the actual air temperature. A large heat sink to the nozzle from the driver tube prevented the first 0.3 seconds of flow from achieving a uniform temperature. The heater had difficulty maintaining a uniform temperature at 180 C. The heater also caused some problems. Oil appears to condense out of the flow during heated runs. The oil forms a film on all the nozzle surfaces and on the instrumentation inside the tunnel. Heating the driver tube also seems to have increased the deterioration of the paint on the inside surface, requiring increased maintenance of the nozzle-throat.

CHAPTER 1 INTRODUCTION

Today there is little talk of the X-15 and SR-71, two of the fastest flying machines ever to take to the air. The space shuttle routinely re-enters the atmosphere and touches down safely on a conventional runway. With many high supersonic and hypersonic research projects in the past, and other successful high-speed flight vehicles, one might think that there is little need for research at high speeds. However, this is not the case, for there are several major areas that have a need for research.

One of these is supersonic and hypersonic boundary-layer transition. The limited knowledge in this area is slowing the design process for single stage to orbit vehicles, like the National Aerospace Plane (NASP). The available data are not accurate enough, or understood well enough to predict transition in the flight regime considered by the NASP and other hypersonic programs.

There is limited flight transition data available mainly due to the expense associated with flight testing a hypersonic vehicle. The available data is not enough to verify computer programs that attempt to predict transition at these speeds. Transition data from most supersonic wind tunnels do not follow the same trend as that seen in flight or indicated by theory. One of the main reasons for this disagreement is that most wind tunnels have relatively high freestream disturbance levels compared to flight. Some wind tunnels have now been designed specifically to prevent a high disturbance freestream. These wind tunnels are termed quiet-flow wind tunnels because the freestream disturbance level is typically an order of magnitude lower than conventional wind tunnels. Quiet flow is generally described as a flow with freastream disturbance levels much closer to those

found in flight, typically with fluctuations on the order of 0.05% of the mean (where conventional wind tunnels usually are at least 0.5%).

The Purdue University Ludwieg Tube is one of the few quiet-flow facilities in operation. Currently the Purdue Ludwieg Tube is capable of Mach 4 flow, with quiet flow to a unit Reynolds number on the order of 40,000/cm. Although this is low when compared with flight Reynolds numbers, it can still be used to gain valuable knowledge on transition.

However, the current facility does have some drawbacks. Its current Mach 4 configuration limits it to the study of mainly first-mode dominated transition. This is because first-mode instabilities usually dominate transition up to about Mach 5 where second mode instabilities then become the dominant instability. It is also limited by its test section size, which is only about 4 by 4 inches.

To overcome these limitations, there are plans to add a larger Mach-6 nozzle. This would allow for the study of second mode instabilities. It is also planned to design a larger test section to accommodate larger models. The purpose of the current study is to accomplish one of the main steps in upgrading the facility for Mach 6 capability.

During expansion through the nozzle to Mach 6, atmospheric temperature air can condense into droplets. Thus, to prevent condensation, the supply air temperature must be increased so the freestream temperature does not fall below the condensation temperature. This must be accomplished while still maintaining quiet-flow conditions in the tunnel. The goal of this study was to develop a heating system that would be able to heat the supply air for the tunnel while still maintaining the quality of flow. A study of the effects of the elevated driver air temperature on the extent of quiet flow was also performed to determine the possible advantages or disadvantages of heating the driver air. This also included an extensive evaluation of baseline-configuration flow noise levels to use for comparison to elevated temperature data.

1.1 Literature Review

1.1.1 Boundary Layer Transition

Boundary layer transition plays an important part in many flight regimes. It can make a significant contribution to the overall forces on the vehicle. At hypersonic speeds, transition can cause extremely high surface temperatures as well. Thus it is of great importance to understand and control the transition process. In his review paper Reshotko (1994) argues that substantial drag reduction opportunities lie in stabilizing the laminar boundary layer. It is estimated that friction drag accounts for 60% of drag in cruise for most transport aircraft with predominately turbulent boundary. This amount could be reduced by maintaining laminar boundary layers so that the maximum amount of friction drag is at laminar levels rather than turbulent levels.

Several review papers present an overall view of the basic elements of transition. In general it is agreed that transition is caused by the growth of linear modes that are amplified in the laminar portion of the boundary layer (Reshotko 1994; Bushnell 1990; Mack 1984; Morkovin 1991; Stetson 1990, 1992; Kendall 1993; Reed and Saric 1989). The process can be broken down into steps (barring large disturbances that cause by-pass transition) including receptivity, linear growth of amplified instabilities, non-linear growth of instabilities, and finally breakdown to turbulence.

Receptivity is viewed as one of the keys to understanding the transition process. In the past, most experiments have focused on simply obtaining transition location data. However, this gives little, if any, information as to the initial growth of instabilities (Stetson 1992). Understanding how the flow field disturbances enter and grow in the boundary layer is the only way to generate reasonable prediction methods (Bushnell 1990, Kendall 1993). Thus, the concept of receptivity was developed.

This is the first step in the transition process. Receptivity is the process by which freestream disturbances enter the boundary layer and the mechanism by which the normal

instability modes are excited (Reshotko 1994). Generally receptivity is limited to the leading edge or any area where the boundary layer must adjust to changing geometric or boundary conditions (Reshotko 1994). Figure 1 (Morkovin 1991) shows several possible environmental disturbances that could influence the receptivity process.

There are different instabilities that amplify or decay under different circumstances. For subsonic flow there are four main modes of instability; the T-S mode (Tollmein-Schlichting) or viscous instability, the Kelvin-Helmholtz or inviscid instability, the Gortler instability, and the crossflow instability (Floryan 1991, Morkovin 1991).

The T-S instability and the Kelvin-Helmholtz instability are both linear 2-d instabilities. Linear stability theory is derived by arranging the Navier Stokes Equations in perturbation form. The perturbations are considered small and thus all non-linear perturbation terms in the resulting equations are ignored (Mack 1984).

The Kelvin-Helmholtz instability comes about by the assumption that viscosity is considered only to be important in the mean flow. In this case an unstable wave can only exist if the boundary layer velocity profile has an inflection point (Mack 1984). The T-S mode comes from examining the equations with the viscous terms. Examination of this form shows that unstable waves can exist under certain viscous conditions (Mack 1984). The most amplified T-S instability waves are aligned perpendicular to the flow (Kendall 1993).

In contrast, the Gortler and crossflow instabilities are more 3-d. The Gortler instability results from centrifugal forces over curved surfaces. The instability produces Gortler vortices which are formed in the streamwise direction and rotate in alternating directions (Floryan 1991). The crossflow instability can amplify if there is a component of velocity perpendicular to the inviscid flow. The instability forms vortices in the streamwise direction like the Gortler vortices, but differs in that they all rotate in the same direction (Reed and Saric 1989). Crossflow instability is common on swept wings, rotating cones, corners, and rotating disks.

Supersonic and hypersonic flows are somewhat different from the subsonic incompressible case. The Gortler and crossflow instabilities remain relatively unchanged

in supersonic flow. Supersonic and hypersonic flows have two other dominant instabilities; the 1st and 2nd mode instabilities. The first mode is the compressible counterpart to T-S waves, except that the most amplified waves are now at oblique angles to the flow (Kendall 1993). The first mode is typically dominant up to Mach 4 or 5. The second mode instability becomes dominant for Mach numbers above this (Reshotko 1994). Second mode waves are high frequency acoustic disturbances. (Stetson 1992).

These instabilities are receptive to different disturbances, and once excited grow in amplitude. This initial growth is weak and occurs over a long length (Reed and Saric 1989). Eventually non-linear interactions occur. These are termed secondary instabilities. This process is much shorter and quickly breaks down to turbulence (Reed and Saric 1989). Turbulence is described by Morkovin (1991) as irregular, three-dimensional vorticity, with diffusive motions far in excess of molecular mixing and dissipation.

Many experiments on the non-linear growth and transition location of the boundary layer have been performed. Unfortunately this focus has caused much of the receptivity problem to be overlooked. There needs to be a shift in emphasis from non-linearity and breakdown, to the initial disturbance field and receptivity layer (Bushnell 1990; Kendall 1993; Reed and Saric 1989; Reshotko 1994).

There is a need for clear data on the subject of receptivity. However, some problems have been found in most wind tunnels that can hamper this effort. It has been shown that at low speeds, a low disturbance freestream is needed to detect and measure the early stages of instability growth. This was demonstrated first by Schubauer and Skramstad (Stetson 1992). High freestream disturbance levels (compared to flight) in supersonic and hypersonic wind tunnels also seem to affect the transition Reynolds number (Kendall 1993). Thus there is a need to simulate the low flight disturbance levels to obtain reliable boundary layer transition data (Reshotko 1994). The development and results of such facilities is discussed below.

1.1.2 Need for Low Disturbance "Quiet Flow" Wind Tunnels

Often transition Reynolds numbers found in wind tunnels did not compare well to flight data at supersonic speeds. In fact, wind tunnel data contradicted flight data trends if one examined the slope of the transition Reynolds number versus Mach number curve (Morkovin 1969). Morkovin (1969) also stated that the existence of a true transition Reynolds number dependence on Mach number could not be found in wind tunnels because of the influence of the radiated aerodynamic noise from the wall boundary layers.

This view is not only based on the disagreement between flight and wind tunnel data. Wind tunnel transition data also contradicted theory. Linear stability theory predicts that transition Reynolds number on a cone is less than that of a flat plate. However, conventional wind tunnel data predicted the opposite (Bushnell 1990). Pate (1961) furthered the case against conventional wind tunnels when he was able to correlate transition Reynolds number data for sharp cones to tunnel wall parameters from data in several different tunnels. This correlation can be seen in figure 2. Laufer (1961) also showed that the high freestream disturbance levels were caused by acoustic radiation from turbulent wall boundary layers. This prompted the need for clear-cut data to definitively show that for the same conditions, wind tunnels and flight produce different results.

Fisher and Dougherty performed such an experiment (Fisher and Dougherty 1982; Dougherty and Fisher 1982). Transition experiments on a 10-deg cone were performed in several different wind tunnels and also in flight. In flight experiments the cone was mounted in front of the nose of an F-15. Comparison of transition Reynolds number versus Mach number (figure 21 in Dougherty and Fisher (1982), reproduced here in figure 3) shows that flight and wind tunnel data agree reasonably well up to about Mach 1.5. However, above that there is a large discrepancy between the two (nearly 50%). The upward trend of flight data is not even followed by the wind tunnel data (Dougherty and Fisher 1982).

The flight freestream noise levels are also much lower than disturbance levels in conventional wind tunnels. Figure 4 (figure 22 in Fisher and Dougherty 1982) shows the

freestream disturbance level for the flight experiments. Notice that the freestream noise levels can be as low as 0.008% of the mean pressure, and even the highest levels are only around 0.03%. This is in contrast to 0.5%-3% found in conventional supersonic wind tunnels (Schneider and Haven 1995). These two noise levels are compared in figure 5 (also reproduced from Dougherty and Fisher 1982); although the fluctuations are normalized by the dynamic pressure rather than mean pressure, the difference is readily apparent.

It was clear that reliable flight approximations from wind tunnels could only be obtained with lower disturbance freestreams. The M=3.5 NASA Langley Low Disturbance Tunnel was developed for this purpose. This is accomplished by maintaining laminar boundary layers on the nozzle wall. Experiments in the tunnel produced some important results. First of all, theory was finally confirmed. Tests showed that transition Reynolds number is lower for a cone than a flat plate (Chen *et al.* 1989). Data with laminar tunnel-wall boundary layers can be compared to data with turbulent tunnel-wall boundary layers. This can be seen in figure 6 which is taken directly from Chen *et al* (1989). The advantage of the low disturbance environment (bleed-slots open) is readily apparent. These transition Reynolds numbers are in the range of the flight transition data, while the turbulent tunnel-wall boundary layer data is similar to conventional wind tunnel data. These results definitely showed the possible benefits of low disturbance tunnels.

1.1.3 Characteristics of Low Disturbance Wind Tunnels

The majority of the low disturbance, or "quiet," wind tunnels were designed and built at NASA Langley. There are some exceptions, including the facility used in the current study, however much of the knowledge used to build them came from the original research at NASA Langley. Thus, the discussion of quiet-flow wind tunnels will mainly focus on Langley work.

Low disturbance wind tunnels have certain requirements that allow them to produce "quiet" flow. These requirements are elements that help maintain an initial low

freestream disturbance and also help maintain laminar boundary layers for as long as possible in the nozzle area. This is done because the dominant noise source for freestreams with $M > 2.5$ is radiation of noise from turbulent boundary layers on the nozzle walls (Wilkinson *et al.* 1992). Delaying transition on the nozzle walls delays noise radiation to the freestream (figure 7). If transition can be delayed long enough, a low disturbance environment will exist where transition experiments can be performed.

There are four main requirements that must be followed to produce the lowest freestream disturbances possible. These are (1) filtering of the supply air (2) creating a very low disturbance supply air prior to the contraction (3) either a smooth long contraction to maintain laminar boundary layers or a method for removing turbulent boundary layers just prior to the throat, and (4) a highly polished nozzle (Wilkinson *et al.* 1992).

The filter is used to remove particulate from the air supply. This is needed because particulate could scratch the surface of the nozzle and possibly degrade its performance (Wilkinson *et al.* 1992). Particulate may also speed transition. It is believed that the wake of the particulate can cause large enough disturbances in the boundary layer to excite instability modes (Bushnell 1990; Reshotko 1994).

A very low disturbance air supply is essential. This minimizes the introduction of disturbances into the boundary that could cause premature transition downstream (Wilkinson *et al.* 1992). In the NASA Langley low disturbance tunnels this is done using a variety of screens and honeycomb material. The Purdue Quiet Flow Ludwieg Tube uses the concept of the Ludwieg tube to alleviate the need for the extensive screen and honeycomb system. Since there is no flow before the run, the air is uniform, and there are also no valves upstream that could cause disturbances (Schneider and Haven 1995).

The requirements for the contraction do not include specific tolerances, but it is important to have a smooth and gradual contraction. This is mainly to prevent flow separation as it is accelerated into the inlet of the nozzle (Wilkinson *et al.* 1992). The Langley quiet tunnels all use bleed slots in the contraction to remove the boundary layer just prior to the nozzle inlet. This produces a new laminar boundary layer. This can be an

advantage since the new boundary layer has a much lower Re_x at any given nozzle location. Bleed slots are not a requirement of all quiet tunnels, since the Purdue quiet flow Ludwieg tube and the Montana-State supersonic wind tunnel do not have bleed slots. This is probably because of the added complexity and cost associated with incorporating bleed slots into the design.

Although some of the above requirements seem complicated, the most sensitive and problematic area of the system is the nozzle (Wilkinson *et al.* 1992). Both 2D and axisymmetric nozzles have been fabricated for Langley quiet tunnels. Each has advantages and disadvantages. Short expansion and long expansion nozzles have also been used (Wilkinson *et al.* 1992).

A longer nozzle does seem to improve quiet flow. The first nozzles were designed to have rapid expansions, with the idea that this would limit the growth of first mode instabilities. However, studies on these nozzles showed that the Gortler instability was dominant and thus responsible for boundary layer transition (Chen *et al.* 1989). Later nozzles incorporated a straight portion in the surface of the nozzle upstream of the inflection point. This delayed the onset of the Gortler instability and also weakened it by allowing larger radii of curvature once the concave portion was reached (Chen *et al.* 1989b).

No matter which design is used for the nozzle, the tolerances for the contour and the surface finish of the nozzle are of utmost importance. According to Wilkinson *et al.* (1992) an appropriate balance between manufacturing capabilities and nozzle performance tolerance limits are typically 0.001-0.002 inches in the throat region and 0.003-0.004 inches downstream in the uniform flow region. The surface finish requirement is also very small, $Re_k < 12$ based on the roughness peak-to-valley height and the local unit Reynolds number. This number is only an estimate based on experience, but Wilkinson *et al.* (1992) also state that all successful quiet nozzles have a mirror-like, near optical finish in the throat region.

It is apparent from the above discussion that the throat area is very sensitive to roughness and thus the flow can be affected by any defects to the surface including

scratches or debris. In fact Wilkinson *et al.* (1992) recommend that there be relatively easy access to the nozzle throat region because it must be frequently cleaned to maintain quiet-flow disturbance levels.

The characteristics of quiet tunnels have been discussed. However, the quiet tunnel design does not mean quiet flow is always present. The freestream disturbance levels must be measured to determine quiet flow. But at what levels is the flow considered to be quiet flow? Commonly flow is considered to be quiet flow if the rms of the static pressure fluctuations are less than 0.05% of the mean static pressure (Beckwith and Miller 1990). This is based on a summary of fluctuation data where transition Reynolds numbers for models in the quiet tunnel agreed with those found in flight. Schneider and Have (1995) found that $P'_{t2,rms}/P_{t2,mean}$ (where $P'_{t2,rms}$ is the rms of the total pressure fluctuations behind the bow shock of the probe) should be less than 0.0006 for quiet flow in the Purdue Ludwieg tube (Schneider and Haven 1995).

Schneider and Haven (1995) also suggested that this is only a guide since the overall disturbances ultimately should determine whether quiet flow exists or not. Since acoustic radiation from the nozzle walls determines the quietness of the flow, the percentage of time these fluctuations are detected in the freestream is a reasonable estimate of the flow quality (Schneider and Haven 1995). Pressure disturbances above 0.2% of the mean were thought to be mostly due to radiated disturbances from the wall boundary layers; the level of quiet flow was thus based on the percentage of time the fluctuations exceeded 0.2% of the mean pressure (Schneider and Haven 1995).

Neither method is seen as a perfect method for determining quiet flow. Both were presented here to give some background as to the different techniques that will be used to evaluate and compare fluctuation data in the current study. However, these criteria bound the low noise flow and create a quiet flow region in the test section (Figure 8). The upstream end of the quiet region is bounded by the onset of uniform flow. The downstream edge is bounded by the Mach line radiated from the location of transition on the nozzle wall. Outside this region the flow is not uniform enough to be useful or does not meet the fluctuation limits described above (Wilkinson *et al.* 1992). Since the current

study deals with the possible influences on the size of this region due to heated driver air, it is pertinent to discuss the possible effects heating could have on the nozzle wall boundary layers.

1.1.4 Effects of Temperature on Boundary Layer Instabilities

The qualitative effects of cooling and heating the wall on boundary layer transition are well documented under some conditions. It is important to note that there are differences between water and air. Heating the wall in water experiments has been found to stabilize the boundary layer, in some cases significantly (Reshotko 1994). Experiments have been performed where the transition Reynolds number for an pipe inlet boundary layer were tripled by only an 8 deg C overheat (Barker and Gile (1981) as cited by Reshotko 1994).

The opposite is true for air. Cooling the wall rather than heating produces a stabilizing affect in most cases. T-S and 1st mode instabilities are stabilized by cooling the wall (Kendall 1993, Reshotko 1994). Flight tests agree with this trend. According to Fisher and Dougherty (1982), cooling the cone significantly delayed transition, while heating the cone resulted in earlier transition. The Gortler instability has been shown to be destabilized by cooling at supersonic and hypersonic speeds (Reshotko 1994).

Second mode instabilities are stabilized by wall heating (Stetson 1992, Bushnell 1990, Kendall 1993). Experiments with a heated Mach-5 nozzle showed a 20% increase in transition Reynolds number for a wall temperature ratio of 1.4 (Harvey 1975). Thus at high supersonic Mach numbers, cooling of the wall can produce unexpected results depending on which instability is dominant. In fact, second modes can become dominant at Mach numbers below 4 when the wall is cooled (Reshotko 1994).

Temperature gradients can also have an adverse effect on the instabilities. Numerical calculations of amplification rates have been performed for a flat plate at Mach 8 for an adiabatic wall, a cooled wall, and a wall initially adiabatic ramped to a cooled level (Gasperas1989). These calculations show that as expected the cooled wall was most

unstable. This is because the second mode is dominant at this speed (Gasperas 1989). However, eventually the ramped case amplification rates began to increase to a similar value as the cooled wall case (Gasperas 1989).

Similarly, heating the nozzle throat in a quiet tunnel may or may not delay transition. Heating may be considered as a solution for roughness-associated problems, since the boundary layer thickness will increase, reducing roughness effects. However this can destabilize the 1st mode and Gortler instabilities which could possibly induce earlier transition on the nozzle walls (Wilkinson *et al.* 1992). Heating the driver air is somewhat similar to cooling the nozzle wall. The unheated nozzle wall will appear cooler to the heated air. Since heating the driver air could adversely affect the performance of the nozzle, it is important to understand the need for driver-air heating.

1.1.5 Need for Heated Driver Tube Air

The converging-diverging nozzle on the Ludwieg tube is a standard isentropic expansion nozzle. When the flow is expanded, the temperature drops according to the isentropic relations. For Mach 4 the temperature ratio is 4.2. As was mentioned above, the future plans call for a Mach 6 expansion nozzle. The temperature ratio nearly doubles to 8.2. Atmospheric stagnation temperature would result in static temperatures on the order of 37 K in the nozzle. Operation of the Mach 6 facility is expected to consist of driver tube (stagnation) pressures of about 150 psi, or 10 atmospheres. These conditions suggest that condensation may occur.

An extensive review of the condensation process is given by Wegener and Mack (1958). During the expansion, part of the flow may reach low enough temperature and pressure to cause a phase change in the gas. Figure 9 shows the coexistence line for air, and the isentropic expansion isentrope for particular stagnation conditions (mainly p and T)(Wegener and Mack 1958). The intersection of the two curves (if this occurs) is the critical point where the pressure and temperature combination causes static liquefaction. The Mach number at this point is the critical Mach number (Wegener and Mack 1958).

This Mach number is the maximum Mach number achievable without static liquefaction. If several isentropes are plotted, a curve can be developed for the critical Mach number for a range of stagnation pressures and temperatures. Figure 10 is a summary of this type of analysis for "dry air" where the critical Mach number can be found if the stagnation temperature and pressure are known (Wegener and Mack 1958).

For the current study one can work backwards to obtain a necessary temperature to prevent condensation during the expansion. Using Mach 6 and 10 atm stagnation pressure, a stagnation temperature of about 450 K is needed to prevent liquefaction. This is a conservative estimate, because supercooling would allow a lower temperature to be reached without condensation.

However, the amount of supercooling is dependent on several parameters including temperature gradients (and hence the nozzle geometry), the availability of particulate and other surfaces of condensation, and of course the pressure and temperature. This makes correlation and prediction of supercooling difficult. Wegener and Mack (1958) present experimental data from Kubota (1956) comparing long and short nozzles (figure 36 in Wegener and Mack 1958). Two nozzles with the same exit dimensions, but different throat radii were compared. The shorter nozzle with a throat radius of 0.3 cm showed much more supercooling than the longer nozzle with an 8 cm throat radius. According to Wegener and Mack (1958) experience has shown that larger hypersonic tunnels usually require preheated air supplies such that the critical Mach number is never reached.

It is apparent that some amount of heating will be needed, however it will be dependent on the supercooling of the gas as it is accelerated. It seems prudent to design a heating system that can achieve a temperature high enough to prevent expansion above the critical Mach number for the expected stagnation conditions.

1.1.6 Temperature Measurement with Hot Wires

Hot wires are used in all types of flows. Depending on the configuration they can be used to sense mass flow, or temperature (Kendall 1993). The wire is placed in the flow at the point of interest and a current is applied across the wire. The magnitude of the current depends on the use. A significant current is used to sense mass flow. This is usually done to try to maintain a constant temperature in the wire. Flow over the wire causes it to lose heat, and this can be calibrated with the amount of mass flow. If a small current that does not cause significant heating of the wire is applied, the temperature of the flow can be measured (Kendall 1993).

Since the present experiment only uses hot wires for temperature measurement, the background information will be limited to this use. Any materials book probably has a section related to a material's electrical resistance variation with temperature. This variation is usually linear over a reasonable range of temperature. The slope of the linear curve varies from material to material. Typically, this relation is expressed as $R_{hot}=R_{cold}(1+\alpha\Delta T)$ where R is the resistance and T is temperature. The hot and cold subscripts indicate heated resistance and a "cold" reference resistance. The resistivity coefficient α has units of C^{-1}.

For temperature sensing, only a small current is applied across the wire (often called the cold-wire mode). This prevents the current from heating the wire significantly, but permits the measurement of voltage across the wire. If the current supplied is kept constant, the voltage changes are directly proportional to any resistance change ($V=iR$, i constant). Thus, any resistance changes due to temperature can be sensed as voltage changes. The equation can be solved for the hot temperature $T_{hot}=(R_{hot}-R_{cold})/\alpha R_{cold}+T_{cold}$. Substitution of $R=V/i$ yields $T_{hot}=(V_{hot}-V_{cold})/i\alpha R_{cold}+T_{cold}$. Thus the temperature can be found by monitoring the voltage output across the wire. It does, however, require that a calibration be performed to determine α. A reference temperature, voltage, and resistance must be recorded for use as reference conditions.

In addition to the calibration there is one other adjustment that must be made to calculate a true temperature for the flow. The wire is immersed in the flow, and thus

should be sensing that temperature. However, there is some cooling of the wire due to the heat loss caused by flow over the wire. This has been studied extensively and it is common practice to use a recovery factor to account for the error due to heat loss (Spina and McGinley 1994). A major contributor to the value of the recovery factor is whether flow near the wire is considered free molecular flow or continuum flow. Flows classified as free molecular flows tend to have recovery factors above 1. This implies that the wire is actually sensing a temperature above the flow stagnation temperature (Spina and McGinley 1994). A Reynolds number at the wire can be calculated using stagnation conditions $Re_o=\rho_1 U_1 d/\mu_2$ (d is the diameter of the wire and the subscripts indicate conditions either upstream (1) or downstream (2) of the normal shock caused by the wire). This is because the majority of the heat transfer occurs on the front edge of the wire near the stagnation point (Spina and McGinley 1994). A Knudsen number can also be calculated using the equation:

$$Kn = \frac{M_\infty}{Re}\sqrt{\frac{\gamma\pi}{2}}.$$

An appropriate recovery factor can be picked from figure 4 in Spina and McGinley (1994).

The size of the wire is important in determining the frequency response and the resolution of the measurements. Typically there are definite advantages to using the smallest wire diameter possible in that frequency response increases. However this must be balanced with the fact that the wires are more fragile as the diameter decreases (Kendall 1993, Kistler 1958).

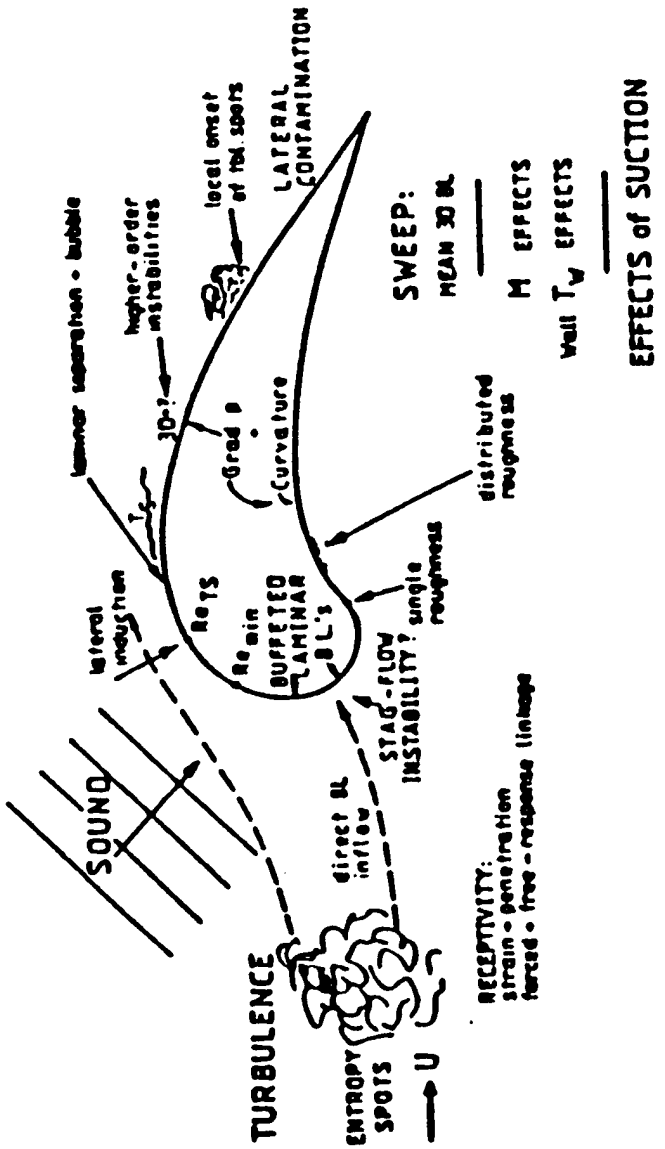

Morkovin (1991)

Figure 1 Possible Sources for Disturbances

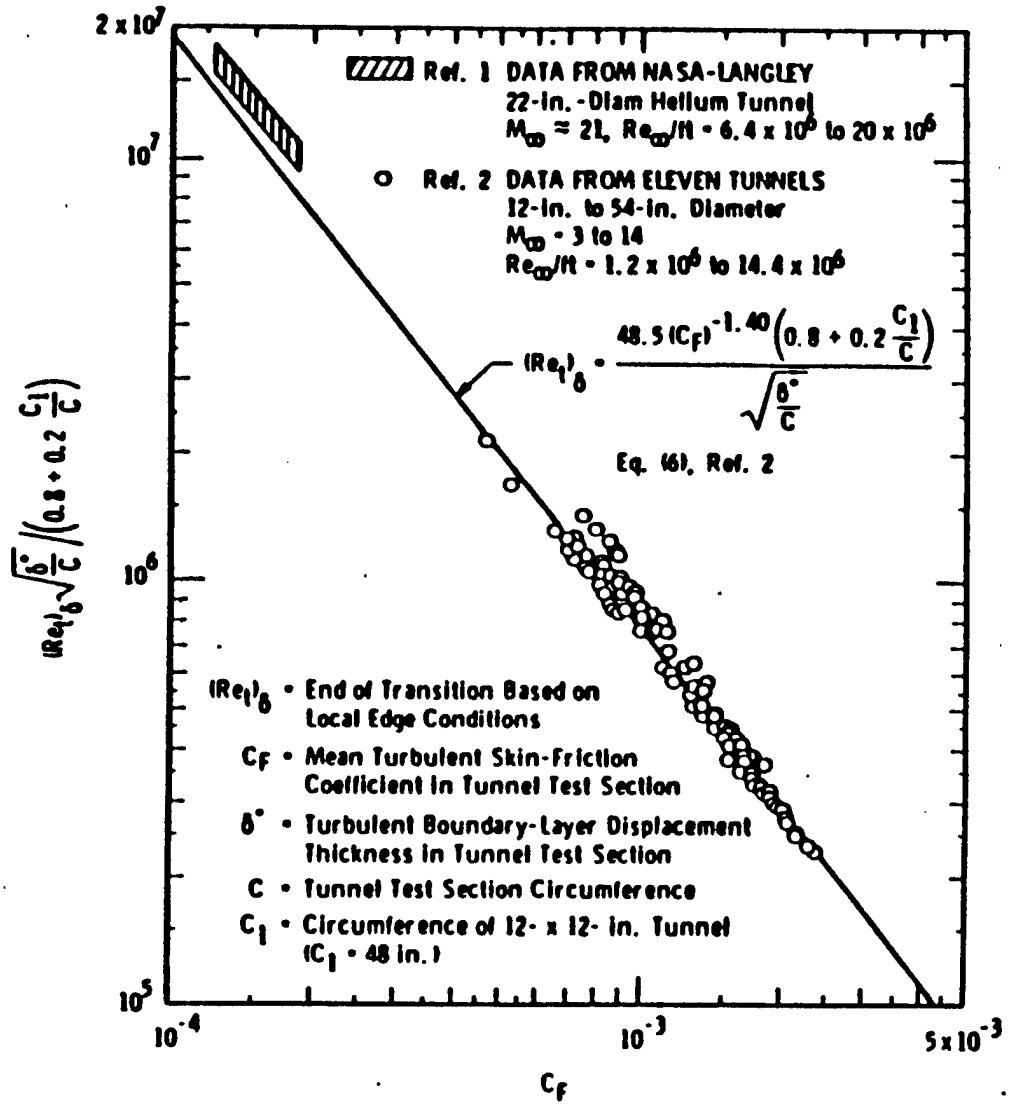

Pate (1971)

Figure 2 Corelation of Transition Reynolds Number

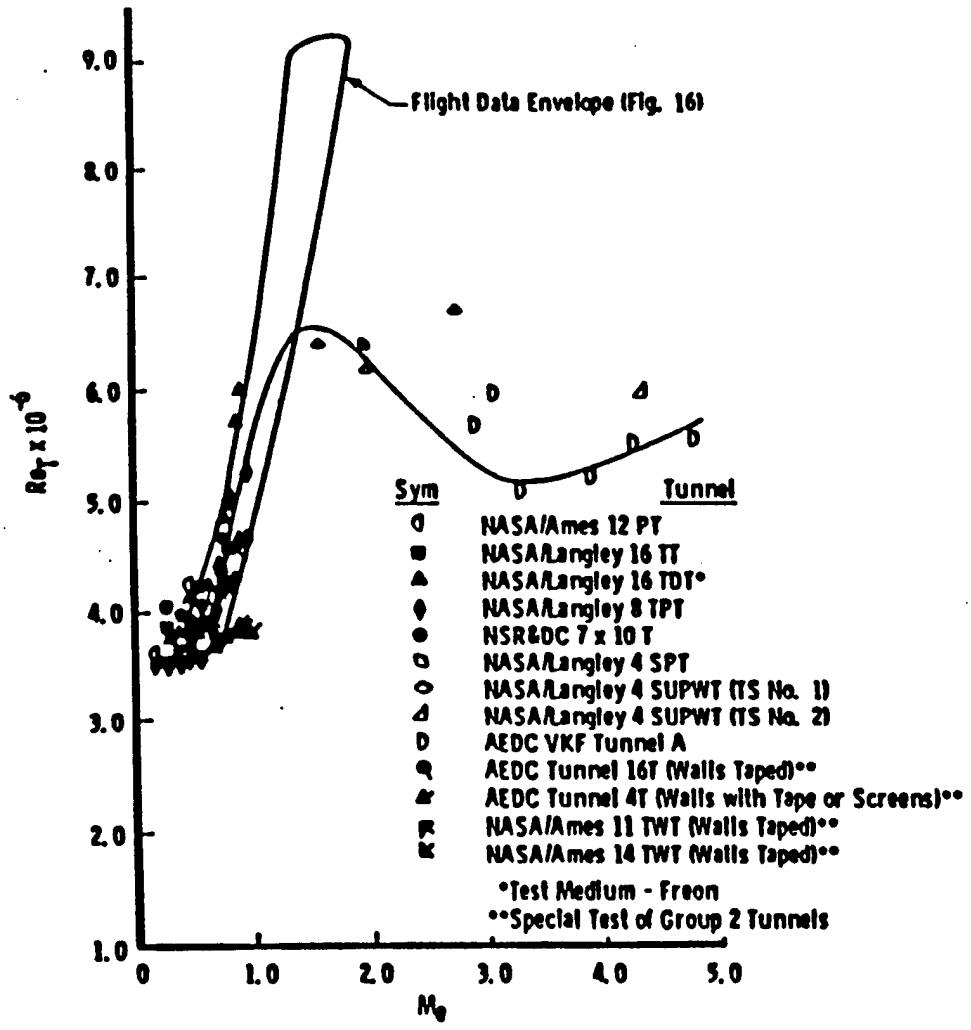

Fisher and Dougherty (1982)

Figure 3 Transition Reynolds Number vs. Mach Number

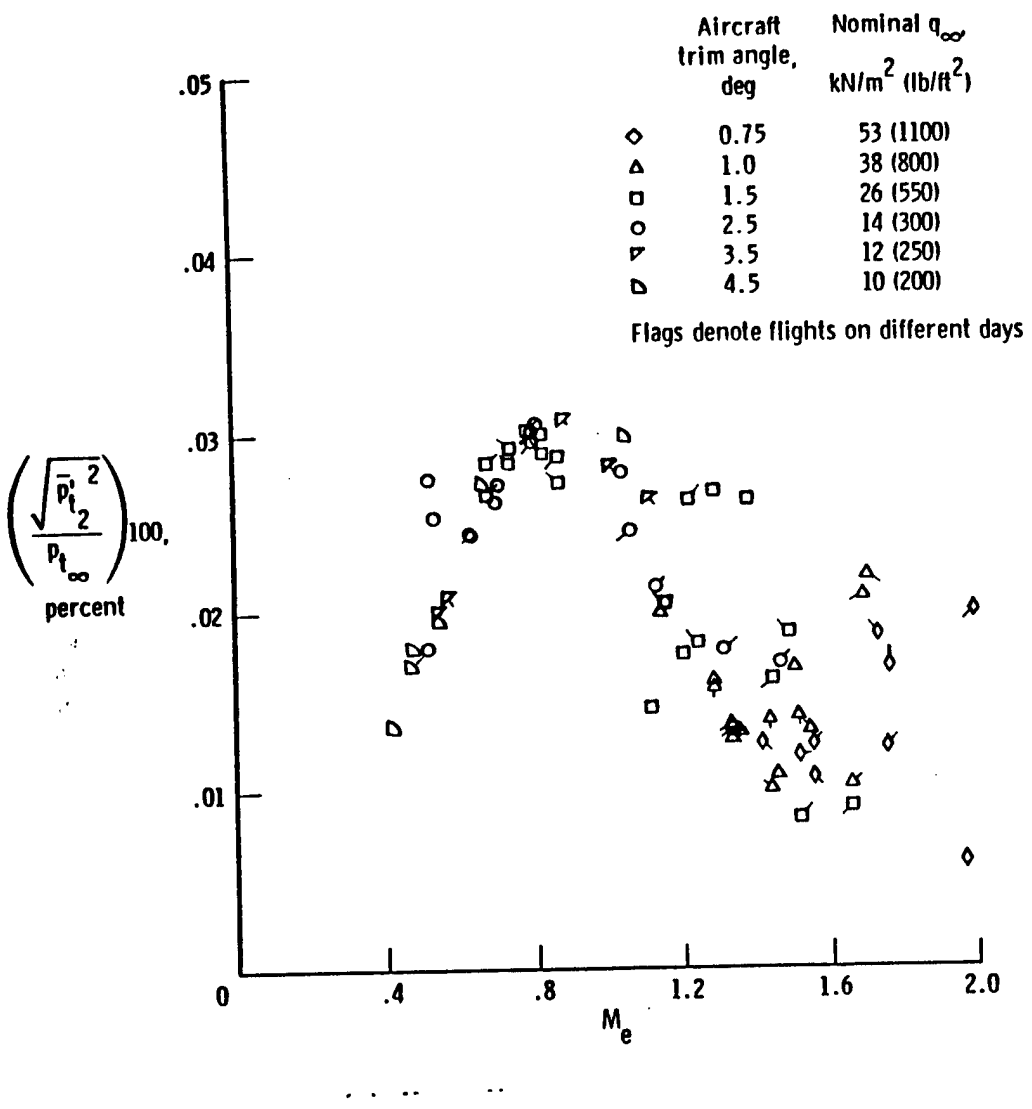

Fisher and Dougherty (1982)

Figure 4 Freestream Noise Levels in Flight

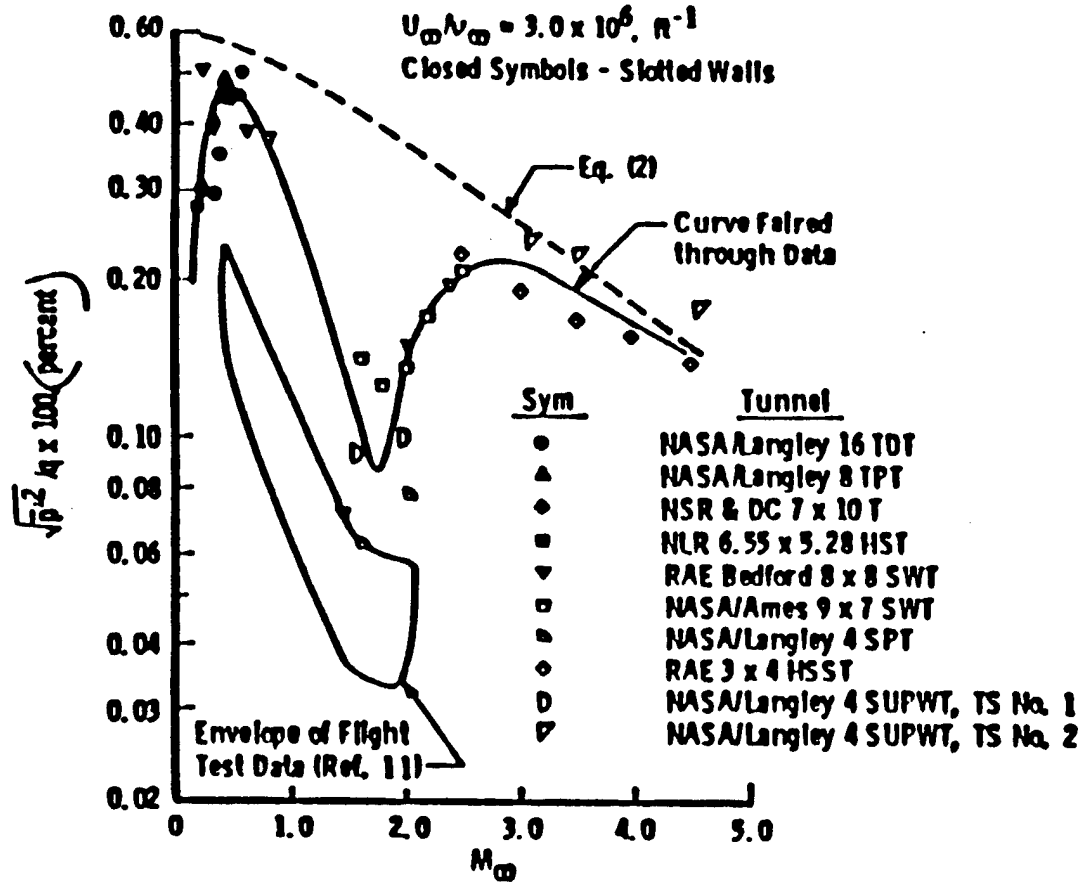

Dougherty and Fisher (1982)

Figure 5 Comparison of Flight and Wind Tunnel Noise Levels

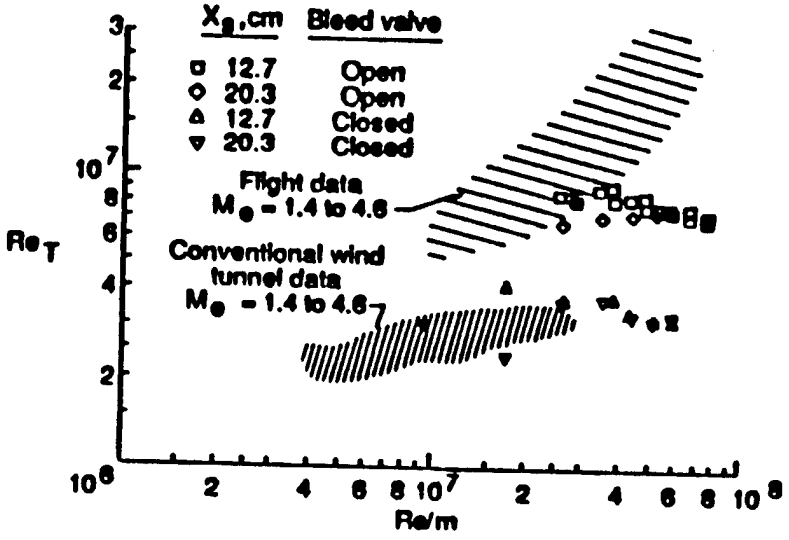

Chen *et al.* (1989)

Figure 6 Quiet-Tunnel Transition Data

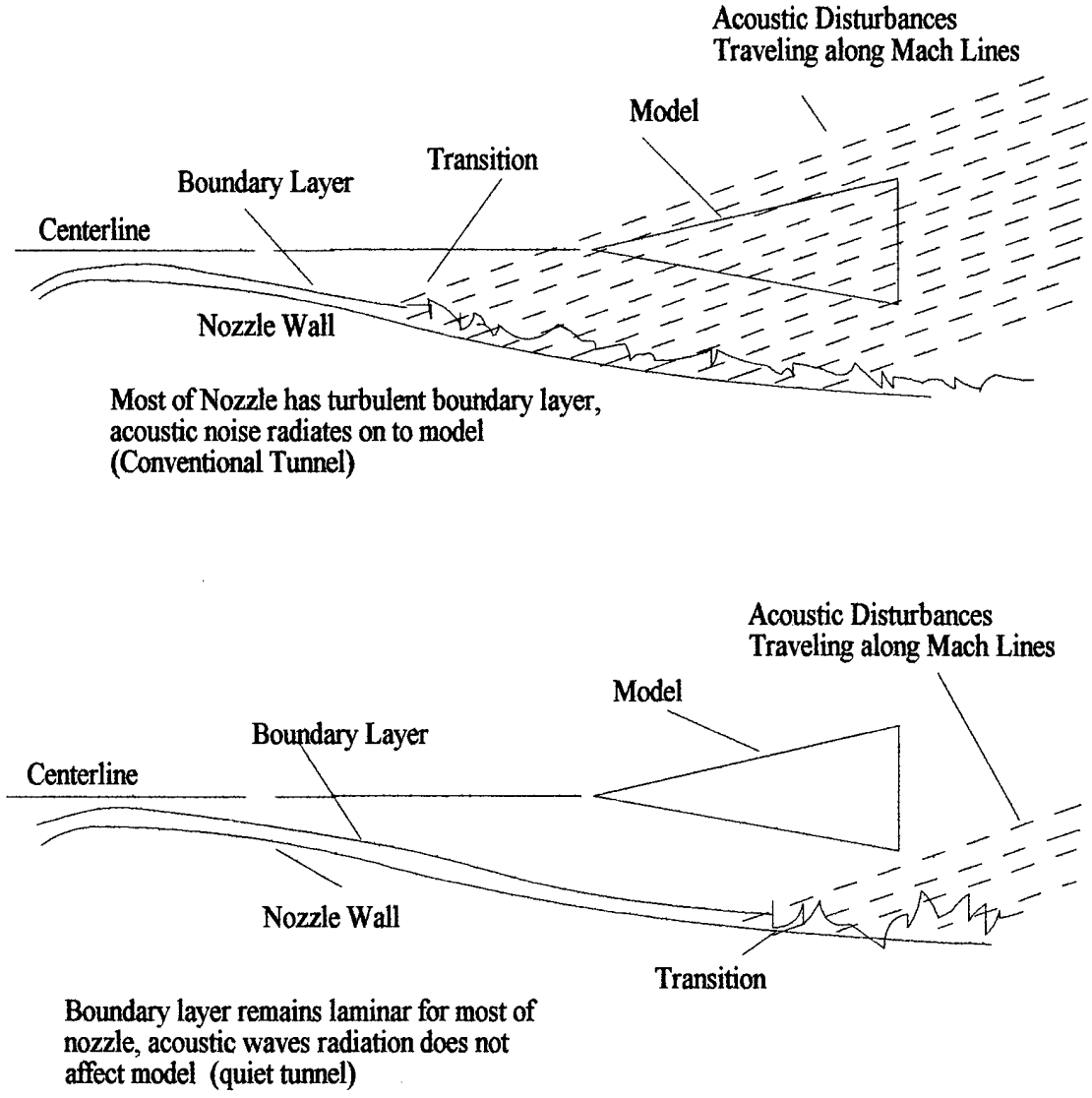

Figure 7 Quiet-Tunnel Boundary Layers

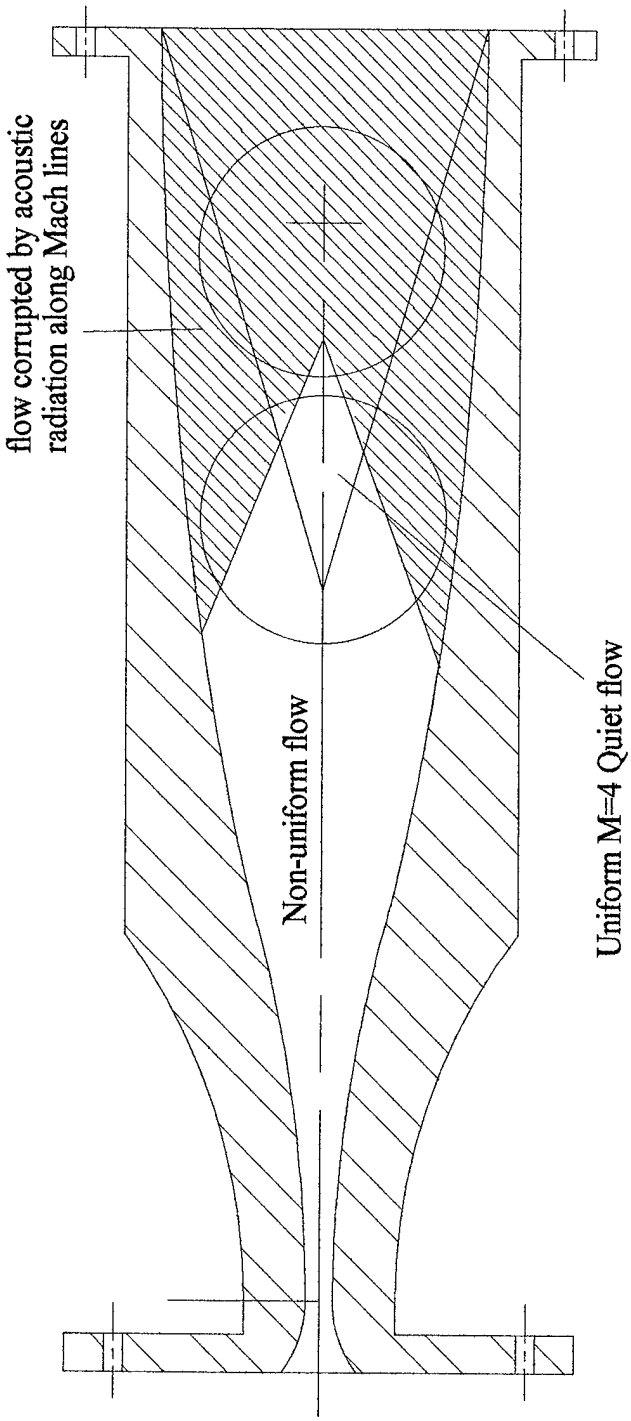

Figure 8 Quiet-Flow-Region Boundaries

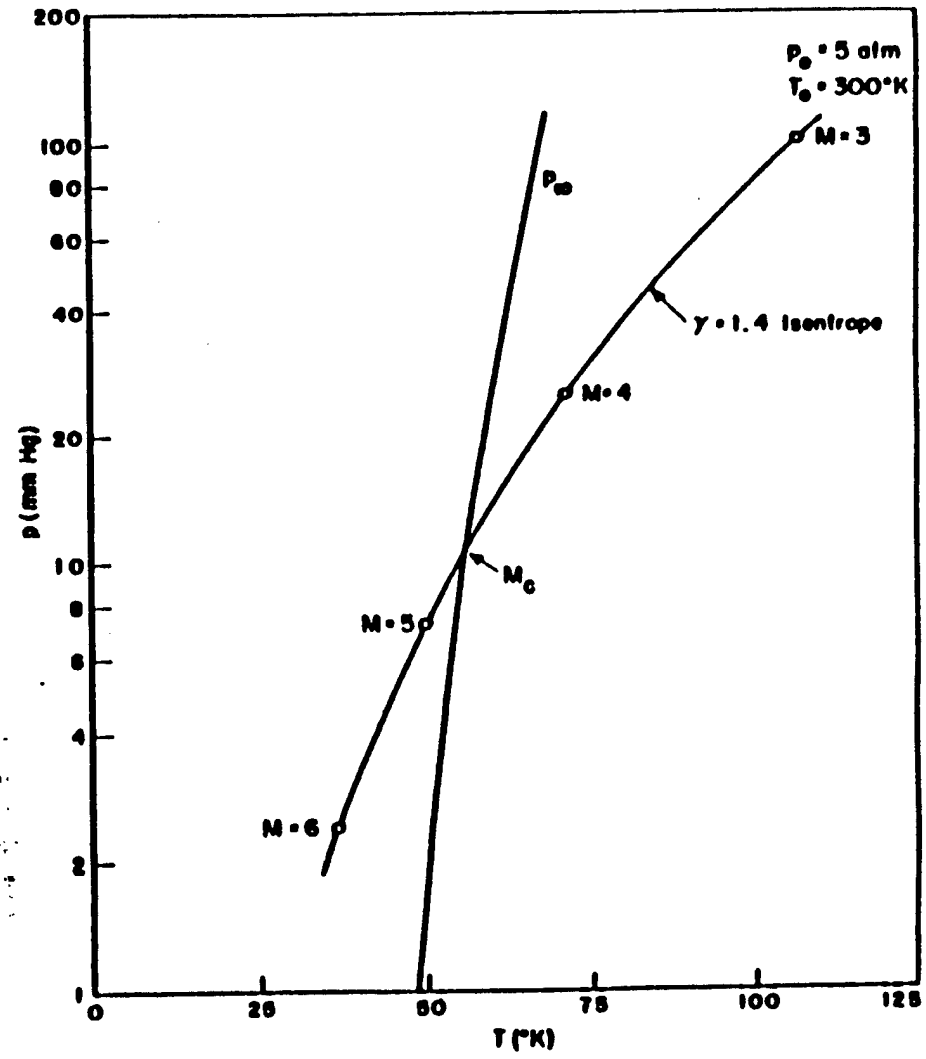

Wegener and Mack (1958)

Figure 9 Determination of Critical Mach Number

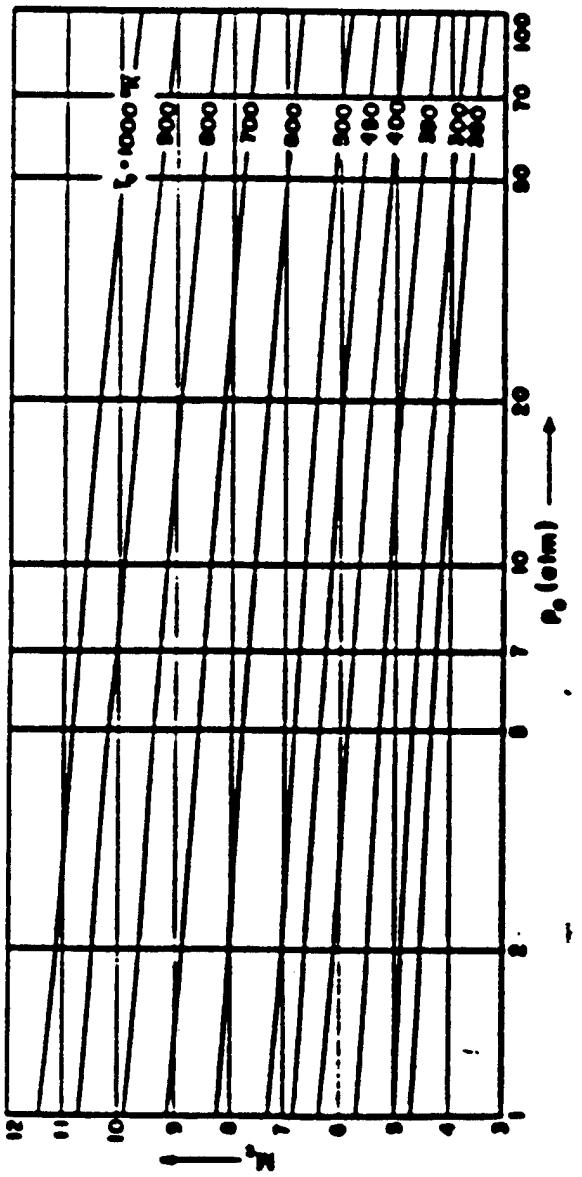

Wegener and Mack (1958)

Figure 10 Critical Mach Number

CHAPTER 2 EXPERIMENTAL APPARATUS

2.1 Purdue Quiet Flow Ludweig Tube

A Ludwieg Tube is a short-duration facility. It consists of three main parts: (1) the driver section, (2) the nozzle and test section, and (3) the vacuum, or driven section (Figure 11). The driver section consists of 12-inch diameter pipe. It is 68 feet long including three 20 foot sections and one 8 foot section connected by standard flanges. The 8 foot section is closest to the nozzle. The nozzle and test section consist of a contraction that extends 12 inches forward into the driver tube, a Mach-4 2-D nozzle with a 3.8 by 4.2 inch exit, and a constant-area test section. The test section contains a double wedge at its downstream end. This serves a double purpose. It has been modified to be the attachment point for stings of models and it forms the second. The Ludwieg tube is similar to a shock tube in that it uses the pressure difference between the driver and vacuum sections to create the flow. However, it is different in that it operatres from an expansion wave instread of a shock wave, allowing a run time of order 1 second instead of order 10ms.

A pressure difference is created between the driver and vacuum sections. The diaphragm is then burst. A shock wave propagates downstream into the vacuum section while an expansion wave moves upstream through the nozzle and into the driver section. The air behind the expansion wave is accelerated, creating flow through the nozzle. Eventually the expansion wave is reflected off the upstream end of the driver section, and then travels back down through the nozzle and test section. This is typically the end of the run. The length of the run depends on the length of the driver section, the pressure difference across diaphragm, and the size of the vacuum section. For the Purdue Quiet

Flow Ludwieg tube the 68 foot driver section gives about 0.122 seconds of flow before the expansion wave returns to the nozzle.

The Purdue Quiet Flow Ludwieg Tube uses the general Ludwieg tube design but also incorporates other technologies to create a very low noise environment during the run. The other major factor in keeping the flow low noise is the nozzle itself. The surface of the nozzle is highly polished. This was done to keep the nozzle wall boundary layers laminar as far down the nozzle as possible. As mentioned in Chapter 1 turbulent wall boundary layers increase the noise in the freestream of the wind tunnel by acoustic radiation along Mach lines. The third aspect of the Purdue Ludwieg tube that helps prevent noise is particulate filtering. It is believed that particulate can make disturbances that contribute to the boundary layer break down to turbulence. The Purdue Ludwieg tube filters the air going into the tube down to 1 micron to prevent this type of disturbance.

All of these concepts help keep the boundary layers laminar on the nozzle walls. However, eventually the boundary layers do become turbulent and radiate acoustic waves into the freestream along Mach lines. Upstream there is a quiet flow region where freestream pressure disturbances are less than 0.05% of the mean total pressure. This region is bounded on the upstream end by the onset of uniform Mach 4 flow and on the downstream end by the acoustic waves traveling along the Mach lines (Figure 12). Different models can be positioned inside the quiet flow region and instability experiments can be performed without the influence of the nozzle wall noise.

The Purdue Ludwieg tube can be run with driver pressures as high as 150 psi. However, pressures this high in the driver section make the Reynolds number large enough in critical regions of the nozzle to cause boundary layer transition on the nozzle walls. Thus, for quiet flow runs the driver pressures and Reynolds numbers are limited. Typically for quiet flow the driver pressure is on the order of atmospheric pressure. This produces a unit Reynolds number of about 40,000/cm.

2.2 Heating Concerns

As mentioned earlier, heating the driver air will be essential when a higher Mach number nozzle is used. In order to successfully heat the driver air, the air must not only be heated, but heated in a way that will not cause disturbances that would destroy the quiet flow. Thus, the heating must not add any particulate to the air, and must be uniform enough so that there are not large convective currents in the driver section at the start of the run. Also there cannot be any device inside the driver section that might cause a wake as the air flows around it during a run. Any of the above factors could lead to disturbances that could propagate downstream and destroy the quiet flow in the test section.

2.3 Heater System

The heater system consists of two main parts, the pre-heater, and the main heater. The pre-heat heater pre-heats the air as it is pumped into the driver section to refill the tunnel after a run. The main heater is the heater responsible for heating the driver pipe and keeping the pre-heated air at the appropriate temperature until the run is made.

The preheat system consists of a circulation heater and a high temperature filter plumbed into the fill line of the driver section. The heater is a Chromolox 4.5 kW, 240 V 3-phase circulation heater (model number GCH-3405/240V/3P). It has carbon steel construction with 3 incoloy heating elements which produce 23 W/in^2. The process is controlled by a single pole thermostat (included with the heater). The process temperature can be varied from 93 C to 288 C (200 F to 550 F) by the user. The purpose of the heater is to heat the air close to the intended temperature as the tunnel is re-filled after a run. To keep the supply air as free of particulate as possible, the air must be passed through a filter once it is heated. Unfortunately the original filter for the tunnel had a maximum temperature of 225 F. To solve the problem a high temperature filter was installed immediately downstream of the circulation heater in the fill line.

The filter is a Van Air Systems F-101-500-HT high temperature filter. The filter removes 99.95% of the particulate down to 0.6 microns. It can filter air at temperatures up to 232 C (450 F) and is rated to 165 psi at that temperature. Its pressure rating is the 150lb flange class (according to Fred Sitter at Van Air Systems, phone 814-774-2631). The filter and heater were mounted on the most upstream support post of the Ludwieg Tube. A bypass line was also added to the fill line at the heater so air can either be sent through the heater or the heater can be bypassed. The lines rejoin after the heater so all supply air passes through the high temperature filter (figure 13 shows original supply line configuration and figure 14 shows the modified configuration). The plumbing for the heater and filter required many threaded connections. High temperature pipe dope (Lat Co Slic Tite heavy duty thread sealing compound) was used to seal the threaded connections. The pipe dope can withstand temperatures up to 260 C (500 F). When assembling a connection care was taken to keep pipe dope off the first few threads. This will hopefully prevent pipe dope from seeping into the pipe and blowing downstream. This was especially important for the connections downstream of the high temperature filter. Before the final connection was made to the driver tube, air was blown through the fill line for several hours. This hopefully removed any sealant or other particulate that may have been in the fill line.

The main heating system heats the driver tube upstream of the nozzle so the heated air doesn't lose any heat to the pipe and atmosphere during the time between the run and re-filling of the tunnel from the previous run. The outside surface was the wake and particulate issues entirely. Since two TCR 30V 200A power supplies were available in the lab, they were chosen as the power source for the main heater system. In order to fully utilize the power supplies, a load resistance of 0.15 Ohms was needed. Originally it was hoped that the pipe of the driver section could be used as the load across the power supplies, but the resistance from one end to the other was calculated as 0.0022 Ohms. This is nearly two orders of magnitude lower than that required for maximum power transfer. The next option was to wrap the driver section in some type of heater wire and let the heat conduct from the wire to the pipe.

The heater wire had to meet several requirements. The wire had to be configured in such a way that its total resistance at the power supply was 0.15 Ohms while covering 34 feet of driver tube (1/2 the total length). The wire also had to be manageable enough to be wrapped around the outside of the driver tube, and it also had to be able to withstand several hundred degrees more than the expected maximum temperature of the heated pipe. This last requirement is because the wire must be significantly hotter than the pipe to transfer a significant amount of heat to it in a reasonable amount of time. Finally, the amount of wire used had to be reasonable. The intention was to wrap the wire continuously around the pipe in a helical fashion. Obviously a wire with a resistance of 0.05 Ohm/ft would not be appropriate since only 3 feet equal the maximum resistance for the power supply. Even if several sections of wire were connected in parallel, it would require a tedious amount of work to configure an appropriate system.

Some theoretical heat transfer calculations were performed that indicated the pipe would need about 4 hours to heat to temperature and the wire would end up being about 300 degrees hotter than the pipe temperature (This was a simple 1-D heat transfer problem estimating the energy input from the power supply, the contact area between the pipe and the wire, and the heat transfer to the air inside the pipe). These calculations also showed that the air inside the pipe would follow the pipe temperature very closely. Several different calculations were performed using different lengths of wire. This essentially simulated the best spacing for the wire coils. A good compromise between efficient heat transfer and the amount of work involved seemed to produce about a 2 inch spacing between each coil of wire. Thus, the final variable for the wire material problem was set, the total length of wire needed to heat the driver section.

Most types of wire normally thought of as heater wire were immediately eliminated since over 650 ft of wire would be needed to wrap 34 ft. of pipe, spacing each coil 2 inches apart. In fact, bare copper wire seemed to be the only wire readily available that came close to meeting the requirements. Even with copper, a fairly large diameter wire would have been needed to have 650ft of wire have a resistance of 0.15 Ohms. This would complicate matters in that cost of the wire would increase dramatically, and one

must remember that the wire has to be wrapped around 12 inch pipe on supports 8 feet above the ground. A reasonable size wire was chosen, 16 AWG (it was large enough so it wouldn't break easily, but small enough to handle without difficulty). A number of lengths of wire were connected in parallel in such a way that the overall resistance would match that needed for the power supply. The fewest number of parallel sections that produced the correct resistance is 6. This takes into account the change in resistance the wire will have due to the temperature increase. Thus, 6 lengths of wire 110 feet long connected in parallel will have a resistance of 0.15 Ohms when the wire is at 260 C (500 F).

Since the pipe itself is an excellent electric conductor the heater wire must be electrically isolated from the pipe or all the current will simply flow through the lower resistance pipe. A good thermal conductor yet electric insulator was needed. The pipe would be covered with the material and the wire wrapped on top. This required the material to be able to withstand the temperature of the heater wire when it is heating the pipe. Fiberglass cloth 1/16 inch thick was chosen for this role. Its maximum temperature is 538 C (1,000 degrees F) so it has no problem with 300 C (~ 600 F) heater wire. It is electrically non conductive, and the thin layer has a minimal thermal resistance.

Heating the driver pipe would not be very effective without insulation to prevent the heat from escaping to the atmosphere. Since the insulation is placed directly over the wire system it needed to be able to withstand at least 300 degrees C. The most reasonable insulation was fiberglass pipe insulation. The maximum insulating value for the most reasonable price determined the thickness. Owens Corning SSL-II Fiberglass Insulation was chosen because of its maximum temperature rating of 450 C (850 F). One of the main factors in determining a thickness was the price. This was mainly because thicker insulations had a significant increase in price, yet no significant increase in insulating value. The 4 inch insulation has an R-value of 12.9 while 5 inch thick insulation had an R-value of 16.7 (both of these are at 350 F). There was a similar difference between 4 inch in 3 inch thicknesses. However, five inch thick insulation was 1.5 times the cost of the 4 inch, while up to 4 inches thick each inch in thickness was only about 1.1 times the cost of

the previous thickness. It was also desirable to keep the insulation at a reasonable thickness since the driver tube extends into common areas of the laboratory and a very thick layer of insulation would reduce clearance underneath the driver section. Since thicker insulations had a greatly increased cost and a 4 inch thickness makes about the same outside diameter as the flanges on the driver section, it was deemed the best choice. Figure 15 shows an overview of the heating system layers.

The heating process must be monitored to assure uniform heating and verify that the heater is in fact heating to the appropriate temperature. This is done using thermocouples mounted on the surface of the pipe. 28 ungrounded sheathed (washer assembly) type J (Omega WTJ-14-S-12, special order for ungrounded) thermocouples are mounted on the outside of the driver tube, beneath the fiberglass cloth of the heating system. Thermocouples were placed around the circumference of the pipe at several streamwise locations. Thus, at each streamwise location, the heating around the circumference can be checked, and having several thermocouples at each streamwise location gives some redundancy. This is important since the thermocouples are not easily reachable underneath the heating system and insulation. Figure 16 shows the themocouple locations.

Originally the intent was to heat the entire driver section. This would ensure that the air was as uniformly heated as possible. However it became apparent that it may not be necessary to heat the entire section since the driver section velocity during the run is only 2.8 m/s. For a 3 second run time this would only move the first 8.4 meters of air through the nozzle. The question arose as to whether or not just heating this amount of air could produce adequate flow conditions for the entire run.

The main reason for answering this question is that on a larger scale much time and expense could be saved if only half the tunnel needed to be heated. It was decided to only heat the first 7.3 meters (24 ft.) of driver section. This would serve two purposes. It should be enough to send almost 3 seconds of heated air through the nozzle. If the flow is satisfactory, it confirms that heating only a portion of the driver section is a viable option for future facilities. However since the average run is typically about 3.5 seconds, it will

hopefully show the transition from heated to unheated air and any adverse affects associated with it.

Thermocouples were placed at approximately 0, 3, 6, 9 and 18 feet upstream of the nozzle throat. These streamwise locations were designated as thermocouple stations 1, 2, 3, 4, and 5 respectively. Emphasis was given to the area of pipe closest to the nozzle, since the first second of flow is most important. At stations 1 and 2 (0 and 3 feet upstream) 6 thermocouples were mounted every 60 degrees around the circumference of the pipe, while at the other three locations 4 thermocouples were placed every 90 degrees (Table 1 shows the upstream distance and angle placement of each thermocouple). The thermocouples and pipe were then covered with the fiberglass cloth, wrapped in heater wire and covered with the insulation (refer to figure 15). Each thermocouple is connected to one of four temperature displays via a switch. Thus four different thermocouples can be viewed at once (figure 17, information is also tabulated in table 1). A fifth switch is used to connect some of the thermocouples to the controller for the heater system.

A controller is used to keep the tube at the desired temperature. An Omega CN9000A PID controller regulates the power supplies. The controller monitors one of three thermocouple temperatures via a switch (TC #6 from station 1 or 2, or TC #4 from station 3) and outputs a 0-10 V DC analog signal (a schematic is shown in figure 18). The signal is sent through a voltage divider to the power supply which accepts a 0-5 V DC signal to scale the total power of the power supply. The factory PID settings were found to be adequate for controlling the temperature. After a short manually controlled pre-heat for the heater wire, the controller will regulate the power to heat the tube to the desired temperature and then maintain that temperature.

The installation of the heater system over the first 24 ft. required 4 of the 110 ft. lengths of wire (figure 19). The ends of each length of wire were connected to large copper wire (1-4 AWG depending on the distance to the power supply) which was attached to one of the power supply terminals. The lead wires were sized such that all the leads had the same resistance even though each was a different length.

All four sections were connected in parallel to the one power supply. Although the overall resistance would not exactly match the power supply impedance, the design specifications for the entire driver tube were used. This would make it easy to install more wire if heating more pipe became necessary. Insulation was also installed over an additional 6 feet of the driver section to prevent excessive heat loss and cooling at the edge of the heated portion of pipe.

Some minor adjustments had to be made to other areas of the tunnel to ensure that the temperature would not adversely affect these areas. Although the driver tube was rated to 315 C (600 F), other parts were limited to lower temperatures. The o-rings used to seal the different parts of the tunnel (material 01, Duro Bun N, Parker O-Ring Inc.) were limited to a maximum temperature of 107 C (225 F). Several of these o-rings were replaced with a high temperature o-rings (material 06, Duro Silicon, Parker O-Ring Inc.) which can withstand temperatures up to 230 C (450 F). O-rings were replaced in the joints between the nozzle and flange of the driver tube, and between the flange and the driver tube. These two o-rings would most likely exceed the 107 C limit since they were adjacent to the heated section of pipe and the intent was to heat as high as 180 C (350 F). The standard o-rings were also replaced with high temperature o-rings in the window inserts and at the nozzle test-section junction. This was done as a precaution since it was not clear how much heat would propagate from the driver tube to the nozzle area.

Early tests using the heating system identified a non-uniformity in the heated air. During the first 0.2 seconds of the run it was noticed that the temperature would slowly increase to the maximum temperature of the run. This indicated that the first air through the nozzle was not as hot as the rest of the air. This was most likely due to the large heat sink provided by the nozzle and flange face for the driver tube (figure 20). These are large surface areas with no heat directly applied to the flange. These areas also could not be insulated very well since large amounts of insulation would impair optical access through the nozzle windows. It was assumed that there was enough heat loss to cause the first part of the driver tube to have a lower temperature than the rest of the pipe.

The contraction probably does not help matters. Once heated, one would think the large thermal mass of the contraction would maintain the heat adequately. However, the contraction is mounted on the flange at the end of the driver tube. Thus there is excellent heat transfer between the two. Although the surface of the pipe may be heated to the same temperature as the rest of the pipe (indicated by the thermocouple readings) there is still a good chance the inside of the contraction is a lower temperature than the rest of the pipe because of the heat transfer.

To counter this heat sink problem extra power was applied to the flange section at the downstream end of the driver tube. This was done using a HP-Harrison 6269A DC 40V 50A power supply. The heating element that best matched the power supply impedance and was about the right length ended up simply being several stainless steel hose clamps clamped together. These were better than wire since there was a much larger surface area that could be in contact with the pipe. The heating element was wrapped around the very end of the driver pipe and around the outside of the flange (Figure 21). The heater element was connected to the power supply and controlled manually as needed. Typically the heater could to maintain the flange area at 100 C with only about 30% maximum power. However full power was required to maintain the flange area at 180 C.

A commercially made ring heater probably would have been the best choice for this task since it could have been attached to the flange face. This would apply the heat to a large surface area and would have directed the heat directly on the face rather than heating the outer part of the flange by wrapping it with the element. Unfortunately, due to the size required to fit around the nozzle, a custom heater ring would have been needed. It was not practical to invest in a custom device since the entire system would have to be redesigned for a Mach 6 nozzle. This is because the Mach 6 design will have bleed slots near the throat requiring a completely different flange/nozzle junction.

2.4 Flow Measuring Instrumentation

There are two main parameters that need to be recorded for this study; total pressure, and temperature. The temperature is needed to determine the effectiveness of the heater in creating a uniform temperature air supply. The mean pressure and its fluctuations must be recorded to determine the quality of the heated flow.

Originally a total pressure rake (figure 22) consisting of 4 pressure transducers was to be used to record experimental data. The pressure rake was mounted horizontally in the flow on a sting attached to a vertical traverse mount. The traverse could position the rake anywhere in the nozzle from slightly upstream of the onset of quiet flow to just downstream of the suspected end of quiet flow. It could also be traversed in the vertical direction. Thus an extensive 2-d study and limited 3-d (limited to the 4 spanwise locations of the pressure sensors) of the quiet flow region could be performed.

The Kulite pressure transducer rake is a double wedge shape about 2 inches square and 0.25 inches thick. Along the leading edge of the double wedge are four 3/16 inch tubes set into the wedge spaced across the span. These four tubes are threaded for set screws that each hold a Kulite pressure transducer. The leads for the transducers are fed through holes in the tubes into a slot at the peak of the wedge on one side and down the sting tube which has a 5/16 inch diameter. The sting tube extends behind the wedge about 7.5 inches. At the back end of the sting tube there are three holes drilled through the tube. The first hole is for feeding the lead wires out of the tube and into the vertical traverse. The other two holes are for two bolts used to secure the rake to the vertical traverse. The double wedge is secured to the vertical traverse such that it is horizontal in the tunnel (Figure 23). The vertical traverse is a brass double wedge 1.5 inches long, 0.25 inches thick and 12 inches tall. When in the tunnel, the vertical traverse projects out through a slot in the tunnel's upper surface and is attached with pins and screws to a traversing mechanism.

Unfortunately the rake vibrated during runs, corrupting the pressure signals. Several attempts were made to eliminate the vibrations including the fabrication of an extra sting support (Figure 24). The sting support mounted onto a window blank and

clamped onto the rake sting. It was hoped this would stiffen the sting structure enough to prevent further vibrations. This reduced the vibrations significantly but did not eliminate them. Since an in depth analysis would have to be performed to rid the rake of its vibration problem, a different single probe device was used in this study.

Since it was not essential to have a 3-d study of the flow to determine the basic effects of temperature a simpler configuration was used to collect data. A single probe mount used in previous experiments was modified for use in this experiment (figure 25). The vertical double wedge fits through a slot in the top surface of the test section. The seal plate covers the rest of the slot. The tube with the sensor mounted in the tip protrudes forward. The length of the tube is such that the sensor is nearly at the beginning of uniform flow when the double wedge is at the upstream end of the slot and at the end of quiet flow when positioned at the back edge of the slot.

The pressure sensor mounted in the probe was a Kulite XCQ-062-25A (serial # 5307-1B-18) absolute pressure transducer. The transducer is 0.064 inches in diameter and is 0.375 inches long. It's pressure sensing device is a silicone diaphragm with a fully active 4 arm Wheatstone Bridge diffused into it. The sensitive area is 0.028 inches in diameter. The transducer was mounted in a set screw in such a way that it extended in front of the rest of the probe. This was done so that the bow shock caused by the probe would be caused only by the tip of the pressure transducer and not by the front face of the set screw or mounting tube. It was mounted so it extended approximately 2 diameters in front of the set screw. The set screw was similarly threaded into the mounting tube.

The leads of the pressure transducer were connected to an amplifier box fabricated in-house (figure 26). The amplifier box produces a 5.0 volt voltage to excite the transducer bridge. The output from the transducer is fed into the box where it is amplified 100 times by an INA103 instrumentation amplifier. A second channel of the signal is then filtered by an 800 Hz high pass filter and amplified another 100 times by a second INA103 instrumentation amplifier. The outputs of the amplifier box are the dc pressure transducer output amplified 100 times and an ac fluctuations channel amplified 10,000 times. These are fed into two LeCroy (model 9304AM) digital oscilloscopes, one sampling at 50,000

Hz and the other at 250,000 Hz (Figure 27). The oscilloscopes can save up to 250,000 points per channel into memory, so once triggered the scopes can save 5 seconds and 1 second of the run, respectively. Expected run times of a Mach 6 facility are predicted to be about 1 second so most of the discussion will present the 1 second of data from the 250,000 Hz oscilloscope. However, the 5 second sampling capability of the 50,000 Hz scope was useful for reviewing temperature data.

To study the effect of driver tube temperature on the noise level in the tunnel, the temperature of the flow must be known. The thermocouples on the outside surface of the tunnel give an estimate of the temperature of the air inside, but this is not necessarily accurate. Therefore the total temperature over the run is required to confirm that the temperature is similar to that displayed on the thermocouples.

The most convenient device available was a cold wire. A cold wire consists of a hot wire operated in low-current constant-current mode rather than constant temperature mode. This configuration responds to change in temperature in the flow by observing the voltage change with respect to a voltage level at a known temperature. The temperature of the wire is calculated using the equations in section 1.1.6. The calculated temperature is also adjusted for the heat transfer of the wire to flow the with the recovery factor.

Several hot wire probes were available since other experiments in this facility use the hot wire probes (Figure 28). Unfortunately all the mounts for these probes used the same slot in the test section as used by the pressure probe. Thus, to obtain both pressure and temperature data, the instrumentation would have to be exchanged each time a different type of data was desired. This left open the possibility that the data could be inconsistent if the temperature was not repeatable enough so that the same conditions were achieved for temperature data and pressure data. Simultaneous acquisition of pressure data and temperature data seemed the most obvious solution.

Since the tunnel expands the flow isentropically the total temperature should be the same no matter where it is measured. This allows for temperature measurement off the centerline of the tunnel. A support was needed that did not use the slot in the test section and was not on the centerline where it would get in the way of the pressure sensor. The

extra support for the original pressure rake solved this problem. A hot wire mount was made to fit the clamp. It was then installed into the tunnel, positioned 0.75 inches below the centerline (figure 29). Care was taken to make sure that it was not positioned in front of the pressure probe, which would possibly cause fluctuations in the flow that could result in erratic pressure measurements.

The wire was connected to an in-house constant-current anemometer (Figure 30). It supplied a constant current of 2.5mA. The voltage across the wire was differenced from a reference offset voltage and amplified 100 times. The constant current anemometer also outputs a channel with ac fluctuations of the voltage amplified 10,000 times, but this was of no interest in the current study and was not recorded. The dc signal was then fed into the LeCroy oscilloscopes in a similar manner as with the pressure transducer signals (refer to figure 27). Thus for each run the dc voltage and ac fluctuation voltage for the pressure, and the dc cold wire voltage, were sampled at the two different rates.

2.5 Experimental Procedure

2.5.1 Kulite Pressure Transducer Calibration

The Kulite pressure transducer outputs the change in voltage across the bridge with change in pressure across the diaphragm. This output is amplified by 100 in the instrumentation amplifier box. If any quantitative work is to be done the voltage output of the Kulite must be calibrated with pressure, frequently. This serves two purposes, first it confirms the factory calibration and second it ensures that the Kulite properties do not change over the course of the experiment. The calibration of Kulite pressure transducers is relatively easy in the Ludwieg tube.

A pressure calibration program has been written and resides on a computer near the Ludwieg Tube (See appendix B for a listing of the code). The program monitors pressure measured on a Precision Paroscientific quartz pressure sensor (model 740) via a

serial port and samples 4 channels on an A/D converter. The program constantly retrieves the current pressure on the Paroscientific and samples the 4 A/D channels when the pressure has changed by a user specified amount. The Paroscientific is normally used to measure the initial pressure in the driver section of the Ludwieg tube before a run. It is connected to a pressure port approximately 2 feet upstream of the nozzle throat, and is accurate to +/- 0.01% according to the manufacturer.

The best method for calibrating the Kulites is to install the Kulite in the tunnel as if preparing for a run. Thus it can be calibrated while mounted in the probe. All calibrations are performed with the tunnel unheated. The tunnel should be closed without putting in a diaphragm. Rather than connecting the pressure transducer to the oscilloscope for data collection, the output from the amplification box is fed to the A/D converter. After the tunnel is sealed the program is started and the user is prompted for an output file, pressure increment at which to sample the A/D channels, and a stop pressure. The operator then pumps the tunnel down to the stop pressure using the vacuum pumps. During this process the program will take A/D samples at the given increment and output the Paroscientific pressure and the 4 voltages from the A/D channels to the output file. This file then contains the pressure/voltage calibration.

The program can also be run while filling the tunnel after a run. However it should be noted that at low pressures the air flow from the fill line seems to impact the transducer causing it to read a dynamic pressure associated with the flow caused by air filling the tunnel increasing the pressure. This is not the same pressure the Paroscientific is measuring since it is mounted in a static pressure port and is also upstream of the nozzle. This problem can be virtually eliminated by raising the pressure slowly (about 0.5 psi/min) up to about 6 psia.

2.5.2 Cold Wire Calibration

As mentioned above, the temperature of the flow is measured by applying a constant current across the wire and monitoring the voltage change due to changing resistance with temperature. There are two parameters that can be calibrated with temperature, each should give the same result. First, the resistance of the wire can be calibrated with temperature. The temperature coefficient (α) is obtained from the calibration, allowing temperature to be calculated from a voltage given the coefficient and a known current. The wire could also be directly calibrated by setting up the cold wire instrumentation system and measuring the output voltage at each temperature.

Since both methods of calibration were not difficult to set up both were used to calibrate the wire simultaneously. The wire was placed in the ASL oven and connected to a set of leads that exit the oven through a small hole. A reference temperature (measured with a thermocouple and temperature display), voltage output from the CCA, and resistance (measured with a precision multimeter) were recorded. The oven was turned on and set to a temperature. The temperature was monitored until it was steady for several minutes. After the temperature was stable, voltage and resistance measurements were taken. The wire was connected to the CCA and the voltage output recorded, and then the wire was connected directly to the multimeter to measure the resistance. This was repeated at several temperatures between 20 C and 200 C.

Once the calibration was complete the data could be plotted. The slope of the resistance vs. temperature line divided by the reference resistance is the resistance coefficient. This can then be substituted into the equations shown earlier to calculate temperature from a voltage. However it is important to note that a reference voltage output, temperature and resistance must be taken once the wire is operating in constant current mode. The reference voltage can be set to zero by adjusting a potentiometer on the CCA circuit. As long as the offset is not changed, only the one reference condition need be taken.

The voltage output can be plotted to give the direct relation between the voltage output and temperature. This relation is correct as long as the offset voltage in the CCA

does not change. If the offset changes, calibration would have to be repeated, unless the offset change is known. The slope of the curve is related back to the resistance coefficient, which tends to remain fairly constant.

2.5.3 Tunnel operation

Normal operation of the Purdue Ludwieg tube is fairly straightforward. A diaphragm is inserted between the driver and driven sections. Once the tunnel is closed the vacuum pumps are turned on to evacuate the driven section. This process takes approximately 15 minutes. For an atmospheric driver pressure run, final instrumentation checks are performed, tunnel conditions are recorded and the tunnel is fired. The diaphragm is broken by using the breaker device described in Schneider *et al.* (1996). The tunnel runs for about 5 seconds. At the end of the run the pressure in the tunnel is about 1.5 psia. A valve (valve #1 in figure 14) in the fill line of the tunnel is opened and the tunnel refills. This takes approximately 10 to 15 minutes depending on the fill rate. The rate is not particularly important unless instrumentation is being calibrated. Once the tunnel reaches atmospheric pressure it can be opened and a new diaphragm inserted. From here the process starts over again. The average time lapse for the entire process is about 45 minutes to 1 hour if the operator is able to make runs without delays (this does not include time to evaluate any data or make major changes in the instrumentation set-up).

When making runs at driver pressures either above or below atmospheric the procedure changes slightly. If a run is to be made with driver pressure below atmospheric, during the pump down a valve (valve #2 in figure 14) can be opened in a line that connects the driver and driven sections. Thus the driver section can be pumped down to the desired pressure by opening the valve until the pressure is reached. Operating the tunnel at higher than atmospheric driver pressures is similar. After the pump down is complete (if it is done during pump down the diaphragm tends to break early) the fill line valve (valve #1 in figure 14) can be opened which will force air from the supply tanks into the driver section.

Once the desired driver pressure is reached, the valve is closed, and normal run procedures take over. For a more detailed step by step procedure for running the Ludwieg tube see appendix A.

Diaphragm thickness is also important to a successful run. The usual thickness for atmospheric runs was 0.007 inches. This thickness was used for runs between 8 and 20 psia initial driver pressure. There were no major problems encountered at the higher end of this range; however, for some of the higher runs (above about 18 psia) 0.010 inch diaphragm thickness was chosen. This was done to make sure an early break did not occur. 0.010 inch thickness was used to pressures as low as 14.5 or so, but this is not recommended since 0.007 inch breaks much more consistently at this pressure. The 0.010 inch thick diaphragms are best used above 18 psia. There were some problems with using 0.007 inch down at the lower pressures (below about 10 psia). These runs had slow or poor breaks of the diaphragm, which sometimes resulted in adverse affects on the noise level of the run. Perhaps a thinner diaphragm would work more effectively here, but only a few runs were made at the lower pressures, and thus resulted in little experience with thinner diaphragms.

2.5.3.1 Tunnel operation with heat

Running with the tunnel "hot" does not alter the procedure significantly. There are only one or two changes. After a run the tunnel pressure is well below atmospheric. Thus, to open the tunnel, it must be refilled with supply air. The tunnel is filled as described above, except that the circulation heater needs to be turned on to the desired temperature (refer to Appendix A for details). It is recommended that air be flowing through the heater before it is turned on. It is a simple process, just after opening the fill valve (valve #1 in figure 14), the heater is turned on, and just prior to closing the fill valve the heater is turned off. The small amounts of time where the heater is off are insignificant when considering that only a small amount of air passes into the tunnel unheated. In fact,

this only occurs when turning the heater on since the heater takes some time to cool after being turned off.

When running the tunnel with low driver pressures there is no change in the procedure other than filling the tunnel. The operator should be aware however that decreasing the driver pressure causes the hot air in the driver section to flow back through the fill line to the junction with the vacuum line (see figure 14). If a large amount of air is drawn back through, the original particle filter could be damaged.

Above-atmospheric-pressure runs have an extra step. In addition to turning on the circulation heater for re-filling the tunnel it must also be turned on to increase the pressure to the desired level (refer to Appendix A for a detailed procedure). This is not such an easy task since the pressure valve and the circulation heater are located at different ends of the tunnel. Because of this difficulty runs were performed using the heater to raise the pressure and also by raising the pressure without turning on the heater. It seems that at pressures slightly above atmospheric there is little need to turn on the heater to raise the pressure. This is probably because there is a small amount of air being added and if it is fairly soon after filling, the circulation heater is still hot.

2.5.4 Heater operation

As mentioned above the heater has two main parts, the main heater and the pre-heater. The pre-heater consists of the circulation heater and the high temperature filter. The circulation heater is only used when filling the tunnel or adding air to the driver tube. It is recommended that air be flowing through the heater at all times while it is on. It is turned on by simply turning the thermostat to the desired temperature.

The main heater system is a bit more complex. The main heater consists of the flange heater and the driver heater. The driver heater is turned on by turning on power to the control panel that houses the controller and temperature displays. The power supply should also be turned on with the current limiters set appropriately (usually maximum voltage and maximum current for starting since most of the power supply's power is used

to heat initially). The power should be slowly increased at the controller starting at about 20% power (to operate the controller see the manual or Appendix A) and increasing 20% every 5 minutes or so until the heater wire is up to about 100 C. Precise timing of increases is not required. The important element is that the wire be given time to settle at a temperature. This can be done by monitoring the temperature of the wire. The power increments can be easily done since the controller has a manual setting that allows the user to manually control the power from 4-100% total power. The process usually takes about 30 minutes. This is very important. The resistance of the wire will increase 50% in this time. If full power is applied without the wire heated, the wire can be damaged, or even melted. Once the wire is sufficiently heated, the controller can be set to automatic mode for the desired temperature.

The controller will monitor one of several thermocouples (via a switch) and output the percentage of power needed by the supply to reach and maintain the desired temperature. Typically for initial heating, it is best to monitor station 1. This makes sure that all parts of the tube are heated to the desired temperature, since it is the slowest to heat. Usually the system is started in the evening the day before scheduled runs and allowed to heat overnight. This allows 4 or so hours for heating and plenty of time for any temperature non-uniformities to settle out.

The flange heater should be turned on at the same time as the driver heater. Although no problems have been encountered with heating the element too fast, it is probably wise to slowly increase its power as well. Usually about 30% to 40% (30 volts, 20 Amps) power is needed to heat the flange area to 100 C (details can be found in Appendix A). Typically with the higher temperatures, more power is required to keep the flange area at the desired temperature. The heater is controlled manually and should be checked occasionally to make sure the temperatures are in the desired range.

The system can be turned off by simply turning off the power of the power supplies. However it is recommended that the driver tube system be turned off by switching the controller into "park" mode and then shutting off the power supply. "Park" mode should turn the power to zero at the supply. Putting the controller in "park"

prevents the controller from trying to immediately achieve temperature once the power is turned back on. One must also remember that the flange heater is completely independent of the driver heater and must be controlled and turned off manually.

Table 1: Thermocouple Locations

TC Name	Dist. upstream of First flange, ft	Angle * deg	Wired to Switch #	Switch Channel	Connected to Controller?
Station 1					
1	0	0	1	1	No
2	0	60	1	2	No
3	0	120	1	3	No
4	0	180	1	4	No
5	0	240	1	5	No
6	0	330	5	1	Yes
Station 2					
1	3	0	2	1	No
2	3	60	2	2	No
3	3	120	2	3	No
4	3	180	2	4	No
5	3	240	2	5	No
6	3	330	5	2	Yes
Station 3					
1	6	0	3	1	No
2	6	90	3	2	No
3	6	180	3	3	No
4	6	270	5	3	Yes
Station 4					
1	9.5	0	3	5	No
2	9.5	90	3	6	No
3	9.5	180	3	7	No
4	9.5	270	3	8	No
Station 5					
1	12	0	4	8	No
2	12	90	XX	XX	No
3	12	180	XX	XX	No
4	12	270	XX	XX	No
Station 6					
1	18	0	XX	XX	No
2	18	90	XX	XX	No
3	18	180	XX	XX	No
4	18	270	XX	XX	No
Other Thermocouples not at a station					
	Ref. Location	Description			
Nozzle	z=9.25 in.		4	2	No
Flange	Flange	Heater element	4	1	No
Wire	7 ft upstream	Heater wire	display 5	XX	No

* Angle 0-359 deg, 0 top of tube, increasing clockwise if facing upstream

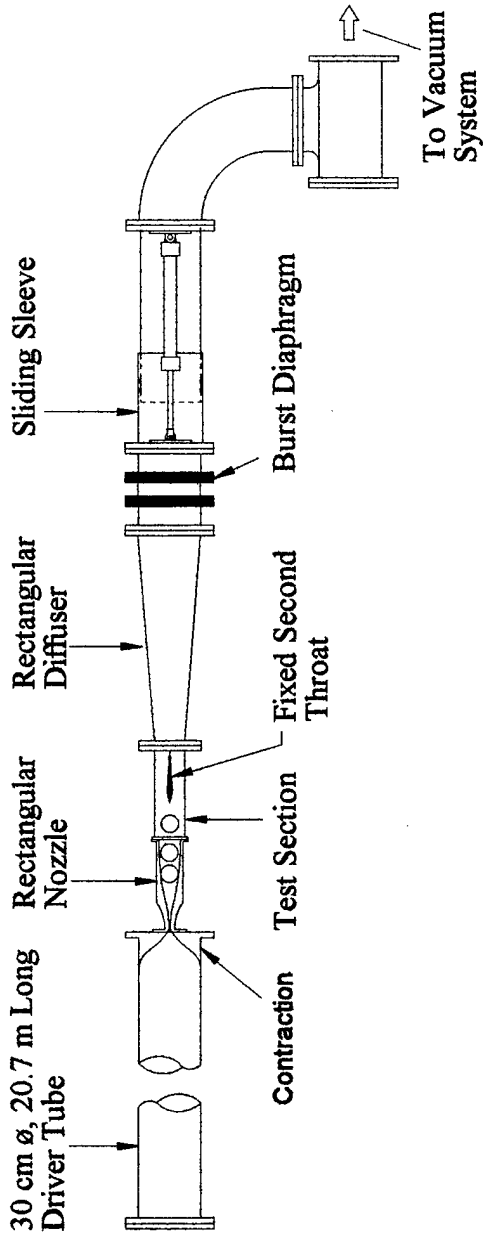

Figure 11 Purdue Ludwieg Tube Schematic

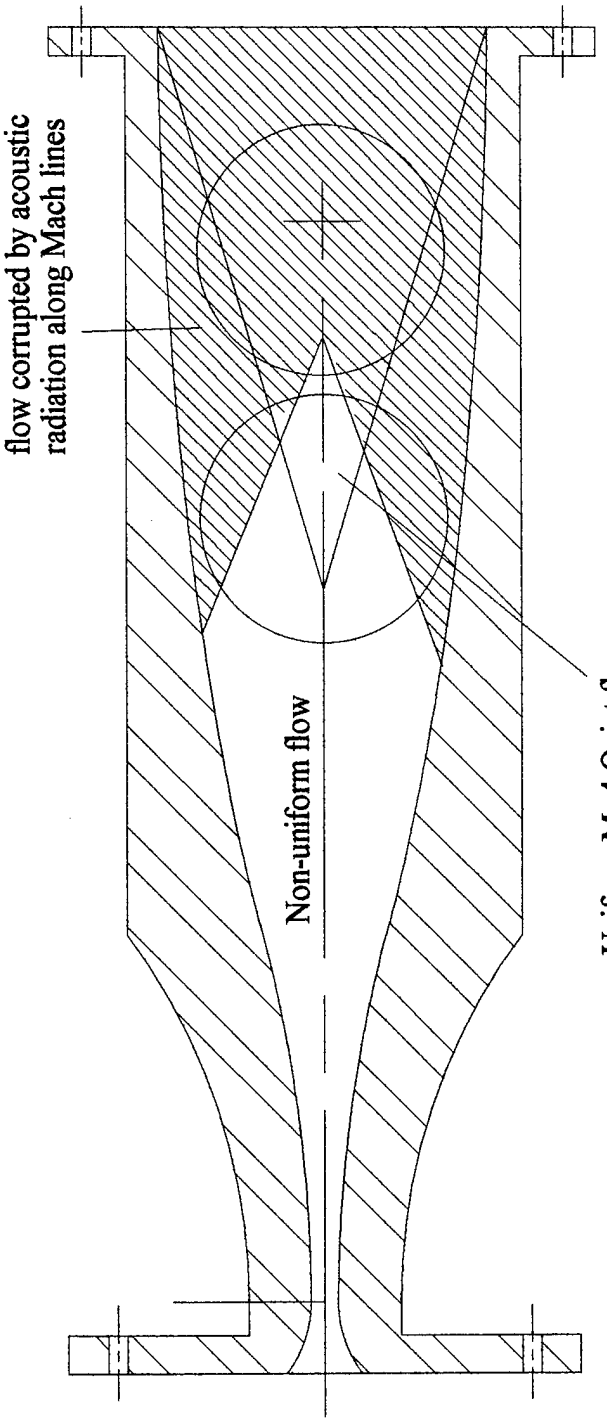

Figure 12 Quiet Flow Region

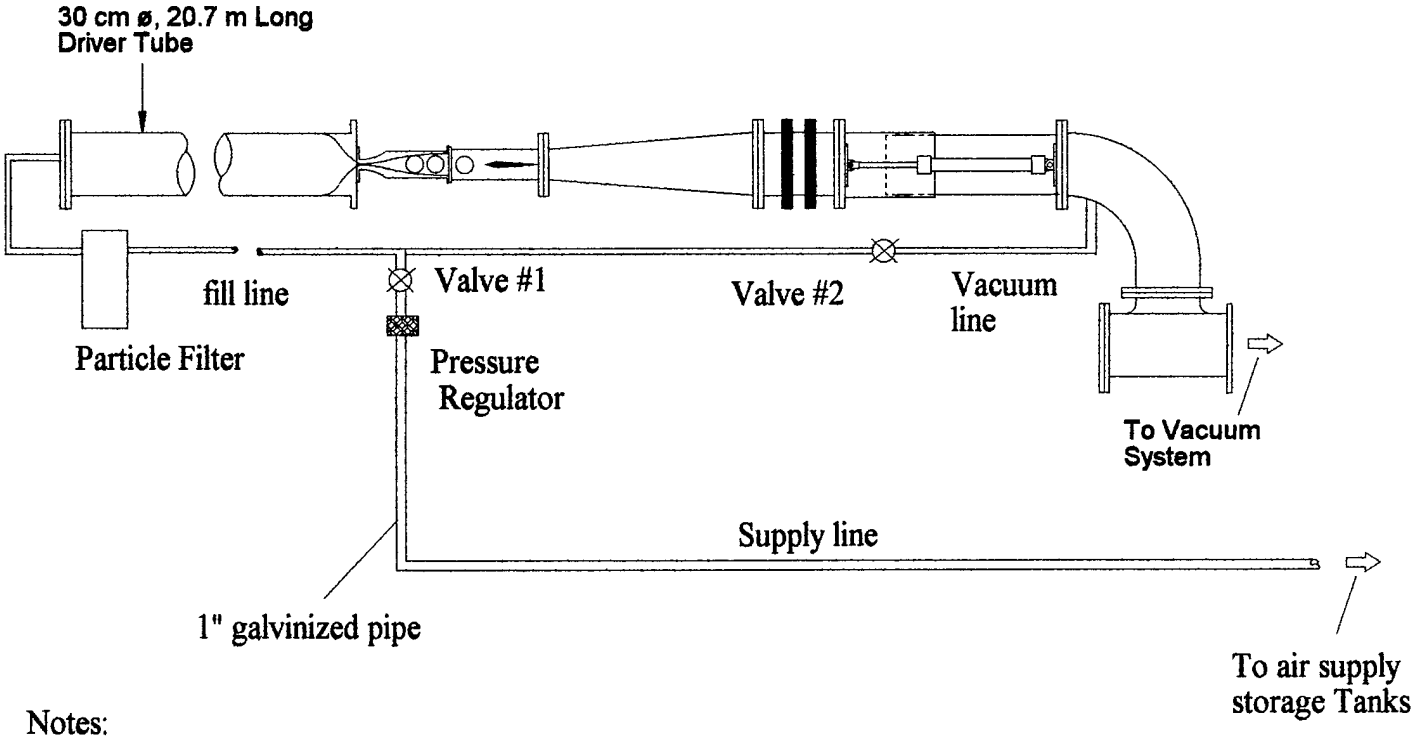

Notes:

To increase pressure in tunnel, open valve #1, set pressure regulator and make sure valve #2 is closed

To lower pressure in tunnel (when diaphragm is in place),
Vacuum side must be at low pressure or vacuum pump must be on
Open valve #2, make sure valve 1 is closed

Figure 13 Original Fill Line Plumbing Schematic

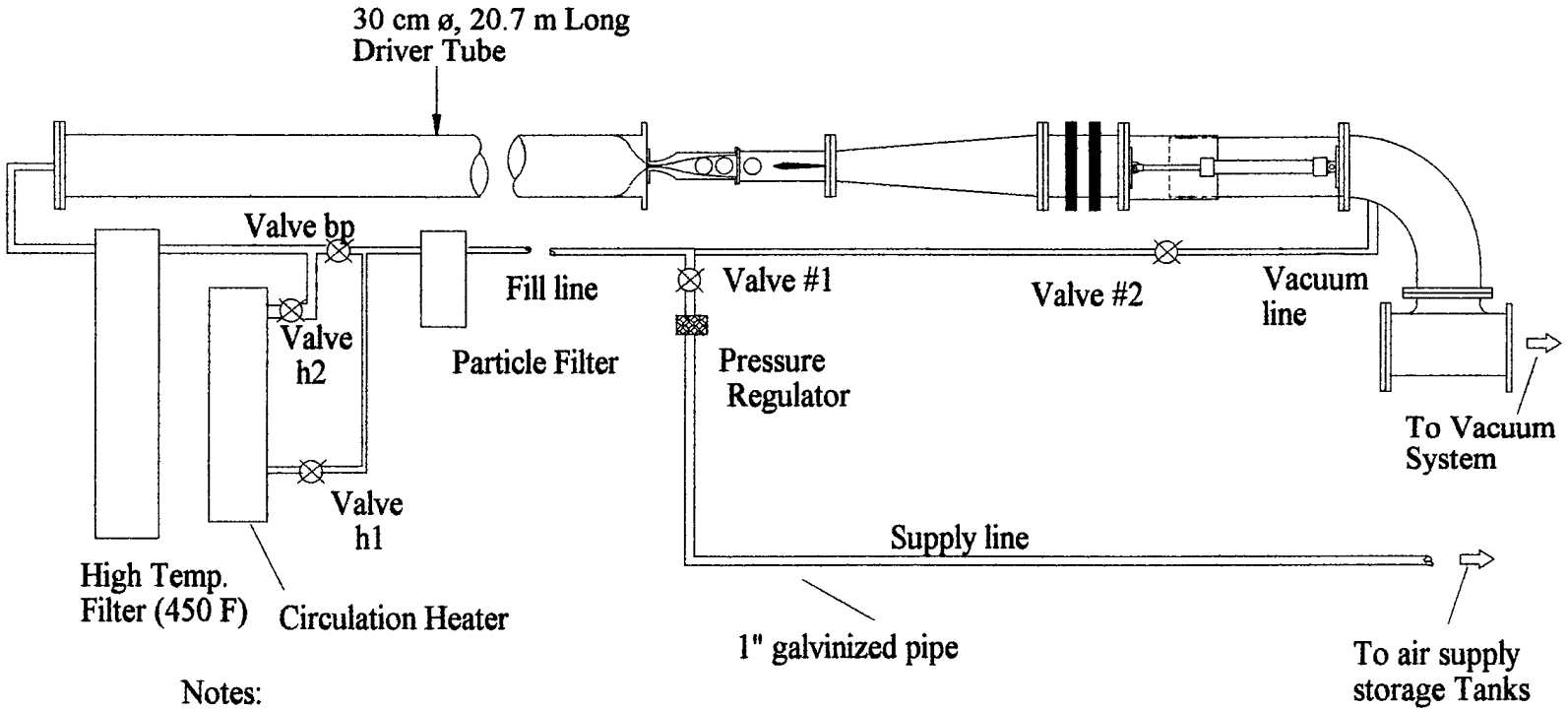

Notes:

When performing heated runs, valves h1 and h2 must be open, valve bp must be closed.
Unheated runs can be performed in either of two configurations:

1. Valve bp open, valves h1, h2 closed (by-pass configuration)
2. Valves h1, h2 open, valve bp closed (heater configuration)

This forces the air either through the circulation heater or the by-pass line.
Unheated runs can be performed in the heated, it is recommended to use the by-pass line.
Never operate circulation heater in by-pass configuration

Figure 14 Modified Fill Line Plumbing Schematic

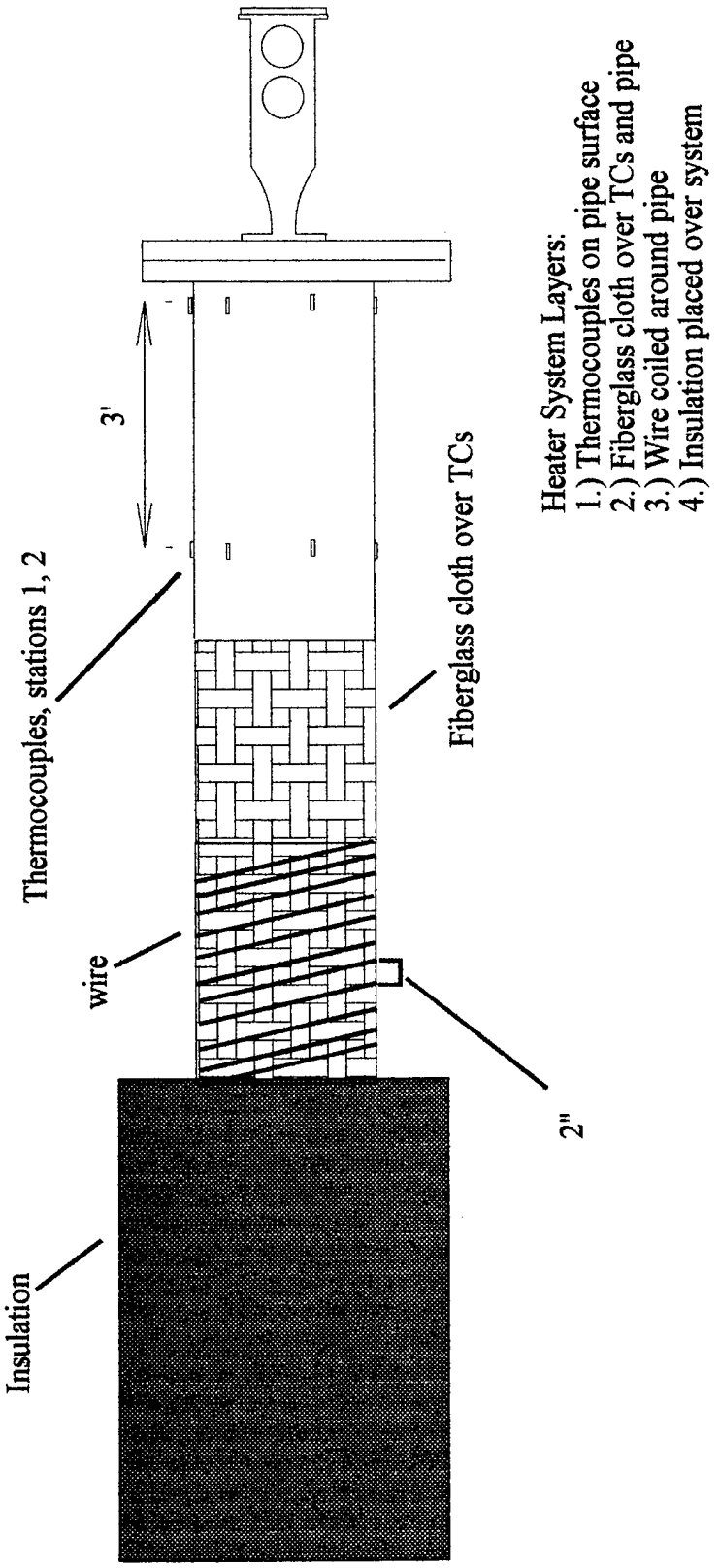

Figure 15 Main Heater System

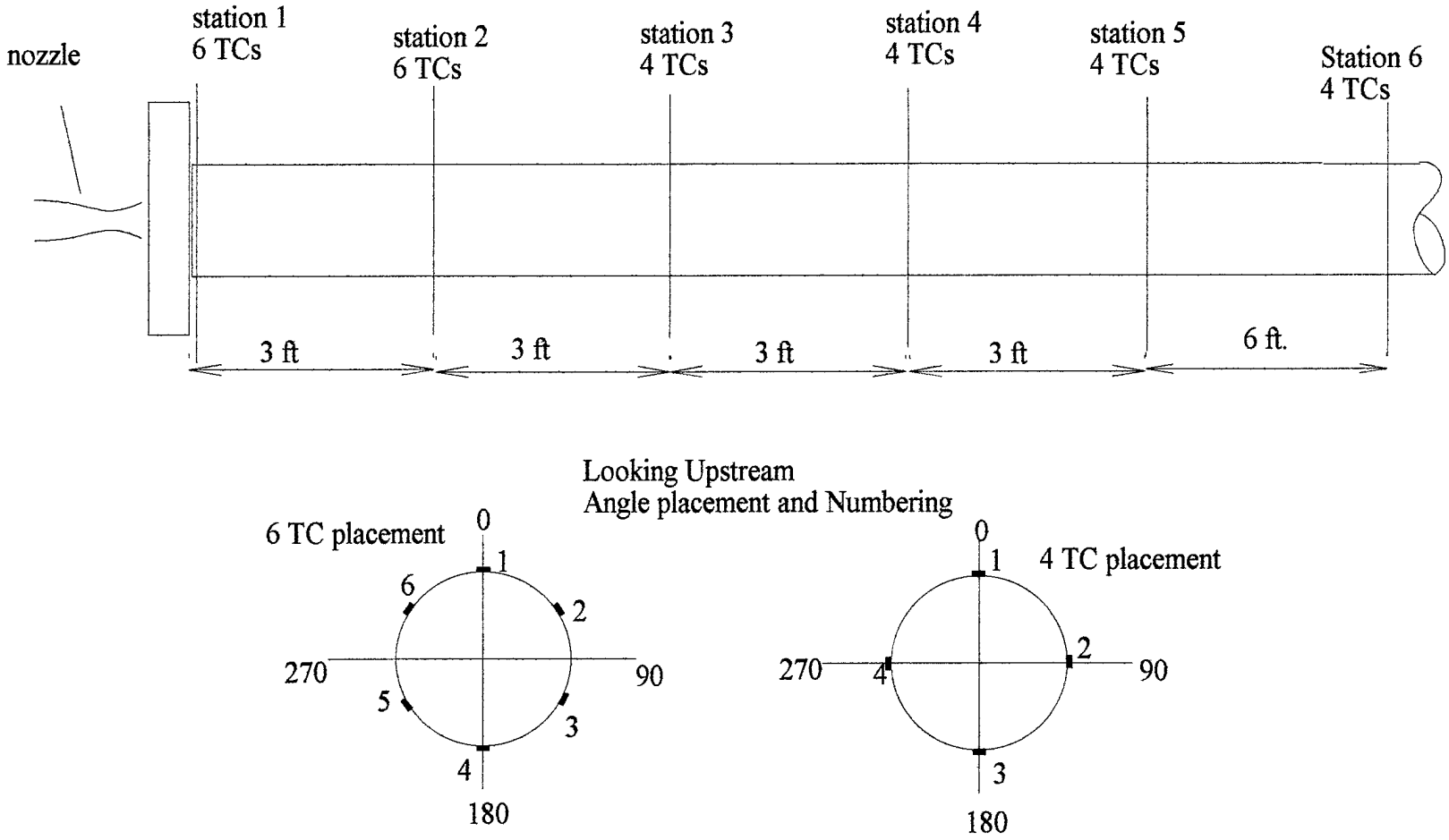

Figure 16 Thermocouple Placement

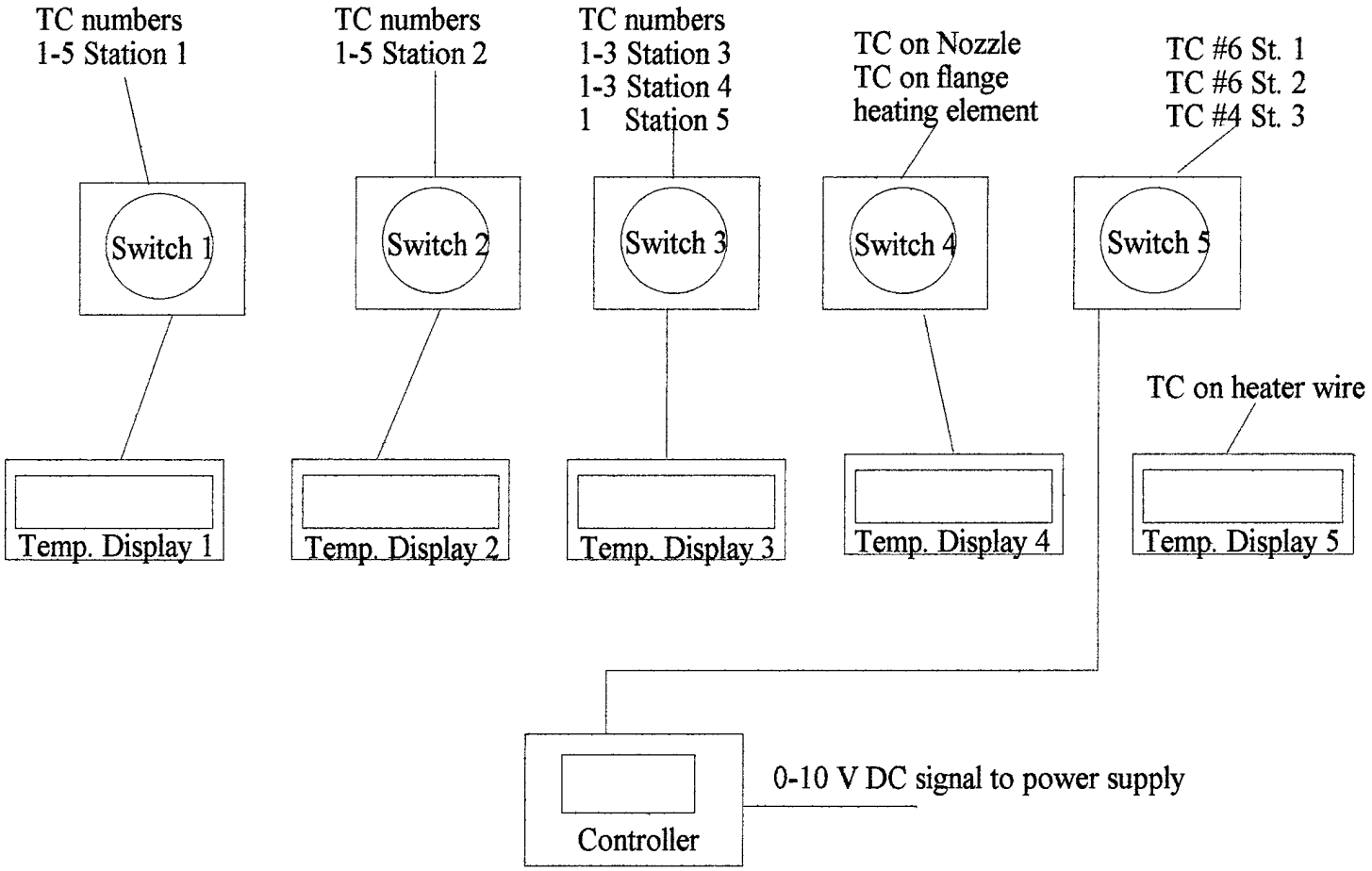

Figure 17 Thermocouple Wiring Schematic

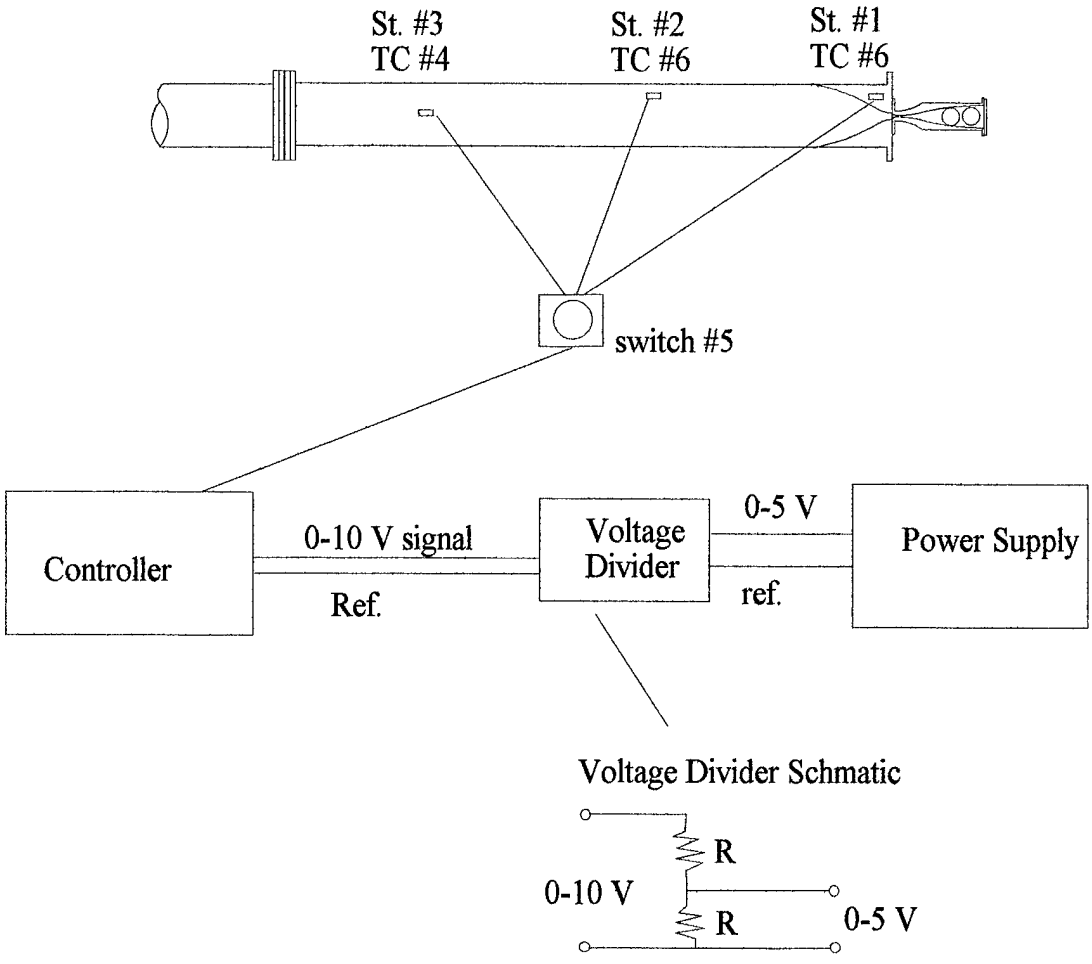

Figure 18 Schematic of Controller Output

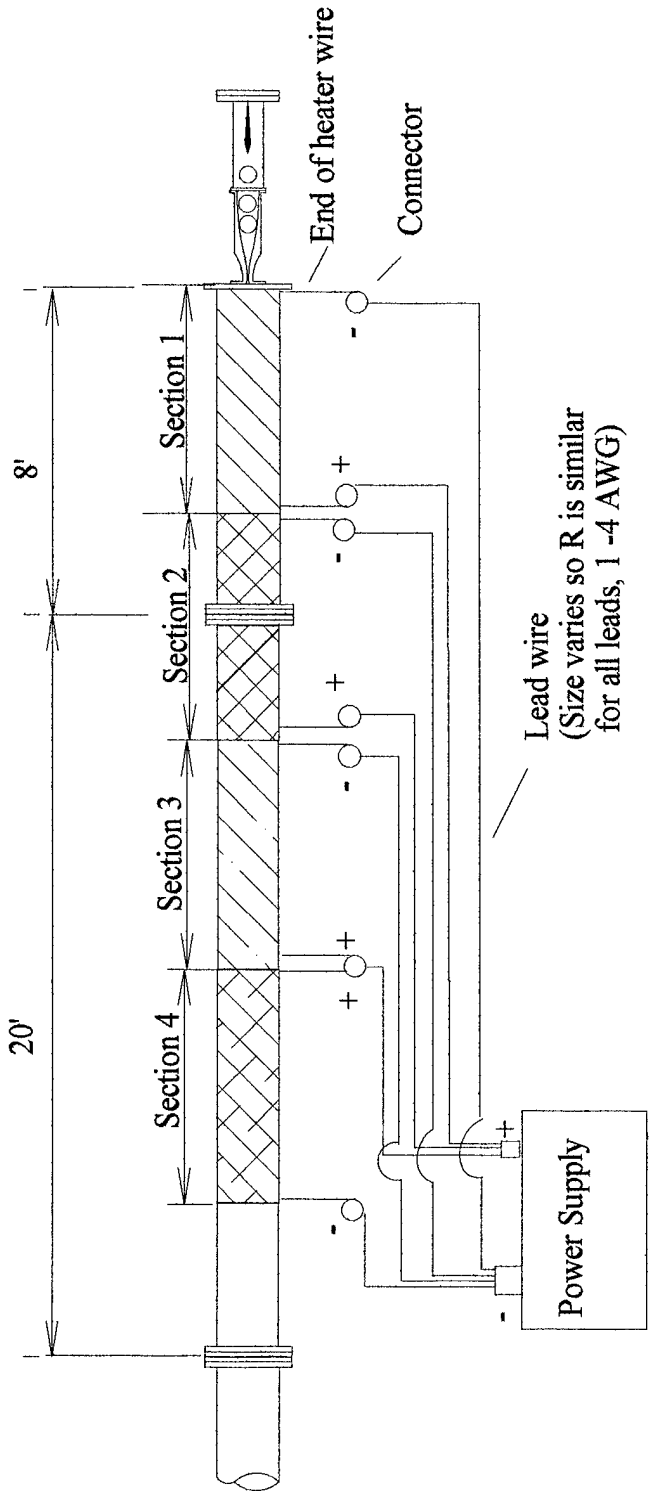

Figure 19 Heater Wiring Schematic

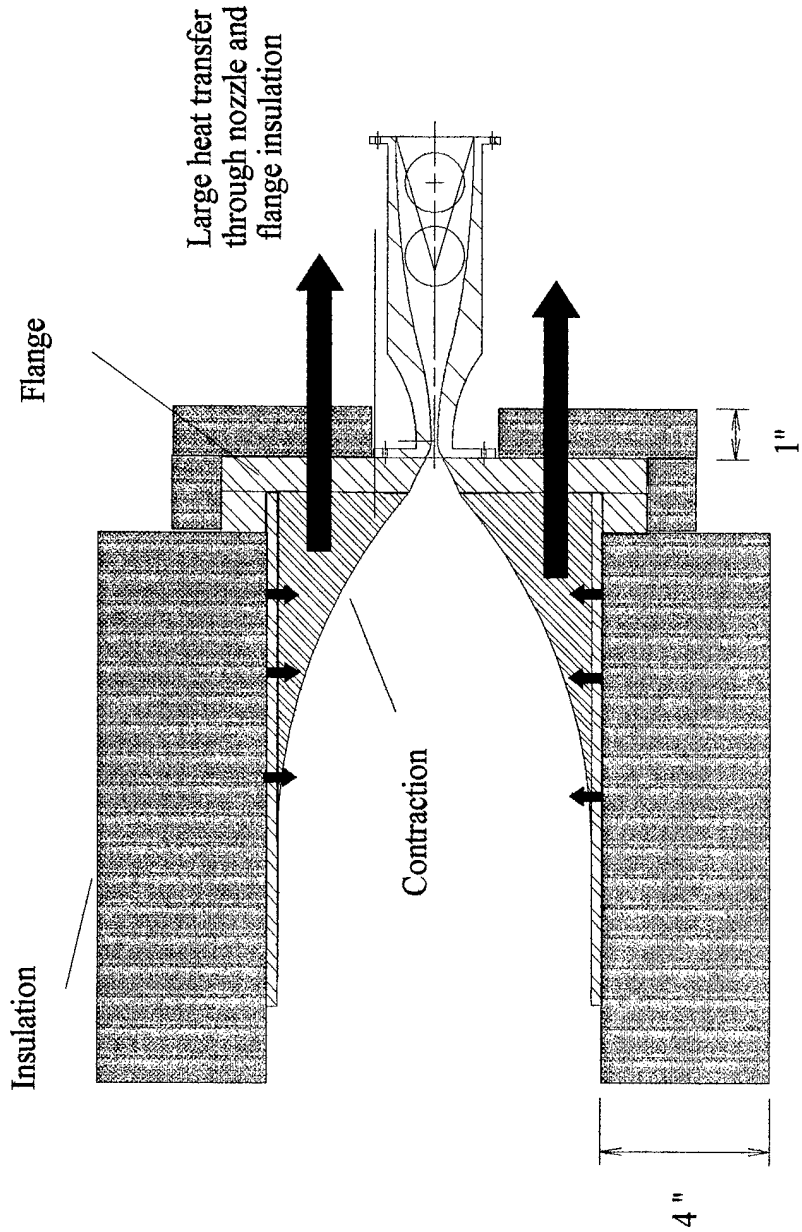

Figure 20 Diagram of Heat Loss at Flange

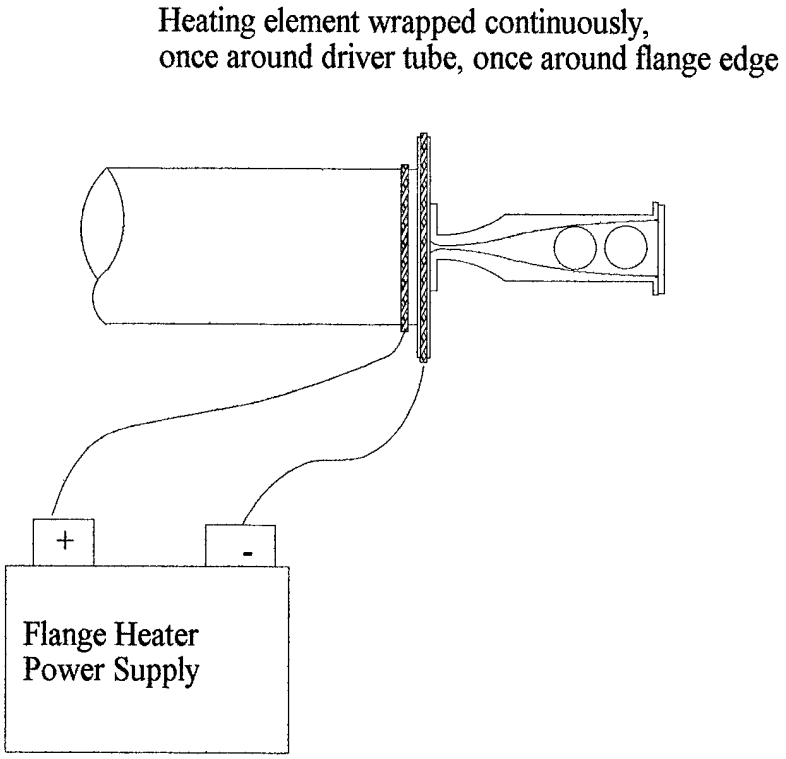

Figure 21 Flange Heater Schematic

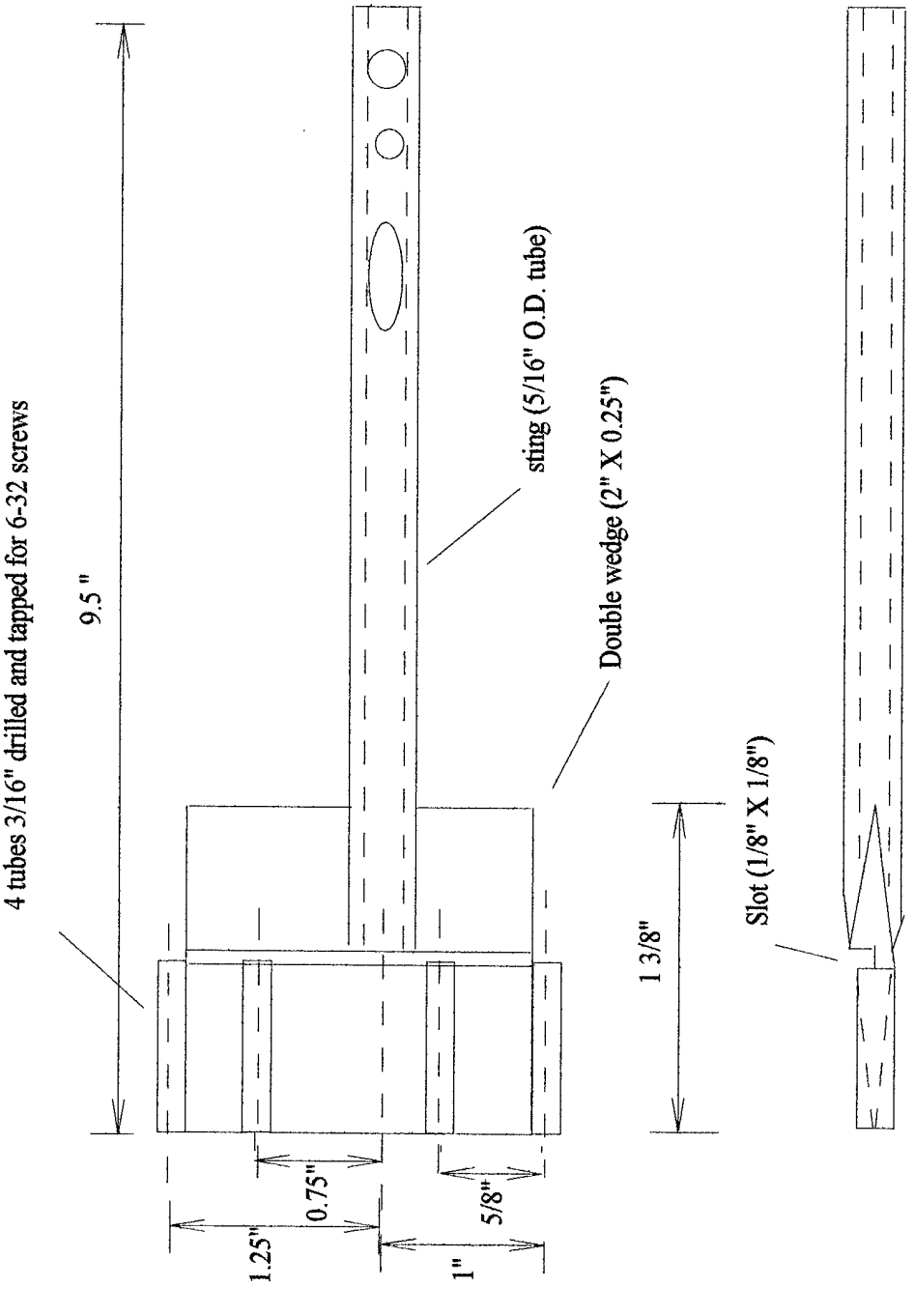

Figure 22 Kulite Pressure Rake

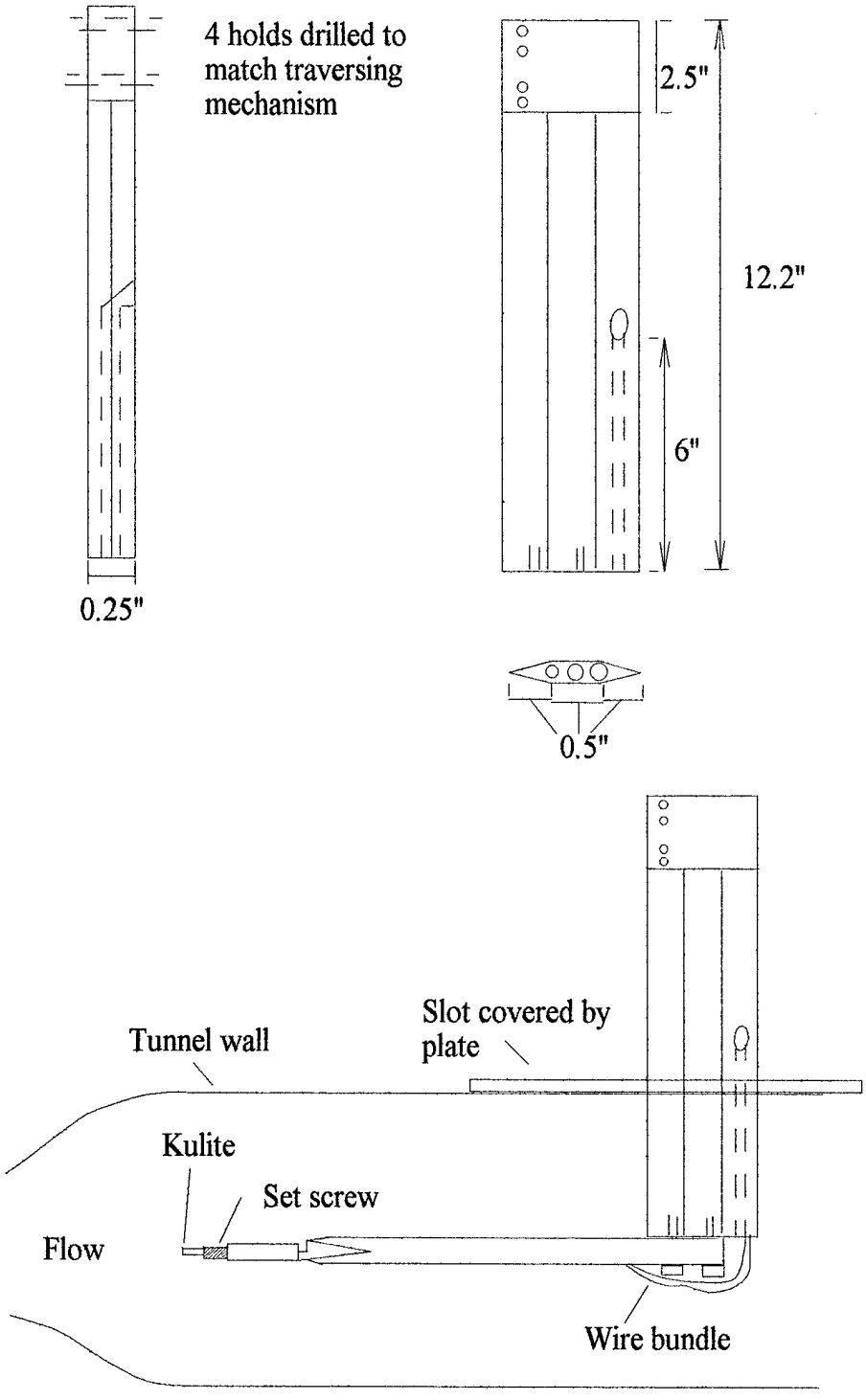

Figure 23 Pressure Rake Traverse and Tunnel Positioning

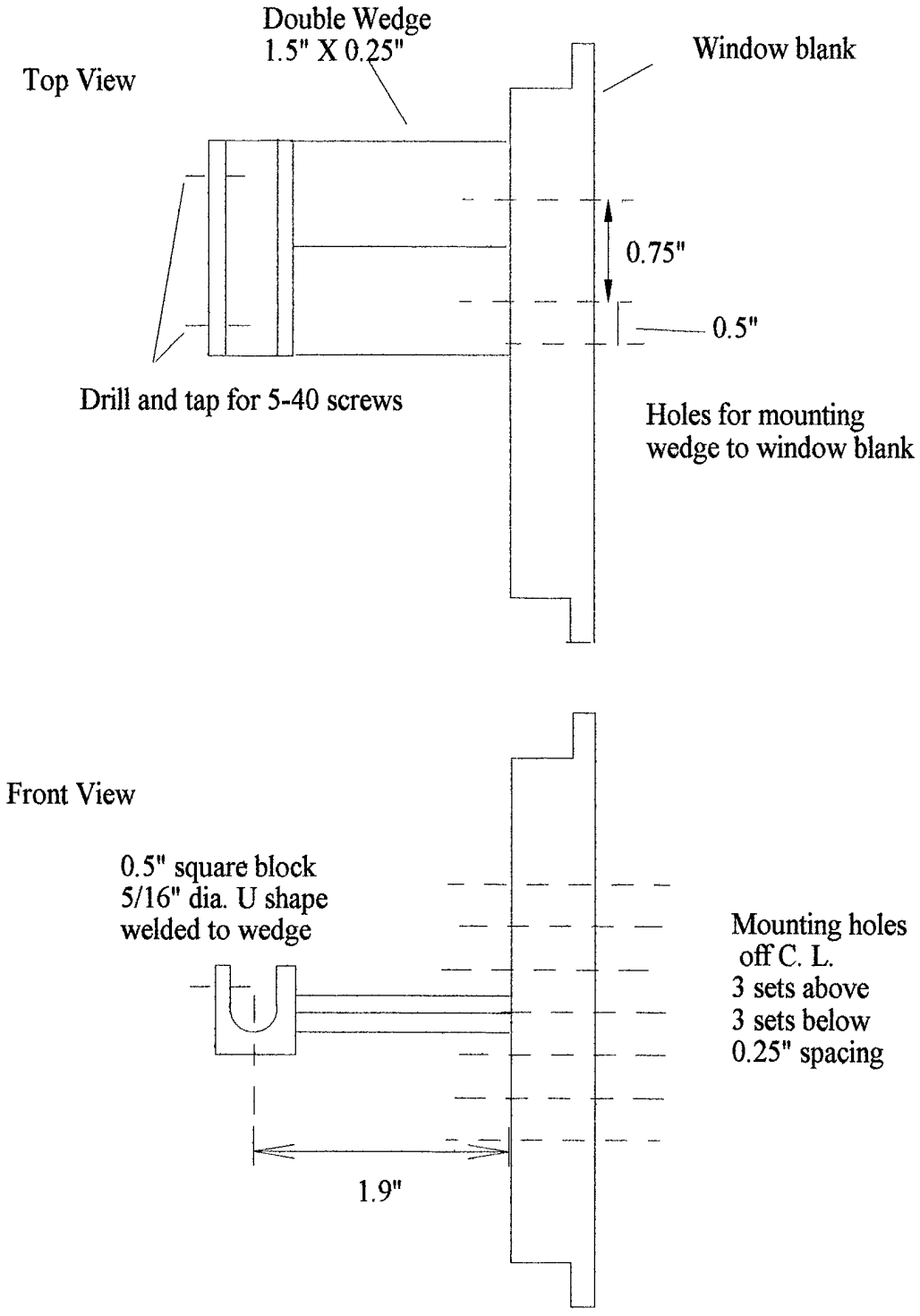

Figure 24 Kulite Pressure Rake Window Support

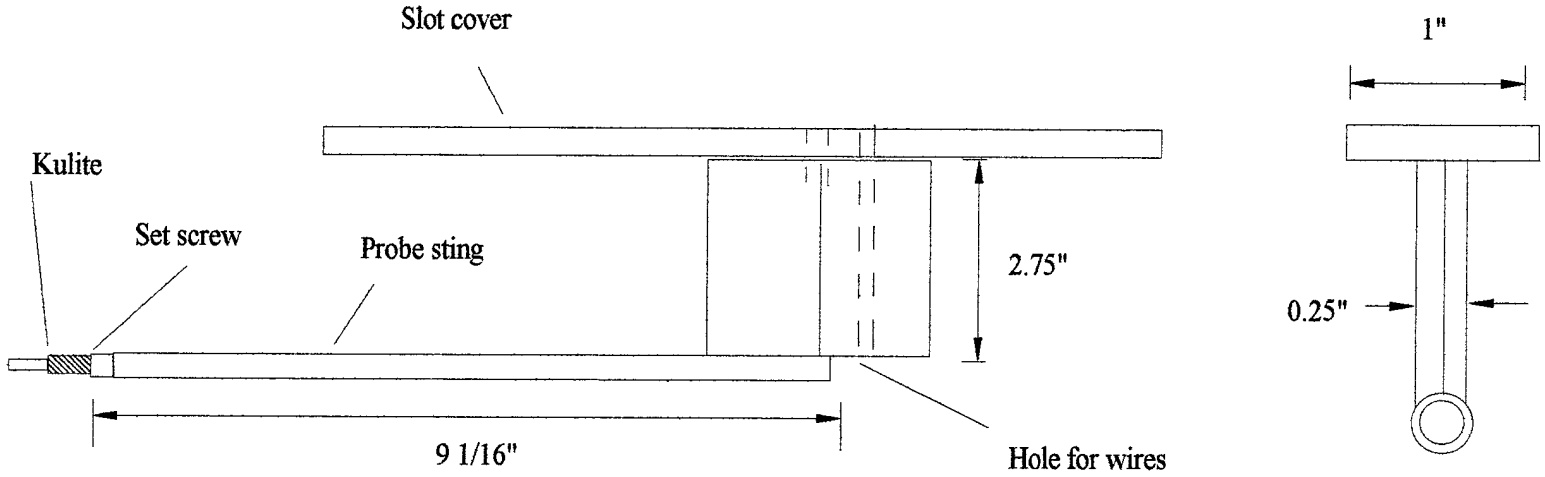

Figure 25 Single Kulite Pressure Probe

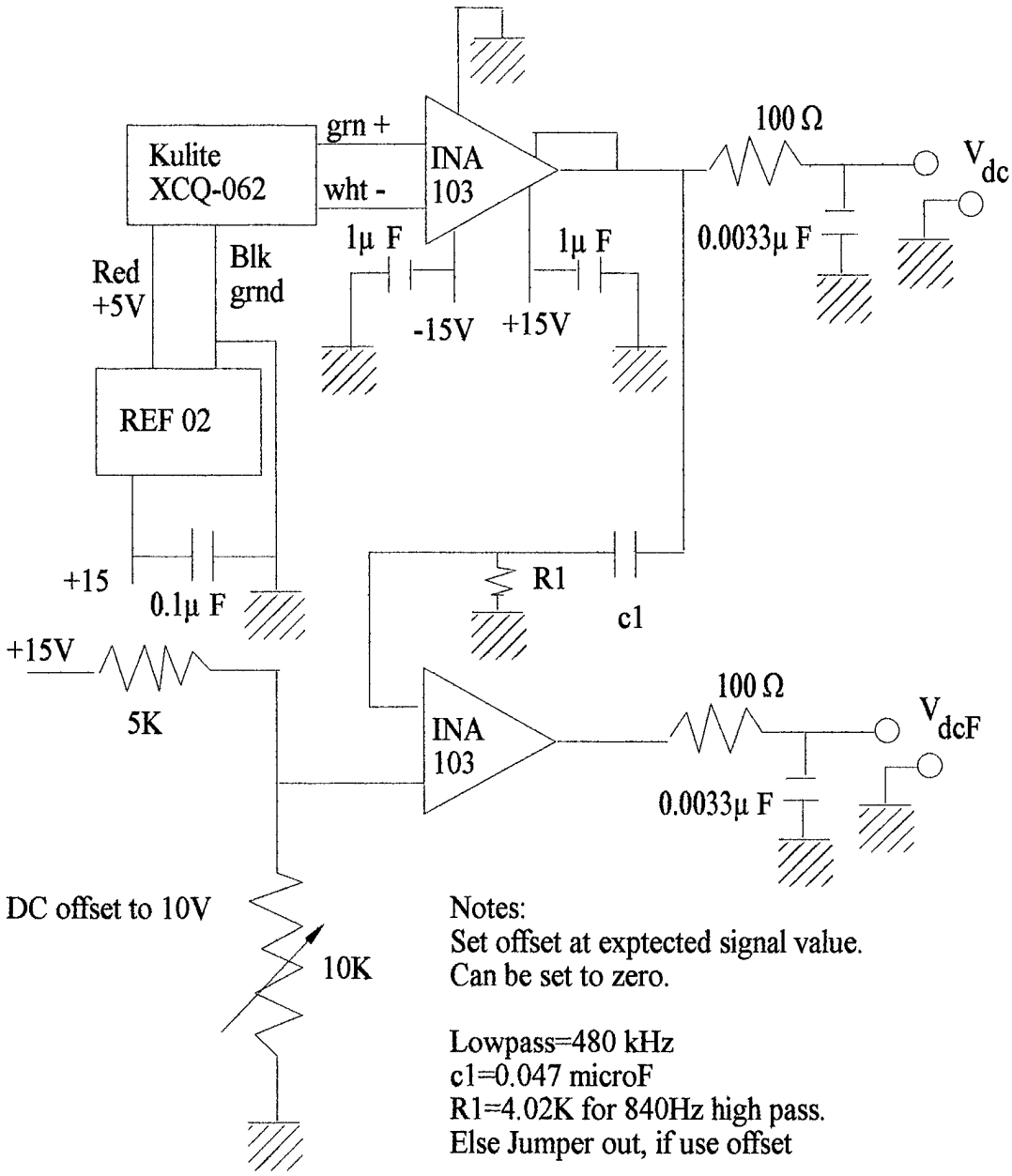

Figure 26 Kulite Amplifier Box Schematic

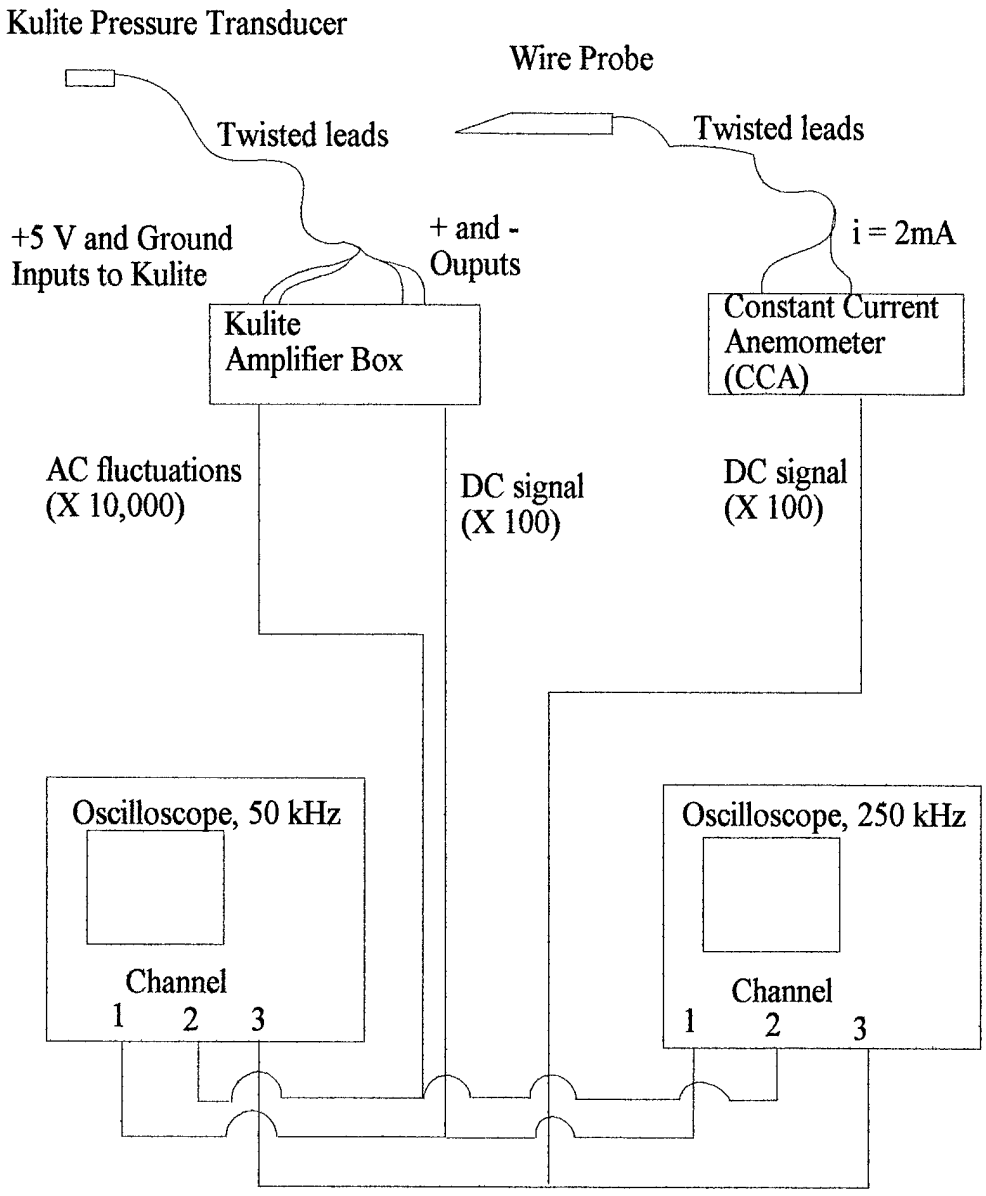

Figure 27 Instrumentation Set-up

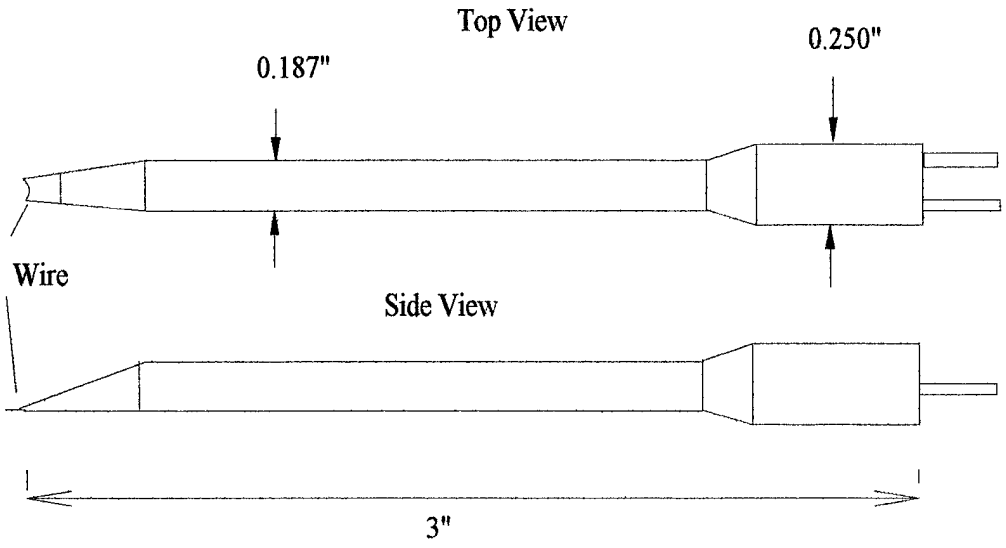

Cold Wire Mounted in Window Support

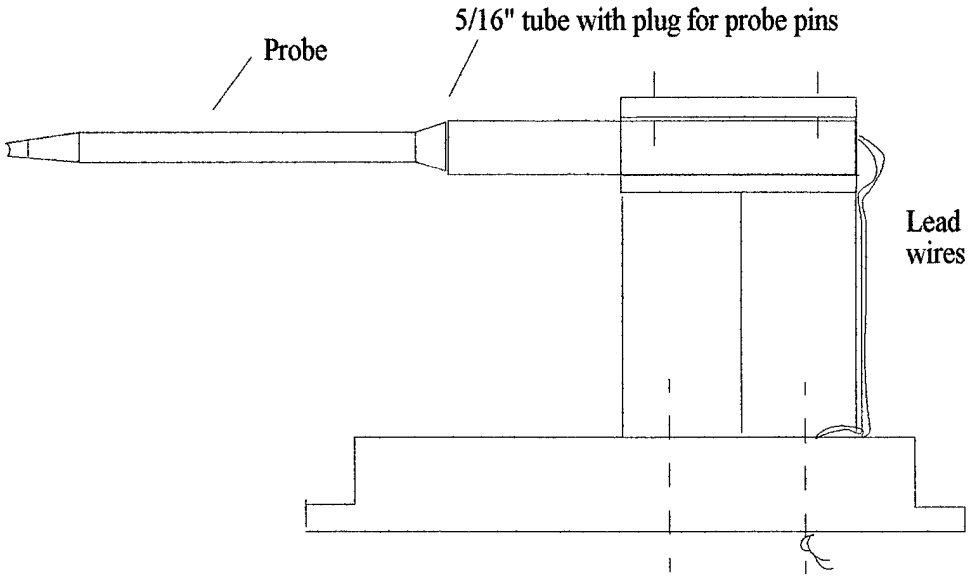

Figure 28 Wire probe and Window Mount

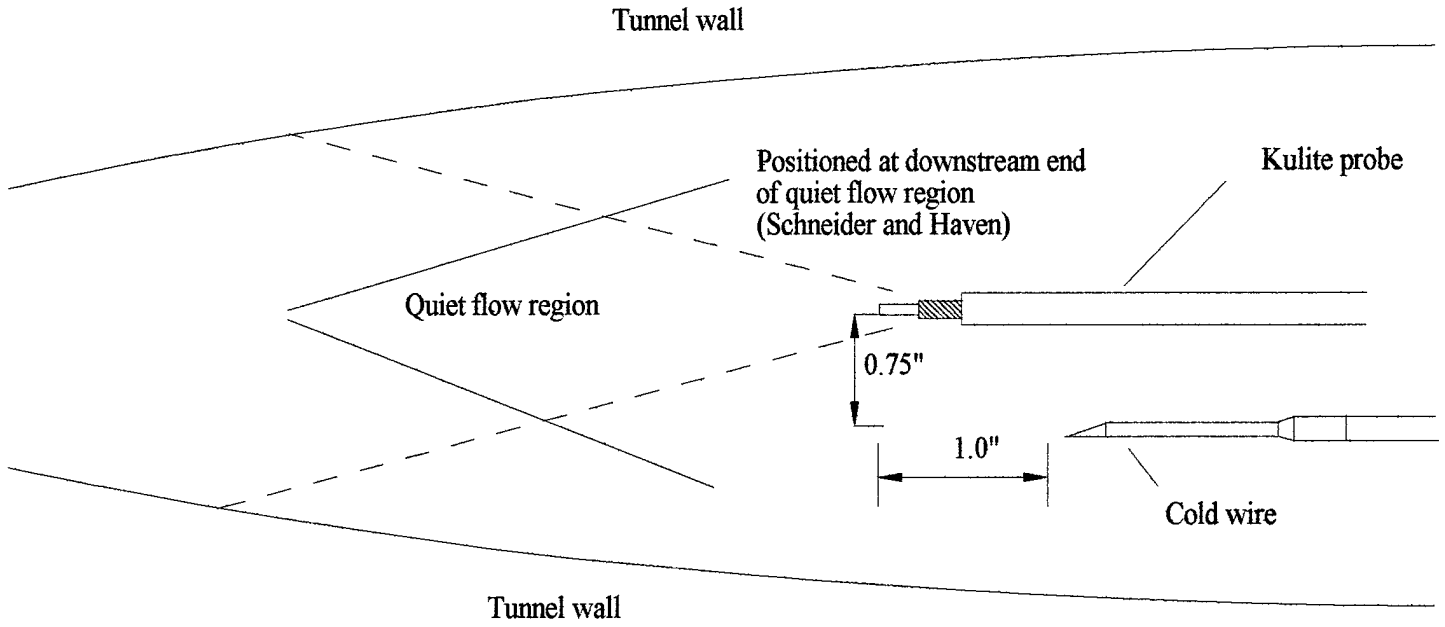

Figure 29 Position of Kulite and Cold Wire Probe

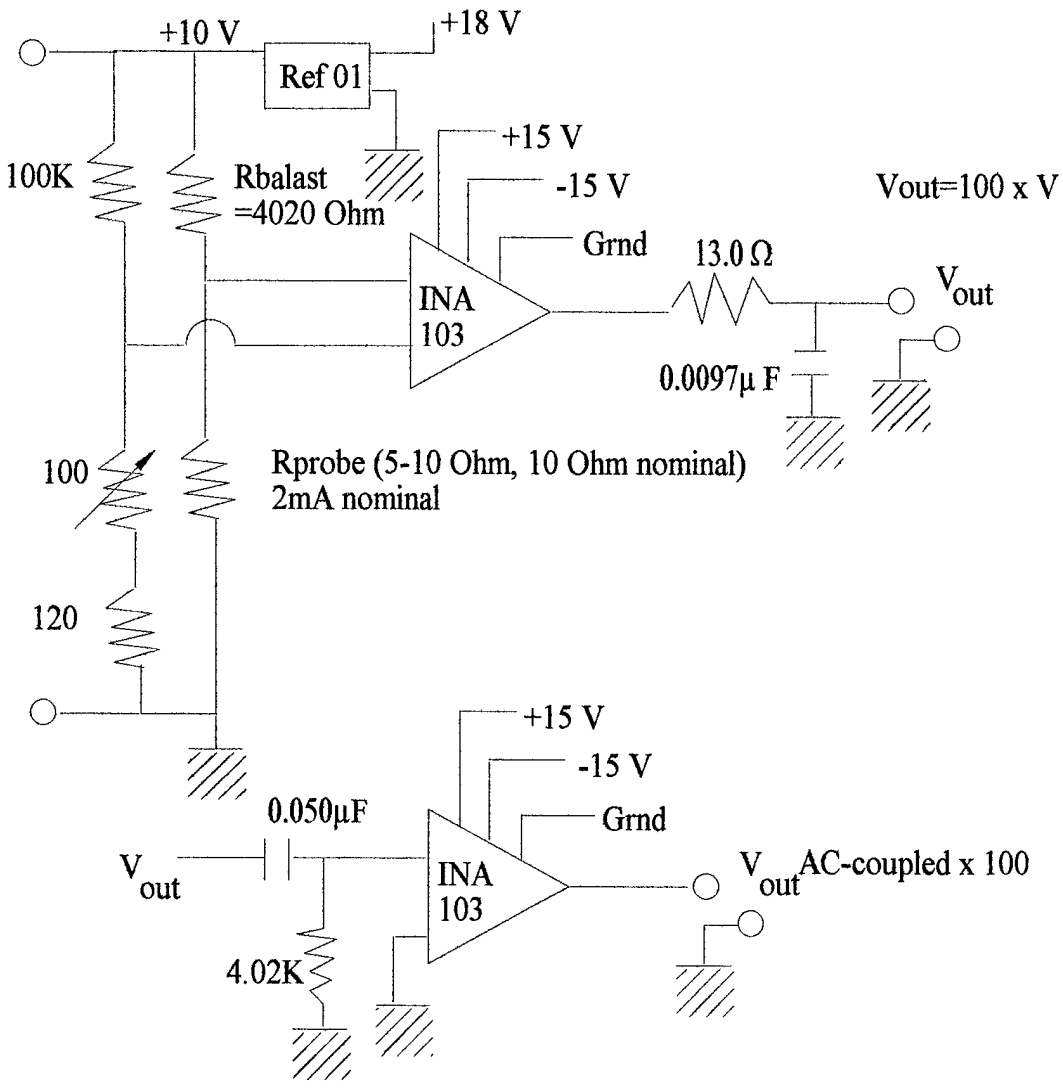

Figure 30 Constant Current Anemometer Schematic

CHAPTER 3 EXPERIMENTAL RESULTS AND DISCUSSION

3.1 Heating System Tests

Before the flow could be studied it was important to evaluate the ability of the heating system to reach and maintain the appropriate air temperature. Initial tests were performed to see if the heater could uniformly achieve temperature in a reasonable amount of time. The main heater system was started at t=0 and temperatures were recorded manually from the thermocouple displays (Figure 31). These tests indicated that most of the pipe could be heated to 100 C in about 5 hours. It was noticed that the nozzle and flange area were large heat sinks. The temperature after 7 hours at station 1 did not increase above 70 C. It was obvious that more heat would have to be added at the nozzle and flange area to boost the temperature of the most downstream portions of the driver tube. The extra flange heater was added to supply the extra power needed to increase the temperature further. The extra heater on the flange/nozzle junction significantly improved the heating results. The entire heated section of tunnel reached a uniform temperature of 100 C to within 10 C, within 5 hours (Figure 32).

The temperature around the circumference of the pipe was within 10 C at any given station (within 5 C at the lower temperatures), with the exception of 1 or 2 thermocouples at each station that were affected by the heat of the nearby heater wire. They showed significantly higher temperatures than the rest of the thermocouples at any given time when the heater system was operating. Once the heater was turned off, these thermocouples quickly settled to within 2 or 3 degrees of the rest of the thermocouples. The thermocouples affected by the heater wire were noted, and not used in determining average temperatures at each station. Figures 33-36 show the indicated thermocouple

temperatures at each station for each of the 4 desired temperatures. Each symbol represents one thermocouple. The temperature of a thermocouple varied little from run to run; at most +/- 2 C. Often there was no change in the temperature within the limits of the display (+/- 0.5 C). Thus, to prevent clutter on the plot the average temperature over all the runs at a particular heater setting is plotted. These plots show the thermocouples influenced by the heater wire. At the lower desired temperatures, the temperatures around the circumference were usually within 5 degrees C (with the exception of those obviously influenced by the heater wire). However, at the higher desired temperatures, the thermocouples show more and more variation around the circumference (as high as 15 C in figure 36). There was no systematic variation of temperature with the angle around the circumference when two different stations were compared. However, at any particular station, the temperature variation between thermocouples was the same. This was true from run to run, and even for different desired temperatures. For example, at station 1, thermocouple 1 always sensed a slightly lower temperature than thermocouple 2. The temperature variation is probably caused by the influence of the heater wire on the thermocouples.

This possibility is supported by observations made during the course of the experiment. At the lower desired temperatures (100 C, 125 C) the heating system did not have to use much power to maintain the desired temperature once reached. This was noted in two ways, first by noting the heater wire temperature, and second by noting the power output of the power supply. In the 100 C experiments, heater wire temperature was typically about 115 C (measured using a custom ungrounded thermocouple placed on the wire). The power supply also used little power to maintain the temperature. Often the power was nearly off to the heater for minutes at a time. When it was on, it was only using up to about 20% of its total power.

However, in the 180 C desired temperature case, the heater wire temperature was typically noted to be about 210 C (wire temperature was recorded prior to each run). The higher the temperature difference between the pipe and the wire, the more a thermocouple

is going to show some influence from the wire. Station 1 is affected by the flange heater which was as hot as 350 C. It was set at maximum power during the entire test at 180 C.

Although these observations support an influence from the heater wire as the main problem with uniform temperature around the circumference, it is confirmed by observing the temperatures when the heater was turned off after completing the experiment. After the heaters were turned off, the thermocouples that were reading higher temperatures began to decrease in temperature quickly. This could mean two things: (1) the thermocouple is decreasing in temperature because the wire influence is no longer present or (2) the tunnel is non-uniformly heated and the temperature is settling out. However, if the second possibility is occurring, the other thermocouples should increase in temperature as the heat from the higher temperature areas spreads out. This was not seen. Thus it was assumed that the variant thermocouples were influenced by the heating elements and decreased to the actual pipe temperature once the heat was turned off.

Even if the thermocouples heavily influenced by the heater wire are eliminated from the temperature statistics there are still some problems with the heating system. The system heats the pipe around the circumference at a given location, but the temperature seems dependent on the streamwise location. Possible heat sinks are also factors in the temperature at a location.

Overall, the temperature spread between stations increases with increasing desired temperature. This is probably one of the best reasons for heating the entire driver tube in the future. As the temperatures increase, any unheated area causes a large heat sink from the heated area, thus dropping the temperature in that region. This causes large differences between regions of the pipe near the heat sink area and those isolated from it. This is especially apparent in the 180 C runs. The middle of the driver tube was excessively overheated (near 200 C) while attempting to heat the upstream end of the heated sections to 180 C. This in turn made it even more difficult to overheat the most downstream portion to account for heat losses in the contraction.

However, the driver tube was reasonably uniform on the surface at the lower temperatures. Thus the next step was to verify that the air temperature was similarly

uniform. The tunnel was run with a cold wire configuration to evaluate air temperature uniformity. These tests produced two main results. First, the temperature does not remain constant during the run. However it is important to note that this is probably not due to the heating. It is probably due to the isentropic expansion of the air as the run progresses and the driver section loses air to the rest of the tunnel. The temperature signal of an unheated run is plotted in figure 37. The raw data are averaged using a smoothing code that averages every 50 points down to one point and taking the mean time for the 50 points (the code is in Appendix B). The temperature drops of the passing expansion wave can be seen about every 0.12 seconds, as well as the fluctuations indicating the end of the run at about 3.5 seconds. Theoretical calculations of the temperature drop of the isentropic expansion compare reasonably well. This can be seen in figure 38 where two unheated runs are normalized by the initial temperature and compared to the theoretical temperature ratio. Although they disagree somewhat, the difference is only about 3% by the end of the run.

The normalized heated data and the theoretical curve agree extremely well. Several curves (maximum temperature of 87 C) are plotted in figure 39, along with the theory. This agreement is surprising since the unheated data does not agree as well. However, this definitely indicates that the temperature drop is due to the expansion of the gas. Also, the temperature must be reasonably uniform in the driver tube. Otherwise the curve would deviate from the theory when gas with a different initial temperature passes the wire. It would essentially be normalized by the wrong initial temperature since the entire curve is normalized by the maximum.

The other finding of the initial runs was that heating of the re-filled tunnel (after a run) took several hours (these tests were before the circulation heater). Figure 40 shows several heated runs. The highest temperature run had a 5 hour wait time after re-filling the tunnel after the previous run, while the others had between 3 to 3.5 hours wait time. One can easily see that the temperature of the air is very dependent on the time between runs. This prompted the need for the circulation heater. Once the circulation heater was installed the temperatures were very consistent. This is evident in the data taken at a

desired temperature of 100 C in figure 41. The wait time between runs was varied from 45 minutes to 3 hours for these runs, but they were still consistently at the same temperature. The temperature is low, but that can be accounted for easily by calibrating actual temperature to indicated temperature and adjusting the temperature setting accordingly.

This was an important step in collecting data, for it was important that the temperature be repeatable from run to run. This made it possible to perform several runs immediately after one another to evaluate the noise level at several pressures at each desired temperature level. However, the temperature was not the only variable that needed to be repeatable. The noise is very dependent on the nozzle cleanliness, and therefore it is important to discuss how this might affect noise measurements.

3.2 Nozzle Condition

The cleanliness of the nozzle is very important in maintaining quiet flow. One speck of dust in the wrong place will produce a disturbance large enough to destroy the quiet flow. When unusually high levels of noise were present in the signal some sort of dust or debris was commonly found near the nozzle throat. It is common practice to clean the nozzle frequently.

There are two major cleanliness issues that have risen from the heating of the driver section. The first and most noticeable is grease that seems to condense out of the air. With the sensitivity of the nozzle to debris one would think this would greatly affect the noise level in the flow. However, after two or three heated runs there is a coating of grease over all the walls of the nozzle and test section (perhaps 0.002 inches thick). This continues to build up with each heated run. This build up does not appear to affect the noise level in the tunnel. In fact, two unheated runs taken after 7 runs of heated flow had no increase in noise levels when compared with previous data even though the windows were so blurred with grease build up that nothing could be viewed through them. The grease does however seem to be more susceptible to catching dust particles and other

debris. It appears that eventually the debris builds up and at some point the noise level increases dramatically.

No source has been identified for the grease. There are three main possibilities: (1) oil in the pipe is vaporized when heated, (2) grease is somehow seeping into the tunnel from a joint, or (3) it comes from upstream of the driver section somewhere. The last possible source is least likely since the oil is not seen during unheated runs and only a small part of the fill line is heated by the circulation heater output. The fill line is used for heated and unheated runs yet, the grease only appears during heated runs. The source of the grease is not the circulation heater because the grease appeared in runs before the heater was installed. The contraction has been removed and examined, but it gives no clear evidence. It does seem to indicate that the grease condenses out since the grease first appears in the contraction near the throat and continues to be seen on the walls downstream to the second throat. This is where the air is significantly cooler, from the expansion in the nozzle, than in other parts of the tunnel. The source of this problem is still unknown.

The other major problem the heating causes is much less of a mystery. The inside of the driver tube is painted with high-temperature paint. This was done to prevent rust on the carbon-steel driver tube. With time, it is obvious that the paint will deteriorate and paint flakes may break off and fly downstream. This has been noticed by other experimenters in the Ludwieg tube. However, it appears that heating has significantly increased the number of paint flakes seen in the nozzle when it is inspected. Before any heating, perhaps three or four flakes (about 0.003 inches diameter) were found on the nozzle when cleaning. Now that the driver tube has been heated several times, it is common to find perhaps as many as two dozen paint flakes. It is suspected that the cycling of the heating process has caused this increase.

It definitely appears that heating the current tunnel causes some problems that need to be investigated further before the system is used routinely. If the conditions worsen it could make running with heat very tedious. The nozzle must be cleaned frequently and sometimes extensively by taking the contraction out and cleaning the throat

area from both sides. This was the case several times during the elevated temperature study. Check runs were made between each temperature setting to verify that the noise level had not changed during the runs. After almost every set of heated runs, the tunnel had significantly higher noise levels (fluctuations on the order of 0.25% of the mean, compared with 0.08% for a completely clean nozzle at atmospheric pressures). Often the nozzle had to be cleaned 4 or 5 times before the noise was at a satisfactory level.

This prevents any extended studies at elevated temperature since the debris build up can cause the increase noise levels only 7 or 8 runs after starting with a clean nozzle. Thus, to prevent corruption of the data, the tunnel must be cleaned frequently when running with elevated driver tube temperatures. The tunnel most likely will have to be unheated for most cleanings since at the higher temperatures the nozzle gets extremely hot to the touch. Also in cases where the nozzle must be removed to clean the contraction, the flange heating system must be removed before removing the nozzle. This frequent cleaning causes more cycling of the heat which in turn can worsen any flaking paint, and it slows down the running of experiments.

Most of these issues will only be resolved by installation of a stainless steel driver pipe, where no paint is needed, and by careful evaluation of the supply air. However, since evaluation of the heating system needed to be performed, freestream pressure and temperature data were taken at several different temperatures to determine the effectiveness and efficiency of the heating system for adaptation to future facilities.

3.3 Data Collection Notes

Since there are many factors other than the temperature that could affect the noise level in the tunnel, care had to be taken to be sure the effects found were in fact from heated driver air. The main barrier is the noise increase that can come from debris on the tunnel walls. Inevitably there will be some build up of debris with time. Thus, a method must be used to identify when this build up begins to affect the data.

Several runs were performed at each temperature. Each run was at the same location with a different initial driver pressure. The basic idea was to produce a noise level versus pressure curve for each desired temperature. The noise level generally increases with increasing pressure (increasing Reynolds number given other conditions remaining constant).

However, noise also increases eventually with time (from one run to the next) because of debris build up. It was important to collect the data in such a way that an increase in noise from debris could be identified. If runs are performed with successively increasing pressure, there is no way to determine if the noise increase is due to pressure or debris. However, if a low pressure run is performed after a high pressure run, the noise should be lower. Thus the noise for the high pressure run would most likely be due to the higher pressure. If debris eventually does cause a noise increase, all the following runs would show a similar increase. If the initial pressure from run to run is set such that it jumps randomly, a debris-caused increase in noise can be found by comparing noise levels. The debris-contaminated measurements will have a definite shift in noise above uncontaminated data. Data was collected in this manner at each desired temperature setting. This method made identification of debris-contaminated data relatively straightforward, as will be seen later.

Once the tunnel was cleaned the single probe pressure transducer and cold wire were installed for data collection. Other current experiments are typically performed at atmospheric temperature and pressure. These are similar to the conditions determined to be the upper limit for quiet flow in the previous freestream noise evaluation (Schneider and Haven 1995). Control data was taken for comparison to previous experiments and as a base for the current study. Several runs were done at different initial pressures with the probe positioned 4 inches back in the quiet flow region ($z=13.33 \pm 0.0625$ inches, $z=0$ at the throat).

The location was determined by placing the tip of the probe in the center of the first nozzle window (the probe was visually lined up in the center of the window by using two specially designed reference rulers that attach precisely to the windows). The probe

location was recorded on the reference rulers. Uniform flow starts at z=9.33 inches, while the window center is at z=10.118. This information was used to determine a location 4 inches downstream of the onset of uniform flow (assuming quiet flow region length of 4 inches). The probe was then moved to this location.

The initial driver pressure was varied from 8 to 19 psia which encompasses pressures ranging from where the flow is very quiet and noise levels are on the order of the electronic noise, to pressures where the noise level is comparable to conventional wind tunnels. Data was taken in a similar manner at 4 different driver-tube temperatures. Runs at z=13.33 (4 inches downstream of onset of uniform flow) were taken with various initial pressures ranging from 10 to 21 psia. This process was performed at 100, 125, 150 and 180 C as indicated on the thermocouples.

The elevated temperature data was usually taken the day after starting the main heater. The only exception to this was the 125 C data which was taken 5 hours after the last 100 C run. The initial driver pressure was varied randomly from run to run, however, there was a conscious effort to have the first and final runs at reasonably low pressure. This would allow for easy detection if any debris contamination occurred. The tunnel was cooled after the 125 C, 150 C and 180 C data sets were obtained. Check runs were then performed to verify that the noise level was nominal. Usually the noise levels were significantly above nominal conditions found in the baseline data. The tunnel was then cleaned until the noise was similar to the baseline level (this usually consisted of several cleanings, and several check runs before an acceptable noise level was obtained). A chronological listing of the runs, their conditions and statistical results, and details of cleaning the nozzle can be found in Appendix C.

A typical screen dump from the oscilloscopes is shown in figure 42. The top signal is the dc pressure signal. The drop near the beginning indicates when the diaphragm bursts and also shows the pressure drop that occurs when the run begins, caused by the pressure being measured behind the normal shock caused by the probe tip. The pre-run portion is also visible in this particular case because of its low initial pressure. Normally the pre-run level of the pressure transducer was off scale so that that a reasonable

resolution of the run signal could be obtained. It is important to note that the signal appears very flat and smooth during the run, this is typical, and only in extremely noisy conditions will any fluctuations be seen on the dc signal. The second channel is the ac fluctuations channel. The pre-run signal can be seen clearly before the large fluctuations of tunnel start-up (the oscilloscopes were set to trigger from the start-up fluctuations and to record a short amount of pre-trigger data). Normally the start-up process takes about 30 to 40 ms before settling into Mach 4 flow. The third channel is the voltage output from the constant current anemometer. Again, the start-up can be picked out easily. This example is an elevated temperature run, and therefore the temperature increases from pre-run to run.

There are two major sets of data that were collected in this study, temperature data and pressure data. Both are equally important in evaluating the overall success of the heating system and its effects on the operation of the Purdue Ludwieg tube. They will each be analyzed in detail in the following sections. One should note that both temperature data and pressure data were collected simultaneously during each run. The discussion will begin with the mean pressure data since it gives many insights into the different aspects of the flow.

3.4 Kulite Pressure Transducer Calibration

Since only the voltage output from the pressure transducer can be recorded, it must be calibrated. Figure 43 shows the result of following the procedure described in section 2.5.1. Several calibrations were performed by both pumping down and by repressurizing the tunnel. The calibration data was fit to a line and the slope was then incorporated into the main data analysis program. It should be noted that the Kulite was calibrated using the amplified output from amplifier box #1 (there are currently 4 similar amplifier boxes) , not the bridge output itself. This must be taken into account when comparing with the factory calibration. The factory calibration must be multiplied by 100

for comparison to the amplified output (this is already done in figure 43). It should be noted that there is a slight slope difference and some offset between the two curves.

This is also the case with several other Kulite pressure transducers used in the Purdue Ludwieg Tube. Since the pressure transducer can be calibrated easily, this drift is noted, and the most current calibration was used to calculate pressures. The A/D converter can resolve a 0.0048 V change which translates into a +/- 0.005 psi pressure change. The Paroscientific is nearly as accurate. The manufacturer guarantees a maximum error of 0.01% of the reading. Using a worst case scenario, the maximum pressure error the Paroscientific could cause in a calibration is 0.0295 psi. If the Parosientific and A/D converter errors added, the maximum possible error in the calibration would be 0.0345 psi. This is less than 2% of typical pressures recorded during a run. If offset errors are excluded, the maximum slope error that could be obtained from the calibration is 0.00042 psi/V. These errors are considered very reasonable for the current study. Thus, if the Kulite is delivering a consistent response to the pressure, the calibration should produce a very accurate method for obtaining pressure.

3.5 Unheated Mean Pressure Results

After a run, the data is transferred to a PC in binary format. Matlab was used for the analysis of the data. A function for reading the data into Matlab variables was developed by Prof. Steven Collicott (listed in Appendix B). This code was used to load the voltage and time into arrays. The pressure was calculated by applying the curve fit from the calibration to each array element (this is a small part of one large code that performed most of the analysis, also listed in Appendix B). Figure 44 is a voltage trace plotted in Matlab while figure 45 is the pressure calculated from the voltage using the calibration in figure 43. Figure 46 is a zoom of figure 45, the detail of the signal can be seen. The resolution is approximately 0.02 psi. This is not excellent resolution; however, there was a trade-off between higher resolution and perhaps missing part of the run due to

improper settings. It was difficult to properly set the offset levels on the oscilloscope to always catch the entire run when working with such a wide initial pressure range.

The data is sometimes smoothed for plotting. An in-house Matlab code (courtesy J. D. Schmisseur, listed in Appendix B) averages a user-specified number of points into 1 point and takes the mean time over those points. It is only used when plotting or in special cases when an averaged signal is helpful. Figure 47 shows the same pressure signal smoothed over every 50 points. It does not seem to change the mean signal, yet makes the signal much more presentable and increases the resolution. Again, this is only used when plotting to produce a less cluttered plot and will be noted as such. All noise level analysis is performed with the entire signal.

Figure 47 displays some important facts about the pressure signal. First, the pressure plotted is the pressure behind the bow shock caused by the transducer. Thus to find the total pressure in front of the shock, this value must be divided by 0.1388 (total pressure ratio for a Mach 4 normal shock). Next, the pressure signal is continually dropping with time during the run. It drops slowly for some time and then there is a sudden sharp drop with a continuing slow drop. The slow drop is caused by isentropic expansion of the gas as it leaves the driver tube. Air mass is leaving, expanding the gas and dropping the pressure. The sharp drops are caused by reflections of the expansion wave in the driver tube. Since the drop in pressure is small between the expansion wave reflections, the flow is considered basically steady in-between each reflection.

Only the portions in-between the expansion reflections provide useful pressure data, thus it is desirable to separate each run into small segments of data equal to the time between the reflections. This is done in two steps using the dc signal. First, the beginning of the run is located, and then the time of each expansion is located. This is a special case where the data is smoothed. Since there is no actual analysis, the process is simplified by smoothing because the large mean pressure changes are more easily identified. The large pressure drop and the fluctuations of the start-up process are thrown out by finding the beginning of steady flow. The beginning of the run is found by fitting a curve to several points in front of and behind the particular point. If the slopes of the two fitted curves are

nearly equal and very small, the time associated with the point is identified as the start of the run. The process is simply repeated at each point in time after the oscilloscope is triggered until the condition is met. Figure 48 shows the pressure signal from figure 47 with the start-up and pre-run removed by use of the algorithm (this analysis is a portion of the main analysis code in Appendix B).

Each reflection of the expansion wave is found in a similar manner. However, rather than using slopes to detect the sudden drop in pressure, a mean signal is calculated over the steady portion of the signal. The signal is searched for a deviation from the calculated mean. When this is found, the time is identified and stored, and a new mean is calculated at the next pressure level. Figure 49 shows the signal from figure 48 re-plotted and marked with the times found by the algorithm. The data is now in a form where it can be analyzed. Each segment between expansion can now be analyzed individually. However, before proceeding with any discussion of the noise levels, it is important to verify that the tunnel and instrumentation are operating as expected.

The normalized mean pressure for the run can be compared to the isentropic expansion theory described in Schneider *et al.* (1996). Figure 50 shows the pressure from the baseline unheated runs normalized by the initial pressure, compared to the theoretical pressure ratio for the expansion of the driver tube air. All the curves tend to collapse on top of each other as expected. This collapse is similar to results found in Schneider *et al.* (1996), but the data does not match the theory as well. The reason for this is unknown, however the difference was not thought to be significant enough to evaluate extensively in this study. The one anomalous run is a low pressure run that had a poor diaphragm break, which seemed to extend the startup process.

During early analysis some anomalies in the data were observed. Some spikes in the dc signal could be seen when the signal was smoothed and plotted (figure 51). The data was more closely examined and the spikes were found to be at 60 Hz. This was determined by zooming in the signal until the precise time between the spikes was found. This was done for several different spikes. The frequency was consistently 60 Hz and was therefore believed to be electronic noise. Although the spikes appeared to be large, they

did not appear to affect the mean pressure signal. Since it does not seem to affect the primary calculations performed on the dc signal (the mean pressure for each data segment) it is insignificant in the analysis of the data.

Before a detailed analysis of the fluctuation data can be performed, it is important to discuss the other main parameter affecting the fluctuation levels - the temperature. The results obtained from the temperature analysis will be used to formulate noise level trends measured on the pressure transducer. The temperature is also needed to calculate the Reynolds number, an important parameter for comparing noise levels.

3.6 Examination of Temperature data

The cold wire measures a temperature change by measuring the voltage change due to the resistance change with temperature. The wire was calibrated using the method described in the calibration section (section 2.5.2). Both the temperature versus voltage and temperature versus resistance relationships were measured. Figures 52 and 53 shows these calibrations. Both data sets are very linear over the entire range, and both were fit to straight lines. The thermal resistivity coefficient, alpha was calculated from figure 52 and found to be 0.0025/C. Both of these curves could then be used to calculate the temperature from the voltage recorded.

Figure 54 shows a typical raw trace (without driver tube heating). It should be noted that smoothing the curve does not change the shape or value of the signal. Since only the mean signal is of interest, and the signal is rather smooth to begin with, the traces were smoothed to speed calculations and to make presentation less cluttered. The start-up is the large "spike" in the signal near the beginning.

In addition to the calibration, the recovery factor for the flow needs to be determined. As mentioned in the section 1.1.6, the recovery factor is used to account for the heat transfer to the flow. Following the process outlined by Spina and McGinley(1994), Re_o for the Purdue Ludwieg Tube is on the order of 4.75 and the Knudsen number is approximately 1.24. Figure 4 from Spina and McGinley (1994)

indicates a recovery factor of 1.11. Thus, the sensed temperature is expected to be higher than the flow temperature. This is a consequence of free-molecular flow.

Unfortunately this recovery factor does not agree with our experimental results. For an unheated run the recovery factor can be found if the stagnation temperature is known. The temperature found can simply be divided by the real stagnation temperature to find the recovery factor. This is essentially the case for an unheated run in the Ludwieg tube. Before flow onset, the cold wire is sensing stagnation temperature. Immediately after the start-up process, the temperature should still be the initial stagnation temperature until the temperature starts to drop due to expanding air. The changes across the weak driver-tube expansion wave are neglected, for the driver-tube Mach number is less than 0.01. The temperature traces for several unheated runs have been normalized by the pre-run temperature in figure 55. The normalized temperature immediately after start-up is about 0.98 of the pre-run temperature. This consistently the case in our facility. Thus, 0.98 will be used as the recovery factor. The cause of the discrepancy with Spina and McGinley (1994) is unknown.

The voltage trace from figure 54 is reduced to temperature via the two calibrations and both are plotted in figure 56. The agreement of the two methods is very good. Since both methods produce the same result, there was no need to calculate temperature using both methods. The data was reduced using only the resistance calibration. For simplicity in analysis, the entire curve is adjusted by the recovery factor even though there is no flow during the pre-run portion of the signal. Since this part of the signal is of no interest, this was not a problem. All cold wire data was processed in this manner to answer three main questions: (1) Does the temperature measured agree with the desired temperature and with the temperatures indicated on the thermocouples, (2) how repeatable is the temperature from run to run, and (3) how does the normalized temperature compare with unheated data and theory?

In order to answer the questions it is important to understand the how the temperature behaves during the run. There are some features of this plot that should be noted. First, the temperature of the beginning of the run is very close to the temperature

before the run (refer to figure 56). This is expected since the temperature should be the same immediately before and after the start of the run (remember that the pre-run is slightly higher than it should be because of the recovery factor adjustment). The second feature is that the temperature decreases with time. This is again due to the expansion of the gas in the driver tube, which supplies stagnation conditions for the flow (remember the cold wire is measuring total temperature which is constant through the nozzle expansion and the shock caused by the wire). The reflecting expansion wave does have a weak effect on the temperature, since the passage of the expansion wave can be seen in the signal. As with the pressure, the temperature can be normalized with respect to the initial temperature and compared with theory. Figure 57 shows two unheated runs compared to theory. Although the agreement is not perfect, the theory does seem to be a reasonable representation of the temperature.

The driver tube was heated to 4 different temperatures, 100, 125, 150 and 180 degrees C, as indicated by the thermocouples. The farthest downstream end of the driver tube was heated to a higher temperature than the rest of the pipe in order to eliminate a much slower rise to maximum temperature than was desired at the beginning of the run.

Heating the pipe to 100 C was not a difficult task for the heater. It was able to achieve a steady temperature in about 5 hours. All thermocouples indicated a temperature within 5 degrees of 100 C. Once at temperature, very little power was used by the main power supply to keep the pipe warm. When bleed air was used, the circulation heater was set to about 100 C (the dial for the temperature setting is not precise, it has increments of 25 degrees F). The runs were made with varying time between runs. Figure 58 shows the CCA data converted to temperature for the 100 C runs. There are several things to note about these results.

First and foremost, the desired temperature is not reached. This is probably an affect of the heater wire influencing the temperature of the surface thermocouples. The thermocouples read a slightly higher temperature than found in the tunnel. For the purposes of these experiments it is not a concern as long as the difference is noted for reference, for future elevated temperature work. Another problem with the temperature is

that it seems to rise from the pre-run temperature to the maximum temperature very slowly. It was hoped that the temperature rise would be complete by the end of start-up. The slow rise is believed to be caused by the large heat sink from the driver tube to the nozzle. If the contraction is cooler, the air near the contraction will be cooler, and the maximum temperature will not occur at the beginning of the run.

As with the pressure data, the passage of the expansion wave can be seen on the temperature traces. It is also interesting to note that at 0.8 seconds from the diaphragm break there is a peculiar drop in the temperature. This drop is not evident in the unheated temperature data, but can be seen in all the heated data. It seems that one particular spot in the tunnel is different and then the normal temperature drop continues afterward. The timing of the drop closely coincides with the passage of the air from near the first flange connection in the driver tube (the driver air moves at 2.8 m/s, at 0.8s the air passing through the nozzle started 2.24 m upstream, the first flange is 2.4 m upstream). However, from run to run, the temperature appears to be very consistent. There is at most a 4 degree difference between any of the runs at any given time.

This is also the case when examining the normalized temperature. The temperature is normalized by the maximum temperature for the run. This is done because it is assumed that the maximum temperature is the initial total temperature before any expansion. Thus, to compare with the theory, the total temperature ratio is calculated. The theoretical temperature ratio is fitted to the data at the maximum temperature for the runs. As seen in figure 59 the normalized temperatures agree better than expected with the theory. One would not expect that the heated data would compare better than the unheated data, especially since the expansion wave travels from the heated into the unheated portion of the driver tube each time it reflects. Overall it seems that the heating system performs well at a desired temperature of 100 C. The only problem that cannot be easily eliminated is the slow temperature rise at the beginning of the run. More heat could have been applied to the nozzle flange area, but as will be discussed later, this can produce other problems.

Unfortunately the data at the higher temperatures are not as clear-cut as the 100 C data. Temperature plots for the 125 C data are shown in figure 60. Two runs appear to be well above the desired temperature. In fact, these temperatures are impossible since they show temperatures well above any of the thermocouple temperatures. This is impossible because the thermocouples are sensing the hotter temperatures, since they are near the heater wire. It is also very unlikely that the circulation heater would cause this difference since the 100 C results were very consistent and the same operating procedure was used. After looking closely at the data, one notices that these two runs have pre-run temperatures well above the other runs. While there is some variance in the temperature before the run due to bleed air passing through the nozzle when changing diaphragms, it is not likely that two runs (that are not back to back) would have pre-run temperatures 35 degrees hotter than all the others. In fact, a thermocouple placed on the outside surface of the nozzle never indicated a temperature above 70 C even when the tunnel was heated to 180 C. Because of this it is believed that these two runs somehow experienced a change in the offset voltage in the CCA, thus causing the calibration to be incorrect for these runs. Unfortunately the cause for the offset change is not known.

All of the other runs are grouped together slightly below the desired temperature, like for the 100 C data. The spread between the runs is quite a bit larger, about 8 C. This appears to be mainly due to the procedure of running the tunnel. The procedure was varied slightly during the experiments to determine the most consistent method. Some experimentation with the use of the circulation heater was performed. For some of the above-atmospheric runs, the circulation heater was not turned on when increasing the pressure before the run. This seemed to only affect the higher pressures (driver pressure of about 17 psia or above). Apparently the amount of air needed to raise the pressure only 1 psi or so above atmospheric does not significantly affect the temperature of the flow.

The flange heater and main heater settings were also changed slightly to try to overheat the contraction area. This did not produce any noticeable difference in the slow rise time in temperature. All the runs seem to reach their maximum temperatures at about 0.3 seconds. However, slight changes can affect the overall temperature of the flow

depending on the thermocouple monitored by the main heater. For instance, if the main heater monitors a thermocouple at station 1, overheating the flange area could cause the temperature of the rest of the pipe to drop. When trying to overheat the contraction area, it is usually best to have the controller monitor station 2 or 3 (station 3 was usually monitored). For most consistent data, the heater settings should remain unchanged for the entire set of runs.

The normalized temperatures again seem to compare extremely well with theory. Figure 61 shows all the 125 C runs (including the two with obvious problems). Since the two problem runs are consistent when normalized, it supports the possibility that the offset in the instrumentation somehow changed for these runs. Since their absolute temperature is obviously incorrect, only an offset change could still produce a reasonable normalized temperature. If a change in slope produced these differences, the normalized temperature would produce a different temperature ratio than the other curves.

The results for the runs at a desired temperature of 150 C are similar. Figure 62 shows the temperature traces versus time (one run is not shown because the oscilloscope was incorrectly set and the signal was clipped). Again most of the runs group fairly close together. The lowest temperature trace is the run at the highest pressure. This is also a run where the air added before the run to increase the pressure was not heated with the circulation heater. This apparently is an important step in maintaining the appropriate temperature air (at least at the higher temperatures). Although this was not seen in the 100 C data, similar but smaller affects were present in the 125 C data. The runs that group together either needed no air added or had the circulation heater on while the pressure was increased. The reason for the higher-temperature run is not known, perhaps the circulation heater was not set exactly the same as in the other runs.

Even though the data is not as consistent as desired, it does collapse very well and agrees with the theoretical expansion temperature ratio curve. This can be seen in Figure 63. This plot also shows the slow rise to temperature very well. For this temperature it seems to take almost 0.3 seconds to reach the maximum temperature. This follows with the idea that the heat loss to the nozzle is causing lower temperatures near the contraction.

As the temperature is increased, a larger percentage of the heat is lost to the nozzle area since heat transfer is exponential with temperature difference. This causes the first air through the nozzle to be cooler, compared to the increasing desired temperature.

Unfortunately the temperature data at 180 C is not correct. During this data set the batteries that powered the CCA began to lose power. Since the offset voltage is directly associated with the voltage across the batteries it also began to decrease. It is believed that this began to occur after the 5th run, but there is no definite way to confirm this. During the experiment it was thought that the drift was because of the high temperature in the nozzle area. Since the tunnel temperature had not been at this level before, it was not known how much temperature variation would be seen in the nozzle in-between runs (due to how long bleed air was blown through the nozzle, the wait time before the run, etc.) Figure 64 gives the temperature traces with the original calibration and offset voltages. Even the curves from the first two or three runs have some differences between them (these are the 2nd, 3rd, and 4th, highest temperature runs). This is most likely because the heating system seemed to struggle to maintain the temperature. The main supply was using more than half of its power to try to keep stations 4 and 5 near the desired 180 C. It was actually never able to reach the desired temperature at those locations. However, in the process, stations 1 and 2 were overheated by as much as 20 to 30 C (refer to figure 36). It is obvious that for operation at 180 C, most of the driver tube will have to be heated to prevent the large temperature gradients near the unheated portion of pipe.

The non-uniform heating of the driver tube is apparent when the normalized temperatures are compared. Since only the offset of the output was affected by the battery problem, the normalized temperatures should be reliable. Figure 65 shows the results. There is a rather large spread in the data compared with the other temperature data sets and the curves tend to deviate from the theory at about 0.68 s. This is most likely due to the non-uniform heating of the driver tube. If the air starts out cooler, it will be below the expected temperature when normalized by the hotter value upstream.

A calibration of the CCA instrumentation system was performed after this last set of data. The voltage versus temperature calibration had an offset drift of nearly 0.5 volts by the time the calibration was performed, but the slope remained the same. The resistance versus temperature calibration was similar in that the resistivity coefficient had remained constant, but the reference voltage had changed significantly for the same reference temperature. The calibrations are compared with earlier calibrations in figures 66 and 67.

It is possible that this calibration may be accurate for the last few runs, if one assumes that the offset did not drift between the last run and the calibration. However, if the data were re-processed with this calibration, the results remain ambiguous. If the temperatures turn out higher than they should be, obviously the calibration is incorrect. But even if the temperatures turn out similar to the previous temperature data sets, one could argue that the calibration is wrong and the actual temperature is much lower than indicated. Thus, since re-processing would not resolve the issue, the CCA was re-wired for +/-15 Volt input from a power supply, replacing the battery power. The intention was to use this more reliable power to repeat the 180 C data. However, time constraints and problems with the Kulite pressure transducer prevented this.

3.7 Unheated Pressure-Fluctuations

Once it was confirmed that the tunnel and instrumentation were working as expected a more detailed analysis of the noise levels could be. As mentioned above, the ac fluctuations of the pressure signal are separated off into their own channel and recorded separately. Figure 68 shows a typical ac voltage for a run. The slow decrease from the start-up fluctuations to the run level is probably caused by the limited frequency response of the AC coupling of the oscilloscope (probably 10 Hz). The pressure is calculated using the same calibration as for the dc channel (the extra amplification must be accounted for by dividing the voltage by 100), but the offset is not used. This is because the pressure fluctuations are fluctuations from the mean, and thus have a different offset, zero. This is

shown in figure 69. Notice that there is a small mean signal. This is probably caused by different electronic ground references between the instrumentation and the oscilloscopes. It does not cause a problem because it can be removed by simply subtracting off the mean of the signal. Figure 70 shows the adjusted pressure signal for the sample ac run. It should be noted that this is a signal for a typical low noise run. Figure 71 is more typical for a very high noise level run, although the amplitude is dependent on the tunnel conditions.

Figure 70 also shows the different parts of the run. Large clipped fluctuations are associated with start-up. This divides the pre-run, and run portions of the signal. One must remember that the mean pressure is dropping with each reflected expansion although it cannot be seen in this plot. However, if the signal is smoothed, or zoomed, some fluctuations corresponding to the passage of the expansion wave can be seen. Thus it is very important to analyze data only between the expansions to prevent the statistical analysis from being corrupted. To avoid any fluctuations from the passage of the expansion wave, 80 ms of signal between reflections (normally about 120 ms apart) was separated into a data segment. This usually results in 7 data segments for each run. Each segment is analyzed individually using only the ac and dc signals corresponding to that segment.

Another important point to notice is that the pre-run fluctuations are similar in magnitude to the fluctuations during the run. Since there is no flow before the run, this is electronic noise in the signal. Some of it can be identified (52 kHz noise can commonly be seen, this is the update frequency of the oscilloscope screen), but some of the noise has not been identified with a particular source. Since the noise level during a low noise run is near the same level as electronic noise a major issue is determining exactly how much of the signal is electronic noise during the run.

3.7.1 Electronic Noise Evaluation and Tare

The simplest solution would be to subtract off some sort of mean value for electronic noise. Since there is some pre-run segment for each run, if each pre-run noise level was subtracted for each run, day to day or even run to run differences in electronic noise could be accounted for. A mean was calculated for each run by taking the root mean square (RMS) of the pre-run portion of the fluctuations signal. This is then subtracted off using an RMS process (Beckwith *et al.* 1983):

$$\sqrt{P'^2_{segment} - P'^2_{pre-run}}$$

(P' is the pressure fluctuation signal and the 'segment' subscript designates the 80 ms of run for one segment of data between expansion waves). This makes the data look very reasonable for some runs, however others seemed to prove this was not a proper method. Figure 72 shows the RMS calculated for each data segment (between the expansion waves), for one run. The first point is the RMS of the pre-run signal and the others are the RMS of each segment without any pre-run noise subtraction. Notice that the pre-run RMS is larger than the RMS of the data segments. If this value were subtracted off during the RMS calculation, imaginary numbers would result when the square root is taken. This is obviously not possible. Thus subtracting off a mean pre-run signal is inappropriate. There are two explanations; (1) the electronic noise changes magnitude during the run where here it has been assumed constant, or (2) the pre-run noise is just not a good representation of the electronic noise during the run. Since there is definitely some electronic noise in the signal, not subtracting anything from the signal seems excessively conservative. Since the pre-run signals have no flow, it was thought that a more detailed look may provide insight into a more appropriate approximation for the electronic noise.

The search for a more reasonable electronic noise estimate produced a possible solution. Figure 73 shows the pre-run RMS versus the driver-tube pressure, measured at the beginning of the run. Also plotted are two RMS levels recorded from the LeCroy oscilloscope during a calibration of the dc signal. There does appear to be a linear relationship even if the two calibration points are included. A line is drawn using the two

calibration points. Notice how the line seems to fit the data very well. The fit was performed using the two calibration points because they provided data near the actual pressures sensed during the runs. Since the curve seems to fit all the data, it appears to be an appropriate representation of the variation of electronic noise with pressure. The curve was used to generate an electronic noise estimate for each run based on the pressure after the completion of start-up. This value (P'_{fit}) was used to correct the data. This estimate was then compared with no noise subtraction, and with the pre-run RMS estimate from above.

The RMS of each segment of data between expansion wave reflections was calculated for the unheated base runs since it is a typical measure of the flow noise level. The two electronic noise estimates were compared. Each estimate was calculated and subtracted off from the squared signal during processing. The RMS calculations were

$$\sqrt{P'^2_{segment} - P'^2_{pre-run}} \quad \text{and} \quad \sqrt{P'^2_{segment} - P'^2_{fit}}$$

for the two different estimates (remember the mean is taken over the 80 ms data segment between expansions). The apparent flow noise levels are shown in figure 74. The problem with simply subtracting the pre-run RMS is readily seen. The zeros are only the real part of the imaginary number created when the larger noise is subtracted from the signal. The pre-run noise estimate produces unreasonable results since even the quietest flows still have some disturbances. Since P'_{fit} produces reasonable results and because it was calculated using definite electronic noise levels, it was used as the estimate for electronic noise. All the ac pressure data was adjusted using this electronic noise estimate before calculating any final noise level statistics.

3.7.2 Determination of quiet flow requirements

Even though the electronic noise has been estimated it is still apparent that determining flow noise levels is not clear cut. In most cases there is a point at which the signal to noise ratio is on the order of 1 when trying to measure low noise fluctuations in

the flow. When this happens, simply taking the RMS of the signal may not be the best way to determine noise level even if the electronic noise is taken into account. It could be argued that the results are affected by over-correction for electronic noise. The adjusted RMS values compared reasonably well with data presented in Schneider and Haven (1995). At z=12.1 inches the noise level of 0.06% of the mean at about 13.6 psi was determined as the quiet flow noise level limit in Schneider and Haven (1995). Here, figure 74 shows the RMS levels starting to increase dramatically around 13 psi, but the pressure probe is located slightly downstream at z=13.33, where the noise level should be higher. Relying on this method alone to determine the quiet-flow levels does not seem totally appropriate even though the results tend to agree with previous experiments.

Another method that can be more directly connected to the flow physics is needed. The time that the amplitude of the fluctuations is above a certain limit is also used to determine the amount of quiet flow. The only problem is that the cut-off amplitude must somehow realistically represent the disturbances causing the noise.

Figure 75 shows a portion of the signal from figure 69. Figure 76 shows a portion of a higher noise signal with a pressure disturbance thought to be caused by noise radiated by the passage of a turbulent spot on the wall boundary layer (Wilkinson, et al. 1994; Schneider and Haven 1995). Since it is the radiation from the turbulent spots that causes the increased noise level (Laufer, 1961), an appropriate amplitude for determining unacceptable noise levels is the amplitude above which the turbulent spot fluctuations are present. Since the fluctuation of a turbulent spot is usually much larger than the basic flow noise the amount of time where turbulent spots are present can be estimated. If figures 75 and 72 are compared, only the disturbance from the turbulent spot has an amplitude greater than about 0.2% of the mean.

Thus a possible estimate for the percentage of time where turbulent spots are present is the percentage of time where the fluctuation amplitude is larger than 0.2% of the mean. As the number of disturbances from turbulent spots increases, so does the percentage of time above 0.2% of the mean pressure. Since these radiated disturbances

make the freestream noisy, it is relevant to relate the criteria for quiet flow directly to the presence of these disturbances.

However, simply looking at two different signals and determining the appropriate cut off amplitude is not necessarily conclusive. To investigate the appropriate amplitude further, several different ac signals with varying degrees of noise levels were compared. Since the RMS noise levels seem to be similar to previous data from 1993, they will also be presented for comparison. Figures 77 -94 shows data for 6 different data segments. The segments have varying levels of noise from nearly quiet to nearly the maximum noise levels recorded during the experiment. Figures 77, 80, 83, 86, 89, and 92 are a portion (5 ms of the 80 ms segment used to compute the statistics) of the signal trace. The RMS noise level and the percentage of time where the fluctuations are above 0.2% of the mean (or τ) are calculated for the entire 80 ms segment (not just the 5 ms portion shown). Figures 78, 81, 84, 84, 87, 90 and 93 are histograms of the 80 ms data segments. It evaluates each data point as a percentage of the mean pressure for that segment. The bins are 0.01% wide. The remaining figures are the power spectra of the signals showing the frequency content.

Figures 77 and 80 show flow that is very low noise, with no turbulent spots present. It is important to remember that each segment is 80 ms long, and that only a 5 ms portion is plotted for clarity; however the plotted portion is representative of the entire segment. The RMS for these two data segments are 0.0416% of the mean and 0.0443% of the mean respectively. Both of these values are within the Beckwith criteria for quiet flow (Beckwith and Miller 1990). τ is 0.23% and 0.14% for the segments. These values are typical for segments where the driver tube pressure is about 11.5 psi. For comparison, Schneider presented values of 0.045% RMS noise and τ=0.3% for a pressure of 11.7 psi at z=12.1 inches (Schneider and Haven 1995). Similar numbers of 0.040% and 0.2%, for the RMS noise level and τ respectively, were found at a pressure of 10.8 psi (Schneider and Haven 1995).

The histograms for the segments show most of the data points are below 0.1% of the mean pressure. Again, this is typical for low noise flow where very few turbulent

spots are seen. Only very small numbers of points fall in the bins above 0.2% of the amplitude. The distributions have a very tight bell shape. Thus both RMS and τ seem to agree that these segments are quiet.

The power spectra for these segments show the frequency content typical for the data in this study. There are a few definite frequencies that cause noise. These are all present in a power spectrum without flow as well, and are thus assumed to be electronic of some sort. The 52 kHz noise is pickup from the update frequency for the oscilloscopes screen. Its harmonic also appears at 104 kHz. The spike at about 30 kHz is always present but has not been identified with any particular source. It also has harmonics at 60 and 90 kHz. The 40 kHz spike is believed to be a harmonic of 20 kHz noise, although the 20 kHz is not as clear in figure 79 as it is in figure 82. It is believed to be related to vibrations of the probe and the associated fluctuations picked up by the pressure transducer.

Previous data with the same probe had a dominate 18 kHz frequency oscillation that corrupted the pressure data and was unexplained. It was guessed that the probe was vibrating, perhaps due to a slight bend in the sting giving the sting a slight angle of attack and causing it to shed vortices. Upon examination, the sting was indeed not parallel to the center line of the tunnel. It was out of alignment by 0.011 inches over the length of the sting (about 9 inches). This was corrected to 0.002 inches. New data after re-aligning did not have the large fluctuations observed in earlier data, but the power spectrum still showed a similar peak at about 18 kHz. This peak is similar to the one in figure 82. Other than this frequency, all the frequencies in the flow seem to have little power compared to the peaks from electronic noise.

In contrast to figures 77 and 80, figures 83 and 86 are data segments that have some turbulent spots. Here the RMS of the fluctuations is higher than the Beckwith criteria for quiet flow. However, does this mean that the flow is no longer considered to be low noise? Beckwith has sometimes classified flows with RMS levels as high as 0.1% as low noise. If one examines the pressure more carefully, one finds that the majority of the signal is quiet flow, interspersed with turbulent spots. This is where the τ can differ

from the RMS. Useful experiments might be carried out if the noisy portion of the record can be identified and discarded. Although the RMS is 0.059% of the mean, only 1.6% of the segment in figure 83 has turbulent-spot disturbances. This is probably borderline for use as quiet flow, but it does show that a large portion of the segment is still very low noise. Figure 84 has a rather definite edge around 0.16% of the mean pressure. Although the Gaussian shape is spreading out compared to figures 78 and 81, there are still only a small number of points that are above the 0.2% cut off amplitude. The power spectrum is similar to those in figures 79 and 82. However, it is exhibiting 1/f characteristics at low frequencies which indicates increased turbulence.

The data segment in figure 86 contains disturbances that probably make it too noisy to be considered quiet flow. The RMS value is outside the criteria of 0.05%, but is only 0.0813%. However, almost 3% of the time is corrupted by large amplitude fluctuations. The histogram of this segment shows that there are several bins above 0.2% that contain more than just a few sporadic points. There is less of a sharp edge to the histogram. This indicates that the signal is beginning to spread out over all amplitudes more equally. All these things seem to point towards the conclusion that the flow is relatively noisy in the data segment in figure 86 and probably could not be considered quiet flow. The power spectrum also seems to indicate this conclusion. A very wide range of frequencies up to 60 kHz is present. This range is beginning to have the same power as the defined sharp electronic noise peaks This indicates that larger, more random disturbances are beginning to dominate the signal.

Figure 89 also cannot be considered quiet flow. One can see that the noise radiated from turbulent spots is becoming common in this data segment. The RMS level is 0.11% and τ is 7%. The flattening of the histogram is very evident in figure 90. The power spectrum is also showing the presence of all frequencies at a relatively high power level compared to earlier figures. The histogram and the power spectrum are beginning to show signs of a random signal where there is a wider Gaussian shape to the histogram and only a few sharply defined frequencies.

Figure 92 is simply an example of noisy flow, very high noise by quiet-flow standards. Although this is low by conventional standards (Dougherty and Fisher 1982) it seems that the acoustic origin on the nozzle wall has a completely turbulent boundary layer. Its RMS value is 0.26% of the mean pressure and has fluctuation amplitudes above 0.2% of the mean over 35% of the time. It is obvious from the signal trace that there are very few portions of the flow with low fluctuation levels. In fact, the flow has turbulent spots present throughout the entire segment. The histogram in figure 93 has a relatively even distribution for all the bins in up to 0.5% of the mean pressure with the exception of the first bin. This segment definitely has random noisy fluctuations. The power spectrum shows a similar result, the frequency content is becoming somewhat uniform for all frequencies at a high power level compared to the other figures. Again this is typical of a noisy signal.

It is apparent from the above discussion that there are two possible criteria for determining the noise levels in the flow. The RMS level of the flow is useful, however, an appropriate cut-off defining "quiet flow" still involves a somewhat empirical comparison to flight data. Finding the amount of time the flow has large amplitude turbulent spots is also useful in determining the flow noise level. The percentage of time where the fluctuations are greater than 0.2% of the mean is valuable in that it estimates the noise based on a qualitative disturbance present in the signal. For completeness both methods will be used to evaluate the affects of elevated driver tube temperature on freestream noise levels. However, before any comparisons are made at different temperatures, the base noise levels without any heat must be examined.

3.7.3 Unheated Quiet Flow Noise Levels

Since pressure is dropping throughout the run, each segment between the expansion wave reflections is individually evaluated. Figure 95 plots the RMS divided by the local mean pressure vs. the mean pressure for each segment for all the unheated control runs. This data can be compared to data from Schneider and Haven (1995) taken

at z=13.06 inches (compared to z=13.33 inches for the current study). These data are shown as well in figure 95. The current data seems to agree well with the previous data.

There are also several letters plotted in figure 95. These are placed near the first data segment for that particular run. The order is important to note. This shows that the noise increase is not associated with debris buildup. Run A is the first run. Run B is at a higher pressure than run A, thus its noise level is higher. Run C is after run B, but its pressure was similar to that of A. Since the noise levels for runs A and C are similar the noise level of B can be attributed to the increase in pressure rather than debris. If debris had caused the increase in noise for run B, run C would have shown a higher noise level than run A, even though it is at a similar pressure. This method was used to eliminate debris as a cause for noise increases in each data set.

The percentage of time the pressure fluctuations are above 0.2% of the mean pressure show a similar trend for the current. Figure 96 is a plot of τ versus the mean pressure for the segment, again for all the unheated segments study (τ was available for a similar location in Schneider and Haven (1995)). The percentage of time above 0.2% of the pressure is relatively constant until about 13 psi. Above that pressure τ increases dramatically. It is apparent that either method seems to find a sharp increase in noise as pressure increases above about 13 psi. Notice that although Schneider and Haven (1995) present data in a small pressure range, the data seems to indicate a noise increase at about the same pressure as the current data. Evaluation of the heated runs in a similar manner will allow for comparison.

The data indicate that the noise levels are relatively constant with pressure, below about 12 psi. This is partially due to the fact that some fluctuations will be present no matter what is done to prevent them. In this case, it is also a possibility that the reducing flow noise levels become masked by the electronic noise levels as the pressure drops lower (below 10 psi, the signal to noise ratio is very near 1). Thus a relatively constant noise level is present rather than a noise level that continues to drop with dropping pressure. However, both methods give a rather clear indication that the flow seems to transition from quiet to noisy flow at about 13 psi total pressure at z=13.33 inches downstream of

the throat. These results compare reasonably well with the data from (Schneider and Haven 1995). This shows that the nozzle performance is consistent even after three years of operation Since this is considered the maximum operational pressure for quiet flow conditions at this location, it will be compared with the maximum pressures found to have mostly quiet flow when the driver tube is heated.

3.8 Comparison of Elevated Temperature Data

As with the base data it is important to verify proper instrumentation and tunnel operation, especially since there is no previous experience in this facility with the Kulites at elevated temperatures. Figures 97-100 give the normalized pressure versus time for all the runs at each of the different driver tube temperatures (the temperatures mentioned in this part of the discussion are all desired target temperature). As can be seen there is some spread among the different runs as compared with the unheated runs. However, on average the spread is not much larger than seen with the unheated baseline runs.

For the 125 C, 150 C and 180 C sets of data, there is one pressure signal that remains constant, which is physically impossible. The pressure cannot remain constant or increase during the run. There is no clear-cut explanation for this anomaly. All the questionable signals have one aspect in common. They were all the first run at their respective temperatures. This is possibly a temperature affect on the Kulite. Before the first run, the nozzle area downstream of the throat remained relatively cool since there is very little flow between the heated and unheated areas. Perhaps, the initial dramatic increase in temperature caused the calibration to change during the run. Although this does bring up the issue of temperature compensation for the calibration of the Kulite, most of the pressure traces seem to agree at least qualitatively with the theory.

Agreement with the theoretical data is not expected to be as accurate as with the unheated runs because the expanding air does not have a constant temperature throughout its volume. The theory assumes no temperature gradients. This is not true for the heated runs since part of the tunnel is unheated. This affects the mass calculation, which assumes

a constant temperature throughout the volume and thus a constant density. The theoretical mass will be lower than the actual mass. For the same mass flow, a smaller percentage of the total mass leaves the volume in the heated case. Therefore, the pressure drop is expected to be lower than the theoretical pressure drop. This result is also apparent at all the different temperatures.

The heated driver tube air also seems to have little affect on the nature of the ac signal. Figures 101 and 102 show typical quiet and noisy ac traces. These are very similar to the unheated ac traces, which is expected. The heated data are analyzed in a similar manner as the unheated data (using the same analysis code from Appendix B). As before, the fitted electronic noise is subtracted off, and the RMS noise level and τ are calculated for each data segment.

Figure 103 is a plot of the RMS values versus the mean pressure, for each segment, for each driver tube temperature. In general, at each temperature the trend with pressure is similar, the noise level remains relatively constant and rather suddenly begins to increase at a particular pressure. However, there does not appear to be a smooth trend of the noise with increasing temperature. The 100 and 150 C data are similar to the unheated values, although they are slightly lower values at any given pressure. Unfortunately it does not appear that a strong conclusion can be drawn from these data alone since the trend with temperature is weak.

While examining figure 103 it was noticed that the pressures for the data segments seemed lower than they should be. For example, the maximum initial driver pressure for the 180 C data (recorded manually before the run) was 20.75 psi. However the maximum pressure for any 180 C segments inferred by calculating the stagnation pressure in front of the normal shock is only 19.5 psi. Some drop between the start-up and the first segment is expected, but over 1 psi is seems too large. Similarly for the 100 C data the maximum initial pressure was 20 psi, while the maximum plotted pressure is just under 18 psi. A similar difference of just over 2 psi occurs for the 150 C data as well. This problem coupled with the pressure signal in the first run of each data set prompted an investigation into the possible errors that could be encountered with the Kulite due to temperature.

3.8.1 Temperature effects on the Kulite Pressure Transducer

According to the specifications the Kulite transducer is temperature compensated between the temperatures of 26 to 82 C (80 to 180 F). There are two types of thermal drift, a zero shift and a slope shift. Within the compensated temperature range, the transducer will have a maximum zero shift of +/-2% full scale (25 psi in this case) per 100 F, while the slope can shift 5% per 100 F. Outside of this range, no guarantees are made and each transducer can shift differently. A 2% full scale shift would be 0.5 psi. This maximum shift is often more than 25% of the mean pressure during the run. This error would be carried back through calculations and could result in the same error when calculating the tunnel stagnation pressure from the stagnation pressure at the transducer. If the slope were also to shift, still more errors could occur.

Even though it is unlikely that this large of a shift could occur, it is apparent that some error is present. Figure 104 is a plot of the percent difference between the initial pressure read from the Paroscientific pressure transducer before the run, P_p, and the inferred tunnel stagnation pressure calculated from the measured pressure for the first data segment of each run, P_k. The difference is also adjusted for the pressure drop that would occur during a nominal start-up process (this drop is insignificant, the Matlab code is listed in Appendix B). The difference between the two pressures is surprisingly high and also has a large amount of scatter. Some of the baseline unheated runs (baseline unheated runs are runs 1-11) have errors as high as 10% or more. These runs are lower pressure runs where the initial pressure is below atmospheric. The percent difference varies from about 5% in some cases to as much as 20% in others and does not appear to have any specific trend. The first run in the 180 C data set seems to have shifted back to the original offset range of first unheated runs. This may be because the Kulite had 3 weeks between the last 150 C run and this run. All other runs were performed within 3 or 4 days after the last heated set. After the conclusion of the experiments, the transducer was returned to Kulite for a damage assessment. Kulite indicated that the RTV in front of the diaphragm had

separated from diaphragm. Air bubbles between the two are suspected as being a cause of zero shifts and other anomalies.

The Paroscientific pressure transducer is very accurate, thus the error is most likely caused by calibration shifts in the Kulite. Hopefully the error is caused by an offset shift rather than a slope shift. If this is the case, the ac signal is unaffected, since by definition the offset is zero. This does appear to be the case, since the factory calibration and calibrations performed in the course of this study all have the same slope, but different offsets (refer to figure 43). Thus, only the mean pressure must be dealt with.

Since a 15% discrepancy in the between the Kulite pressure and the actual pressure can significantly change the noise level comparisons, a more reliable mean pressure must be used. The only other possibility is the Paroscientific pressure transducer. The Paroscientific is a very accurate pressure transducer (+/-0.01% of the reading), which is why the Kulite is calibrated using it. It is connected to the tunnel via a pressure line, so it is not exposed to high temperatures like the Kulite. Unfortunately, the Paroscientific is a low frequency transducer and is not recorded during the entire run. Therefore only a pre-run initial driver-tube pressure is recorded. The only reasonable option is to use the theoretical pressure drop with time using the Paroscientific pressure as the initial pressure. This should have less of an error because the theoretical pressure drop was nearly identical with the pressure drop when compared in Schneider *et al.* (1996). The equation used to generate the pressure ratio is

$$\frac{p}{p_o} = \left\{ 1 + (\gamma - 1) A^* \left[g T_o \gamma \left(\frac{2}{\gamma + 1} \right)^{\frac{\gamma+1}{\gamma-1}} \right]^{1/2} \frac{t}{2V} \right\}^{\frac{2\gamma}{1-\gamma}} \quad \text{, and} \quad \frac{T}{T_o} = \left(\frac{p}{p_o} \right)^{\frac{\gamma-1}{\gamma}}$$

It must be assumed that the pressure drop comparison with theory in figure 50 is not as good because of the errors associated with the Kulite.

The theoretical pressure curve for each run was calculated using the theoretical pressure ratio drop and the initial pressure before the run. The original pressure curve was

still used to detect the expansion wave passage, but the mean theoretical pressures for each segment were calculated to use in the statistical analysis.

3.8.2 Comparison of Elevated Temperature Data Using Theoretical Pressure

Figure 105 is the same RMS data as figure 103 except it is plotted versus the theoretical pressure for the segment. A monatonic trend with temperature can now be seen. As the temperature is increased, the pressure where the noise level begins to rise also increases. The noise increase occurs at about 14.5, 15.5 and 18 psi for 100 C, 150 C and 180 C respectively. This would tend to indicate that the boundary layer on the nozzle wall is more stable as the temperature is increased, and thus transitions to turbulence at a higher pressure as the temperature is increased. One should note however that the 125 C data was not included in figure 105. This was because the 125 C data is believed to be corrupted by debris on the nozzle surface.

The 125 data was taken after the 100 C data without cleaning the nozzle in-between temperature changes. The 125 C data is believed to be corrupted because of unusually high noise levels at all pressures. Closer examination revealed that the noise level on the 2nd to last 100 C run was significantly higher than a previous run near the same pressure. Figure 106 shows the RMS levels for both data sets. The second to last 100 C run seems to group better with the 125 C data, which has a totally different trend (almost linear) with pressure than do any of the other data sets. The last 100 C run was at a higher pressure where the flow is normally noisy anyway, and thus it tends to blend in with the rest of the 100 C data. Because of these relationships, it appears that debris collecting on the nozzle surface eventually caused enough disturbances to prevent normal quiet flow operation of the tunnel.

After the 125 C data the tunnel was cooled and the unheated noise level was checked at atmospheric conditions. The RMS noise levels for two check runs were 0.25% of the mean pressure. This is more than twice the value normally found when operating at this location at atmospheric pressure. Dirt was found on the nozzle and the nozzle was

cleaned several times before the noise levels were found to be at normal levels. Because the 125 C data is corrupted by other disturbances, it is not useful for comparisons in this study and therefore will not be included in further analysis.

Continuing with the comparison of the 100, 150 and 180 C data, similar results to figure 105 are found using the second method of determining quiet flow. Figure 107 is a plot of τ versus the theoretically calculated pressure. The percentages are very low up to a particular pressure, but increase dramatically from that point. This figure also supports a conclusion that increased temperature improves the quiet flow range of the Ludwieg Tube.

The increasing temperature may raise the operating pressure at which quiet flow can be achieved, but its affect on the quiet flow region is yet undetermined. The quiet flow region is usually measured by the quiet flow Reynolds number, or the maximum length Reynolds where quiet flow conditions exist. This is because of the desire to match flight Reynolds numbers under quiet flow conditions. As with most wind tunnels, the quiet flow Reynolds numbers in the Purdue Ludwieg Tube are much lower than flight. Thus it is hoped that the increased maximum quiet flow pressure will increase the Reynolds number compared to unheated operations. However one must remember that the higher temperatures also means lower density and higher viscosity.

The unit Reynolds number was calculated using the tunnel conditions.

$$\frac{Re}{L} = \frac{\rho_\infty U_\infty}{\mu_\infty} \text{ where } \rho_\infty = \frac{P_0}{RT_0(36.15)},\ U_\infty = 4\sqrt{\gamma R \frac{T_0}{4.2}} \text{ and}$$

$$\mu_\infty = \mu_r \left(\frac{T_0}{4.2T_r}\right)^{1.5} \frac{T_r + 111}{\frac{T_0}{4.2} + 111} \text{ (Sutherland's Law)}$$

The stagnation values are shown in the equations with appropriate Mach 4 expansion ratios to convert them to freestream conditions. This was shown because the stagnation conditions are already measured. T_r and μ_r are reference values for temperature and viscosity used to calculate a viscosity at a non-reference temperature. The theoretical pressure value for each segment was used as the pressure and total temperature was found

using the theoretical drop for temperature and the maximum temperature recorded by the CCA. The theoretical temperature drop was used to simplify the calculations. It had to be used for the unheated data since only an initial temperature was recorded. This doesn't really affect the data where the total temperature was recorded since the theoretical curve agrees very well with the calculated temperature ratio (see section 3.6). This did allow the theoretical curve and an estimated maximum temperature to be used for the 180 C data. This is because the temperature data in the 180 C case is not correct (see section 3.6). The maximum temperature was estimated to be 165 C which is similar to the temperatures recorded before the errors occurred.

Figure 108 is the percent RMS of the fluctuations vs. the length Reynolds number. Even if the 180 C data is not included it can be seen that with increasing temperature the maximum quiet flow unit Reynolds number decreases. The unheated data shows a maximum at about 400,000 which is comparable to previous experiments (Schneider and Haven 1995). The 100 C data is slightly lower at about 375,000 while the 150 C data is lower yet at around 340,000. If the 180 C data is assumed reasonable with the temperature estimate, its maximum quiet-flow Reynolds number is about 330,000. Error bars are also shown for selected data points. The bars are the maximum difference that results from using the theoretical pressure and temperature as opposed to the Kulite pressure and cold wire temperature in the Reynolds number calculations. The small bars represent data at the beginning of the run, where the only difference between the two methods is the initial pressure. The large bars represent data at the end of a run where there is some difference between the Kulite pressure ratio and the theoretical pressure ratio (refer to figure 50). Any increase in Reynolds number that could have been gained by increased pressure seems to be offset by an increase in viscosity and a decrease in density at the elevated temperatures. As temperature increases, the Reynolds number where a particular noise level occurs decreases. This implies that the wall boundary layer transitions to turbulence at a lower Reynolds number when the driver air is heated.

Similar results are deduced from figure 109 which is a plot of τ versus unit Reynolds number. It definitely appears that the flow is affected by the increasing

temperature. To make sure the data show a definite trend, the RMS values are plotted again in figure 110. However, only the first two data segments for each run are plotted. This excludes the data associated with the larger error bars. The 180 C data is also removed from this figure since the temperatures are ambiguous for this data set. The remaining data still show the decrease in Reynolds number with increasing temperature.

A comparison can be made with Harvey *et al.* (1975). At Mach 5, a 20% increase in transition Reynolds number was obtained by heating the nozzle to a wall-to-total temperature ratio of 1.4. In this experiment, heating the air is similar to cooling the nozzle wall. An accurate temperature map of the nozzle surface was not obtained, but the nozzle temperature was recorded for each run at approximately z=9.0 inches downstream of the throat. Thus an estimate of the wall-to-total temperature can be calculated. For the 100 C data, the wall-to-total temperature ratio was 0.89, and a 7% drop in quiet-length Reynolds number occurred. The 150 C data had a temperature ratio of 0.85 and a corresponding drop of 15% in quiet-length Reynolds number.

Since the data at 180 C was not completely accurate, it was hoped to repeat some of the data and confirm the unit Reynolds number decrease at 180 C. However problems with the Kulite pressure transducer prevented this. During some runs after the 180 C the Kulite appeared to be failing. Since there were no other pressure transducers readily available for use in these experiments an evaluation of the Kulite began in an attempt to correct the problem and collect more data.

3.9 Discussion of the Possible Failure of The Kulite Pressure Transducer

It is apparent that the Kulite pressure transducer did not perform as well as hoped for the experiments. In fact, some of the data was to be repeated to try to remove some of the problems that occurred with the pressure, and to also confirm some temperature data. However, after the runs at 180 C the Kulite began to show signs of failing. After cooling, the tunnel was cleaned and runs were made without heat to verify the baseline noise level. During these runs, the Kulite apparently was measuring extremely large

fluctuations during the run on the order of 3 psi peak to peak. Barring some extreme problem in the tunnel, these fluctuations are obviously incorrect. A second pressure transducer was used to verify that the tunnel indeed did run properly and achieve Mach 4 flow. The large fluctuations were present in several runs, and eventually most possible causes were ruled out; including large debris causing blockage upstream, a scratch in the nozzle or contraction, and blockage downstream in the vacuum section. The Kulite was removed from the tunnel and a hot wire was used to sense the fluctuations in the freestream near the same location. The hot wire did not show the same fluctuations, in fact, it indicated that the flow was relatively low noise. The cause for the fluctuations appeared to be failure of the transducer.

The transducer was re-installed and calibrated several times without heat. These calibrations were all very similar, but they differed from previous calibrations. The offset had changed by about 0.5 psi (figure 111). According to other experimenters who had used Kulite pressure transducers, this shift was typical when a Kulite began to fail. Unfortunately no other pressure transducers were available to install in the probe and repeat any data. All others were currently being used, and the risk of causing a second transducer to fail was too great. The failure mode of the transducer was not known, it was been returned to the manufacturer to determine the cause. According to the manufacturer, the RTV coating over the sensing diaphragm separated from the diaphragm. Apparently the RTV causes the fluctuations when it vibrates.

It is possible that the high temperatures caused the failure. The specified maximum temperature is 120 C, but through correspondence with technical staff at Kulite, the short duration at the higher temperatures should not have caused the failure. The tip of the probe was inspected for damage under a microscope. Some small paint flakes could be seen stuck in the RTV coating over the diaphragm, but this has also been observed in Kulites that have not failed. At this point, taking more data was no longer a viable option due to the failure of the Kulite, the need for other experimenters to use the facility, and the need to complete the project.

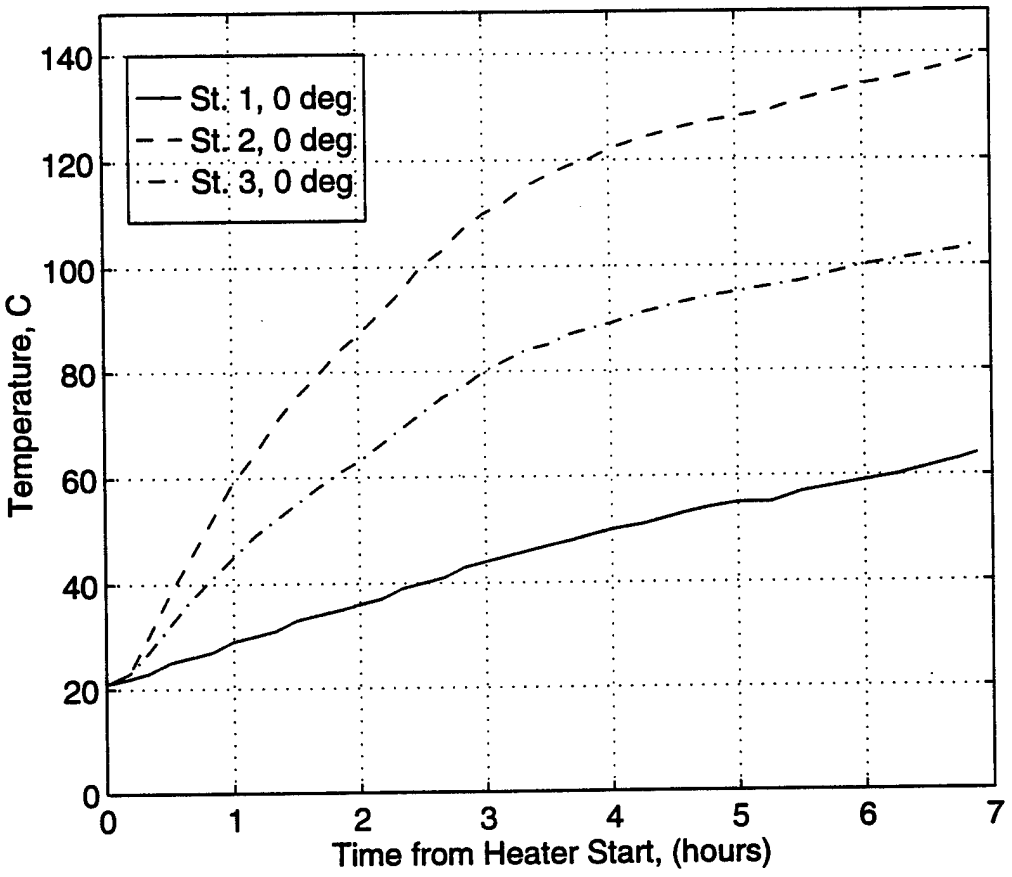

Figure 31 Initial Heating Test

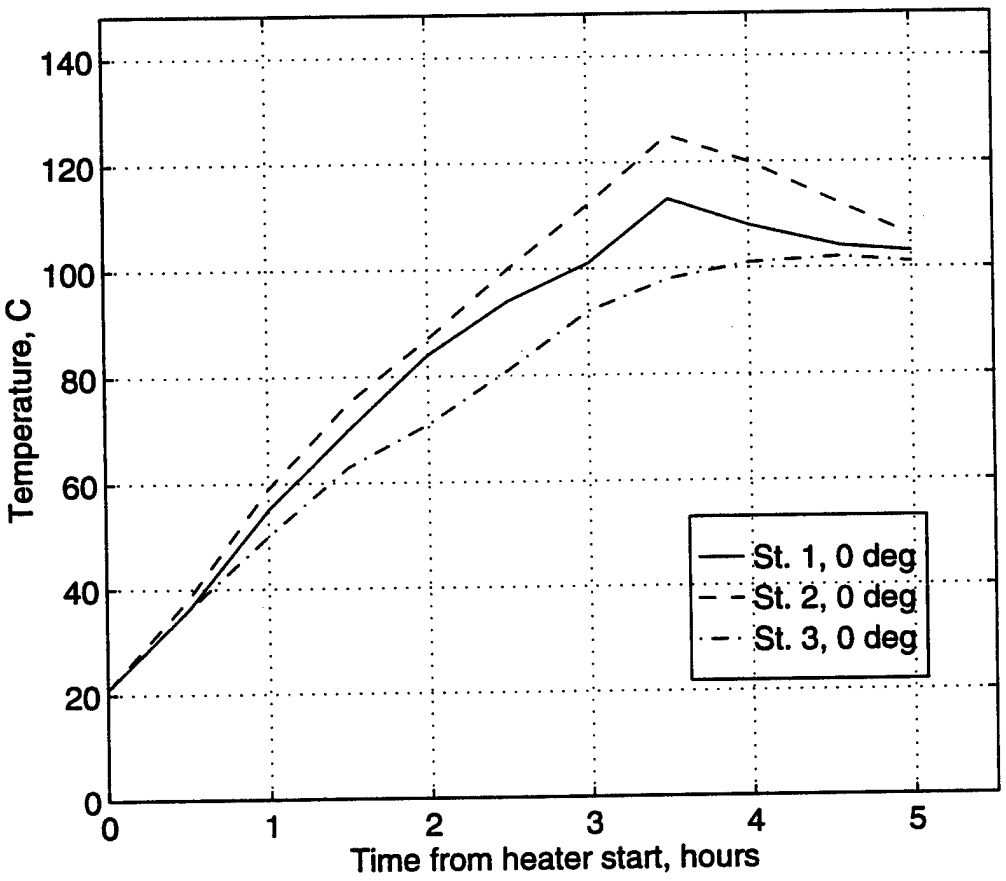

Figure 32 Heating Test After Installation of Flange Heater

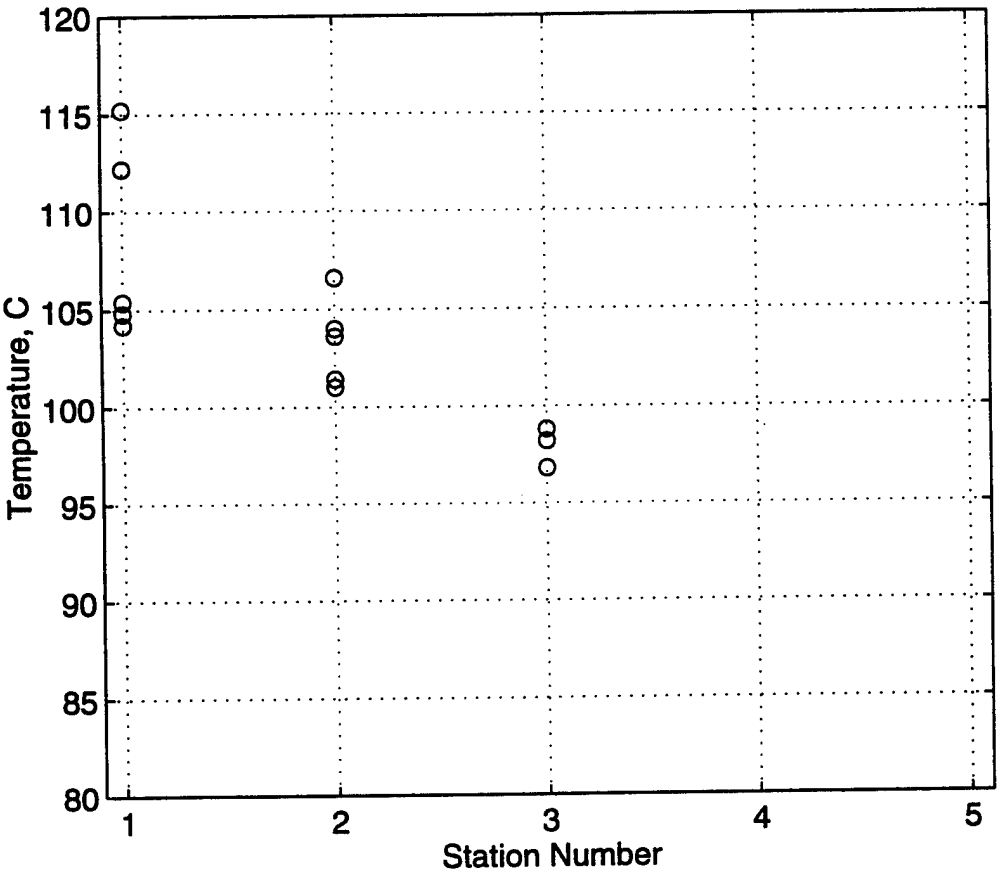

Figure 33 Thermocouple Temperature vs. Station, 100 C

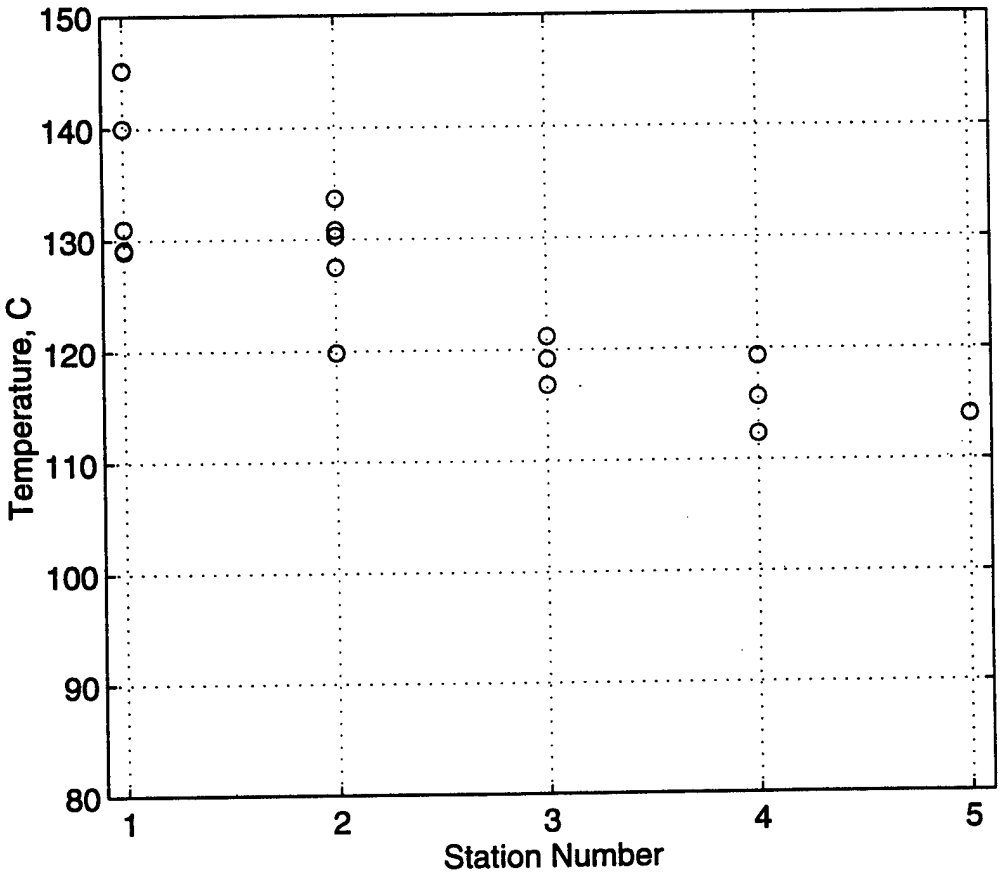

Figure 34 Thermocouple Temperature vs. Station, 125 C

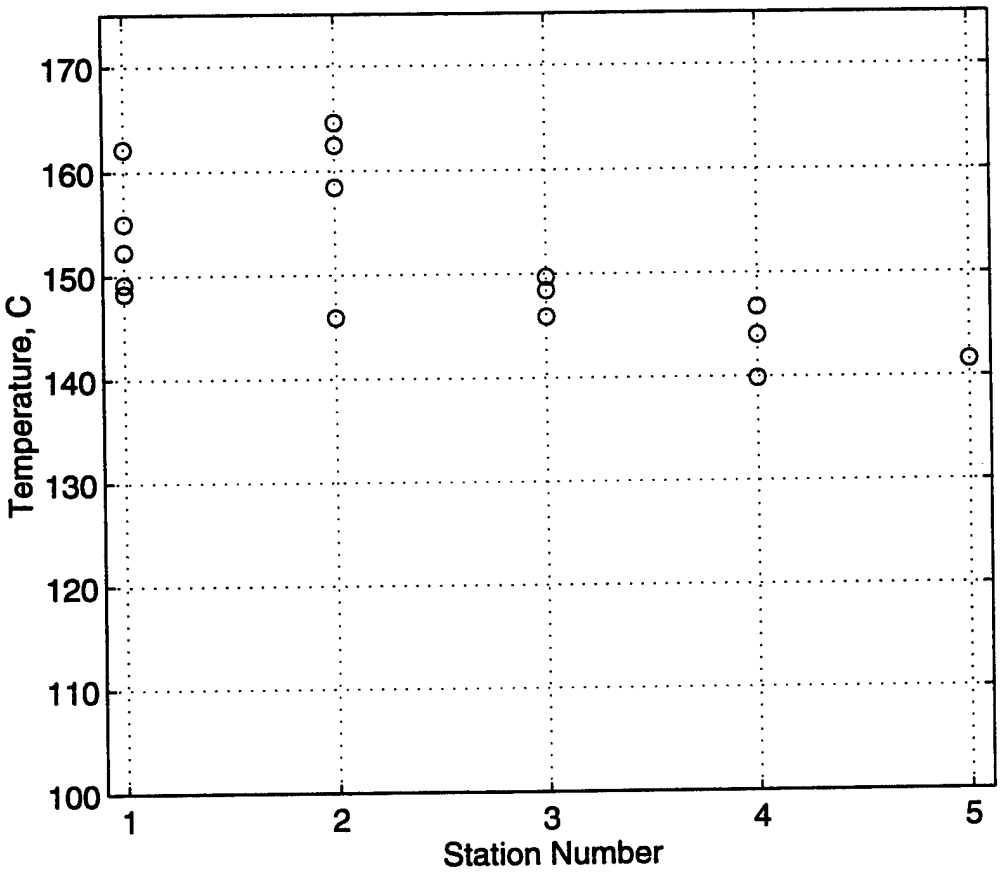

Figure 35 Thermocouple Temperature vs. Station, 150 C

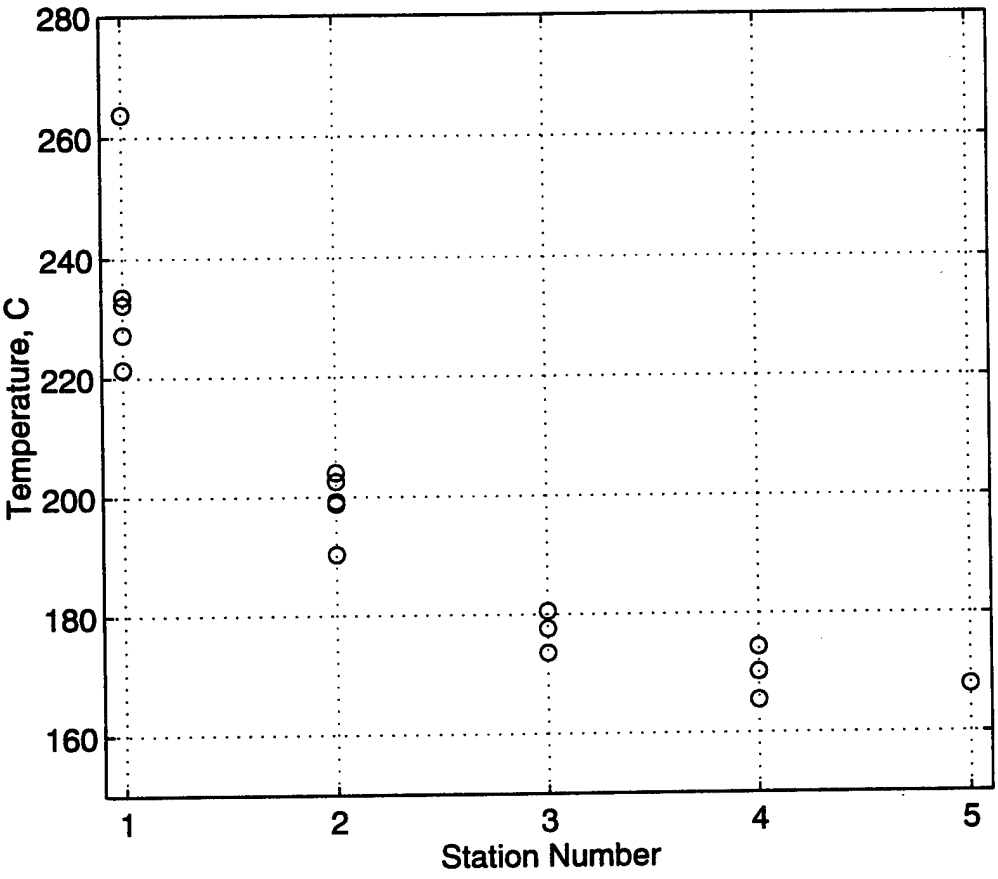

Figure 36 Thermocouple Temperature vs Station, 180 C

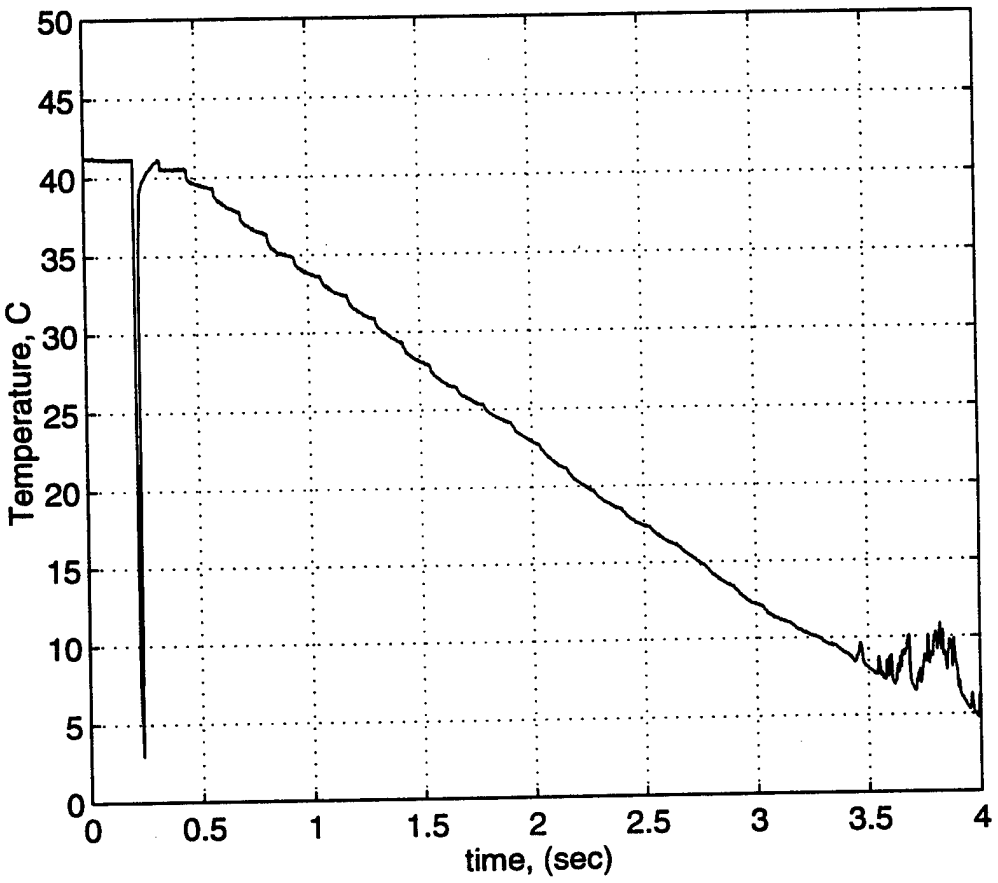

Figure 37 Temperature vs. Time, unheated

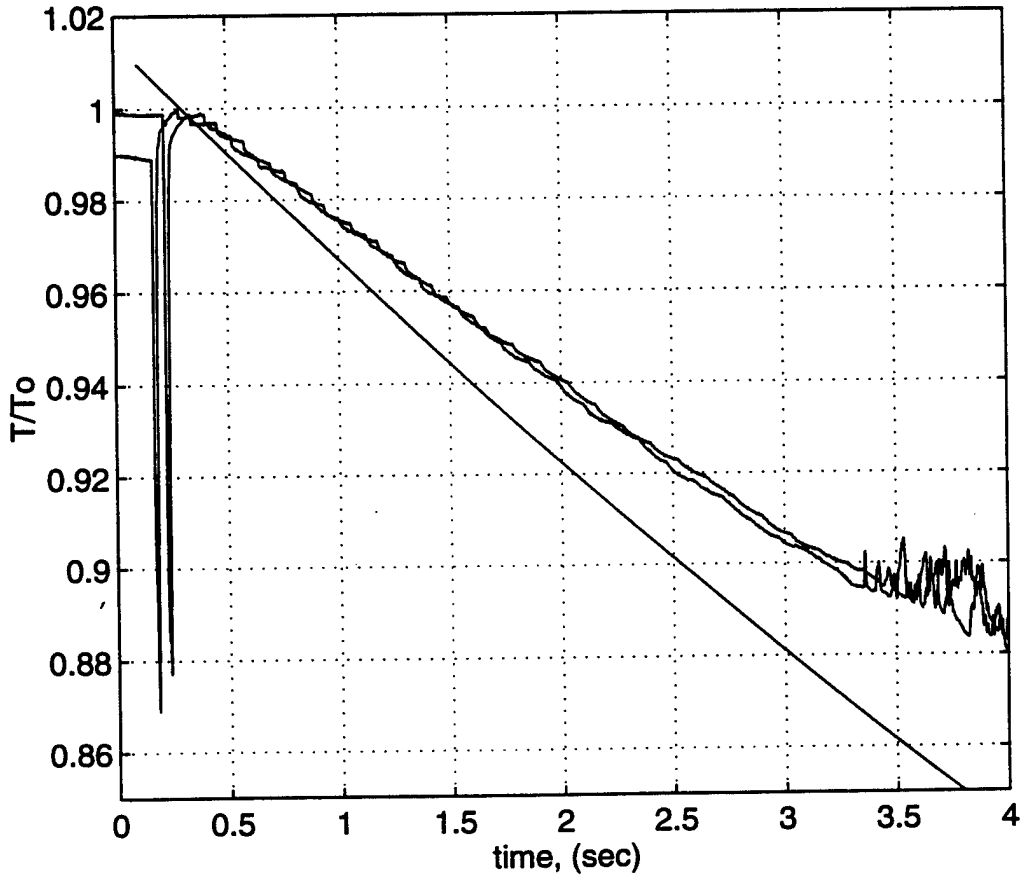

Figure 38 Normalized Temperture Comparison to Theory

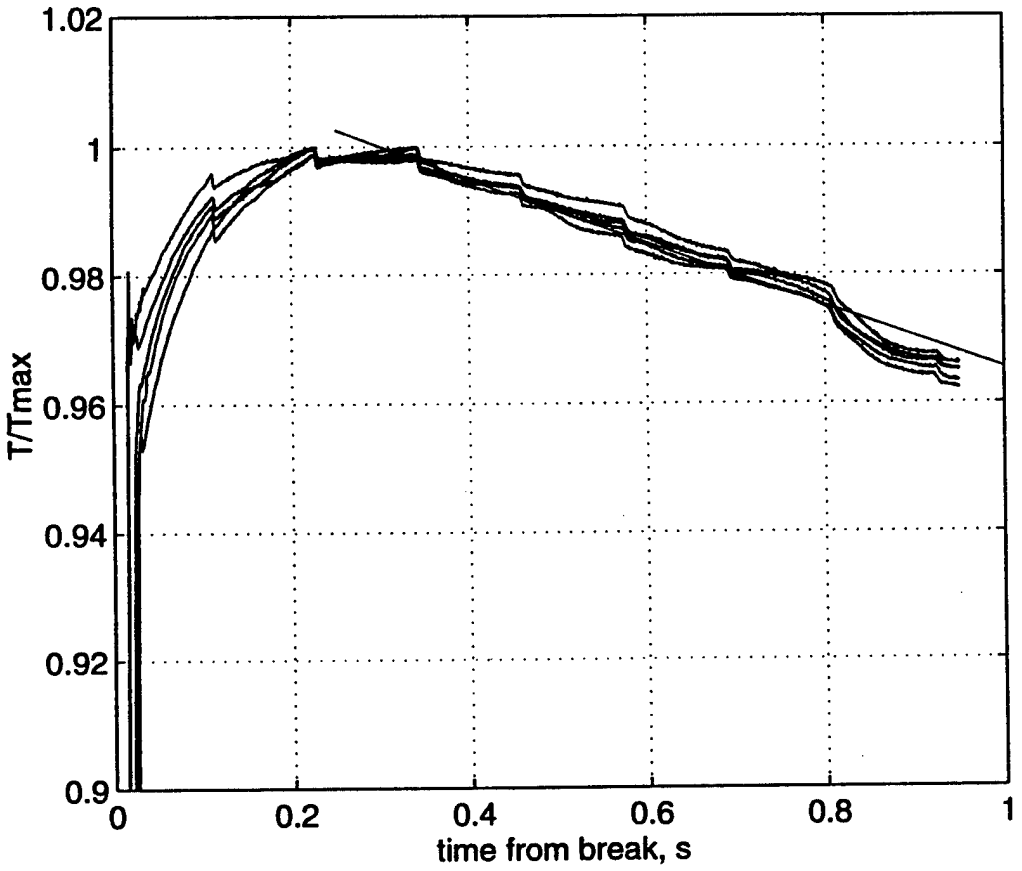

Figure 39 Normalized Temperature Comparison to Theory, Heated

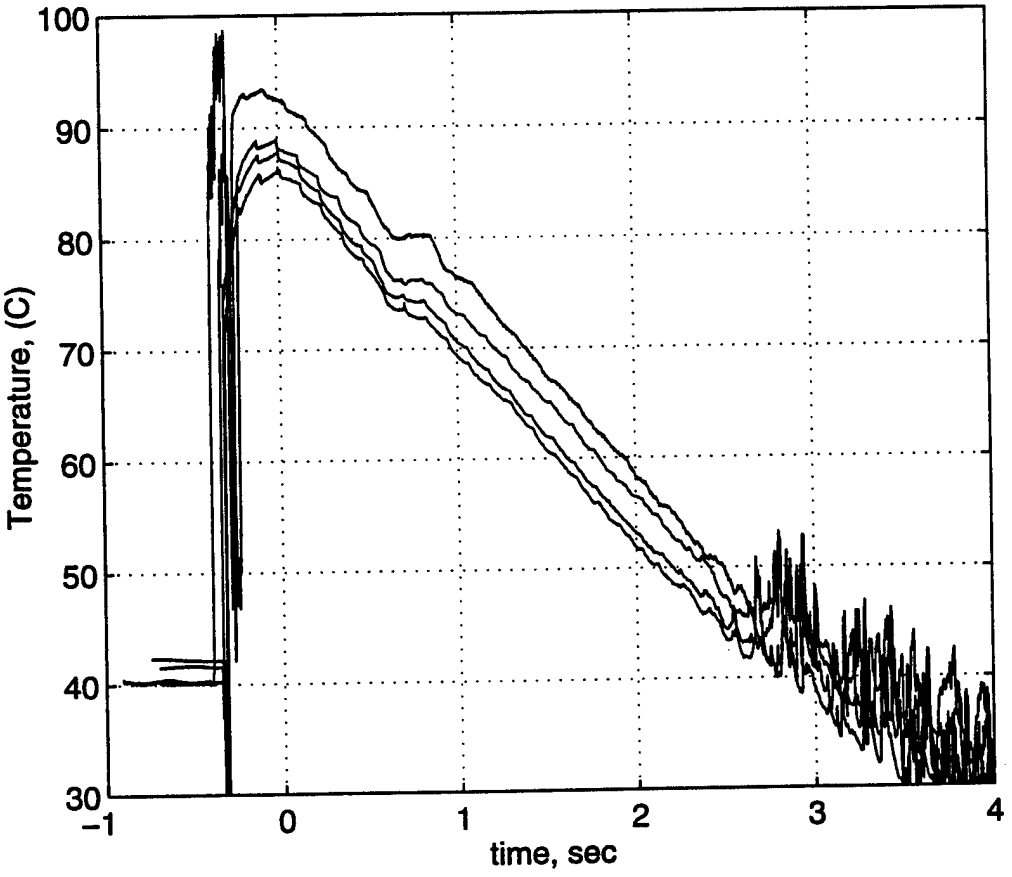

Figure 40 Heated Runs with Different Settling Times

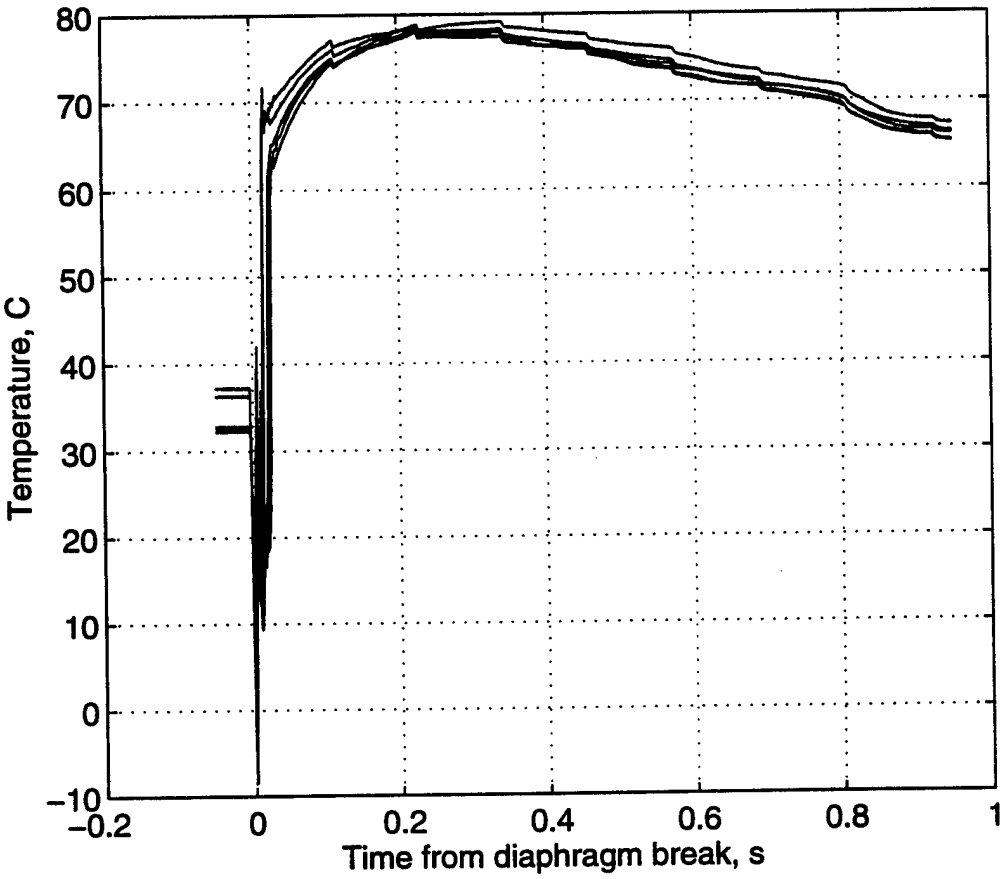

Figure 41 Heated Runs After Installation of Circulation Heater

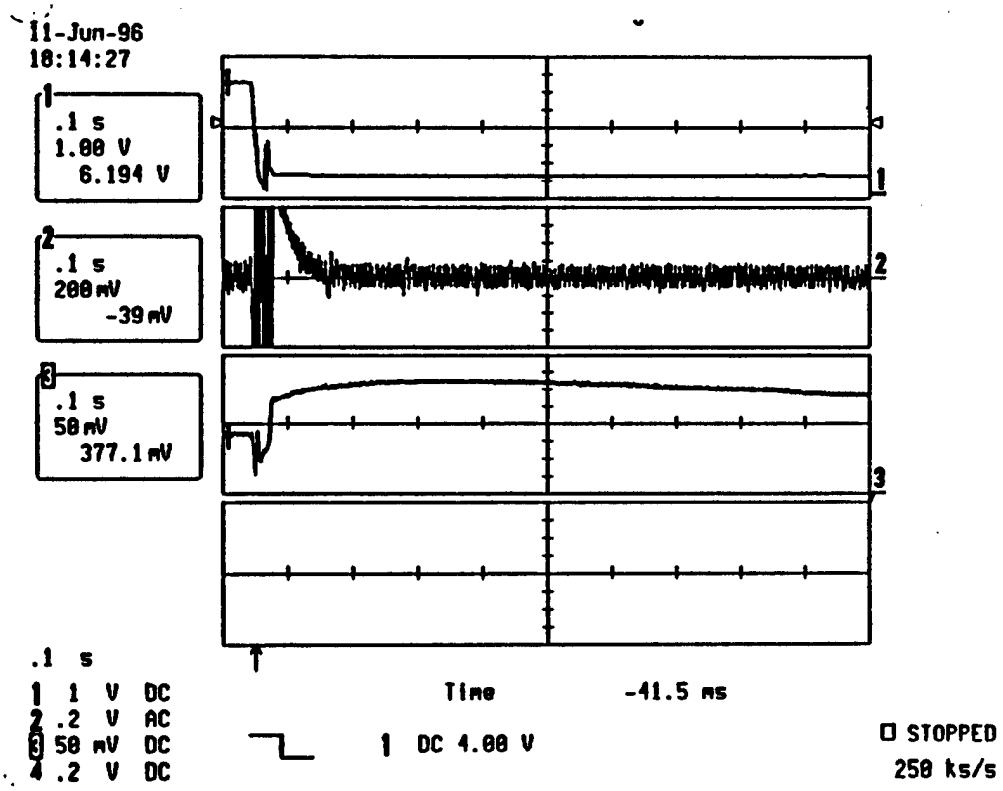

Figure 42 Sample Oscilloscope Screen Dump

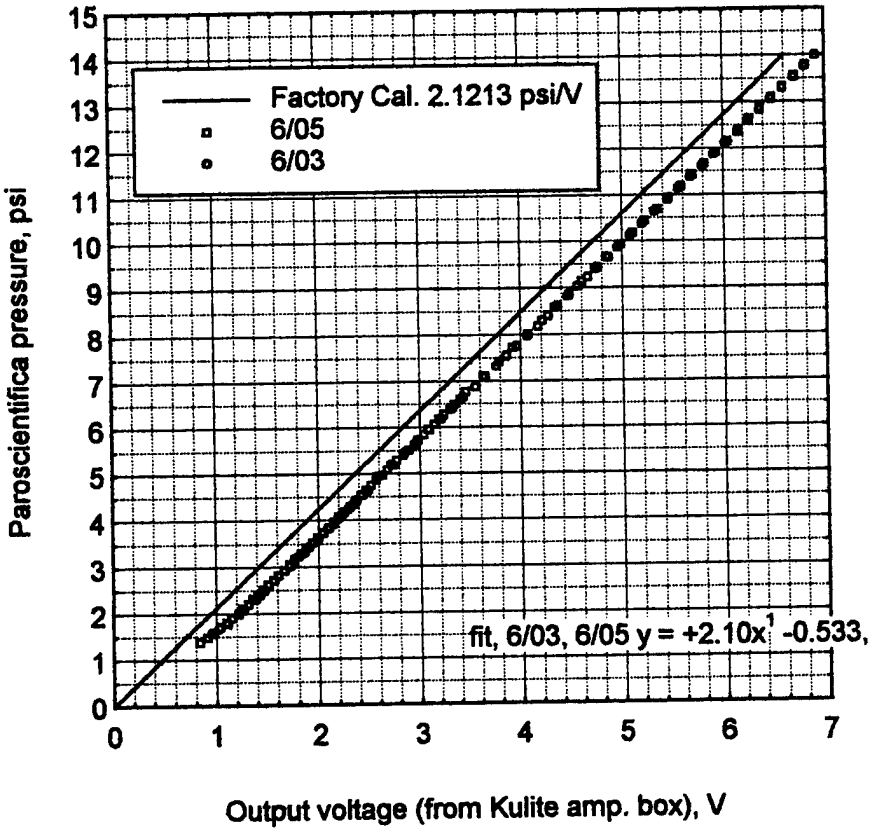

Figure 43 Kulite Pressure Transducer Calibration

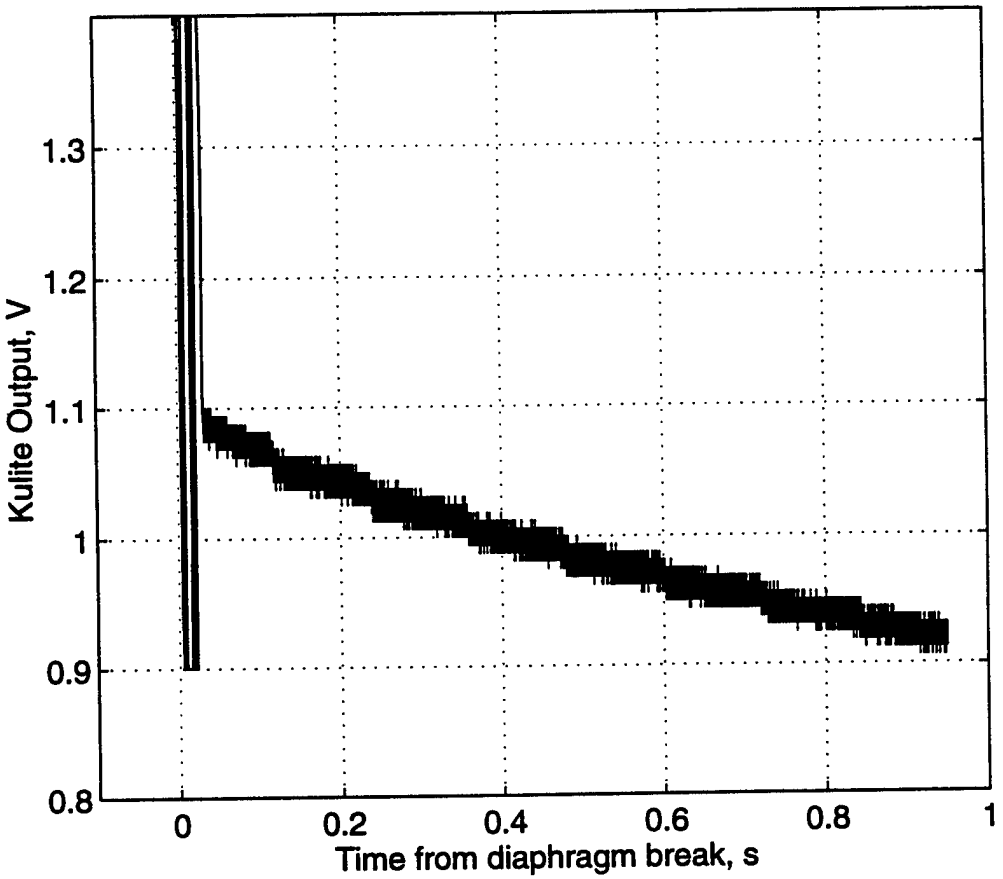

Figure 44 Sample Kulite Output

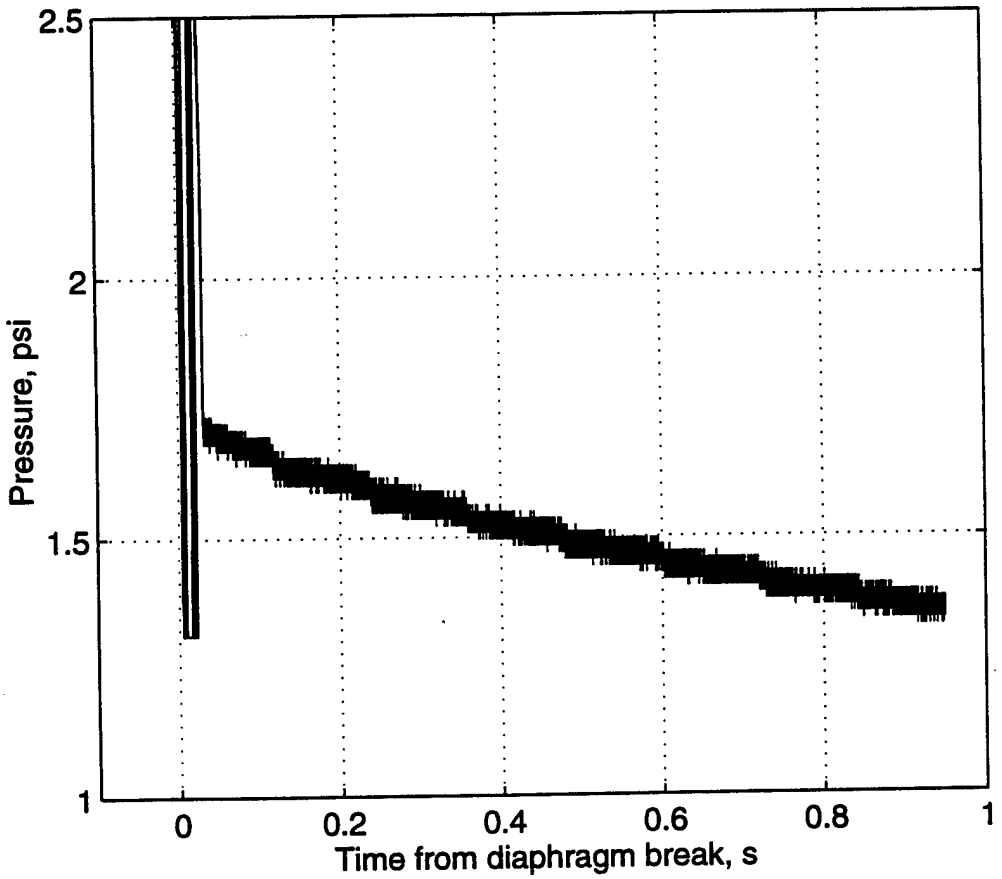

Figure 45 Sample Kulite Pressure Trace

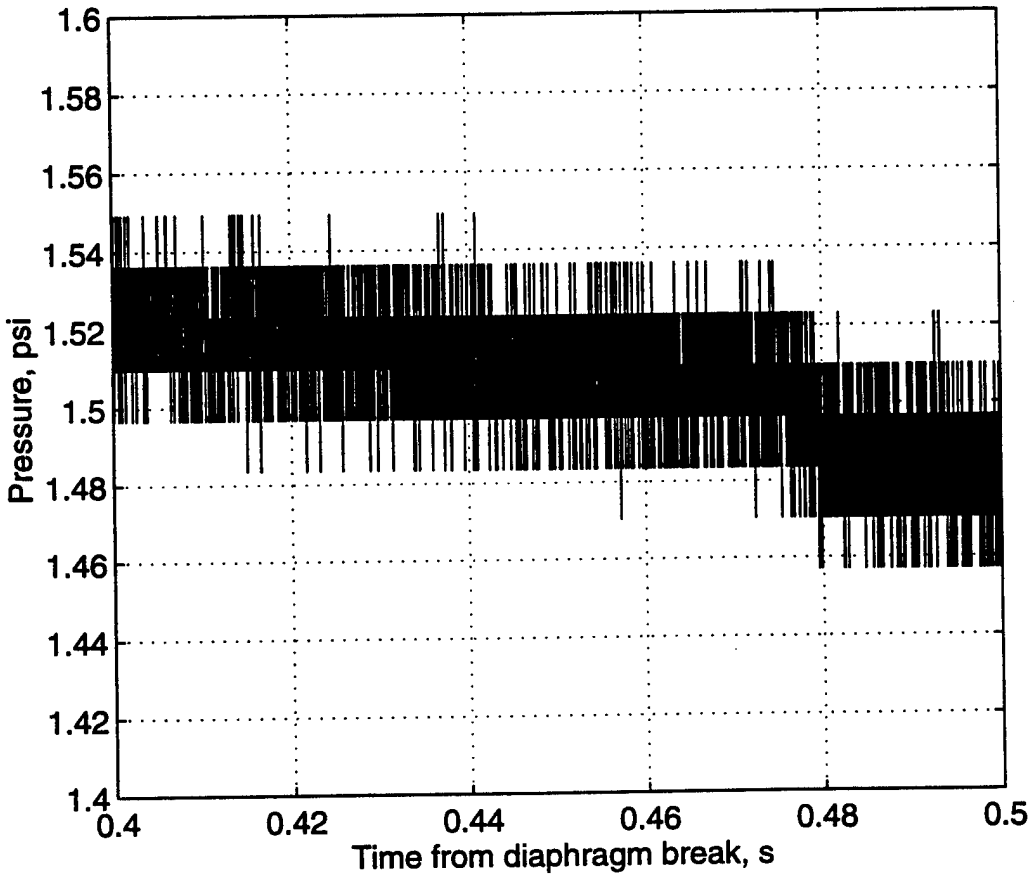

Figure 46 Zoom of Pressure Trace

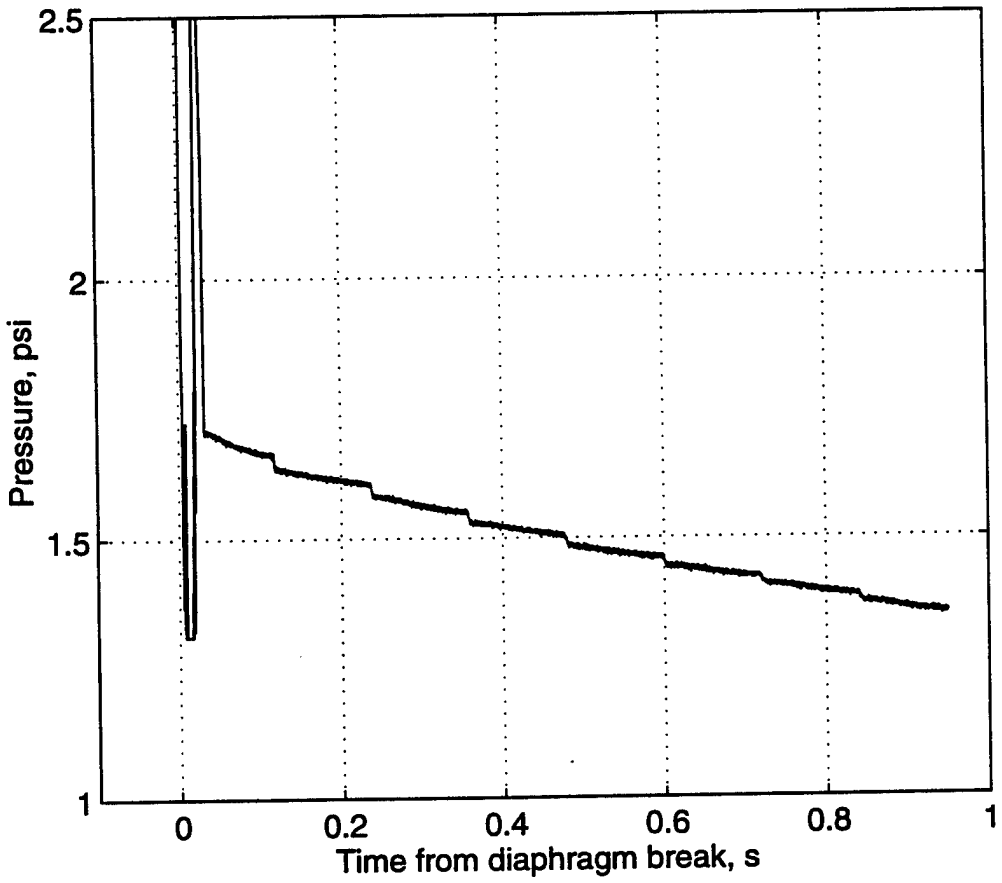

Figure 47 Example of Smoothed Pressure Trace

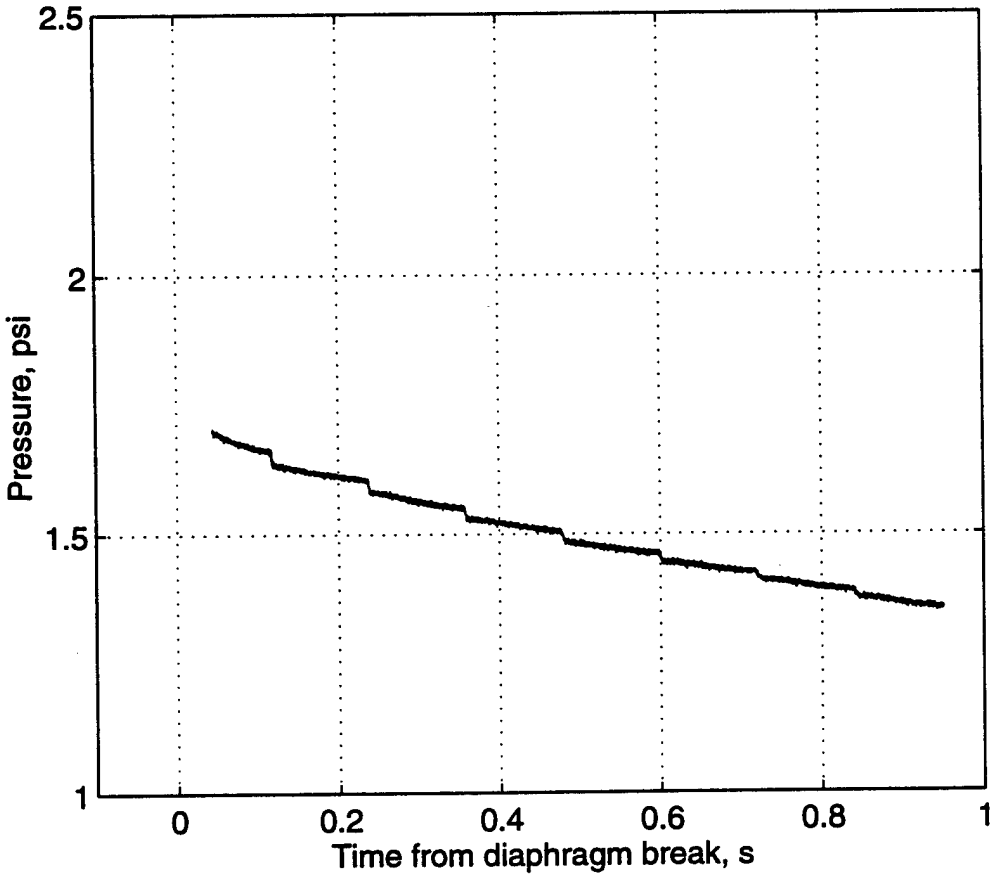

Figure 48 Pressure Trace with Start-up Removed

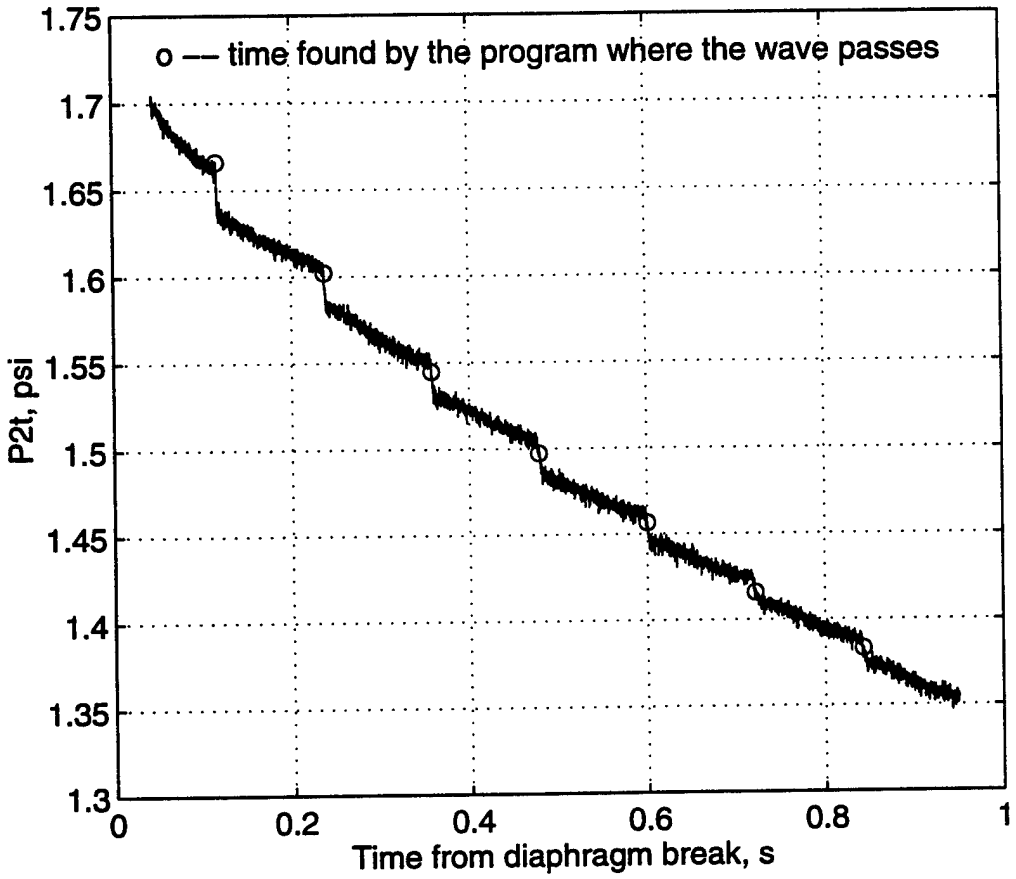

Figure 49 Pressure Trace with Segment Times

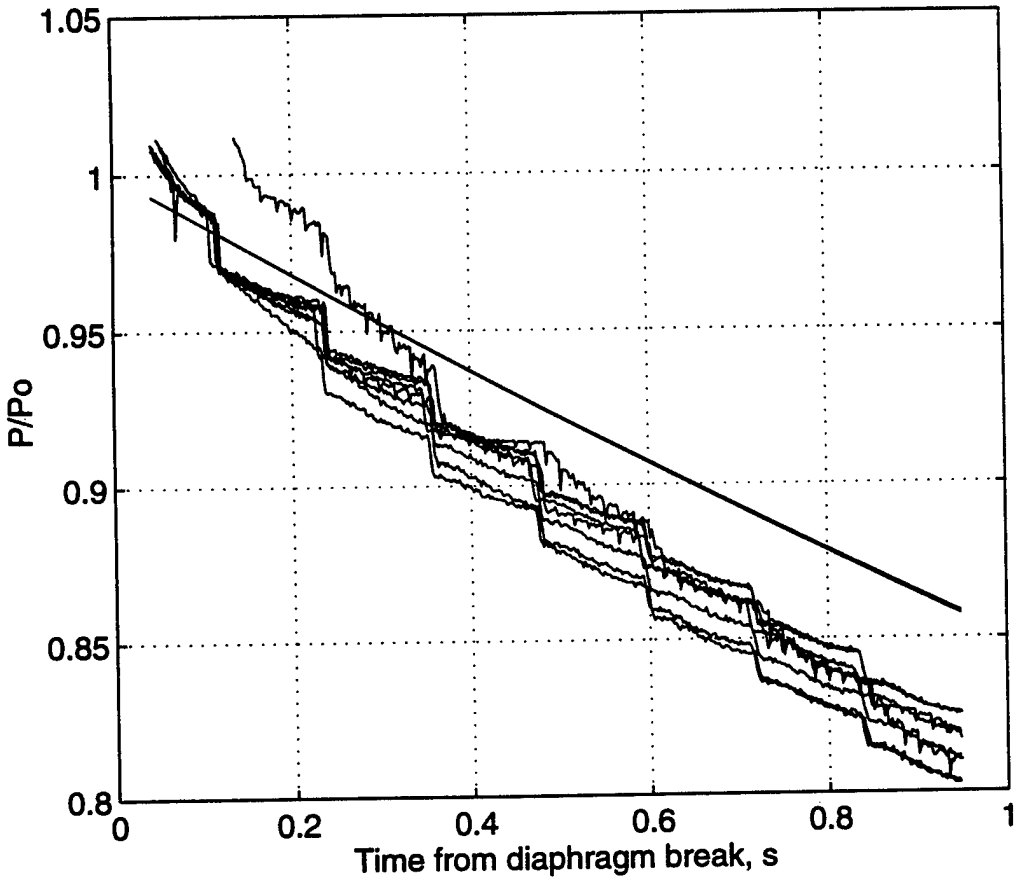

Figure 50 Normalized Pressure Comparison to Theory, Unheated

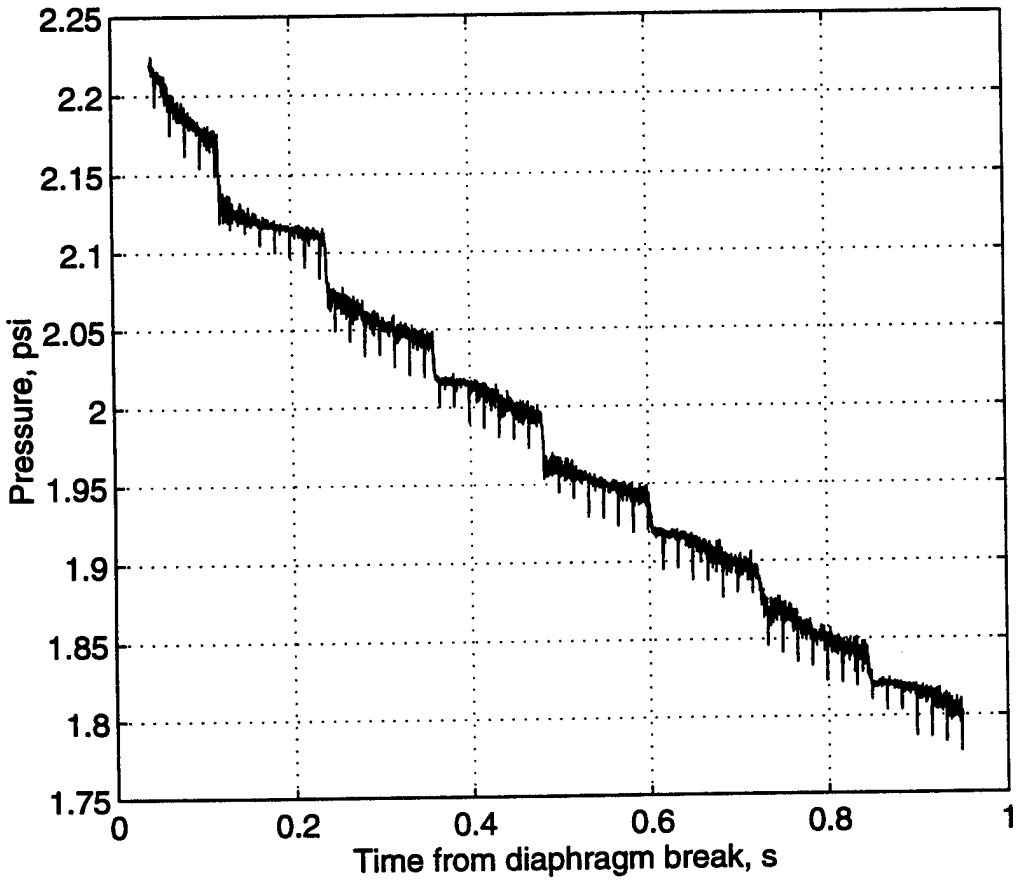

Figure 51 Example of 60 Hz Noise in Pressure Signal

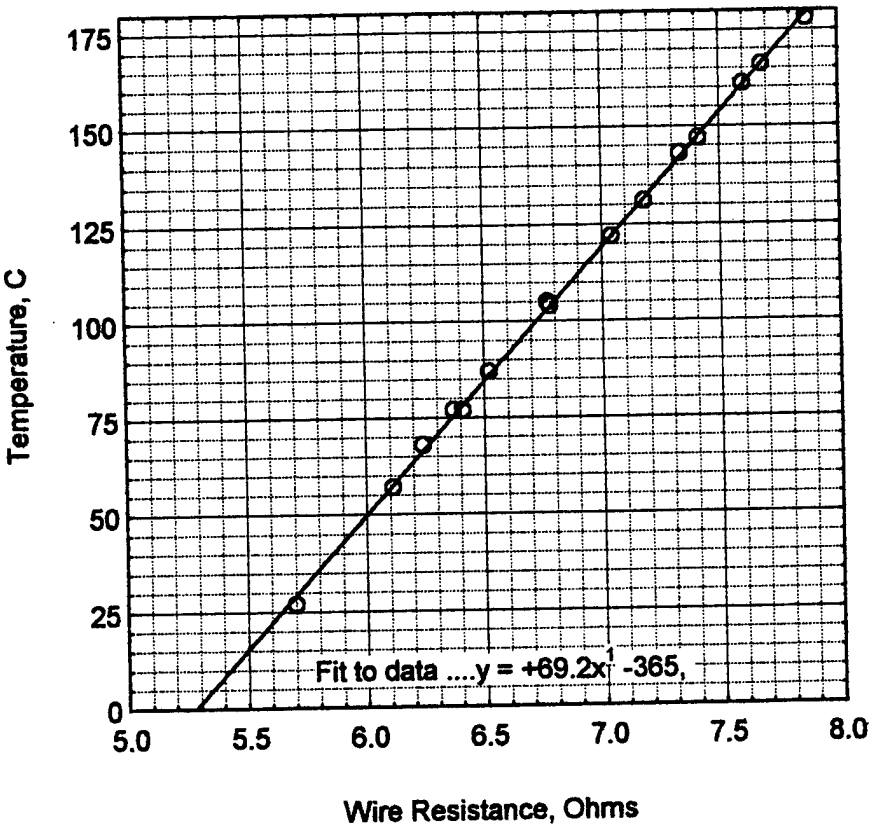

Figure 52 Cold Wire Calibration, Temperature vs. Resistance

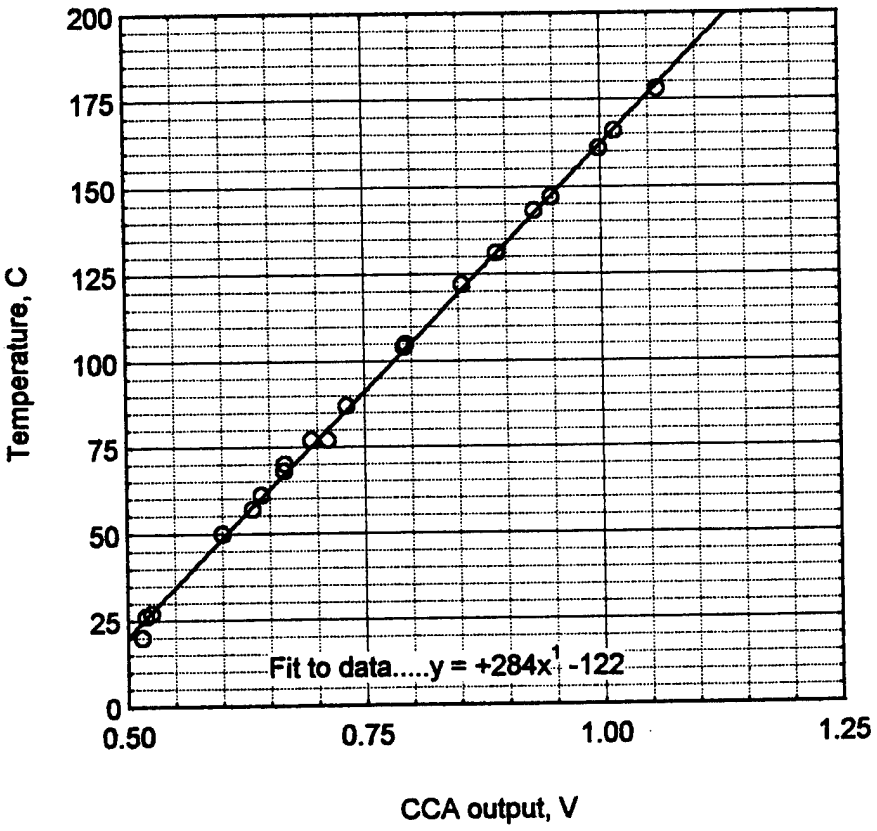

Figure 53 Cold Wire Calibration, Temperature vs. CCA Output

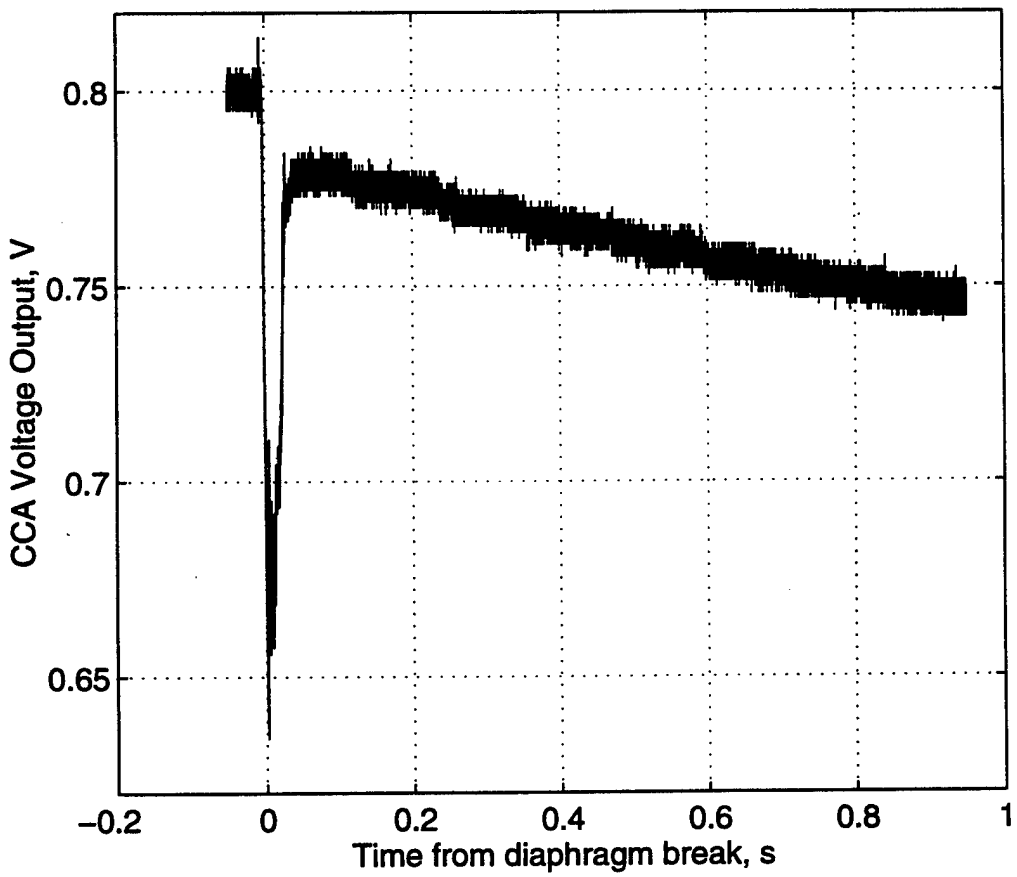

Figure 54 Sample CCA Voltage Output

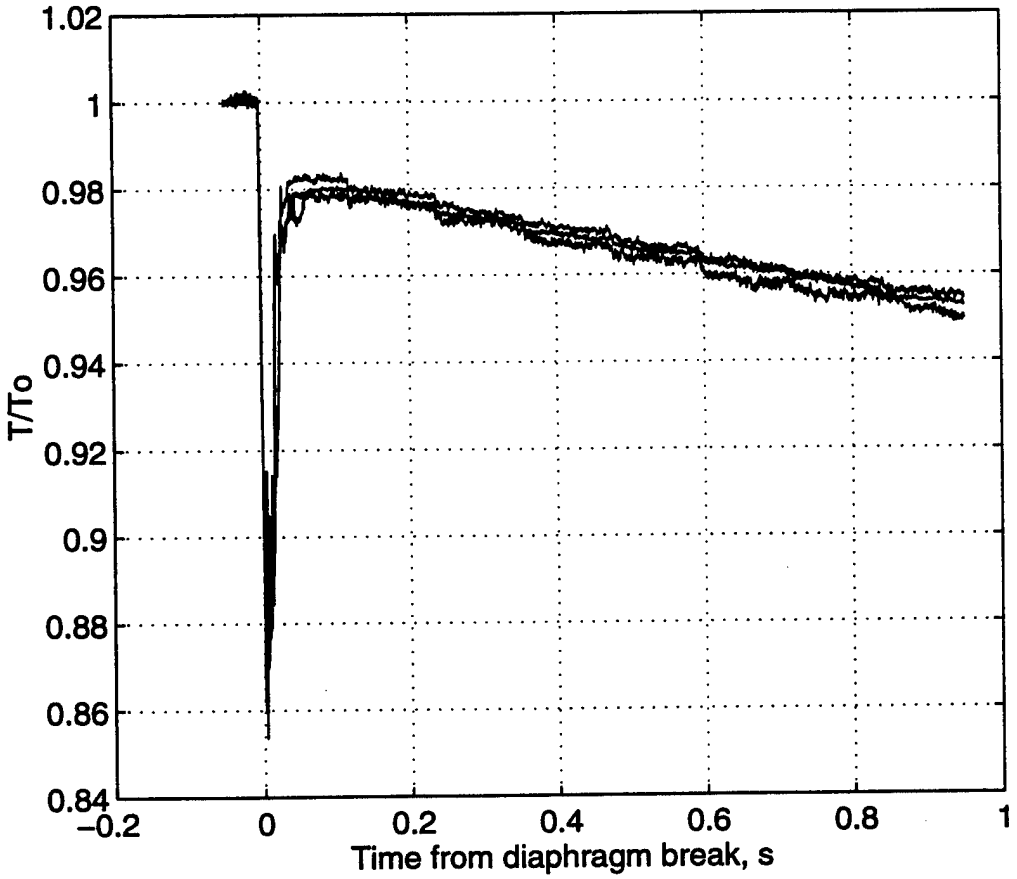

Figure 55 Normalized Temperature Showing Recovery Factor

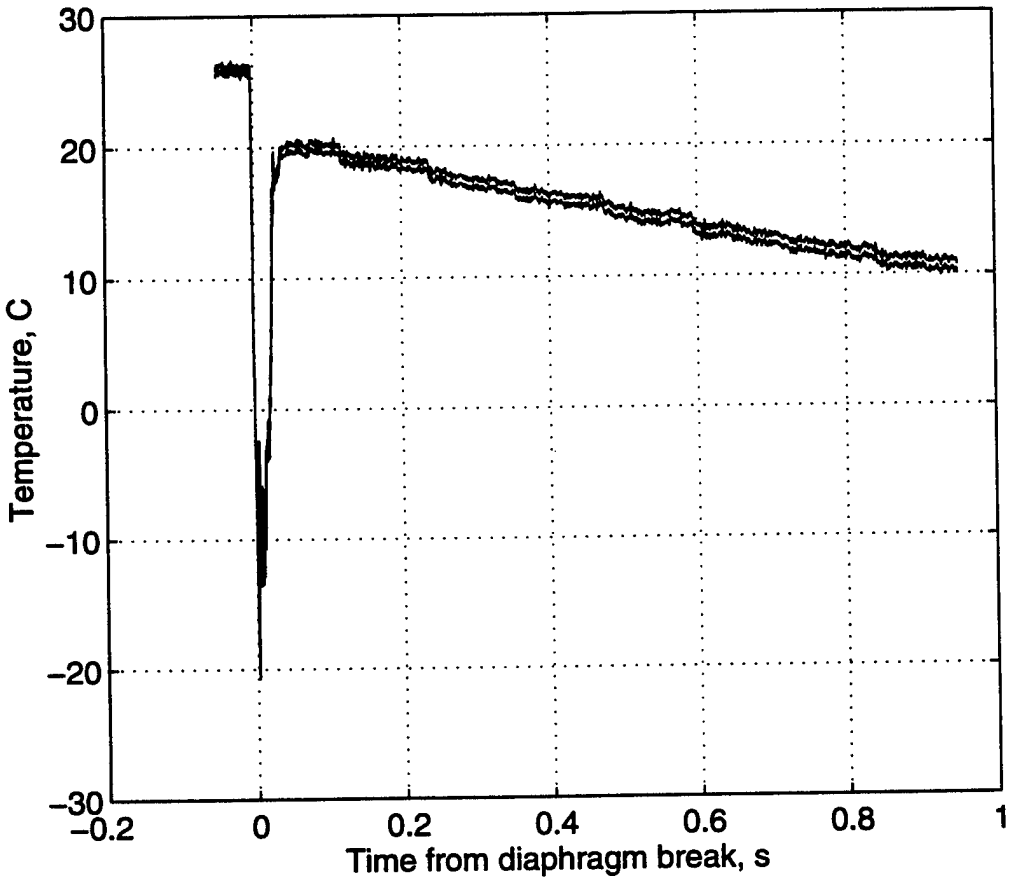

Figure 56 Comparison of Cold Wire Calibration Methods

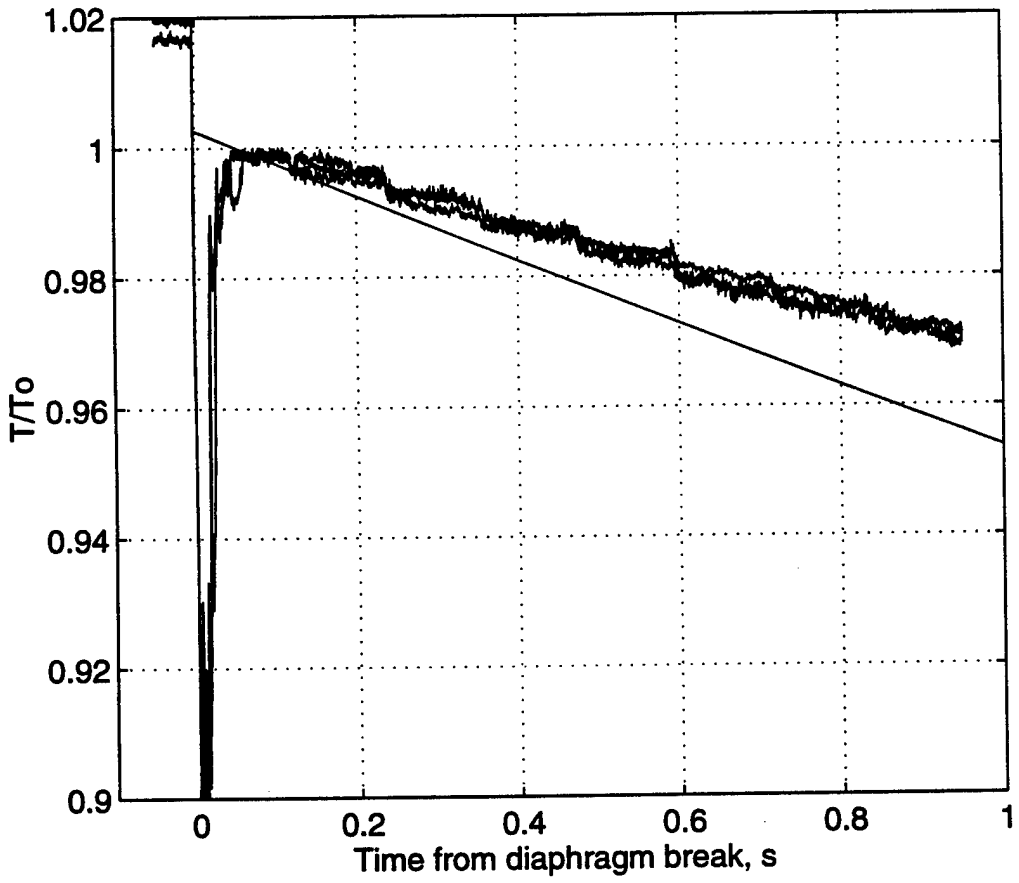

Figure 57 Normalized Temperature Comparison with Thoery

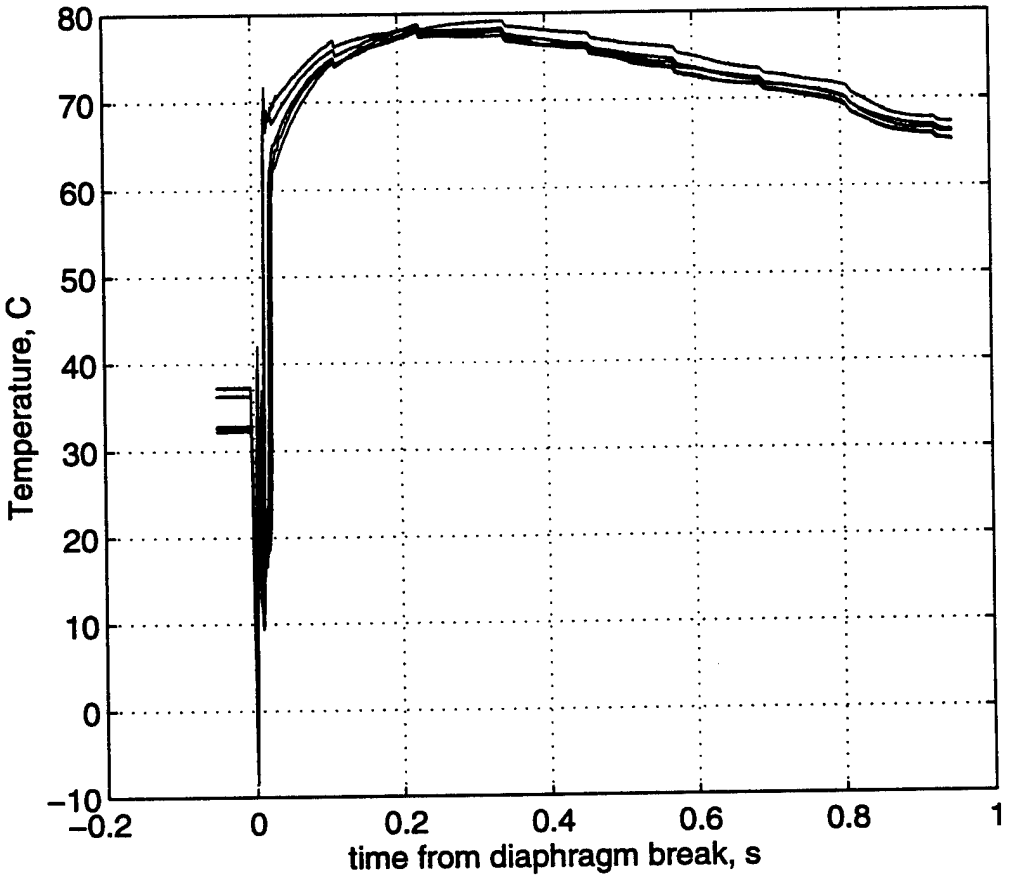

Figure 58 Temperature vs. Time, 100 C

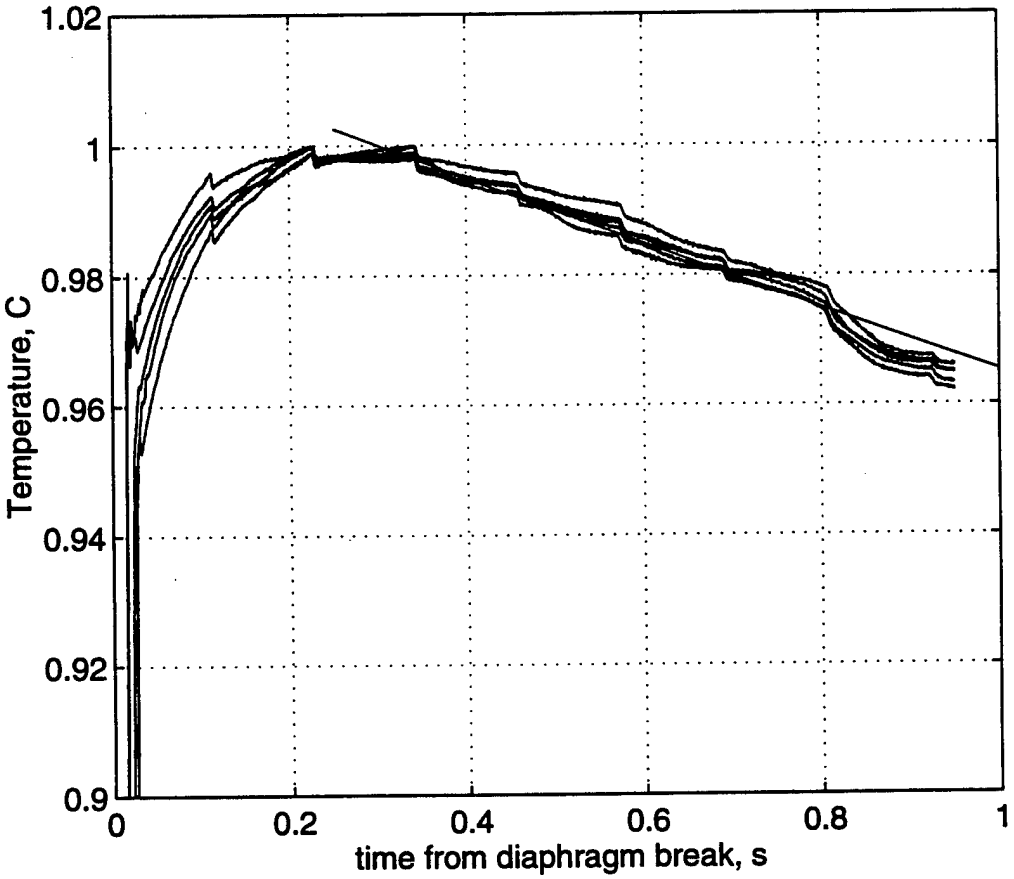

Figure 59 Normalized Temperature Comparison with Theory, 100 C

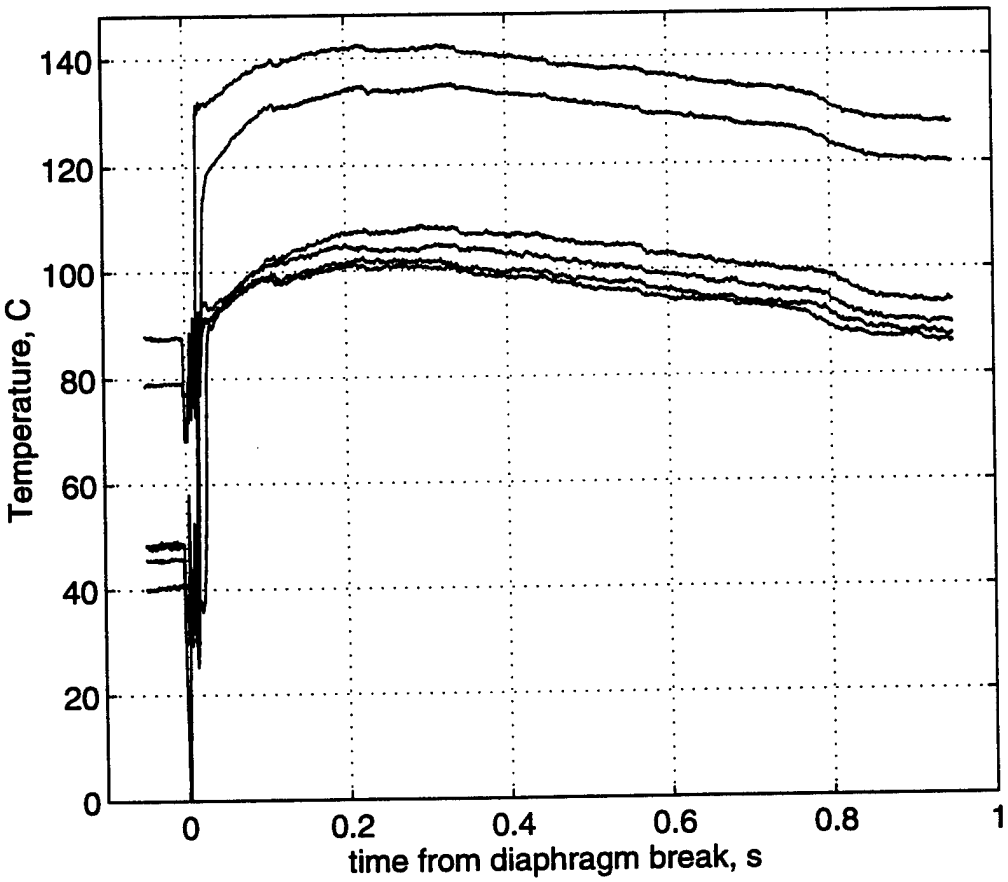

Figure 60 Temperature vs. Time, 125 C

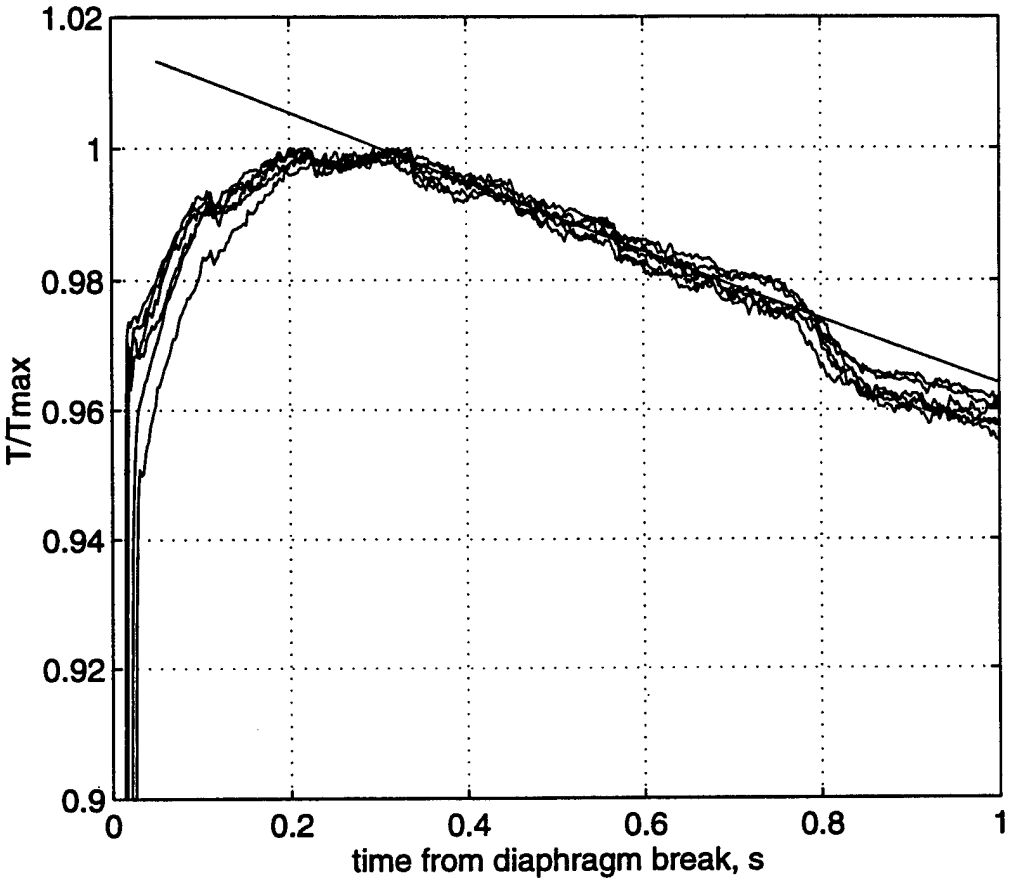

Figure 61 Normalized Temperture Comparison with Theory, 125 C

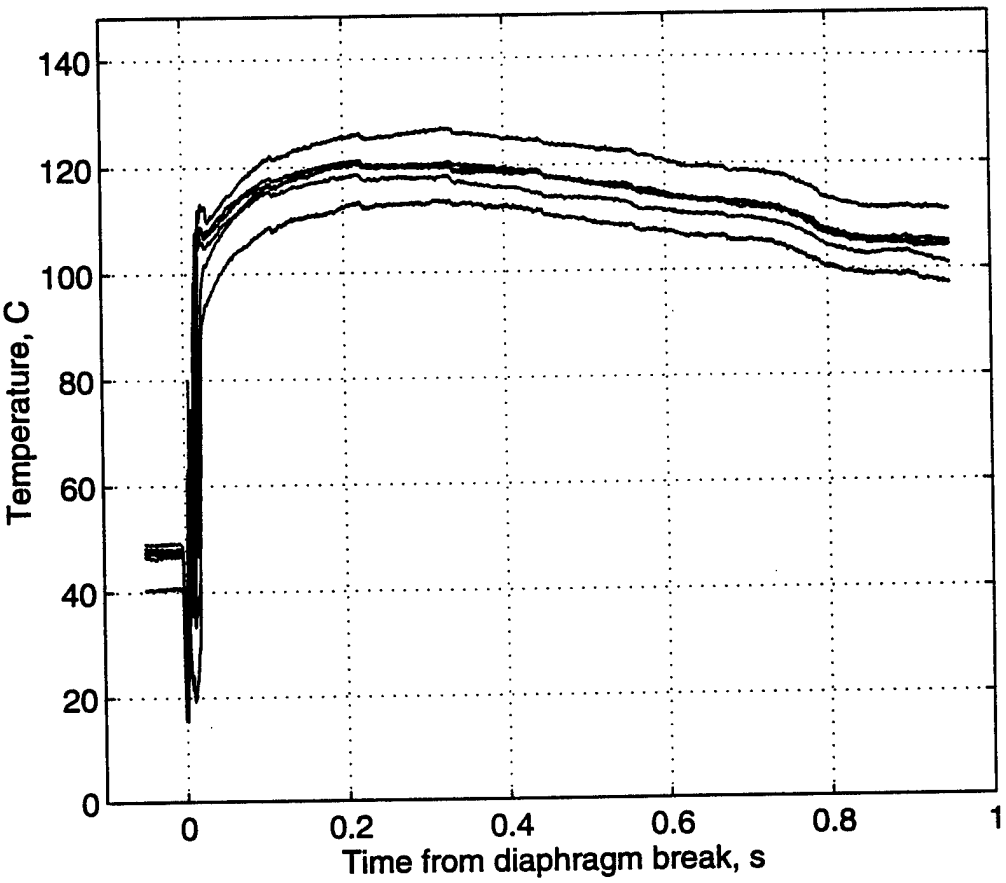

Figure 62 Temperture vs. Time, 150 C

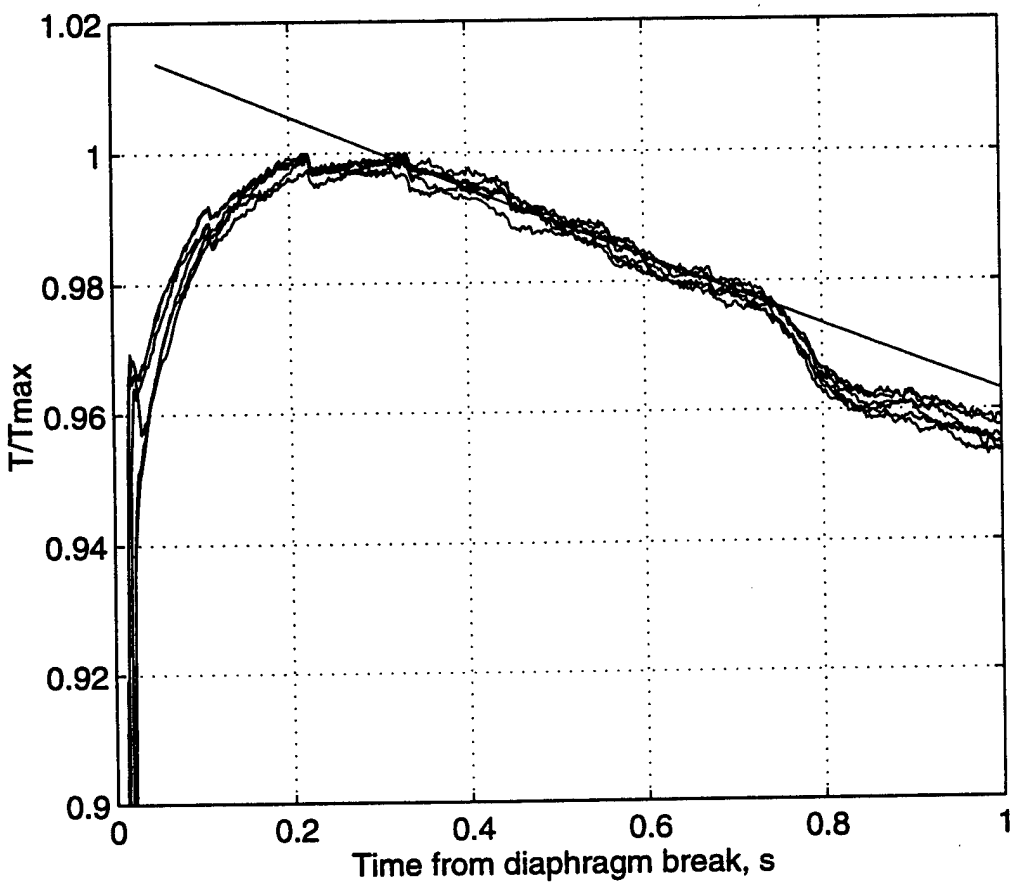

Figure 63 Normalized Temperture Comparison with Theory, 150 C

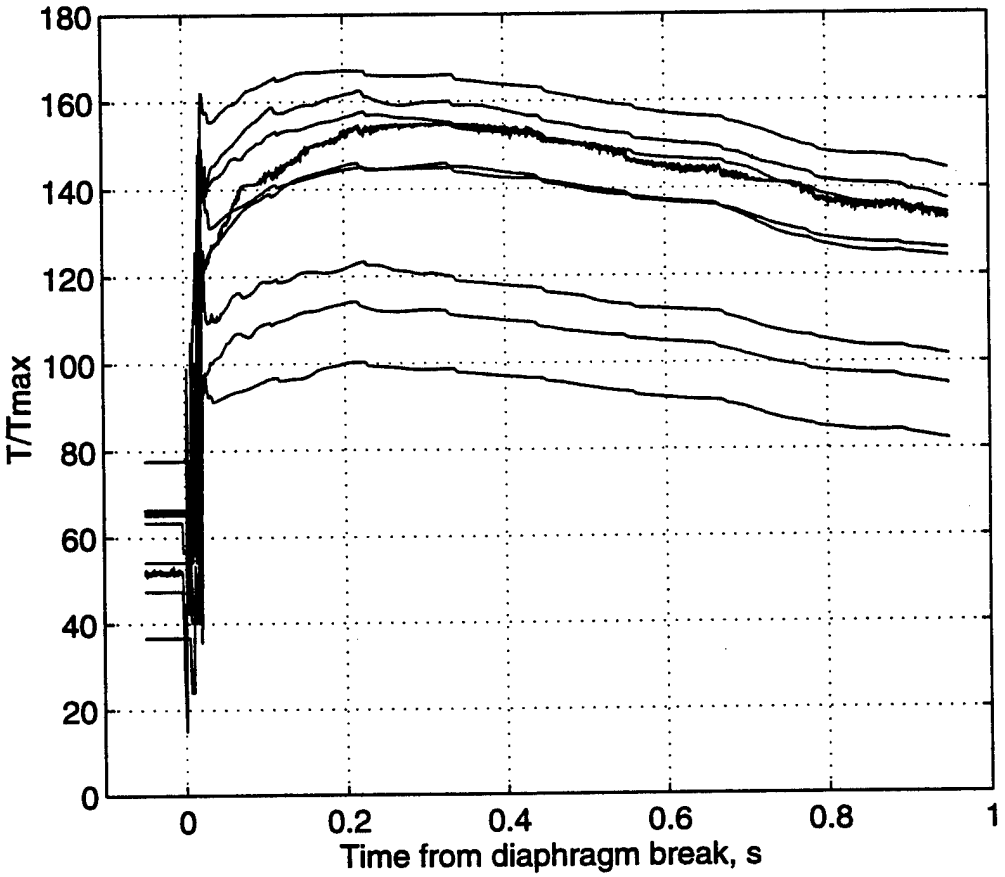

Figure 64 Temperature vs. Time, 180 C

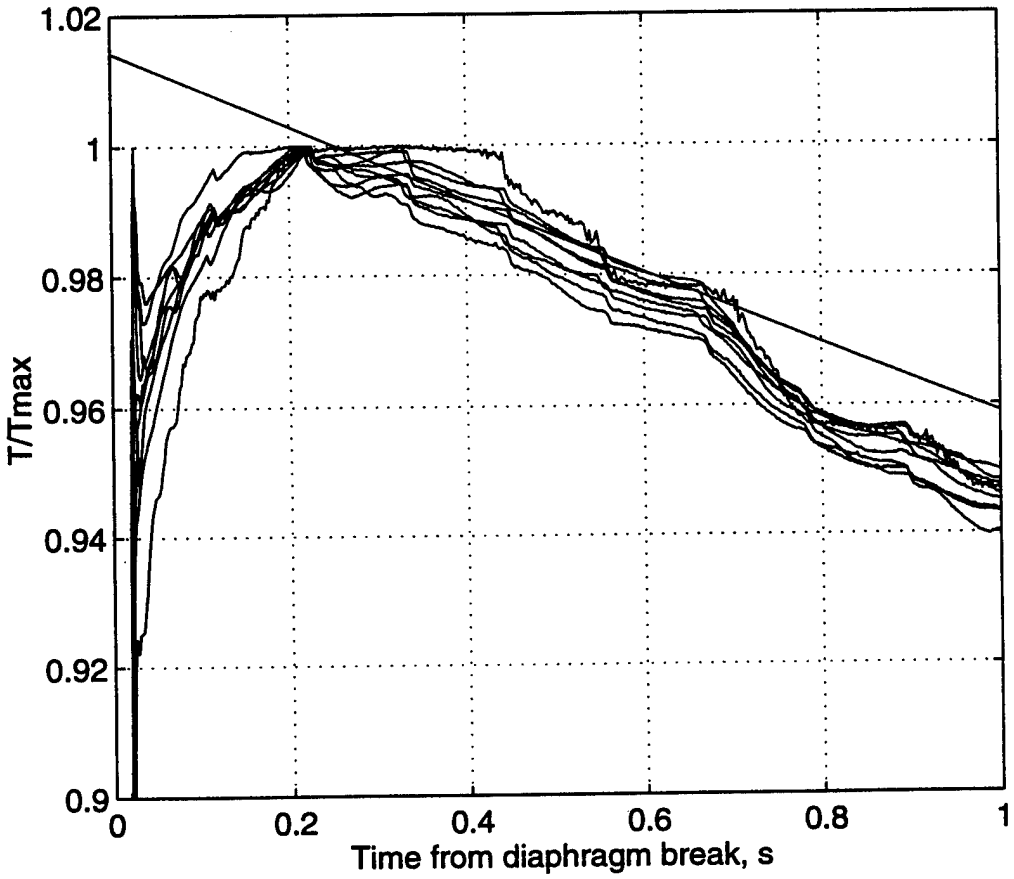

Figure 65 Normalized Temperature Comparison with Theory, 180 C

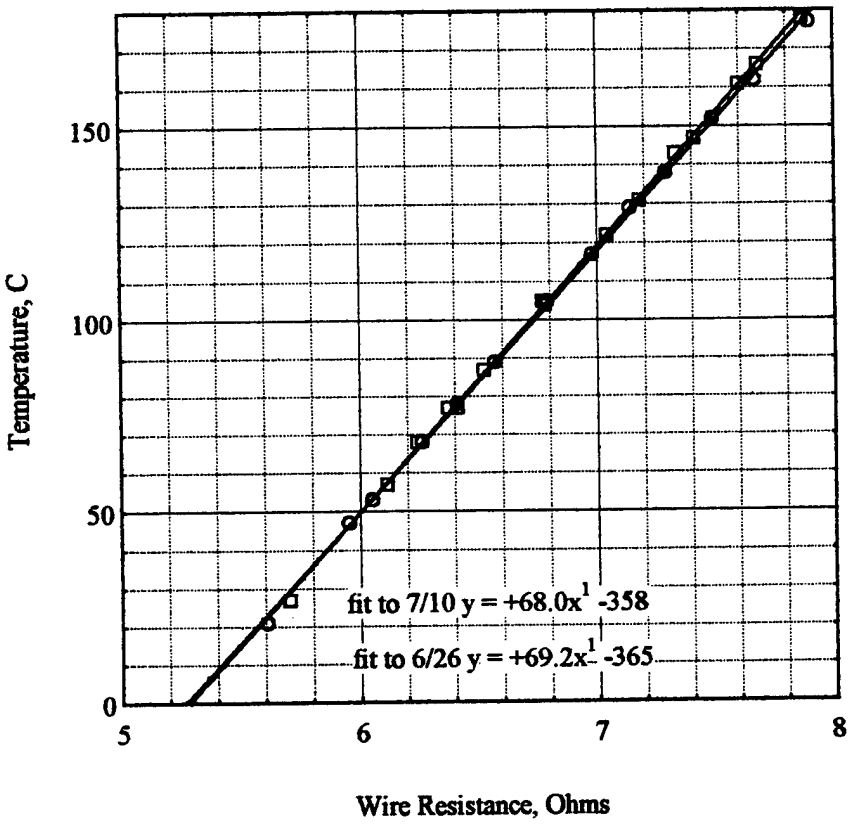

Figure 66 Cold Wire Calibration After 180 C Data, Temperature vs. Resistance

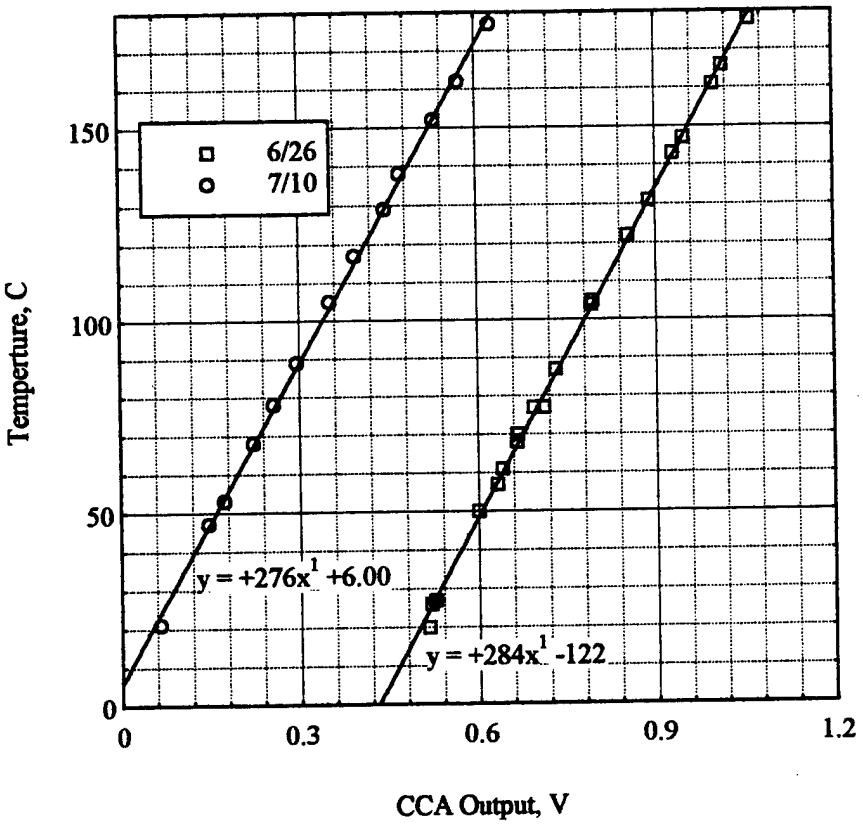

Figure 67 Cold Wire Calibration After 180 C Data, Temperature vs. Voltage

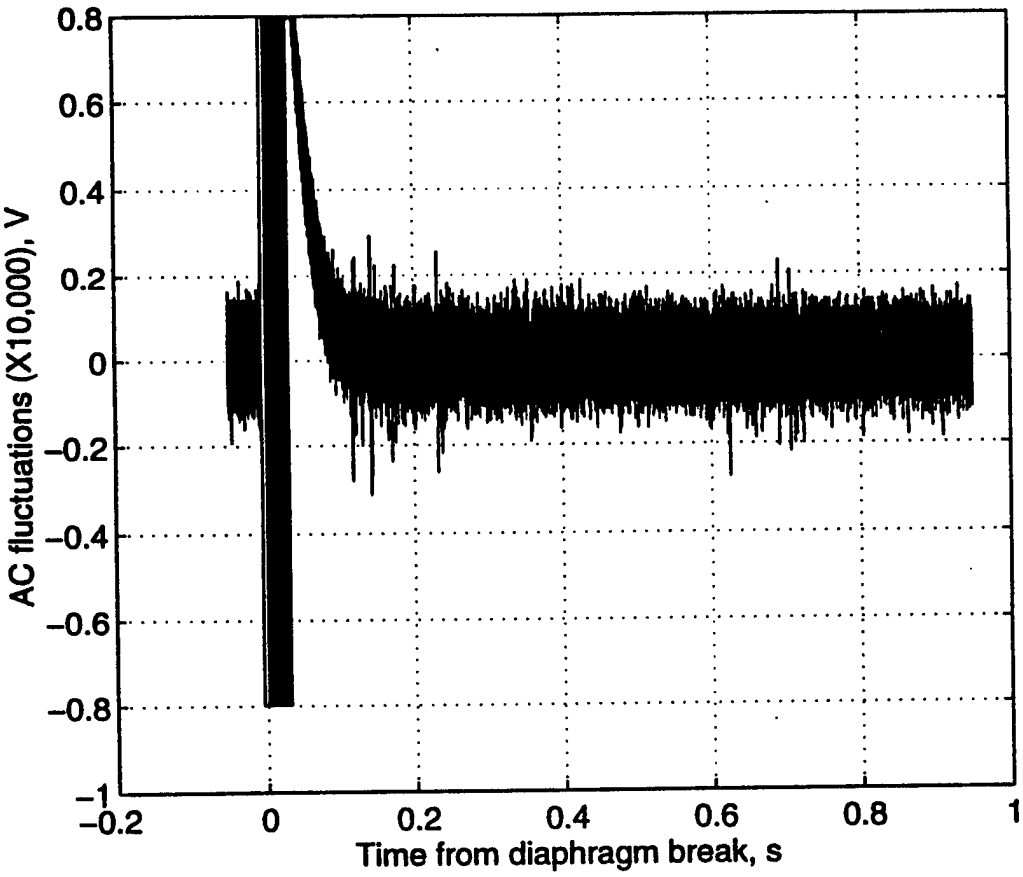

Figure 68 Sample Fluctuation-Voltage Signal

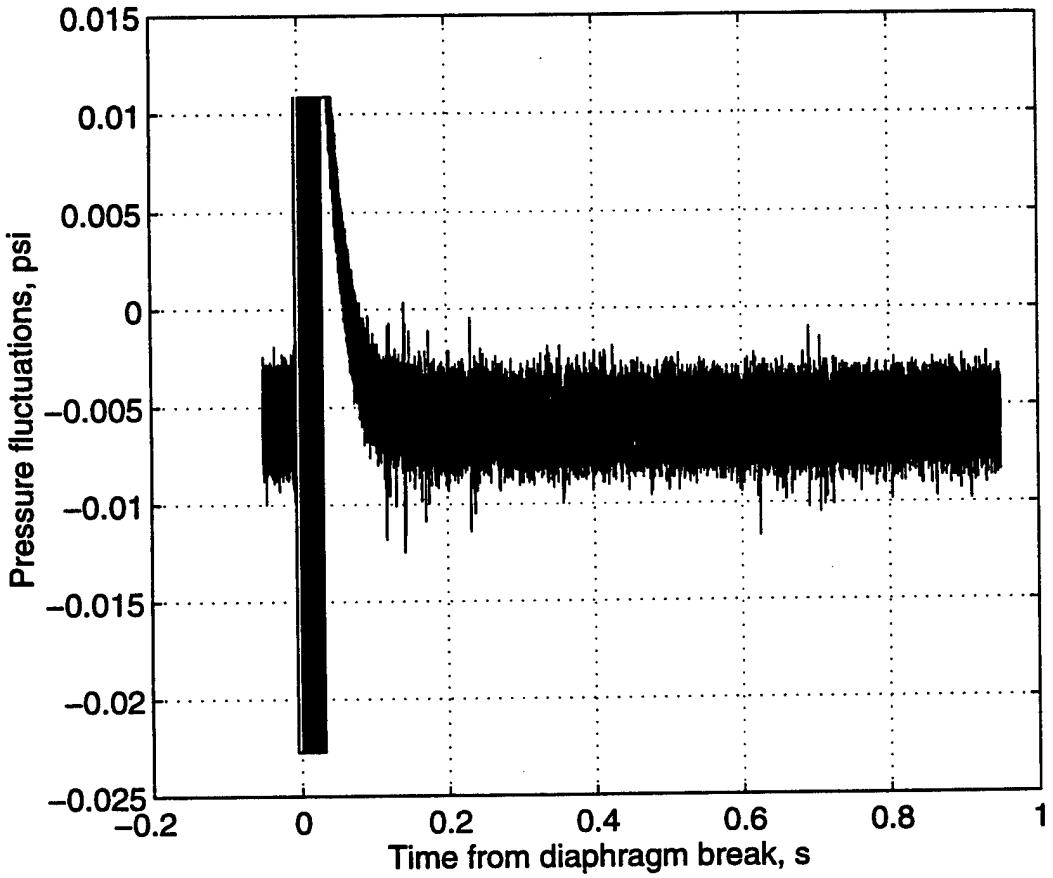

Figure 69 Pressure Signal with Slight Offset

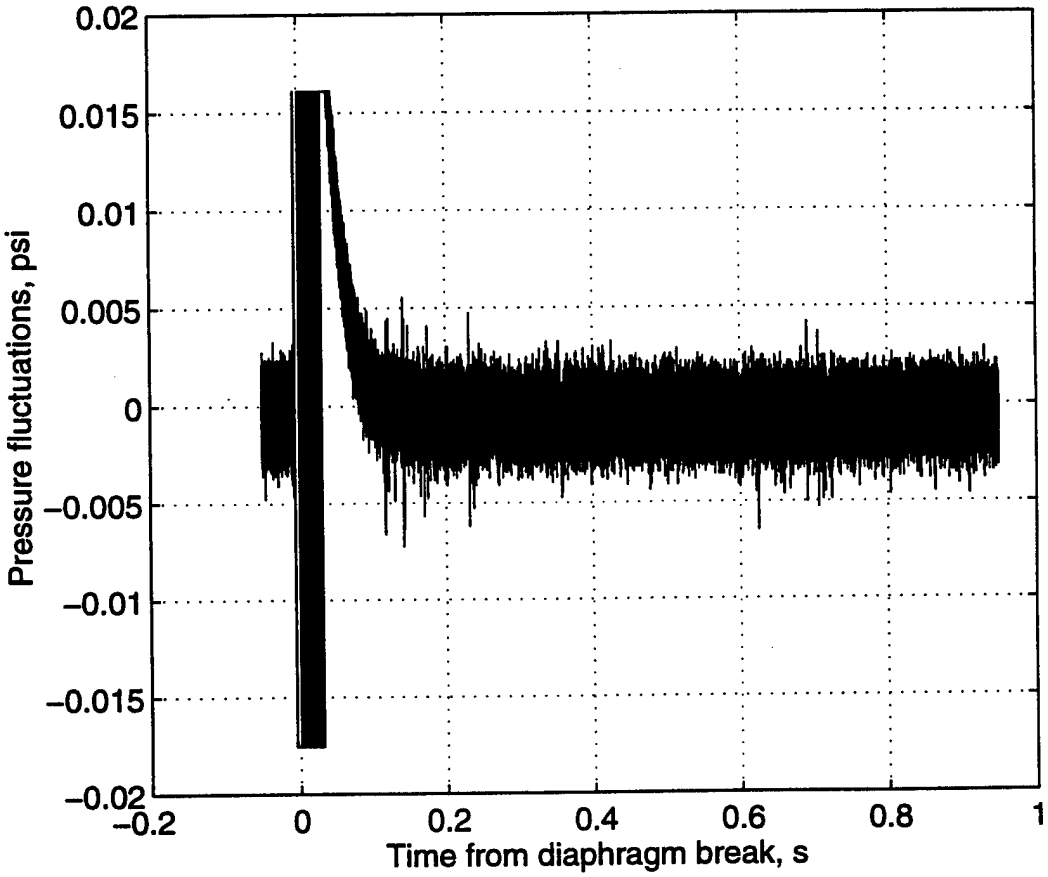

Figure 70 Pressure Signal After Mean Value Subtracted Out

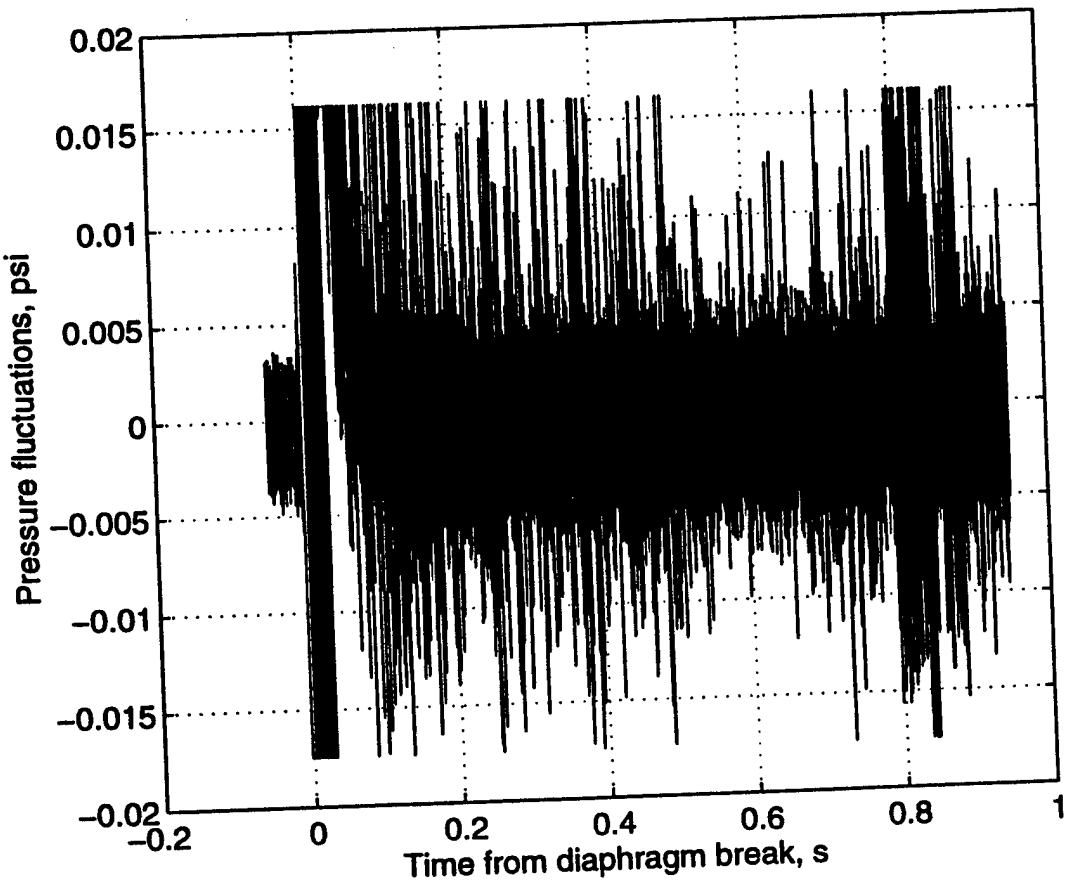

Figure 71 Noisy Pressure Signal

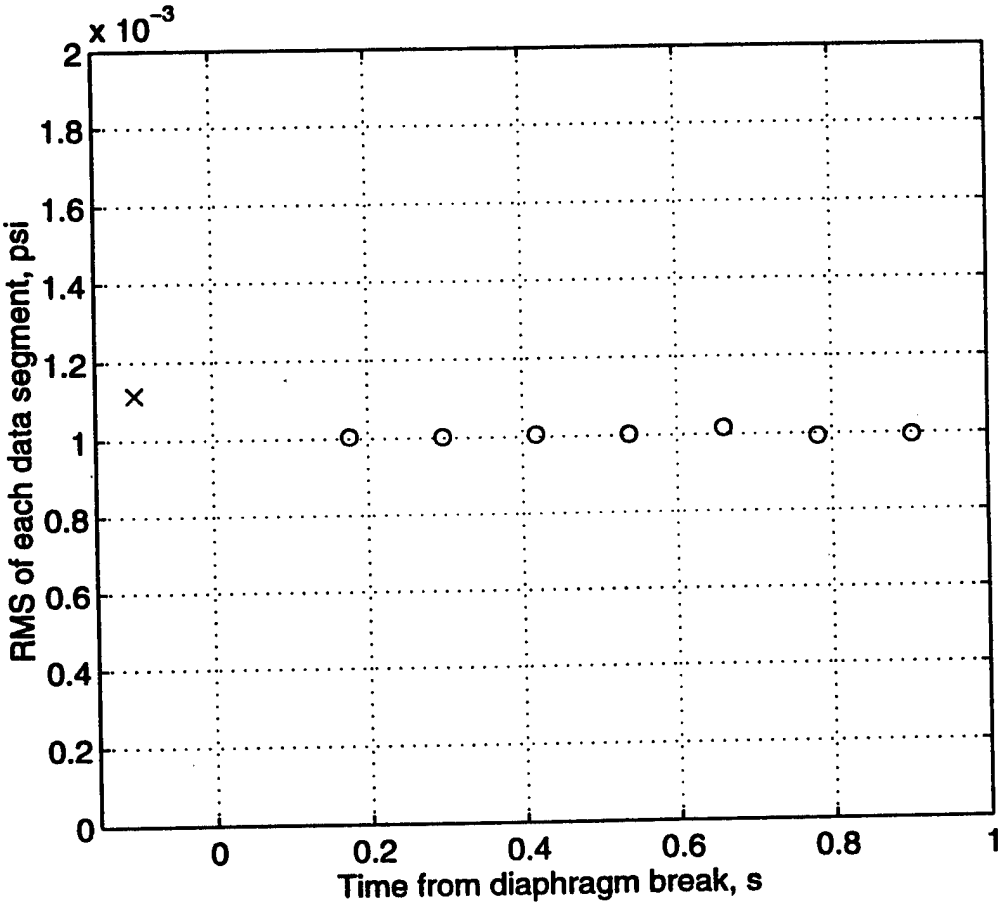

Figure 72 RMS of Fluctuaions: Comparison Between Run and Pre-Run

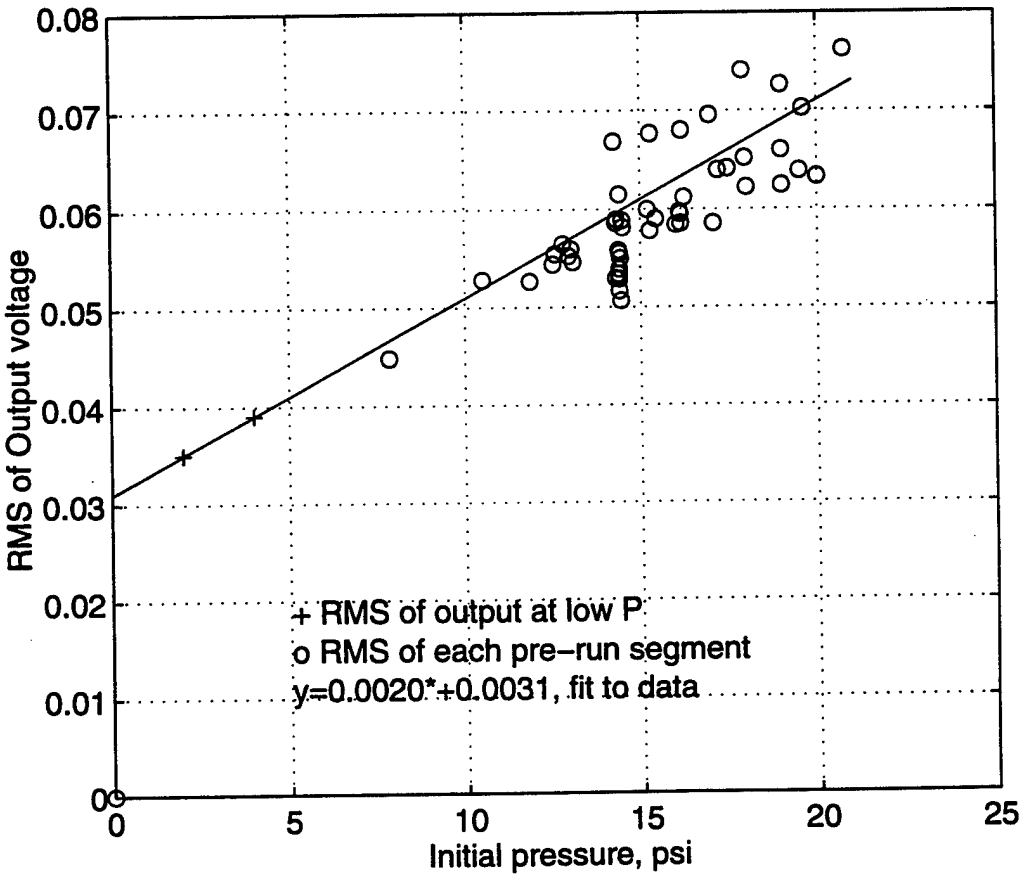

Figure 73 Fitted Pre-Run Noise Level vs Pressure

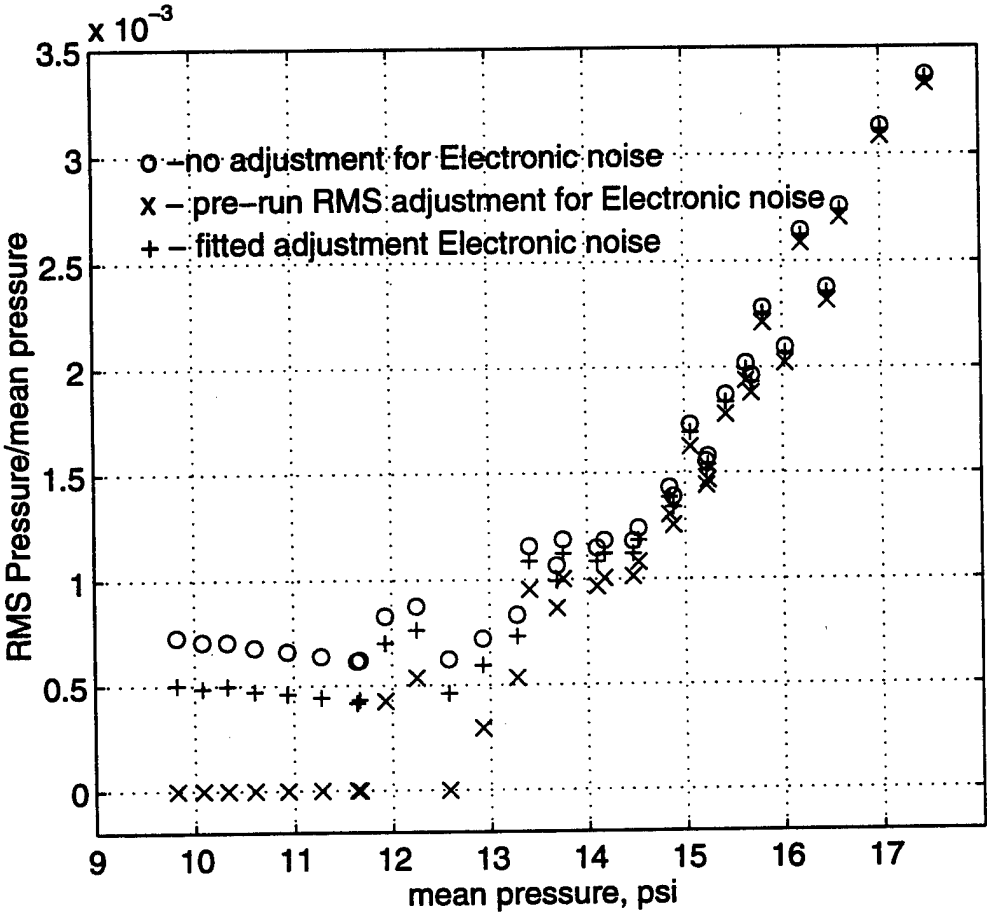

Figure 74 Comparison of Electronic Noise Estimates

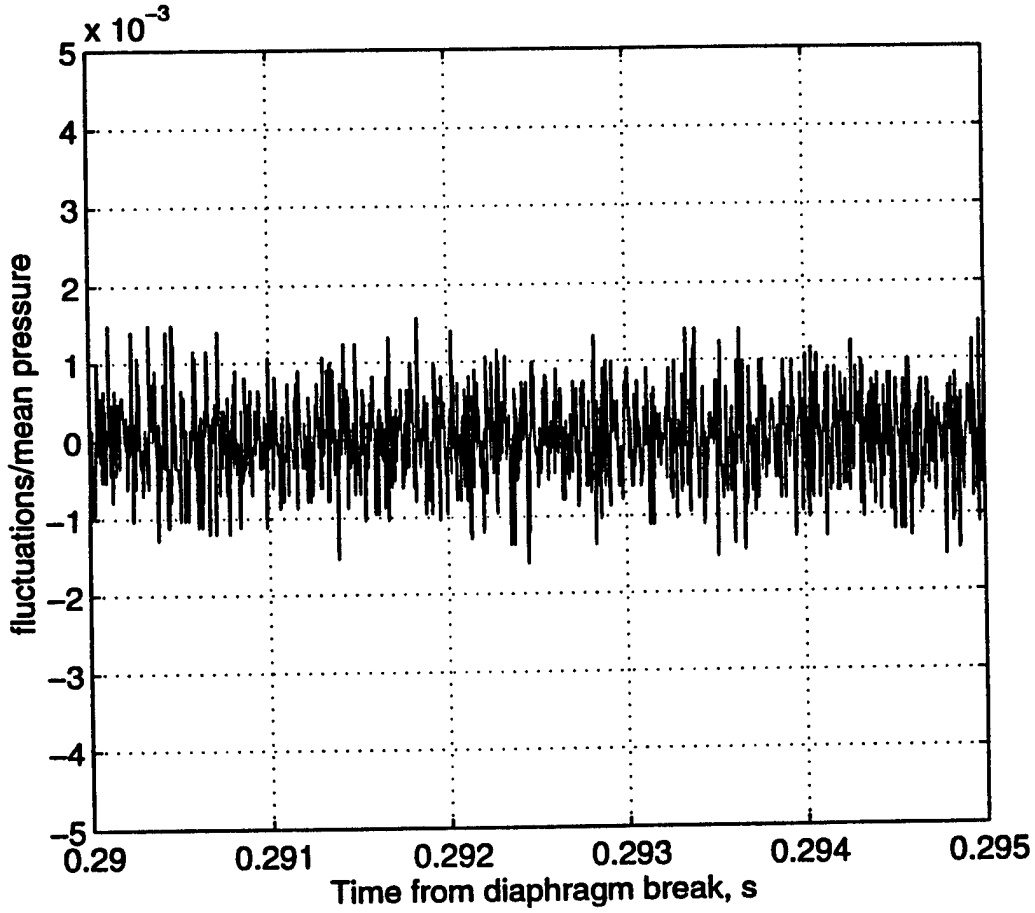

Figure 75 Sample Low Noise Pressure Signal

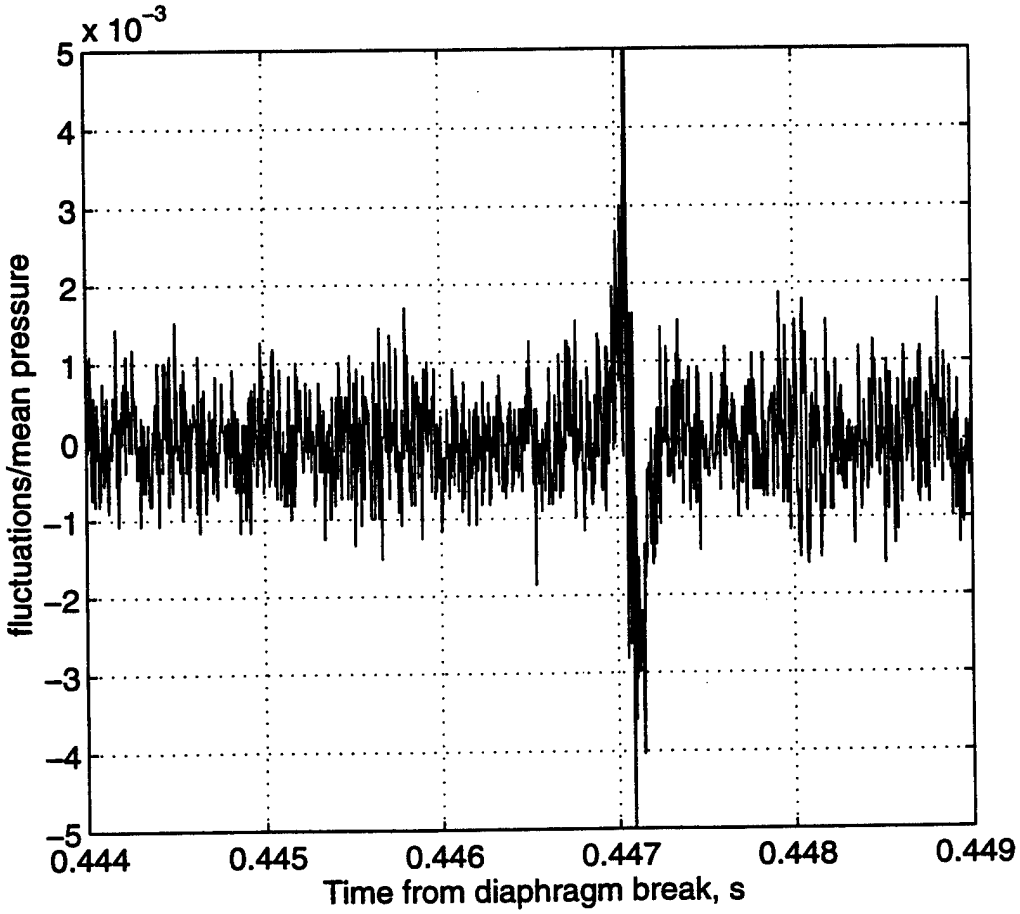

Figure 76 Example of Pressure Fluctuation Due to Turbulent Spot on Nozzle Wall

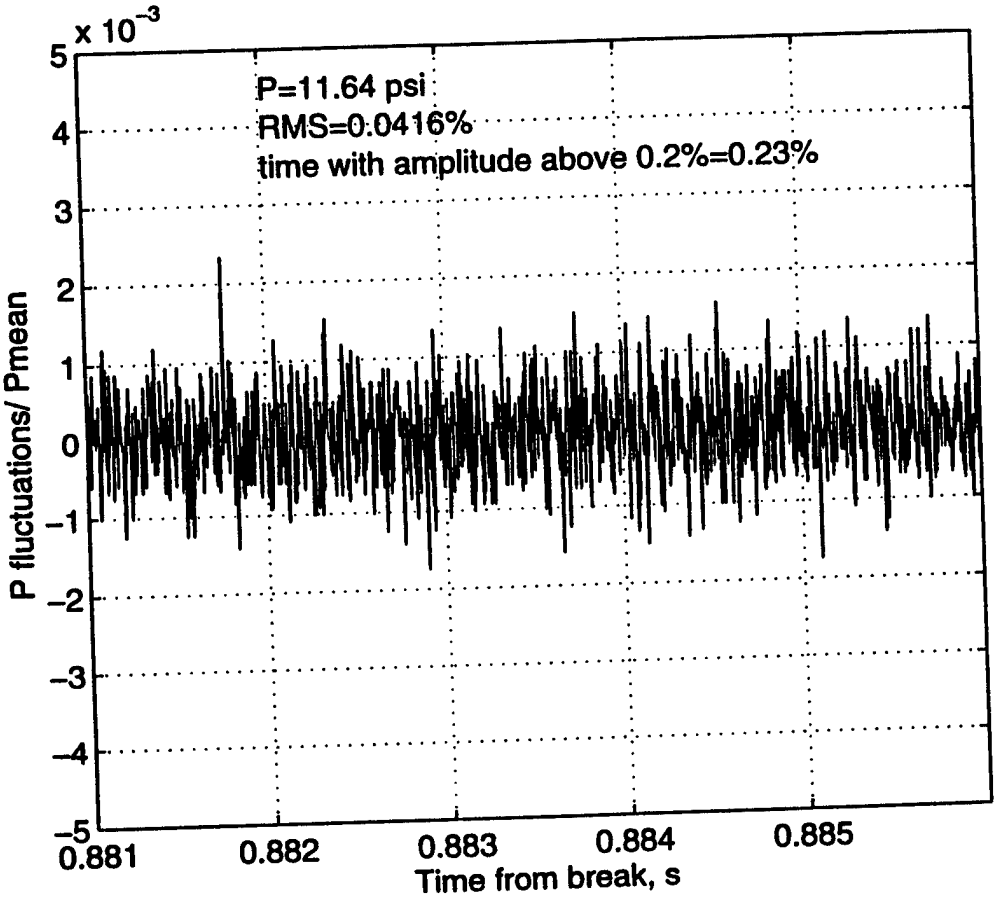

Figure 77 Portion of Low Noise Pressure Signal

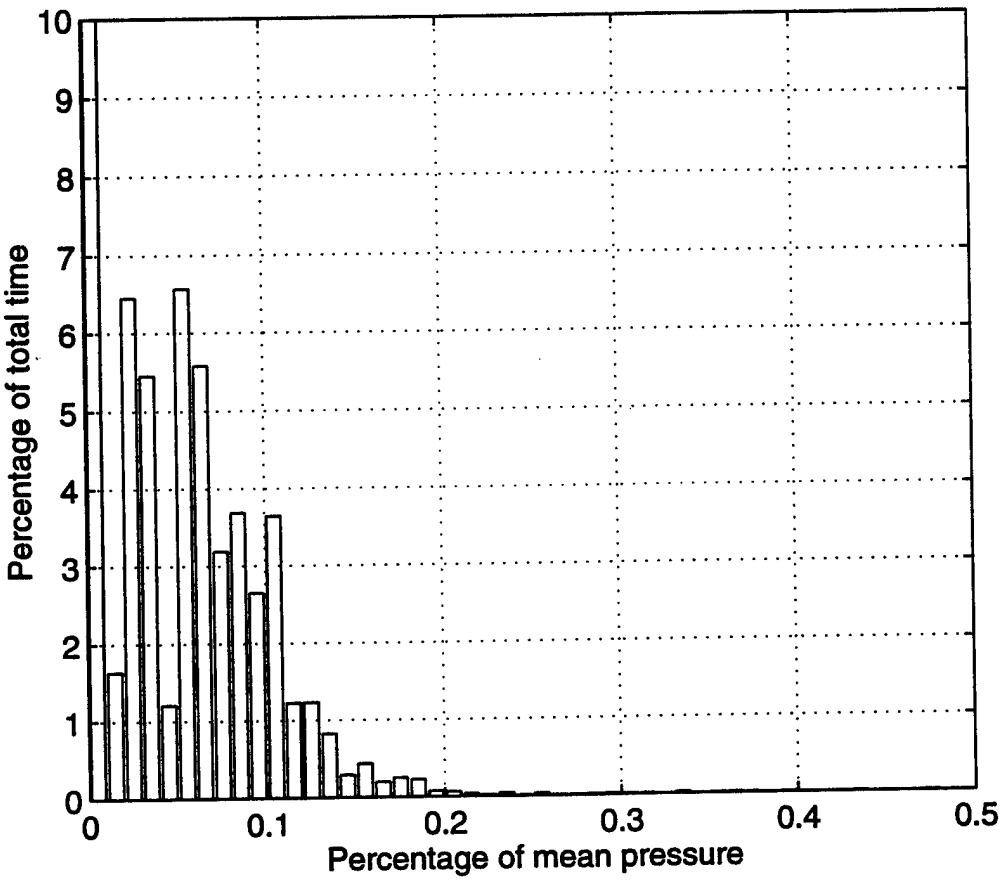

Figure 78 Histogram of Low Noise Segment

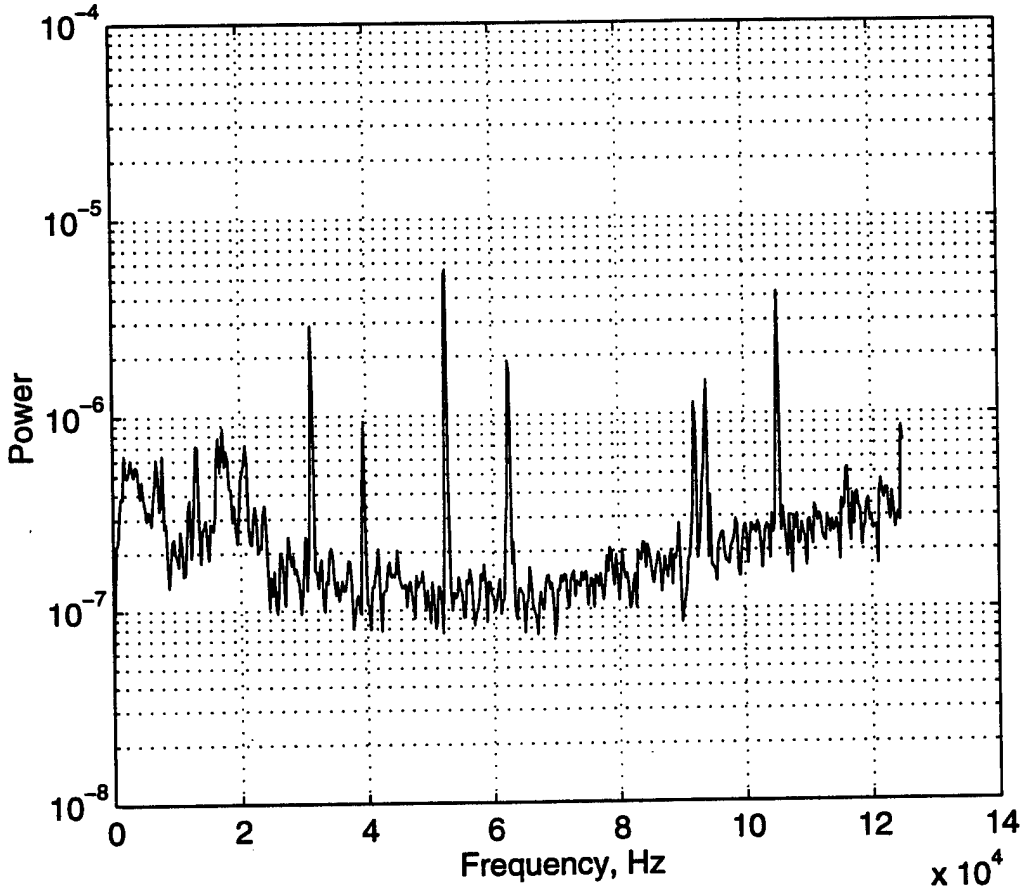

Figure 79 Power Spectrum of Low Noise Segment

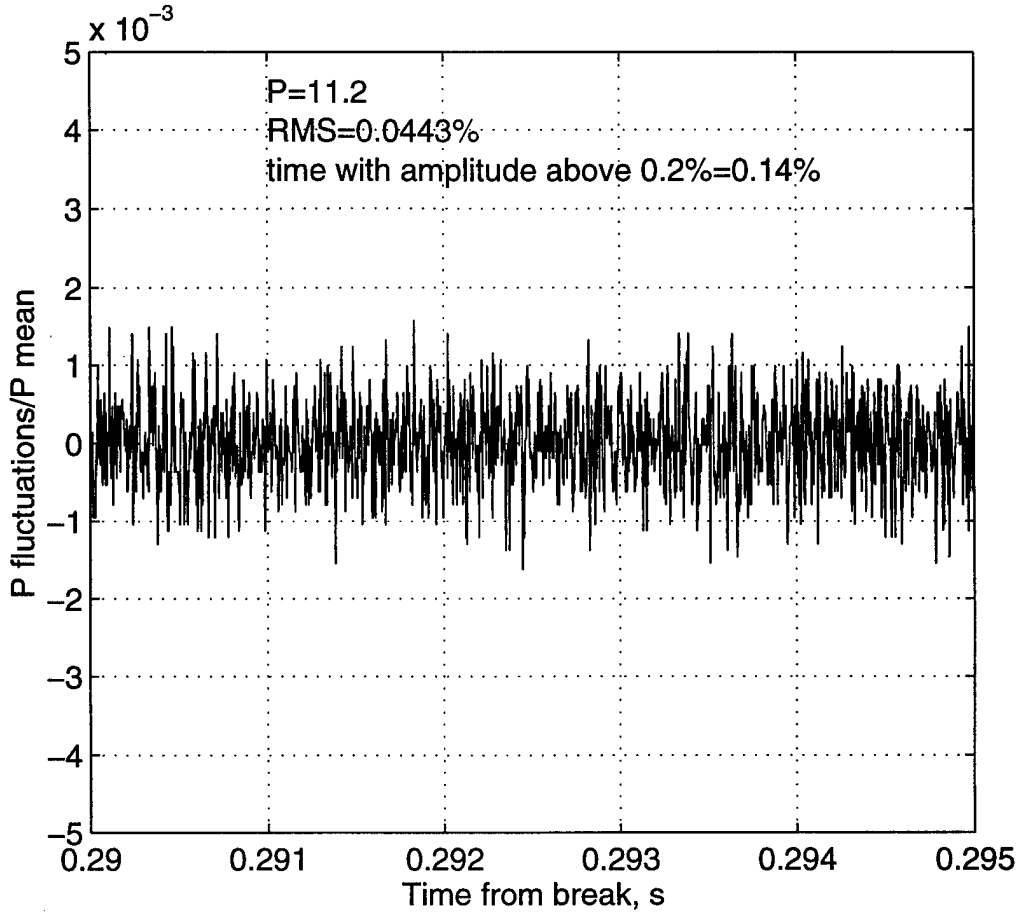

Figure 80 Another Low Noise Segment

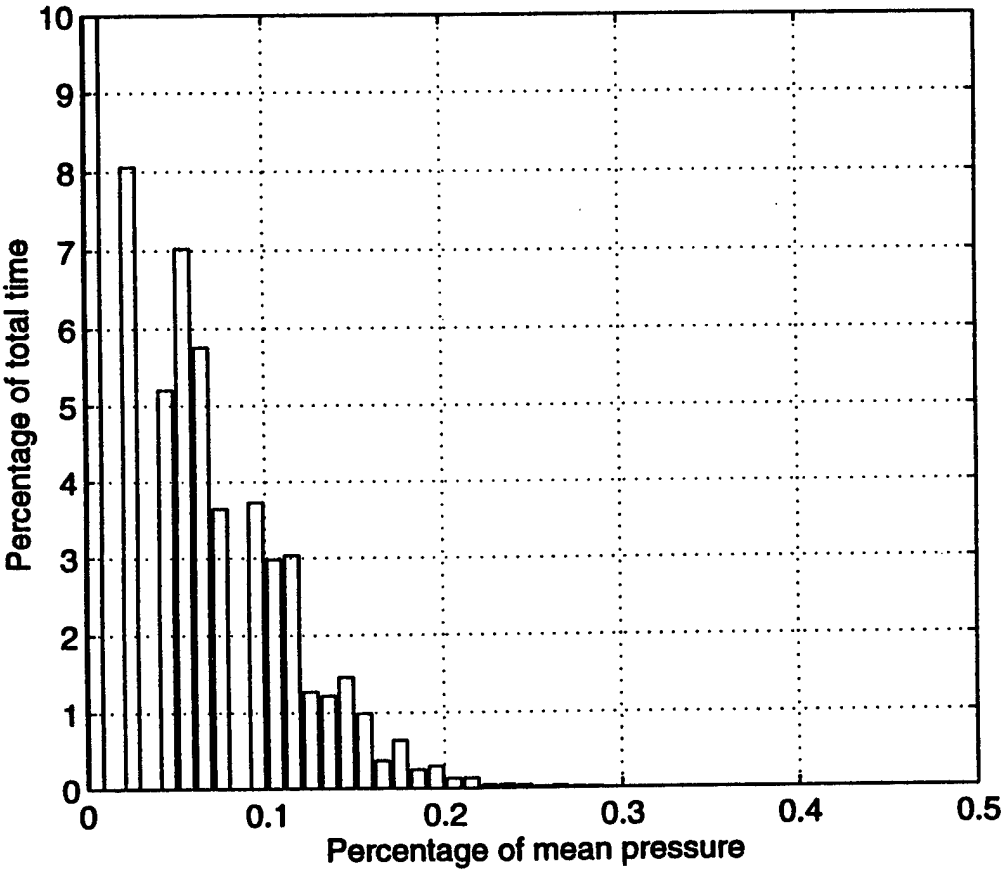

Figure 81 Histogram of Another Low Noise Segment

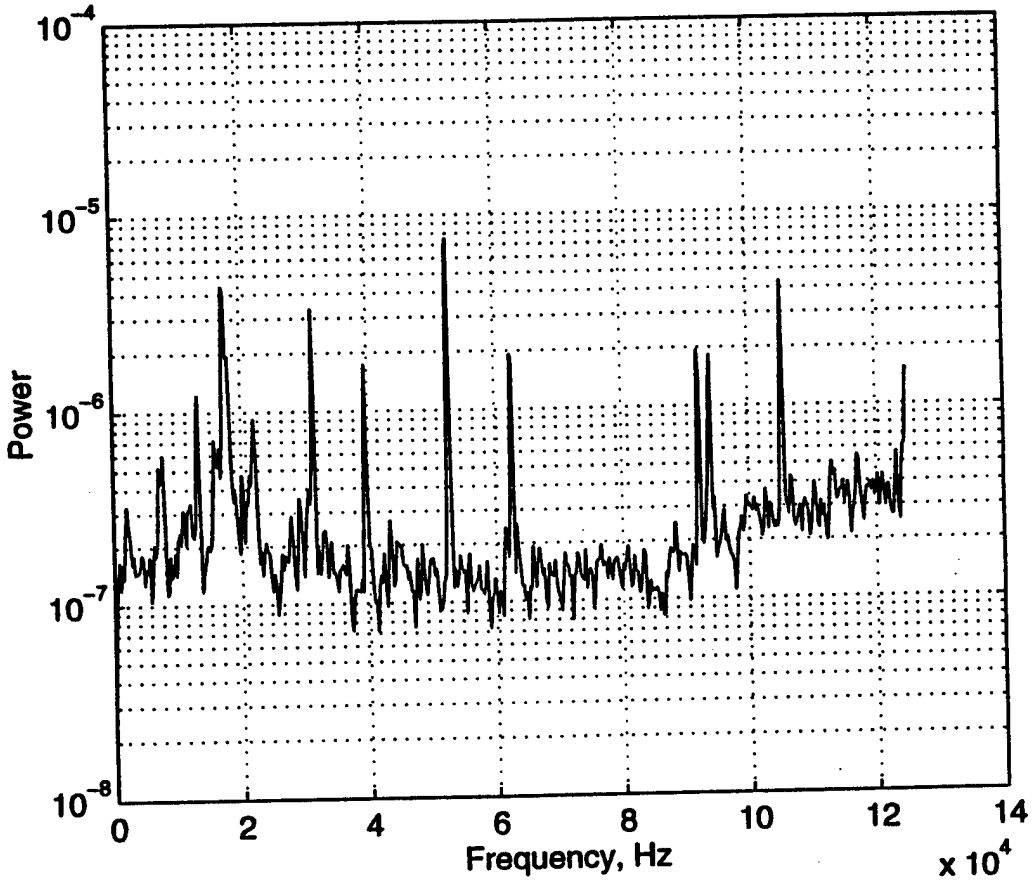

Figure 82 Power Spectrum of Another Low Noise Segment

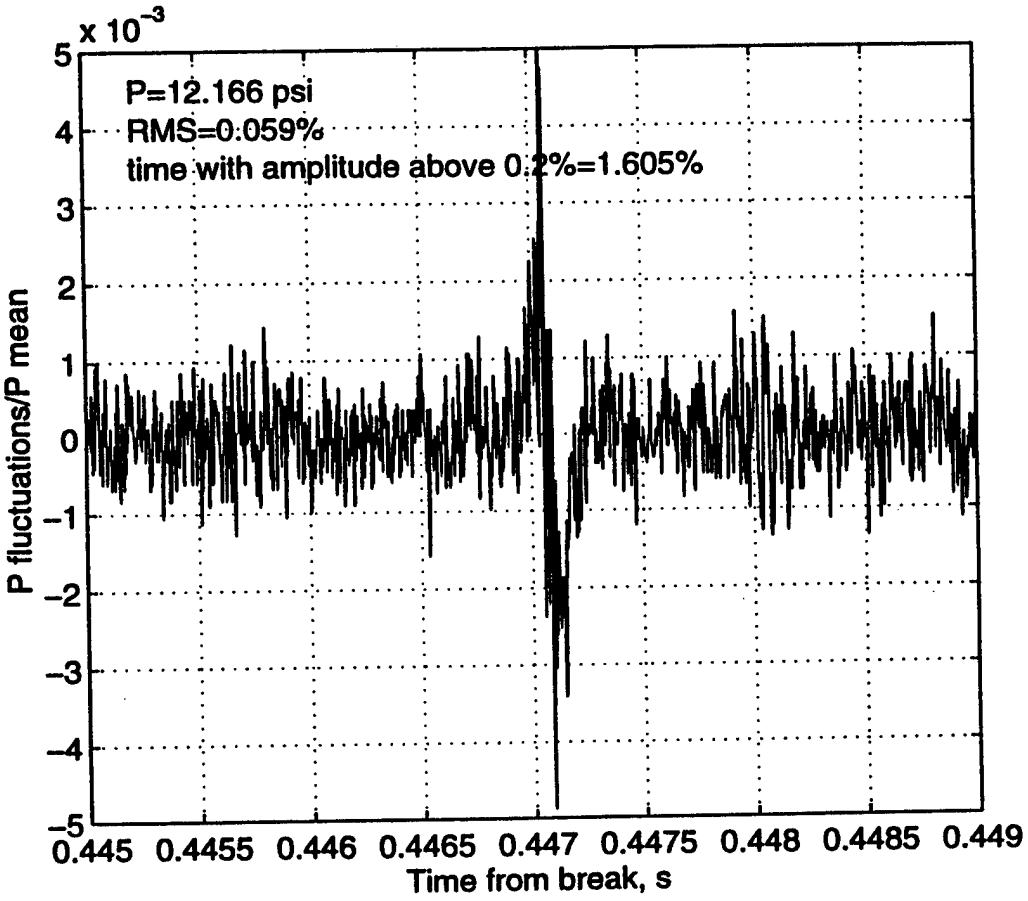

Figure 83 Portion of Slightly Noisy Segment

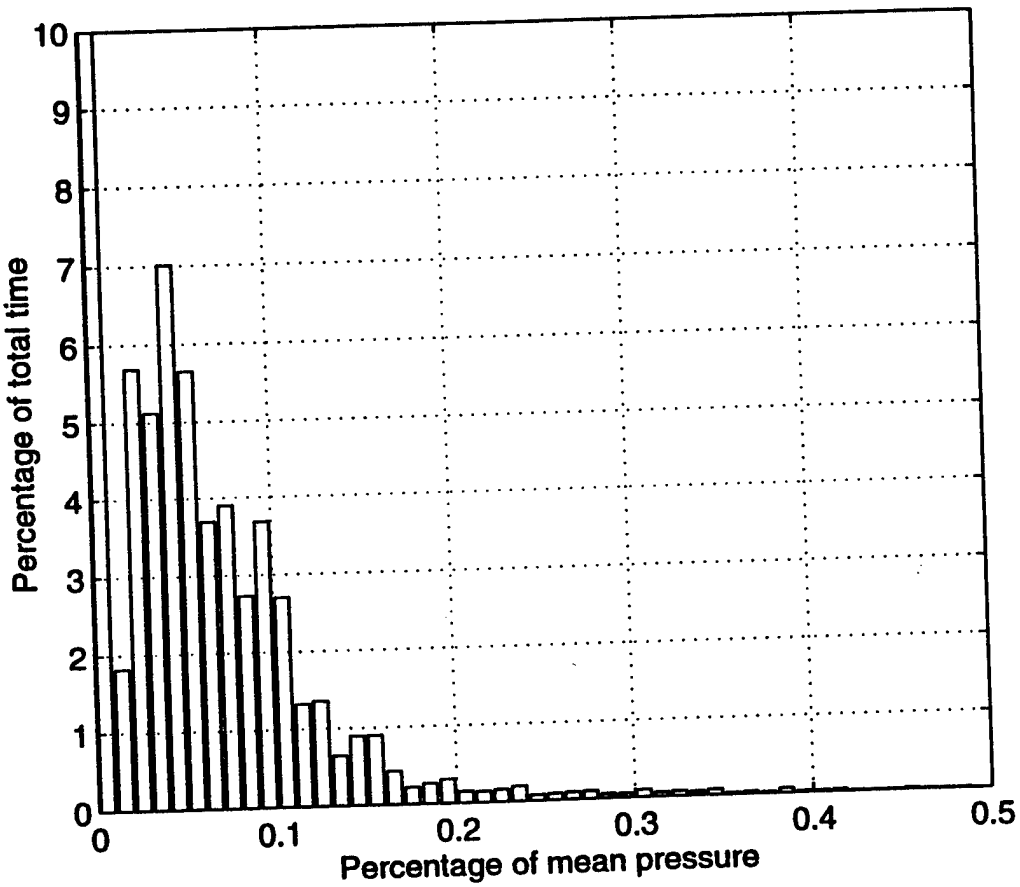

Figure 84 Histogram of Slightly Noisy Segment

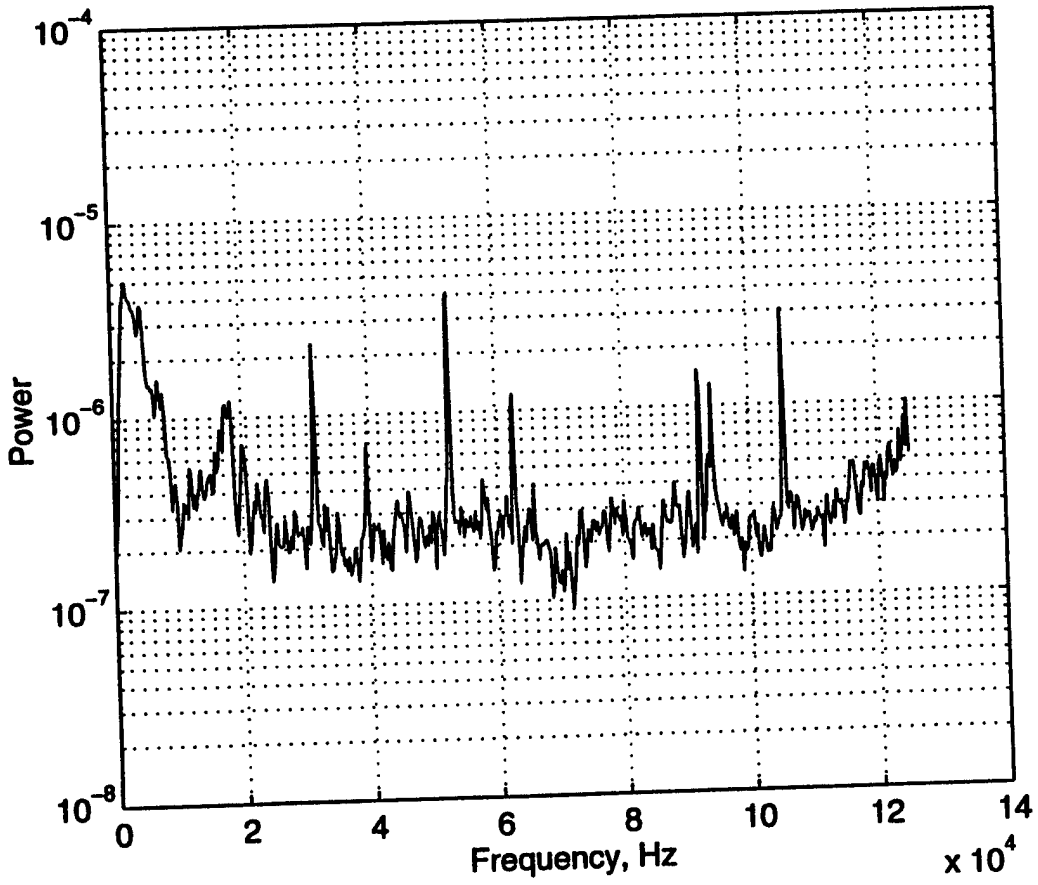

Figure 85 Power Spectrum of Slightly Noisy Segment

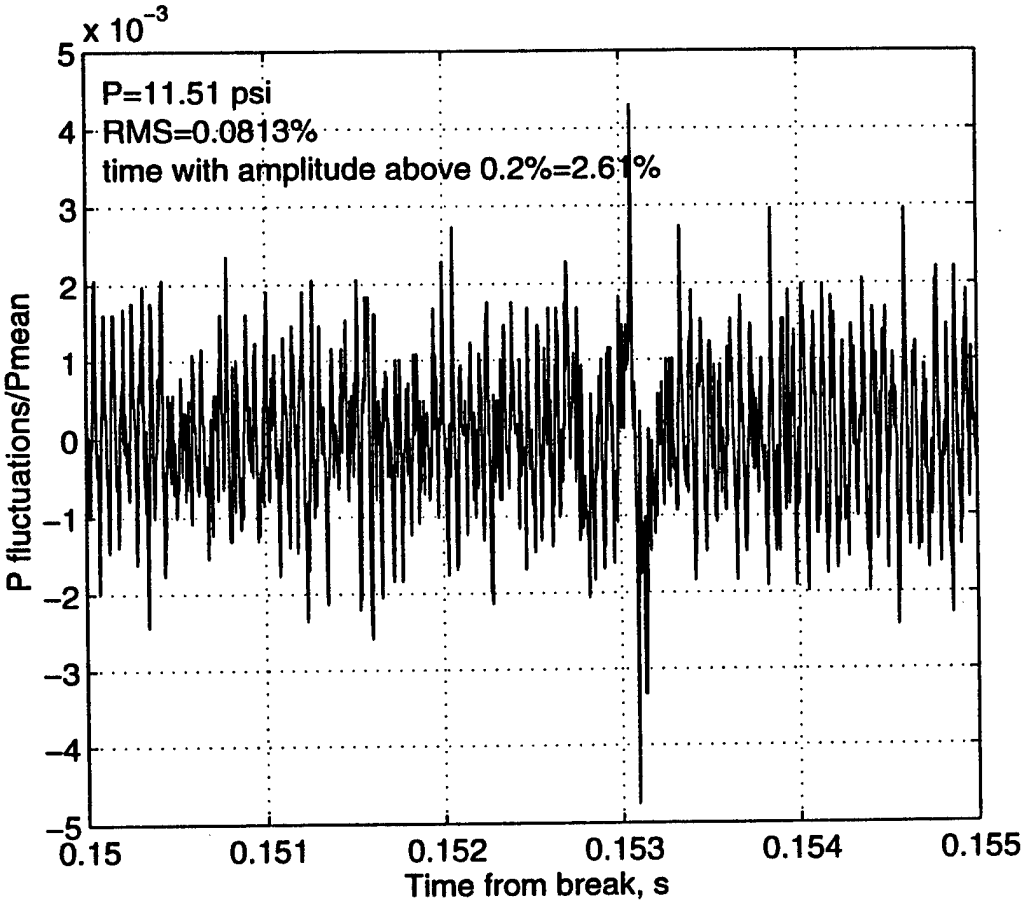

Figure 86 Portion of Moderately Noisy Segment

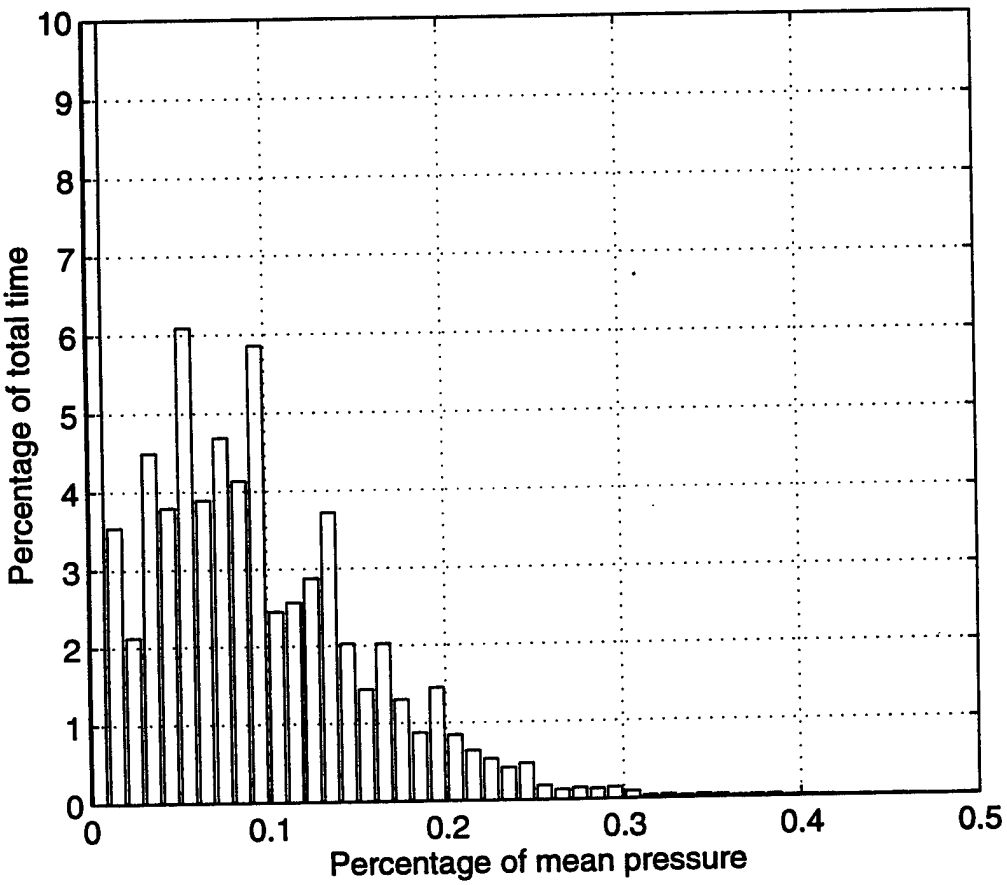

Figure 87 Histogram of Moderately Noisy Signal

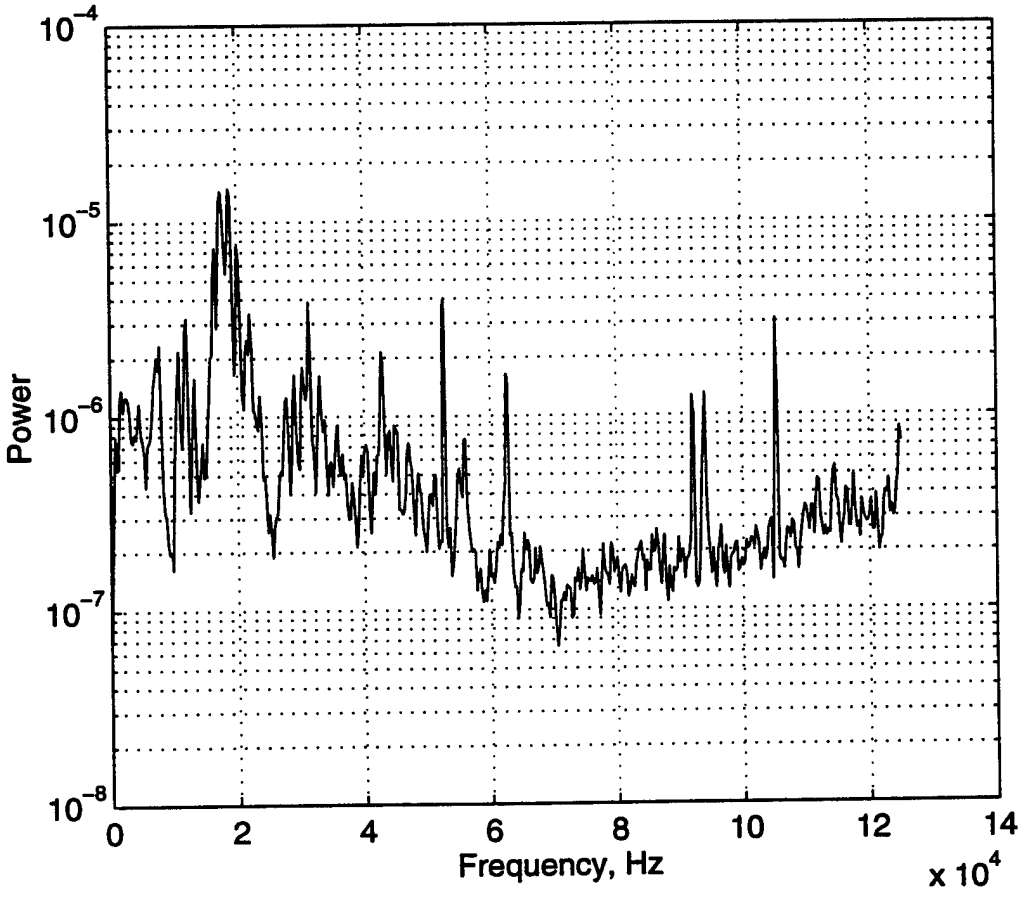

Figure 88 Power Spectrum of Moderately Noisy Signal

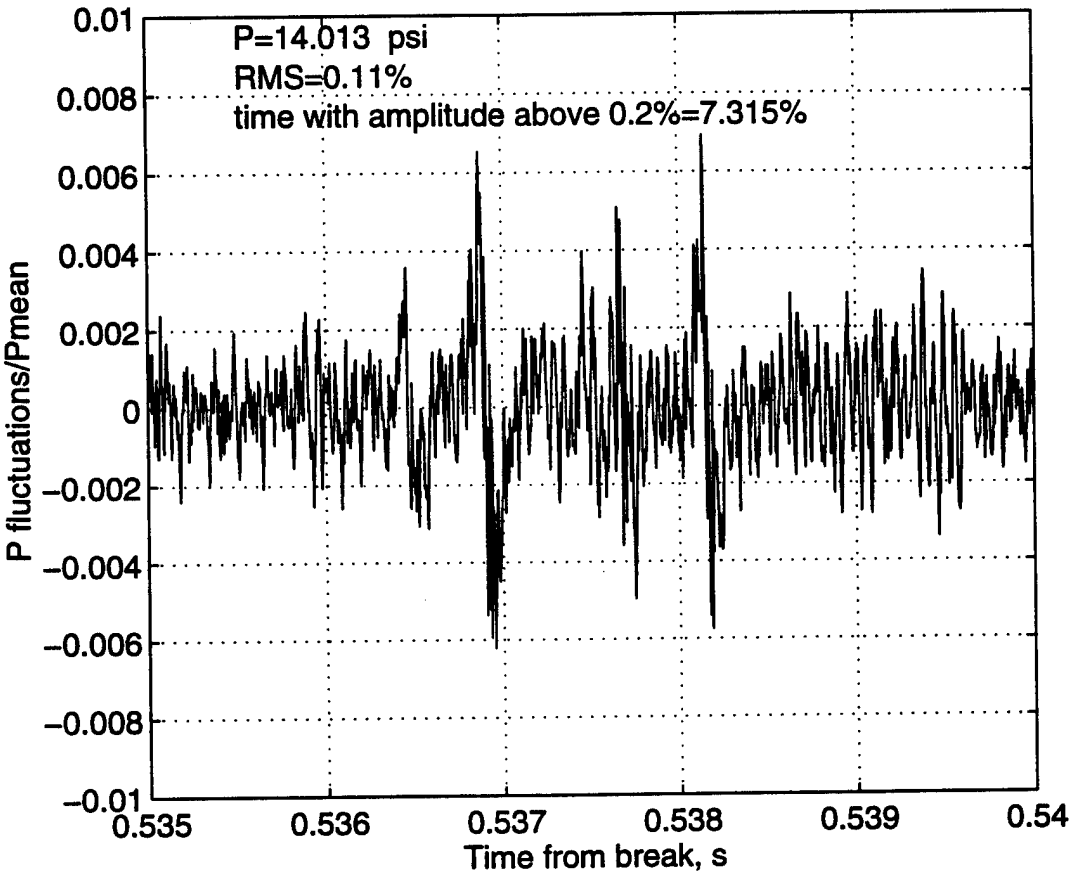

Figure 89 Portion of Noisy Signal

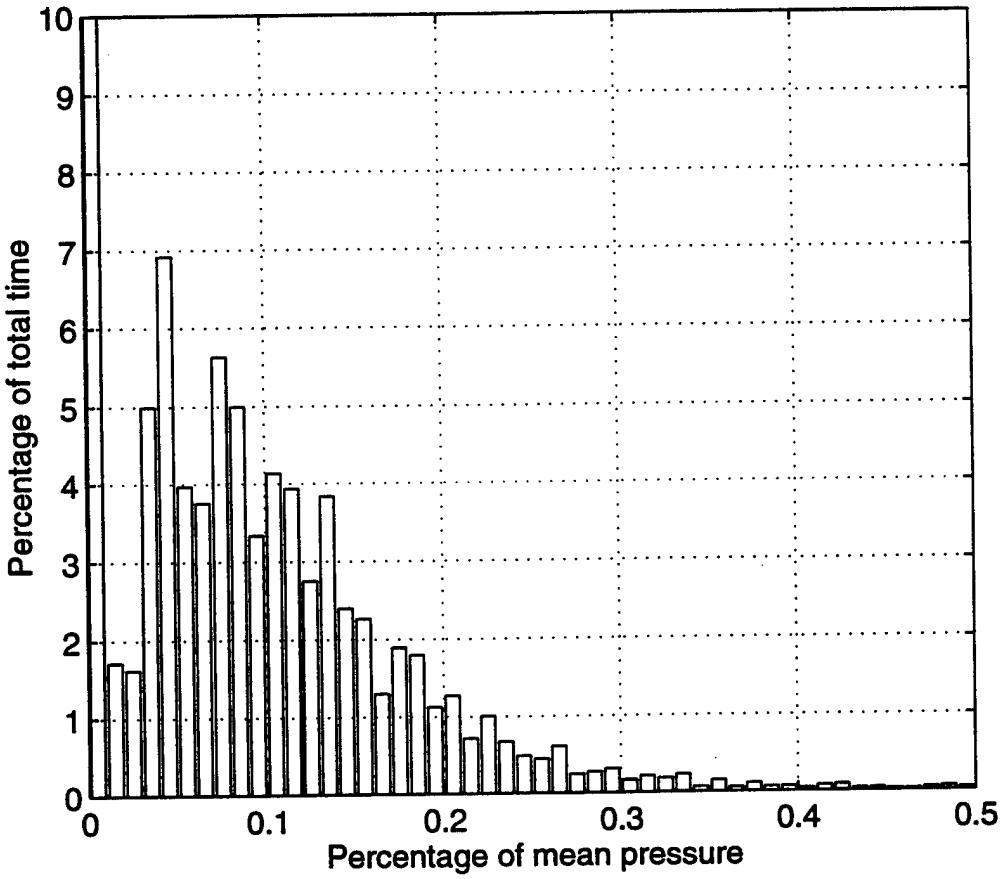

Figure 90 Histogram of Noisy Signal

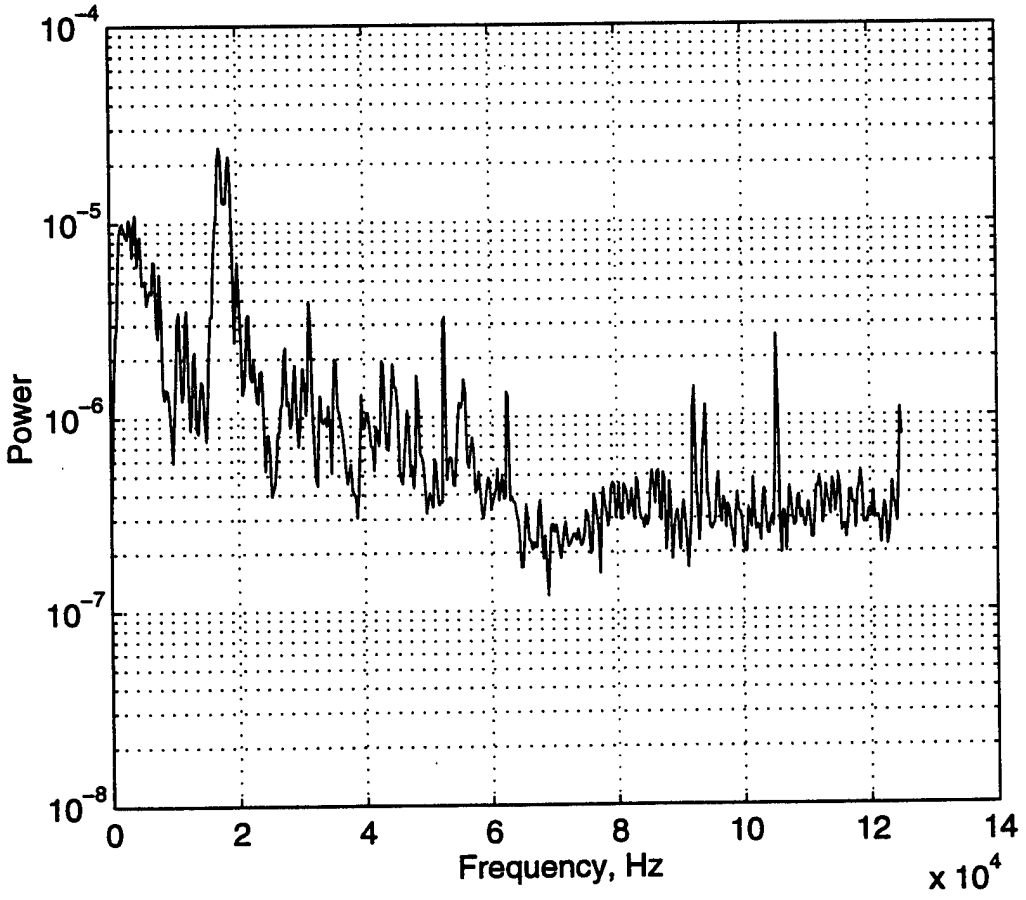

Figure 91 Power Spectrum of Noisy Signal

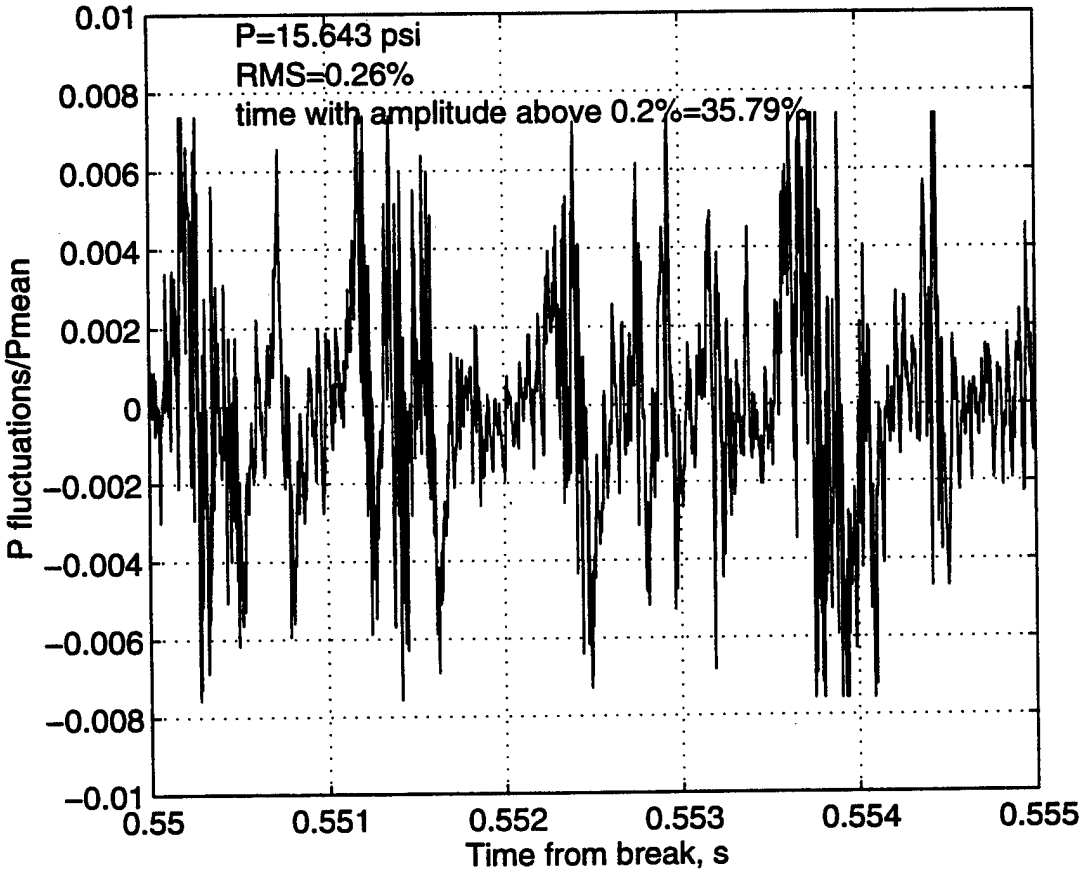

Figure 92 Portion of Very Noisy Signal

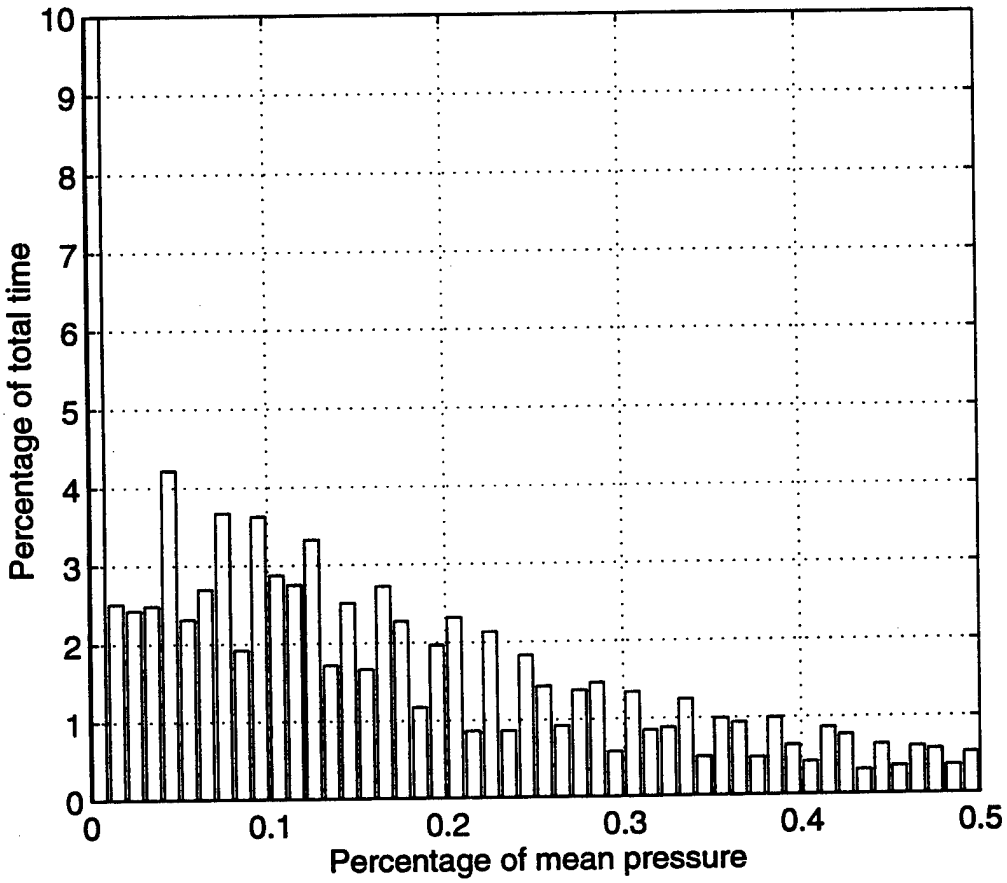

Figure 93 Histogram of Very Noisy Signal

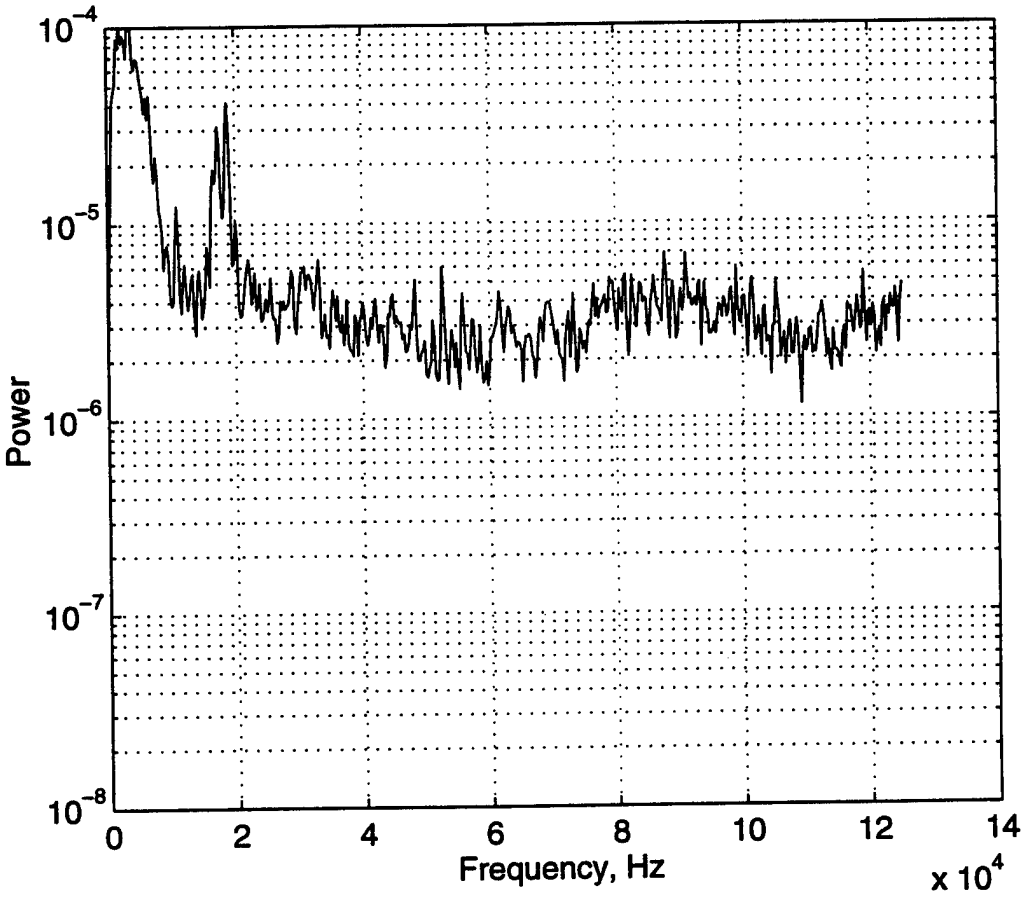

Figure 94 Power Spectrum of Very Noisy Signal

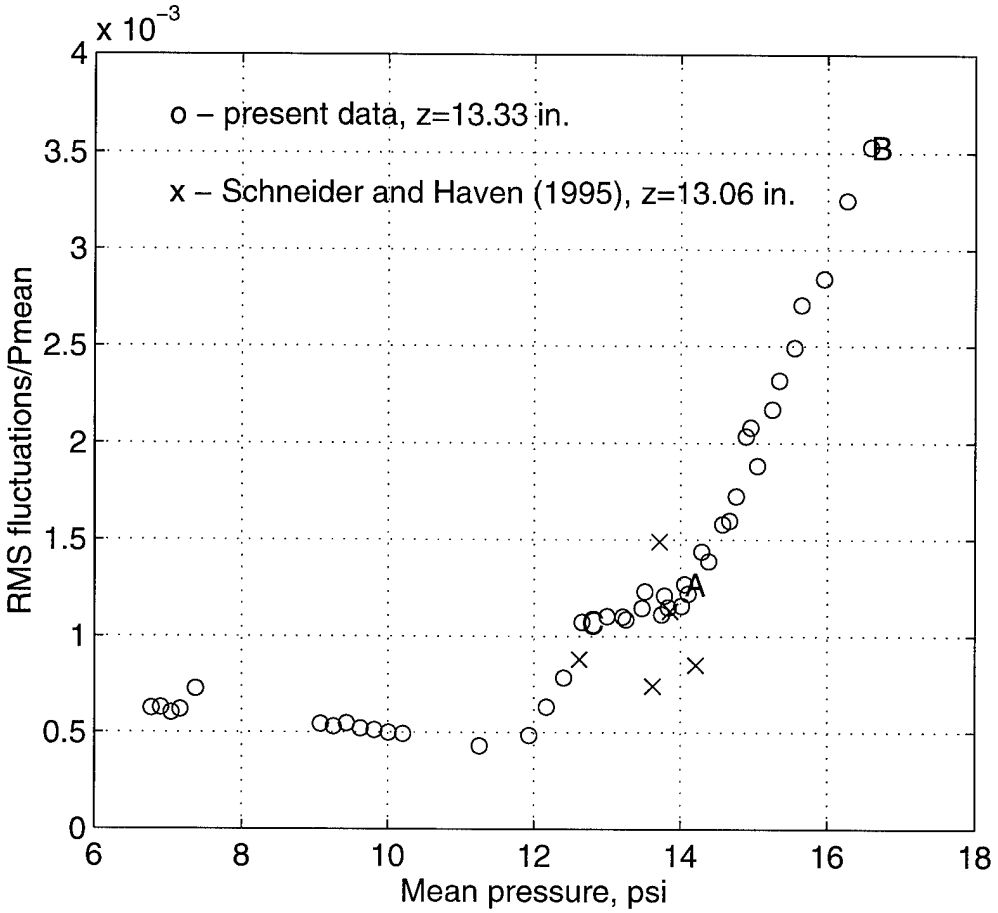

Figure 95 RMS Noise Levels vs. Pressure, Unheated

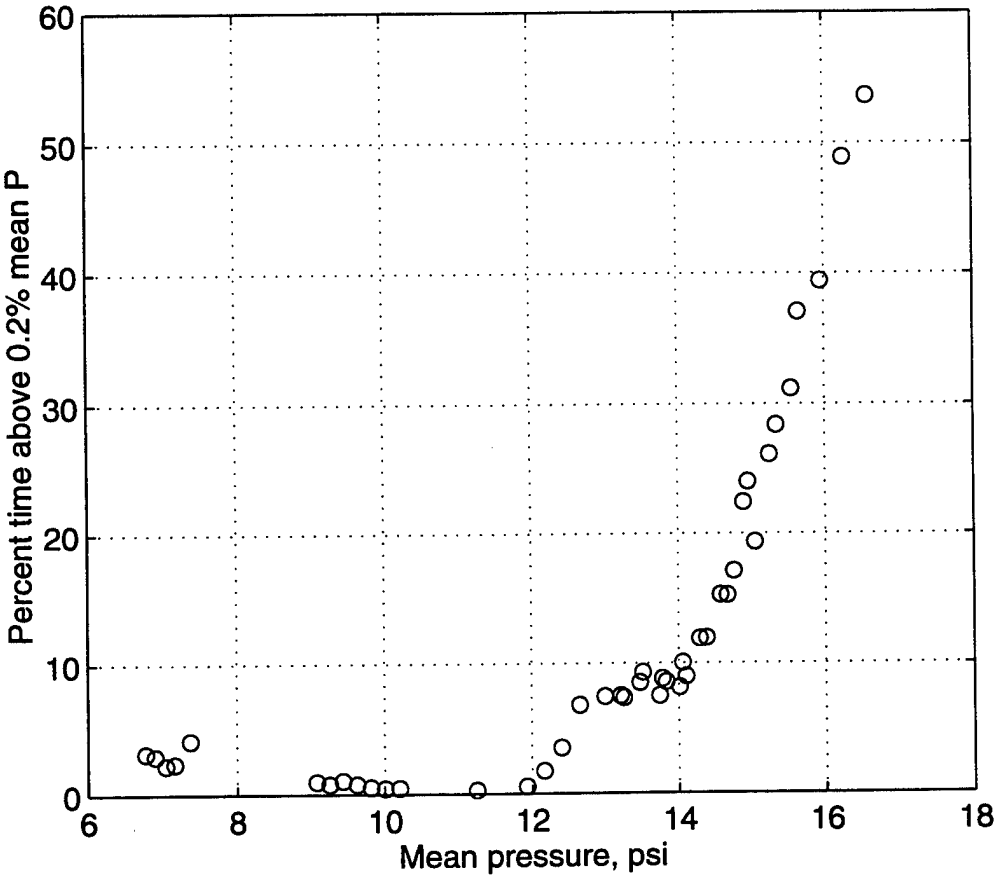

Figure 96 τ vs. Pressure, Unheated

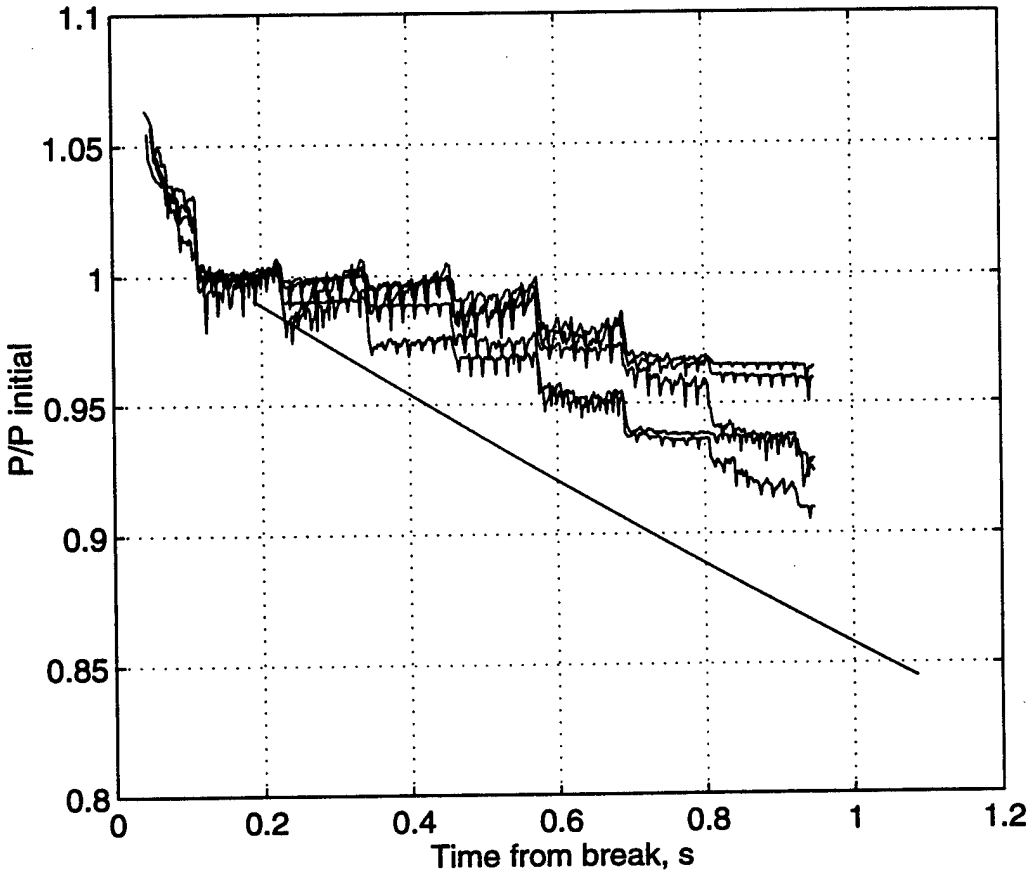

Figure 97 Normalized Pressure Comparison with Theory, 100 C

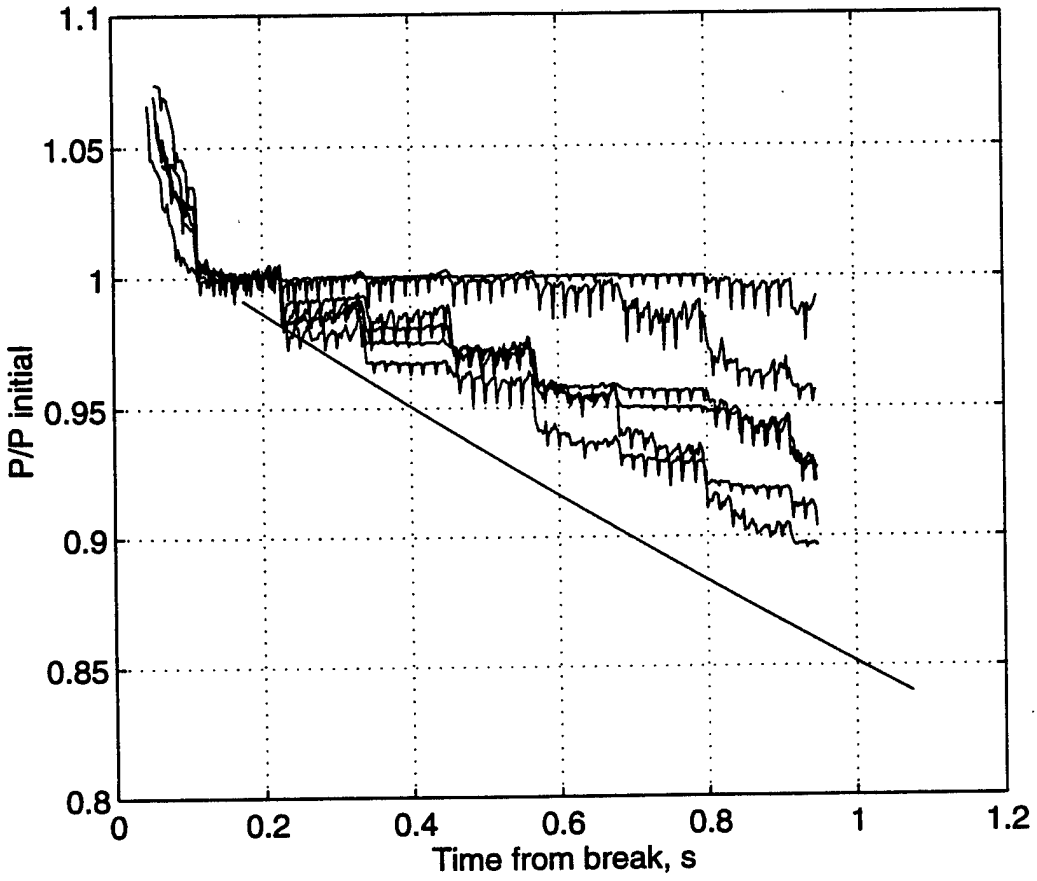

Figure 98 Normalized Pressure Comparison with Theory, 125 C

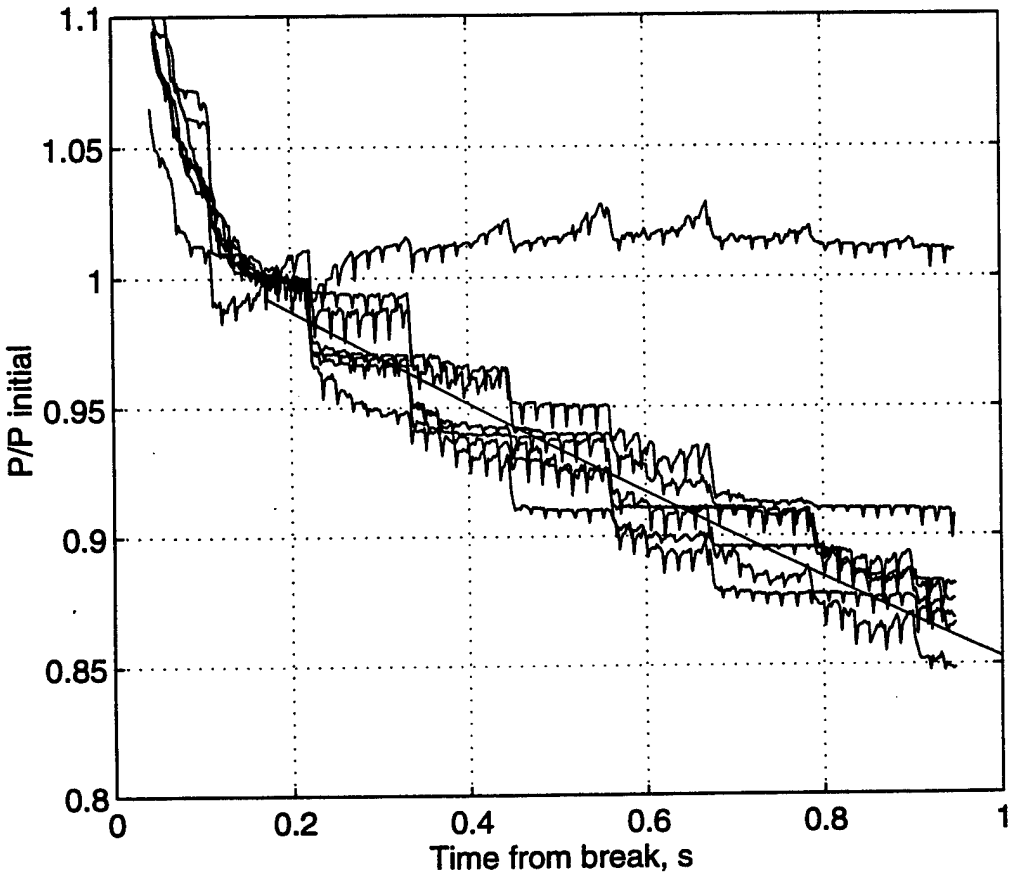

Figure 99 Normalized Pressure Comparison with Theory, 150 C

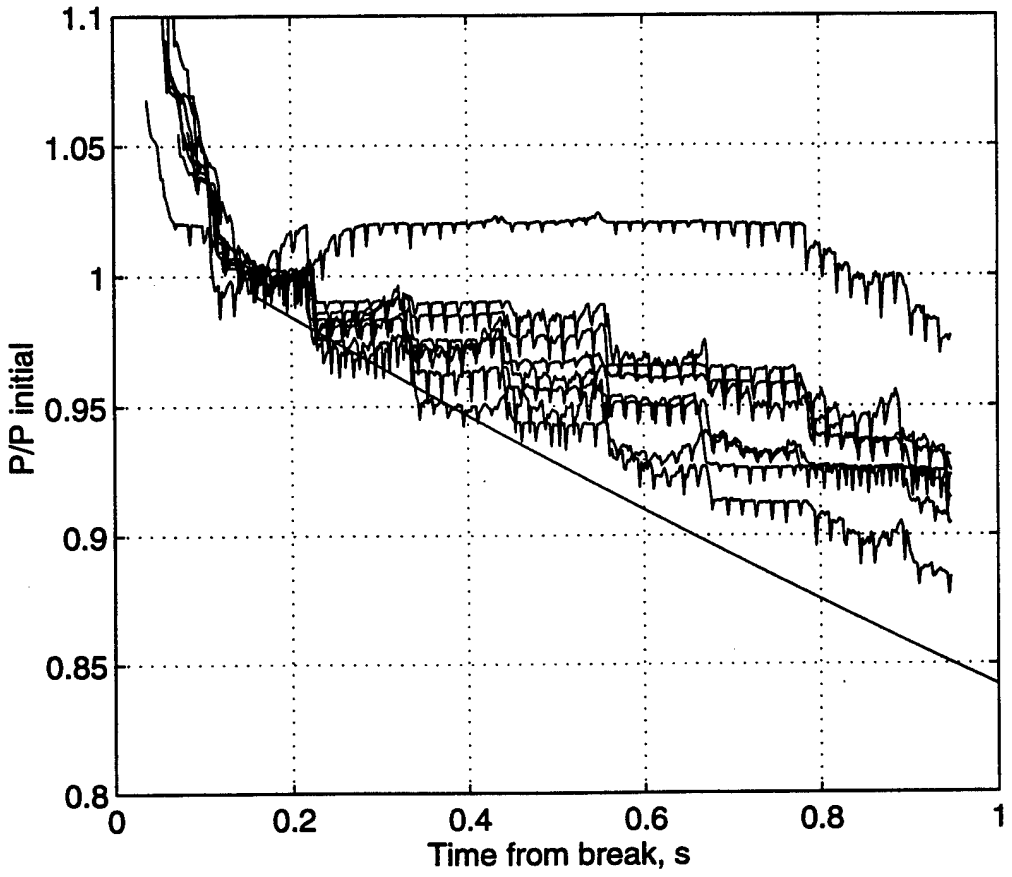

Figure 100 Normalized Pressure Comparison with Theory, 180 C

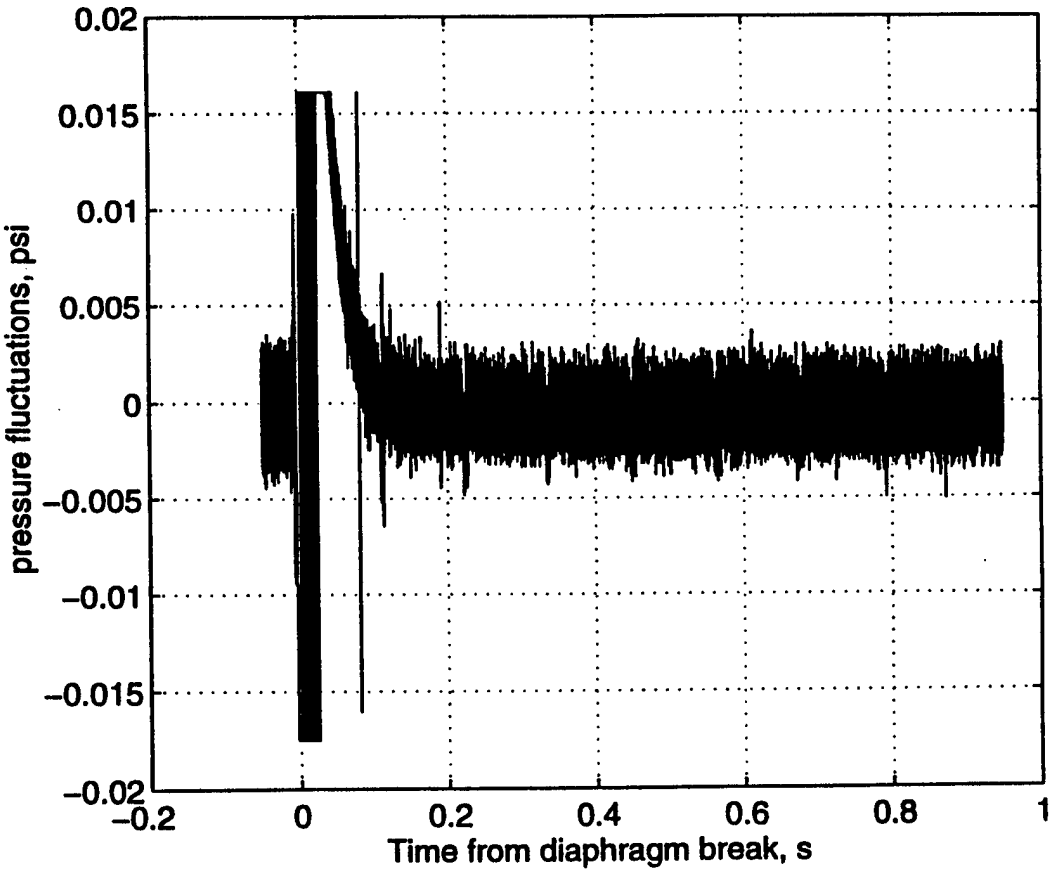

Figure 101 Sample Heated Pressure Signal, Low Noise

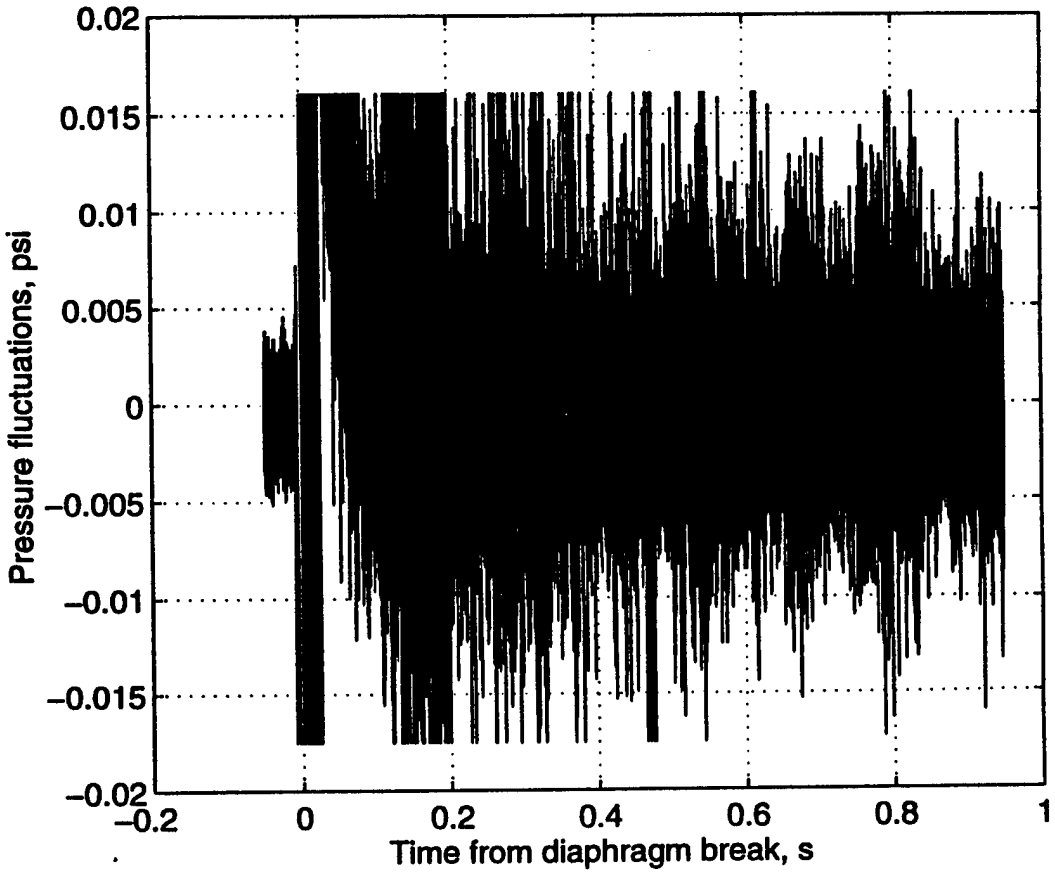

Figure 102 Sample Heated Pressure Signal, High Noise

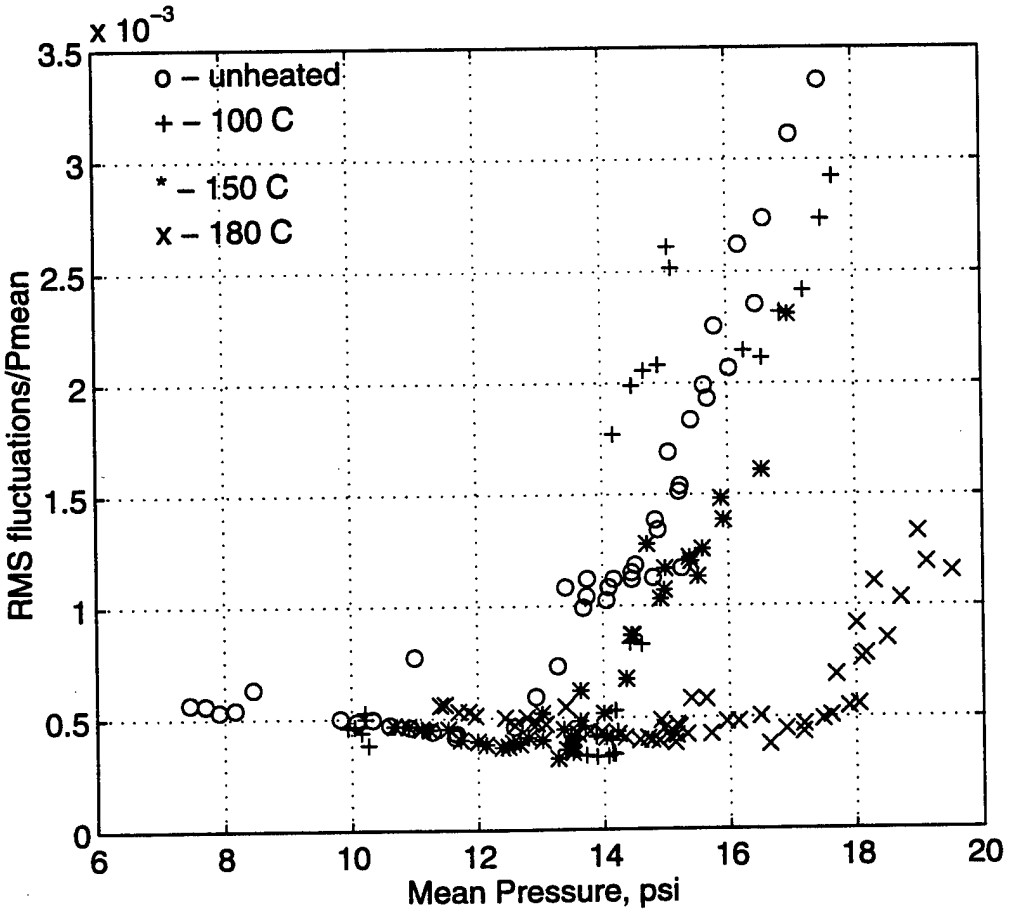

Figure 103 RMS Noise Level vs. Pressure

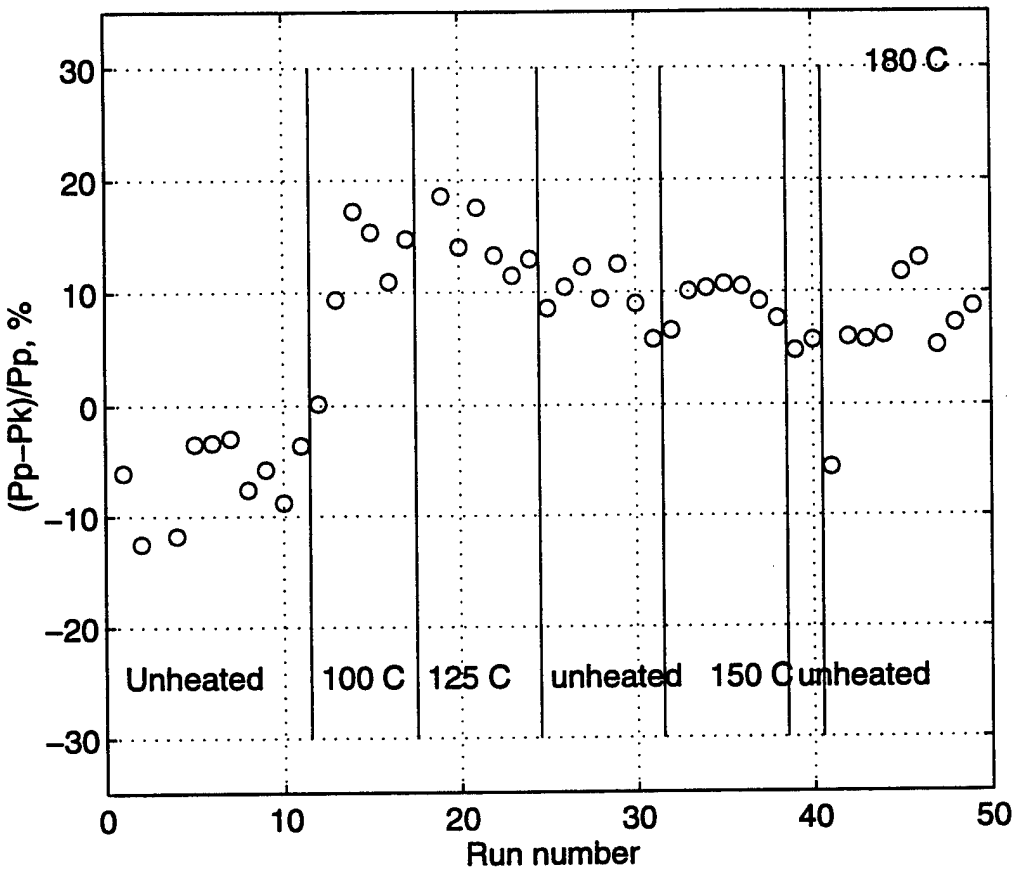

Figure 104 Percent Difference Between Kulite and Paroscientific Pressure Transducers

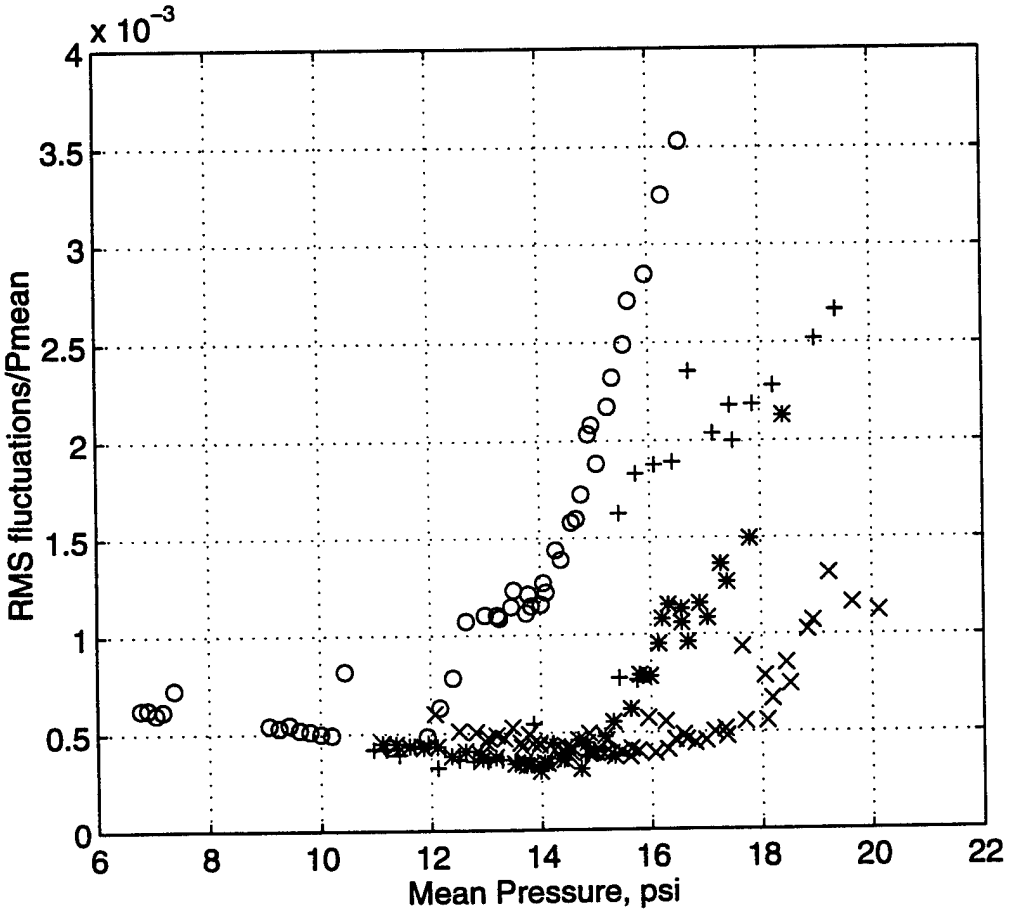

Figure 105 RMS Noise Levels vs. Theoretical Pressure

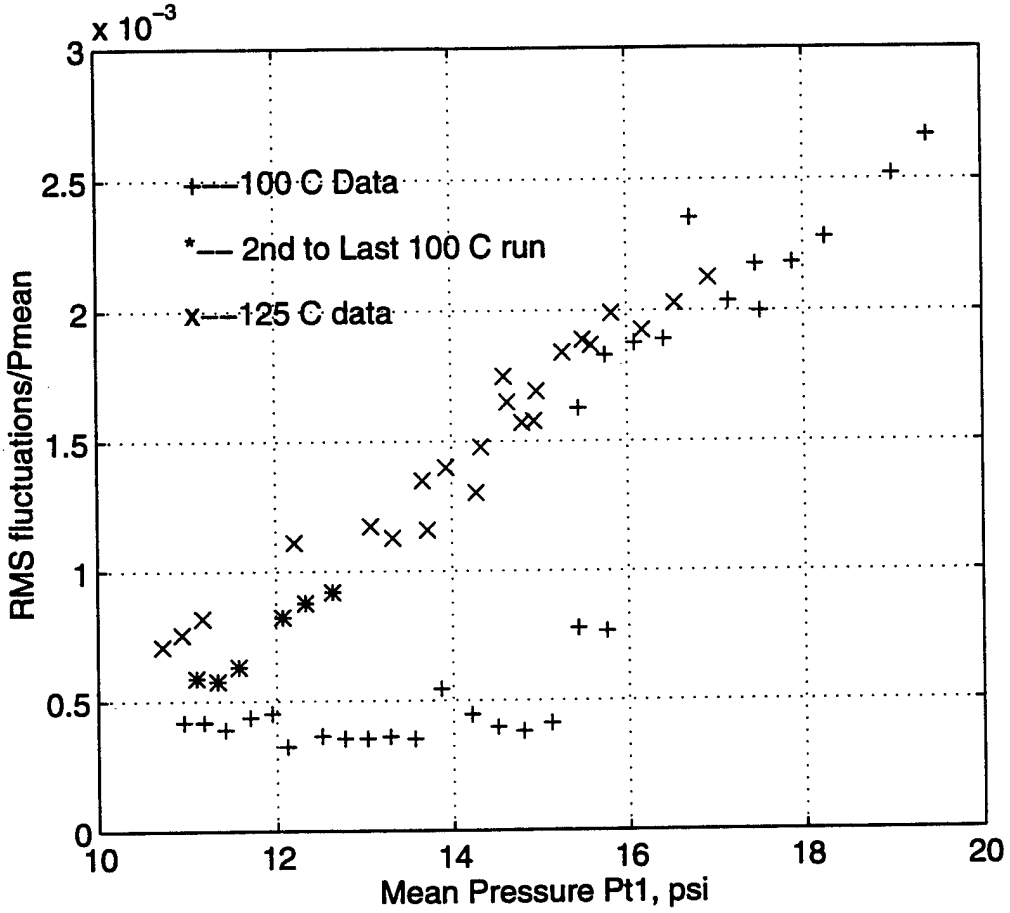

Figure 106 Comparison of 100 C and 125 C Data

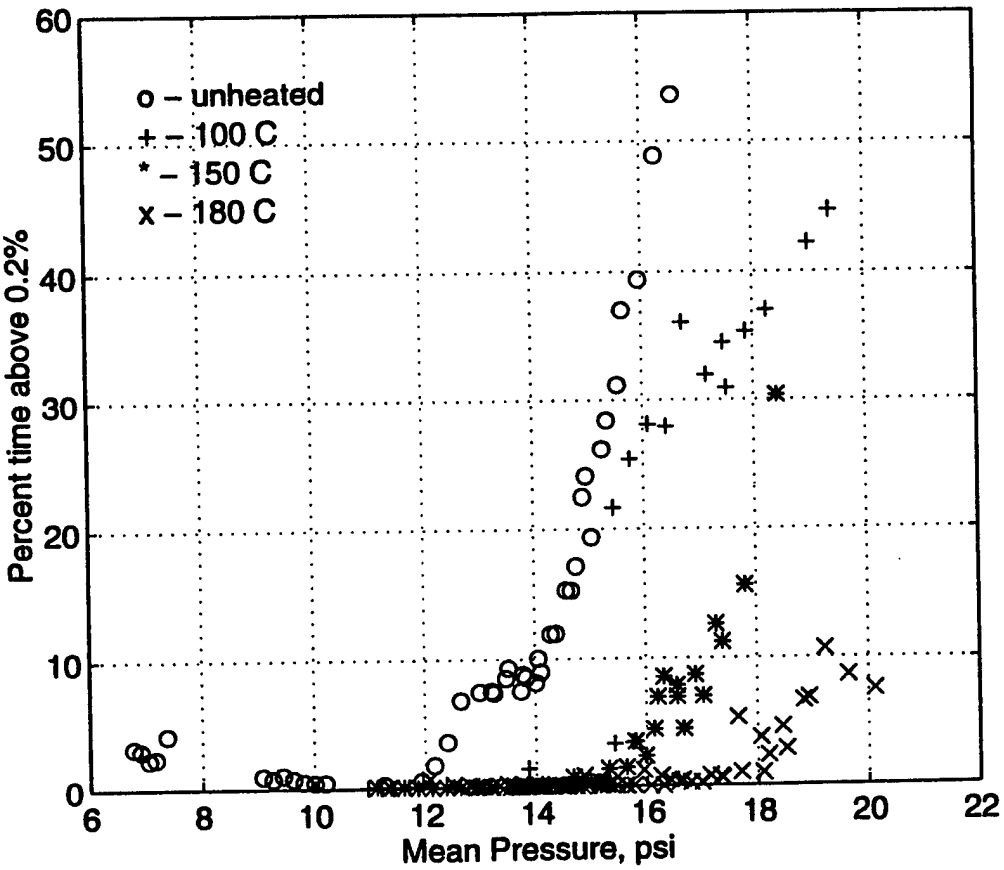

Figure 107 τ vs. Theoretical Pressure

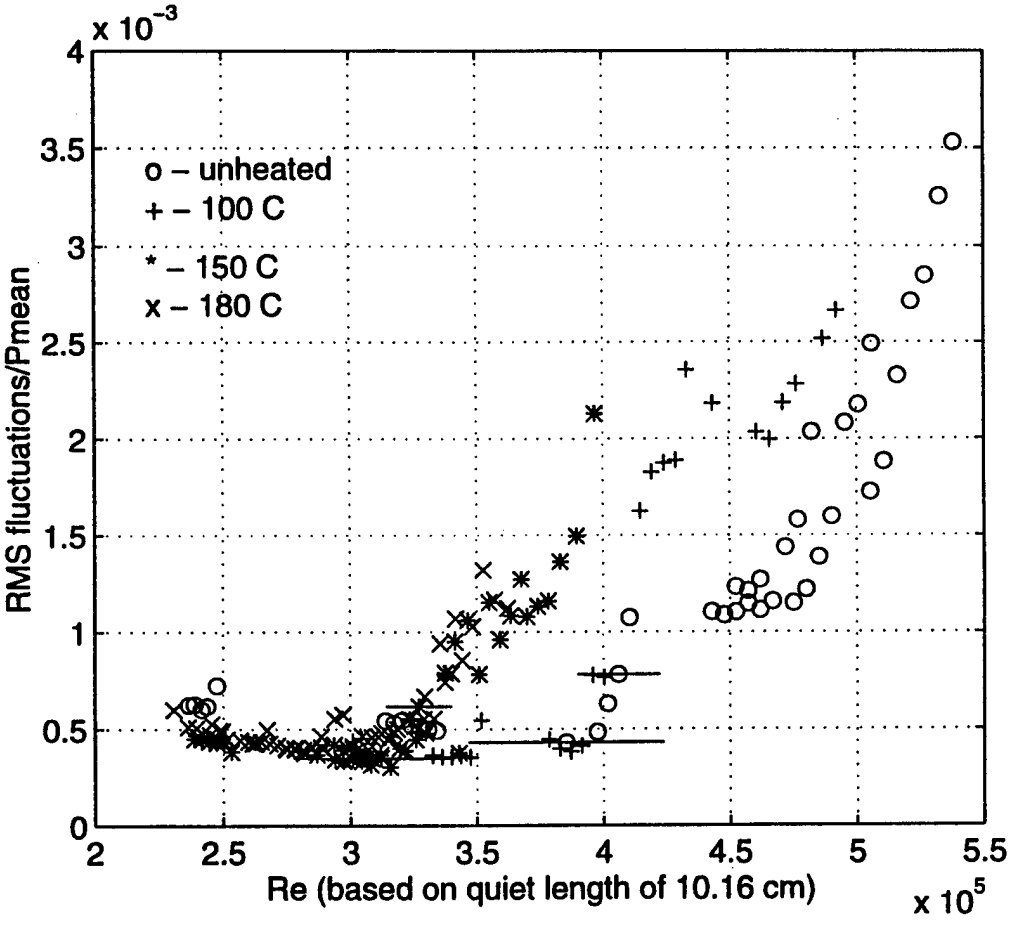

Figure 108 RMS Noise Levels vs. Reynolds Number

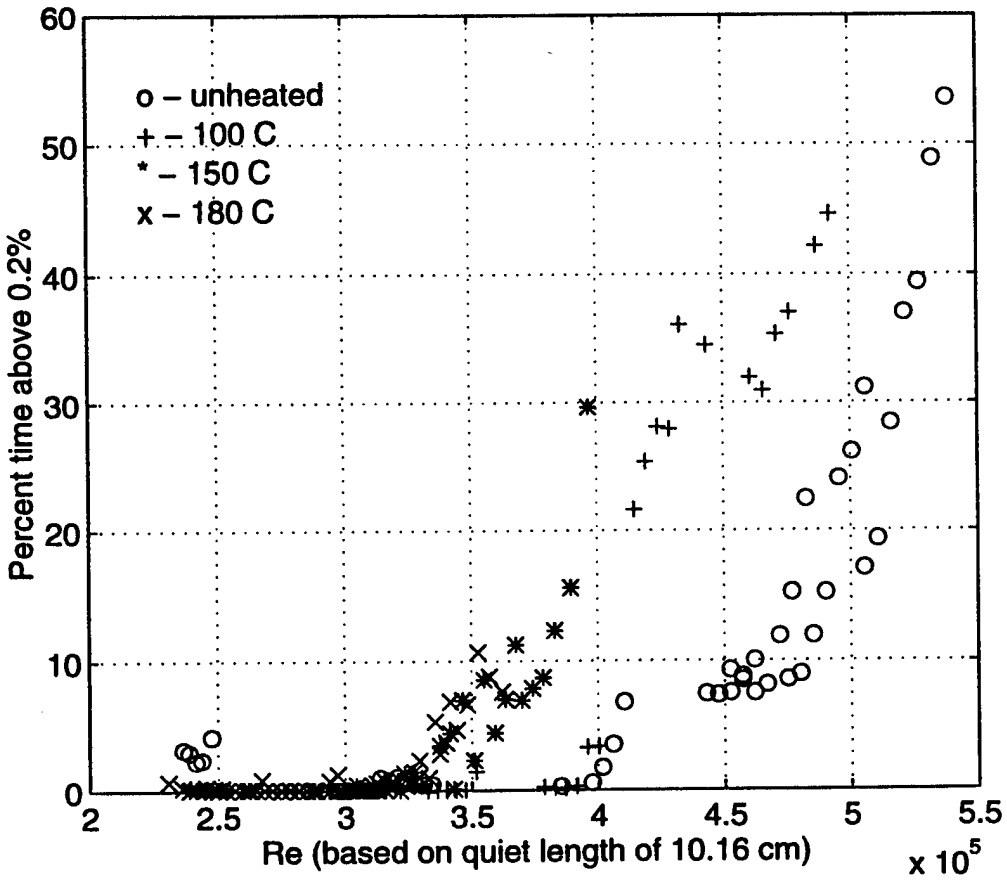

Figure 109 τ vs. Reynolds Number

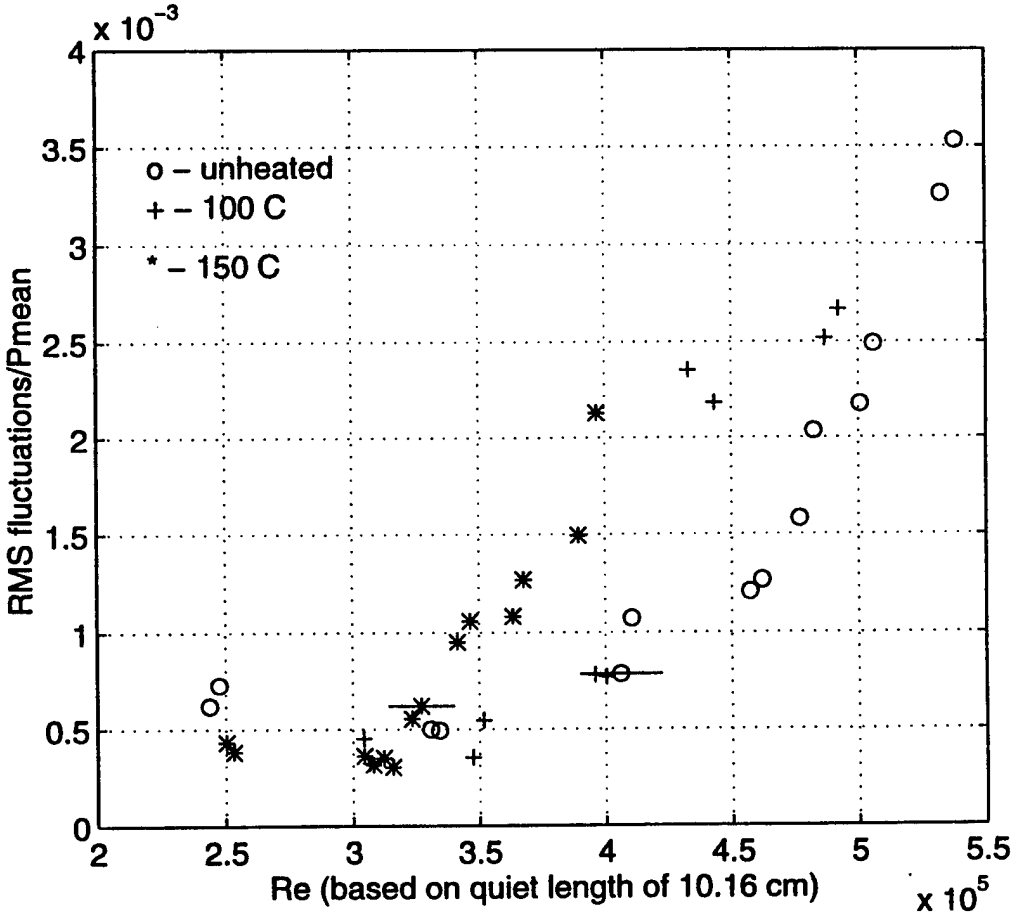

Figure 110 Most Reliable RMS vs. Reynolds Number

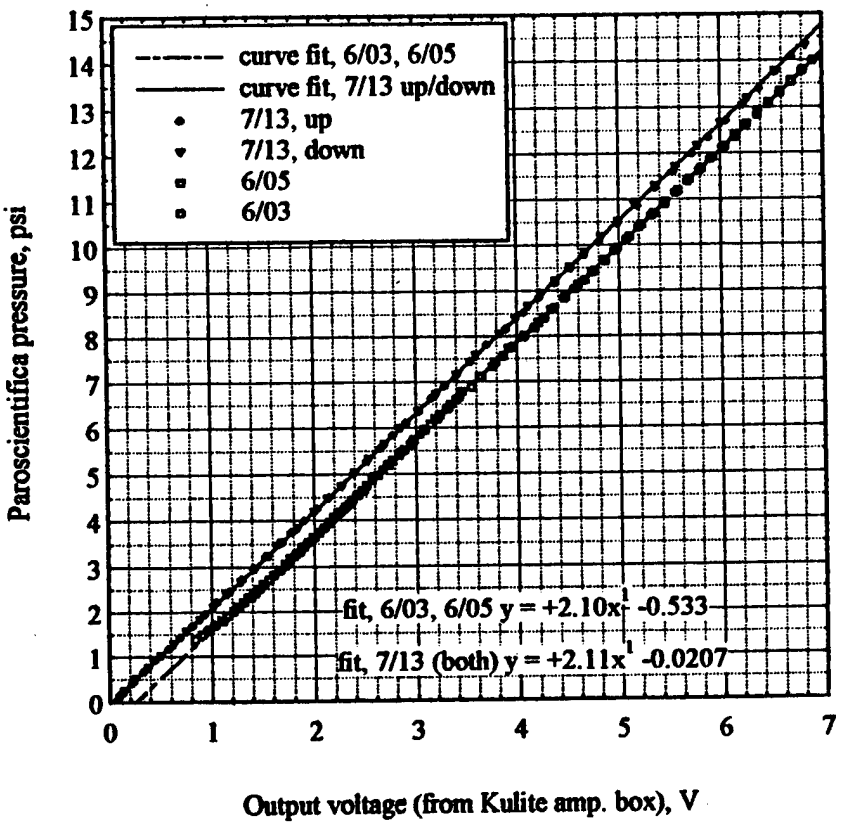

Figure 111 Comparison of After 180 C Kulite Calibration and Earlier Calibrations

CHAPTER 4 CONCLUSIONS AND RECOMMENDATIONS

4.1 Conclusions

First, the major goal of the experiment has been met satisfactorily. This research has shown that the Ludwieg Tube driver air can be heated without a major change in the quiet-flow capability of the tunnel. This has been done for the moderate air temperatures around 80 C without much problem. The tunnel still has quiet flow to z=13.33 inches back from the throat (4.0 inches downstream of onset of uniform flow) up to an quiet length Reynolds number of 380,000. This heated condition is very repeatable from run to run. Unfortunately the maximum quiet flow Reynolds number continues to decrease with increasing temperature. It is down to about 340,000 at about 130 C. The highest temperature data is not conclusive due to unknown actual temperature, however an estimated temperature (160 C) does produce a slight drop in Reynolds number to about 314,000.

The reduction in Reynolds number can also be compared with the wall-to-total temperature ratio. A 15% decrease in Reynolds number occurs for a wall-to-total temperature ratio of 0.85. This can be compared to Harvey *et al.* (1975) where a 20% increase in nozzle wall transition Reynolds number was achieved with a wall-to-temperature ratio of 1.4. Although, the data from 1975 was at Mach 5, the experiments produce opposite effects for opposite heating conditions.

Although temperatures above 100 C are not quite as repeatable, they are fairly consistent. The scatter in the temperature from run to run is probably due to several

small details, such as the wait time, circulation heater temperature setting, and amount of overheat on the nozzle flange area. With more fine tuning, the repeatability could probably be improved.

It also appears that all the data other than the 180 C data showed uniform heating of the gas in the driver tube except for near the contraction. The data matched the isentropic theory extremely well. If large non-uniformities existed in the gas, they most likely would have made the temperature ratio deviate from the theory. This is very useful, because basic running procedure only has to be slightly modified to produce these results. It is clear that the current heating system is not capable of heating to temperatures high enough to prevent local temperature at Mach 6 from reaching the static liquefaction limit (187 C). There are two areas that need improvements. Once these are made it is likely the heating system will be capable of heating to the maximum desired temperature. These areas are the downstream and upstream ends of the heater system.

There is a definite heating problem near the contraction. The flange face and nozzle provide a very large thermal mass for heat to escape from the driver tube. This makes the air that is initially near the nozzle cooler. This cooler air is the first air through the nozzle after start-up, resulting in a very slow rise to the maximum temperature (on the order of about 0.3 s). This can be compensated for to a certain degree by overheating this area of the driver tube. Unfortunately at the higher temperatures, even this did little to prevent a slow rise to temperature. This essentially causes the first 0.3 s of a run to be useless because the temperature is not uniform. Any attempt to alleviate this problem by adding more heat is hampered by the fact that very little insulation could be used to cover this region because of the short nozzle. Large amounts of insulation would clutter and hinder optical access to the nozzle area. A special heating system will definitely have to be designed to solve this problem. Part of the Mach 6 design is to include a commercial strip heater attached directly to the flange face. This would apply heat more directly to the cool area. A similar heat loss occurs at the other end of the heater system.

There is also a heating problem at the upstream end. This is most likely due to the large heat sink created by the unheated portion of the driver tube. To resolve this

problem, the entire driver tube will have to be heated. As discussed earlier, it was hoped only heating part of the driver tube could save much time, energy, and money, since air from only the first 1/3 to 1/2 of the driver tube passes through the nozzle during a run. However, it appears that this cannot be done without sacrificing flow quality at higher temperatures.

Even with these problems, the quiet flow region was not seriously affected by the heated air. Any connective currents present, although hopefully small, do not cause drastic changes to the overall flow. The quiet flow Reynolds number does decrease with the increasing temperature. This is unfortunate, but it will not prevent elevated temperature work in the quiet flow environment. If the nozzle is overheated with respect to the gas the trend is likely to reverse, as in Harvey *et al.* (1975).

4.2 Recommendations

There are some fairly straightforward improvements that need to be made in order to make the heating system more repeatable. First of all, the entire driver tube probably must be heated and insulated to prevent non-uniformities in temperature at higher temperatures (above 150 C). It seems reasonable at this point to simply continue the same type of heating system to the rest of the tube. There does not seem to be a problem with reaching the desired temperatures, where the tube is well insulated and isolated from large heat sinks.

Some way of thermally insulating the supports from the driver tube may also need to be developed. At the lower desired temperatures, only slight heating of the supports occurred, but at the higher temperatures, the upper portions of the structure became very hot to the touch. This is not necessarily a safety issue, but more of a heat-loss issue. The strange dip in the temperature traces occurs at approximately the time where air originally near the support and associated flanges is passing through the nozzle.

It is also apparent that a nozzle/flange heater will have to be specially designed for any future facility. This also applies to the current facility if it is to be routinely operated

at elevated temperatures. At minimum, a specially made ring surface heater should be installed on the exposed surface area of the flange. More insulation in this area would also be helpful. A longer nozzle will have more room between the end of the driver tube and the optical access windows for more insulation.

Some way of dealing with the oil and paint flakes will also have to be devised. While cleaning the nozzle frequently allows one to run experiments, it is time consuming and unpredictable as to how often it must be done. As discussed earlier, it does not seem to come from upstream of the filters because it does not occur during unheated runs. Obviously a solution must be found since the film forms on all the surfaces including the optical windows and sensors.

The paint problem was easily identified, but the best solutions are probably rather expensive. There are only two solutions outside of frequently cleaning the nozzle. The driver tube will have to be replaced with a stainless steel tube, or the current tunnel will have to remain a facility that does not require heating for routine operation. It is the feeling of the author that routinely heating the current driver tube will eventually cause much more trouble than benefit.

Another problem with the current configuration is the vacuum line. If a below-atmospheric driver pressure is desired, air is bled from the driver tube back through the fill line. However, this creates a problem when performing heated runs. If the air is heated above 225 F it can damage the original particle filter. Some method of lowering the driver pressure without passing heated air through the original filter should be developed.

4.2.1 Suggestions for Repeatable Data

Aside from making the modifications to the heating system, there are some things that can be done to possibly make the data more repeatable. Following a consistent procedure is very important in obtaining consistent data. This includes making sure to set the circulation heater to the same temperature when re-filling the tunnel, and using the circulation heater when increasing pressure for above-atmospheric-pressure runs.

Installation of a remote on/off switch for the circulation heater would be helpful in this. In this case, the temperature could be left at the same level and the switch could be flipped to turn on the heater when the fill line was opened.

Another possible way of obtaining more repeatable data is to keep the time between runs as consistent as possible. Before installation of the circulation heater this was the only way to ensure two runs would have similar temperature. Having a consistent wait time gives the same amount of time for any differences between air and pipe to settle out. The wait times for this study were intentionally varied to verify that the circulation heater could consistently heat to the desired temperature without a long wait. However, for best results a consistent wait time should be used, whether it be the minimum turnaround time, or a set amount of time chosen by the experimenter.

4.2.2 Instrumentation Recommendations

It is definitely recommended that for any work to be performed at elevated temperatures that the instrumentation be rated for the intended temperature range. Even though the Kulite was only exposed to the high temperatures for a short time, it seems that the calibration was greatly affected by the temperature. The temperature also most likely caused the failure of the Kulite. Hopefully future experiments can use a pressure transducer specifically designed and compensated for high temperatures.

If possible, it would also be helpful to calibrate the transducer at different temperatures to verify any compensation problems and be able to quantify them. This however is probably unfeasible since it would be very time consuming to try to calibrate a pressure transducer at each desired temperature. If this were attempted with the current calibration procedure with the probe installed in the tunnel, a method for monitoring the actual probe temperature would be needed. A more feasible solution would be to calibrate the transducer as often as possible and keep a record of any changes that occur.

The cold wire system overall worked very well. The change from battery power to power from a supply should eliminate the problems seen in this experiment. Even with

this improvement it is always good to frequently take reference voltage, resistance and temperature measurements. Thus if any drift does occur, adjustments can be made in the processing of the data. The resistivity of the wires, α, was very consistent, even for different wire probes (same wire material).

LIST OF REFERENCES

LIST OF REFERENCES

Barker, S. J. and Gile, D. 1981 Experiments on Heat Stabilized Laminar Boundary Layers in Water. *J. Fluid Mech.*, **17**, 139-158.

Beckwith, I. E., Chen, F. -J., Wilkinson, S. P., Malik, M. R., Tuttle, D. G. 1990 Design and Operational Features of Low Disturbance Wind Tunnels at NASA Langley for Mach Numbers From 3.5 to 18. AIAA Paper 90-1391.

Beckwith, I. E., Creel, T., Chen, F. -J., and Kendall, L. 1983 Freestream Noise and Transition Measurements on a Cone in a Mach 3.5 Pilot Low-disturbance Tunnel. NASA TP-2180.

Beckwith, I. E., and Miller, C. G., III 1990 Aerothermodynamics and Transition in High-Speed Wind Tunnels at NASA Langley. *Annual Review of Fluid Mechanics.* **22**, 419-439.

Blanchard, Alan E., Lachowicz, Jason T., Wilkinson, Stephen P. 1996 Performance of the NASA-Langley Mach 6 Quiet Wind Tunnel. AIAA Paper 96-0441.

Bushnell, D. M. 1990 Notes on Initial disturbance Fields for the Transition Problem. *Instability and Transition*, (edited by M. Y. Hussaini and R. G. Voight), pp. 217-232. Springer-Verlag.

Bushnell, D. M., Malik, M. R., and Harvey W. D. 1988 Transition Prediction in External Flows via Linear Stability. Symposium Transsonicum III, IUTAM Symposium Gottingen (edited by J. Zierep and H Oertel), pp 24-27. Springer-Verlag.

Chan, C. -L., Malik, M. R., and Vinh, H. 1995 Linear and Nonlinear Stability of Compressible Swept-Wing Boundary Layers. AIAA Paper 95-2278.

Chen, F. -J., Malik, M. R., and Beckwith, I. E. 1989 Boundary-Layer Transition on a Cone and Flat Plate at Mach 3.5. *AIAA Journal*,. **27**, No. 6, 687-693.

Chen, Fang-Jenq, Malik, Mujeeb R., and Beckwith, Ivan E. 1989 Advanced Mach 3.5 Axisymmetric Quiet Nozzle. NASA High Technology Report No. HTC-8903.

Chen, F. -J., Wilkinson, S. P., and Beckwith, I. E., 1991 Gortler Instability and Hypersonic Quiet Nozzle Design. AIAA Paper 91-1648.

Demetriades, Anthony 1994 Stabilization of a Nozzle Boundary Layer by Surface Heating. AIAA Paper 94-2501.

Demetriades, A., Mueller, R.L., Reda, D. C., and King, L. S. 1994 Boundary-Layer Studies in a 2-D Supersonic Nozzle for Quiet-Tunnel Applications. AIAA Paper 94-2507.

Demetriades, Anthony 1992 Cooling and Roughness Effects on Transition on Nozzle Throats and Blunt Bodies. *Journal of Spacecraft and Rockets*, **29**, 432-436.

Dougherty, N. Sam Jr., and Fisher, David F. 1982 Boundary-Layer Transition Correlation on a Slender Cone in Wind tunnels and Flight for Indication of Flow Quality. AEDC-TR-81-26.

Fisher, David F., and Dougherty, N. Sam Jr. 1982 In-Flight Transition Measurement on a 10 deg. Cone at Mach Numbers From 0.5 to 2.0. NASA TP-1971.

Floryan, J. M. 1991 On the Gortler Instability of Boundary Layers. *Prog. Aerospace Sciences*, **28**, 235-271.

Gasperas, G., 1989 Effect of Wall Temperature Distribution on the Stability of the Compressible Boundary Layer. AIAA Paper 89-1894.

Harvey, W. D., Stainback, P. C., Anders, J. B., and Cary, A. M. 1975 Nozzle Wall Boundary-Layer Transition and Freestream Disturbances at Mach 5. *AIAA Journal*, **13**, No. 3, 307-314.

Holden, M. Bower, D., and Chadwick, K. 1995 Measurements of Boundary Layer Transition on Cones at Angle of Attack for Mach Numbers from 11 to 13. AIAA Paper 95-2294.

Incropera, Frank P., and Dewitt, David P. 1990 *Fundamentals of Heat and Mass Transfer*. 3rd edition. John Wiley and Sons.

Kendall, James M. 1993 Experimental Methods and Results on Supersonic Boundary-Layer Stability and Receptivity. ICASE Short Course on Stability and Transition, NASA Langley. To be published by Oxford University Press.

Kistler, Alan L. 1958 Fluctuation Measurements in Supersonic Turbulent Boundary Layers. Balistic Research Laboratory Report no. 1052.

Lachowicz, J. T., and Chokani, N. 1996 Hypersonic Boundary Layer Stability over a Flared Cone in a Quiet Tunnel. AIAA Paper 96-0782.

Laufer, John 1961 Aerodynamic Noise in Supersonic Wind Tunnels. J. Aerospace Sci. **28**, 685-692.

Laufer, John 1964 Some Statistical Properties of the Pressure Field Radiated by a Turbulent Boundary Layer. Physics of Fluids, **7**, No. 8, 1191-1197.

Mack, Leslie M. 1984 Boundary-Layer Linear Stability Theory. In AGARD Report No. 709: Special Course on Stability and Transition of Laminar Flow.

Malik, M., and Balakumar, P. 1992 Instability and Transition in Three-Dimensional Supersonic Boundary Layers. AIAA Paper 92-5049.

Mayle, Robert Edward 1991 The Role of Laminar-Turbulent Transition in Gas Turbine Engines. *Journal of Turbomachinery*, **113**, 509-537.

Morkovin, Mark V. 1969 Critical Evaluation of Transition From Laminar to Turbulent Shear Layers with Emphasis on Hypersonically Traveling bodies. Air Force Flight Dynamics Laboratory TR-68-149.

Morkovin, Mark V. 1991 Panoramic View of Changes in Vorticity Distribution in Transition Instabilities and Turbulence. *Boundary Layer Stability and Transition to Turbulence*, (edited by D. C. Reda, H. L. Reed, and R. Kobayashi,) Vol. 114, pp. 1-12. Fluids Engineering Division, American Society of Mechanical Engineers, New York.

Narasimha, R. 1985 The Laminar-Turbulent Transition Zone in the Boundary Layer. *Prog. Aerospace Sciences*, **22**, 29-80.

Narasimha, R., and Dey, J. 1989 Transition-zone models for 2-dimensional boundary layers: A review. *Sadhana*, **14**, Part 2, 93-120.

Pate, S. R. 1971 Supersonic Boundary-Layer Transition: Effects of Roughness and Freestream Disturbances. *AIAA Journal*, **9**, 797-803.

Pope, Alan, and Goin, Kennith L. 1965 High Speed Wind Tunnel Testing. Wiley.

Reed, Helen L., and Saric, William S. 1989 Stability of Three-Dimensional Boundary Layers. *Annual Review of Fluid Mechanics*, **21**, 235-284.

Reshotko, Eli 1994 Boundary Layer Instability, Transition and Control. AIAA Paper 94-0001.

Schneider, Steven P., and Haven, Christine E. 1995 Quiet-Flow Ludwieg Tube for High-Speed Transition Research. *AIAA Journal*, **33**, No. 4, 688-693.

Schneider, Steven P., Collicott, Steven H., Schmisseur, J. D., Ladoon, Dale, Randall, Laura A., Munro, Scott E., and Salyer, T. R. 1996 Laminar-Turbulent Transition Research in the Purdue Mach-4 Quiet-Flow Ludwieg Tube. AIAA Paper 96-2191.

Spina, E. F., and McGinley 1994 Constant-Temperature Anemometry in Hypersonic Flow: Critical Issues and Sample Results. *Experiments in Fluids*. **17**, 365-374.

Stetson, Kenneth F. 1990 Comments on Hypersonic Boundary-Layer Transition. Wright Research and Development Center TR-90-3057.

Stetson, Kenneth F. 1992 Hypersonic Boundary-Layer Transition. *Advances in Hypersonics: Defining the Hypersonic Environment*, **1**, (edited by J. J. Bertin, J. Periaux, J. Ballmann), Birkhauser.

Stetson, Kenneth F., and Kimmel, Roger L. 1992 On Hypersonic Boundary-Layer Stability. AIAA Paper 92-0737.

Wegener, P. P. and Mack, L. M. 1958 Condensation in Supersonic and Hypersonic Wind Tunnels. In *Advances in Applied Mechanics,* Volume **5**. (edited by H. L. Dryden and Karman),

Wilkinson, S. P., Anders, S. G., Chen, F. -J., and Beckwith, I. E. 1992 Supersonic and Hypersonic Quiet Tunnel Technology at NASA Langley. AIAA Paper 92-3908.

Wilkinson, S. P., Anders, S. G., Chen, F. -J., and White, J. A. 1994 Status of NASA Langley Quiet Flow Facility Developments. AIAA Paper 94-2498.

Wright, R. L., and Zoby, E. V. 1977 Flight Boundary Layer Transition Measurements on a Slender Cone at Mach 20. AIAA Paper 77-719.

APPENDICES

Appendix A Operation Instructions

Normal (unheated) Operation of the Ludwieg Tube

This procedure assumes that the model has been installed, and all accompanying instrumentation has been set up and is operating.

1.) Insert an appropriate thickness diaphragm in the diaphragm holder and place in tunnel, making sure to plug in the breaker wires. Close the tunnel.
2.) Turn on vacuum pumps (before operating vacuum pumps one should be familiar with their operation procedures.)
3.) If the initial driver pressure is to be less than atmospheric follow a, b, c. Otherwise go to step 4.
    a.) Open valve #2 (figure 14) making sure valve #1 is closed.
    b.) Monitor driver pressure via the Paroscientific pressure transducer.
    c.) When the appropriate pressure is reached, close valve #2.
4.) When the desired vacuum pressure is reached, shut off the vacuum pumps.
5.) If the initial driver pressure is to be above atmospheric, follow a, b ,c . Otherwise go to step 6.
    a.) Open valve #1 (figure 14) and regulate flow with the pressure regulator.
    b.) SLOWLY increase pressure until the desired pressure is reached, monitor pressure via the Paroscientific pressure transducer.
    c.) Close valve #1 and turn pressure regulator to zero.
6.) Record initial conditions and fire tunnel when ready.
7.) The pressure is now well below atmospheric. To re-fill the tunnel, open valve #1 (see figure 14). Monitor pressure via the Paroscientific pressure transducer.
8.) When atmospheric pressure is reached, valve #1 can be closed, and the tunnel can be opened to replace the diaphragm (remember to open valve #1 for bleed air when the tunnel is open).

Operation of the Ludwieg Tube for Heated Runs

This procedure assumes that the model has been installed, and all accompanying instrumentation has been set up and is operating.

This procedure further assumes that the tunnel has been heated by the main system, and the fill line has been configured for heated runs (see figure 14).

Steps that are different from normal operational procedure will be designated with a *.

1.) Insert an appropriate thickness diaphragm in the diaphragm holder and place in tunnel, making sure to plug in the breaker wires. Close the tunnel.

2.) Turn on vacuum pumps (before operating vacuum pumps one should be familiar with their operation procedures)

3.) If the initial driver pressure is to be less than atmospheric follow a, b, c. Otherwise go to step 4.

   a.) Open valve #2 (figure 14) making sure valve #1 is closed.

   b.) Monitor driver pressure via the Paroscientific pressure transducer.

   c.) When the appropriate pressure is reached, close valve #2.

   d.*) Be aware that this brings heated gas from the driver tube back through the original particle filter which has a maximum temperature rating of 225 deg. F.

4.) When the desired vacuum pressure is reached, shut off the vacuum pumps.

5.) If the initial driver pressure is to be above atmospheric, follow a, b ,c . Otherwise go to step 6.

   a.) Open valve #1 (figure 14) and regulate flow with the pressure regulator.

   b.*) Turn on circulation heater to desired temperature

   c.) SLOWLY increase pressure until the desired pressure is reached, monitor pressure via the Paroscientific pressure transducer.

   d.*) Turn off circulation heater (heater should not be on when there is no air flow)

   e.) Close valve #1 and turn pressure regulator to zero.

6.) Record initial conditions and fire tunnel when ready.

7.) The pressure is now well below atmospheric. To re-fill the tunnel, open valve #1 (see figure 14).

8.*) Turn on circulation heater. Monitor pressure via the Paroscientific pressure transducer.

9.*) When atmospheric pressure is reached, turn off circulation heater.

10.) Close valve #1, and the tunnel can be opened to replace the diaphragm

11*) Remember to open valve #1 for bleed air when the tunnel is open and have circulation heater on to continue heating the incoming air.

Main Heater operation

Start up procedure:

These are the steps to heating the driver tube initially prior to any heated runs.

1.) Turn on the power supply and set the current limiters (volt and amp knobs) to the maximum positions. The power supply should be in remote mode and therefore the voltage and current should not change when the knobs are turned up. The controls are only limiters in this mode. Turning the knobs to the maximum positions will allow the supply to use maximum power to get the tube to temperature.

2.) Turn on the power at the control panel.

3.) Push the flush button labeled 'P'on the controller. The display should look like '3.0' with the 0 flashing. The number to the right of the '.' is the current menu. 0 is the control menu (The user should be familiar with the basic operations of the controller, especially with sections 3.1-4, 3.8 and 3.9 of the operations manual. Some helpful hints may also be found in the "Quick Start" pamphlet). The 3 is the current option for the 0 menu and signifies that the controller is in 'park' mode (no voltage out to the power supply)

4.) To change the current menu option push the '*' key. The 3 should now be flashing. The flashing number is the one that will change, so be sure the 3 is flashing.

5.) Change the menu option by pushing the up arrow key until 20 is displayed in place of the 3 (any number between 4 and 100 on the '.0' menu signifies a percentage of total power the controller will output to the supply).

6.) Push the flush button again and the display should read '20H' (20 flashing). The controller should be outputting a 20% signal to the supply. The square light on the display above 'sp1' should be flashing, this indicates that an analog signal is being output. The supply should be reading about 20% of 30 V in the voltage display.

7.) This setting should be left until the temperature of the wire seems to level off or only increase very slowly. I usually just left it alone for 10 minutes which is usually plenty of time.

8.) Once the wire temperature is rather stable, repeat steps 3-6 increasing the power by 15% each time until the wire temperature gets to 100 C or so. After pushing the flush button, the display should read '**.0' where **=the last power setting input.

9.) Once the wire reaches 100 C, the controller can be set to automatic control. This is done by following the above steps to set the 0 menu to 0, thus the display should read '0.0'. This puts the controller in automatic mode. Push the flush button again.

10.) The display will now show the measured temperature for the thermocouple that is being monitored. One of the arrows or square box should be lit on the left side of the display. This indicates whether the current temperature is above, at, or below the setpoint (see manual for details).

11.)Use switch 5 to select the thermocouple the controller should use to control the process (refer to table 1 or figure 17).

12.)To check the setpoint of the controller, push and hold the far left button ('*' button). The setpoint temperature will be displayed. It can be changed by continuing to hold the far left button and pushing the up or down arrow buttons as desired.

13.)As a safety precaution it is usually a good idea to set the current limiter to just above the power being used by the supply. If the controller is signaling to use full power, the voltage indicator on the supply should read 30 Volts. Because the impedance isn't

exactly matched, the supply may not be using maximum amperage. To set the limiter turn the amp knob down until the amperage starts to decrease. Turn the knob up slightly so it will limit current just above the current at that time. This will prevent the power supply from increasing current in the event of a problem.

Flange Heater

The flange heater should be slowly incremented to the desired power as well.
Just to be consistent, I usually increment the power to the flange heater at the same time as the main heater.

1.) Turn on the flange heater supply. Turn the current knob to zero and the voltage knob to the maximum setting.
2.) Increase the current to 5 amps. The voltage display should increase accordingly to about 2.5 V (the heater element resistance is about 0.5 Ohms).
3). When incrementing the main power, I usually increment the flange heater about another 5 Amps.
4.) It should eventually take about 20 Volts and 30 Amps (the resistance of the element increases as it heats) to heat station 1 to about 100 C. One should remember that this is only a guide, and actual heating will probably vary somewhat depending on the conditions. I have had the power supply to maximum voltage and maximum current. This makes the flange heating element on the order of 300 C or so and extreme care should be taken around the flange area as it is very hot.
5.) The temperature of the flange heating element can be monitored on temperature display 4 when switch 4 is set to channel 1.

Appendix B Analysis Codes

READLEC.M

```
% Reads in a Lecroy file, writes a MATLAB variable into your workspace.
% Written to be run from within MATLAB.
%
% Matlab usage:
% [v,t] = readlec( <lecroy filename>, [optional verbose flag (0, 1, or 2)]);
%
% Original: S. Collicott, March, 1995.
%

%
% Modifications:
%
%**********************************************************************
******
% Modified June 26, 1995 by Collicott:
%   - tolerate extra 7 or so bytes prepended by the GPIB transfer
%     from Lecroy scope to PC.
%**********************************************************************
******
%
%**********************************************************************
******
% Modified September 1, 1995 by Collicott:
%   - reads in Fourier transform traces.  Note the fftflag variable.
%
%**********************************************************************
******
% Modified March 6, 1996, by Collicott:
% Switched to +trigger_offset[i] and +pixel_offset in creation of
% time vector based on observations of Schmisseur that the pre-triggering
% was coming out incorrectly on the Matlab data.
%
%**********************************************************************
******
% Translated to m-file, S. Collicott, March, 1996.
%   - Reading subroutines into separate m-files:
%   - longread.m
%   - wordread.m
%   - flotread.m
```

```
%   - dbleread.m
%
%*********************************************************************
******
%
function [volts_out, time_out] = readlec( lecroy_file, verbose)
%
% set verbose flag
%
if nargin == 1
 verbose = 0;
end
%
% Open file, proceed if successful.
%
lec_ptr = fopen(lecroy_file);
if lec_ptr  == -1
 fprintf(1, 'Exiting: Error opening LeCroy file: %s\n', lecroy_file);
 volts_out = [];
 time_out = [];
else
%
% Read until WAVEDESC is found.Typically 11 bytes extra at start, unless
% sent over GPIB from o-scope to PC, then a command is echoed for extra
% bytes which may contain 'WAVE' and other strings.
% No, I don't know why.Collicott, June, 1995.
%
 wavedesc_found = 0;
 descriptor_name = sprintf('1234567812345678');
 while ~wavedesc_found
  descriptor_name(1) = fread( lec_ptr, 1, 'char');
  if descriptor_name(1) == 'W'
   descriptor_name(2) = fread( lec_ptr, 1, 'char');
   if descriptor_name(2) == 'A'
    descriptor_name(3) = fread( lec_ptr, 1, 'char');
    if descriptor_name(3) == 'V'
     descriptor_name(4) = fread( lec_ptr, 1, 'char');
     if descriptor_name(4) == 'E'
      descriptor_name(5) = fread( lec_ptr, 1, 'char');
      if descriptor_name(5) == 'D'
       descriptor_name(6) = fread( lec_ptr, 1, 'char');
       if descriptor_name(6) == 'E'
        descriptor_name(7) = fread( lec_ptr, 1, 'char');
        if descriptor_name(7) == 'S'
```

```
            descriptor_name(8) = fread( lec_ptr, 1, 'char');
            if descriptor_name(8) == 'C'
              wavedesc_found = 1;
            end
           end
          end
         end
        end
       end
      end
     end
%
% Read in the other 32 of the first 36 bytes.
%
 descriptor_name(9:16) = fread( lec_ptr, 8, 'char');
 template_name = fread( lec_ptr, 16, 'char');
 comm_type = fread( lec_ptr, 2, 'char');
 comm_order = fread( lec_ptr, 2, 'char');
 if verbose > 1
  fprintf(1, '%s\n', descriptor_name(find(descriptor_name ~= 0)));
  fprintf(1, '%s\n', template_name(find(template_name ~= 0)));
  fprintf(1,'%d%d, %d%d\n', comm_type(1), comm_type(2),...
   comm_order(1), comm_order(2));
 end
%
% Swapping flag set for Suns.
%
 if comm_order(1) == 1
  swapflag = 1;
 else
  swapflag = 0;
 end
%
% Read block lengths.
%
 wave_descriptor = longread( lec_ptr, swapflag);
 user_text       = longread( lec_ptr, swapflag);
 res_desc1       = longread( lec_ptr, swapflag);
 if verbose > 1
  fprintf(1,'wave_descriptor: %d\nuser_text: %d\nres_desc1: %d\n',...
   wave_descriptor, user_text, res_desc1);
 end
%
```

```
% Read array lengths.
%
 trigtime_array = longread( lec_ptr, swapflag);
 ris_time_array = longread( lec_ptr, swapflag);
 res_array1     = longread( lec_ptr, swapflag);
 wave_array_1   = longread( lec_ptr, swapflag);
 wave_array_2   = longread( lec_ptr, swapflag);
 res_array2     = longread( lec_ptr, swapflag);
 res_array3     = longread( lec_ptr, swapflag);


 if verbose > 1
  fprintf(1,'trigtime_array = %d\n', trigtime_array);
  fprintf(1,'ris_time_array = %d\n', ris_time_array);
  fprintf(1,'res_array1 = %d\n', res_array1);
  fprintf(1,'wave_array_1 = %d\n', wave_array_1);
  fprintf(1,'wave_array_2 = %d\n', wave_array_2);
  fprintf(1,'restime_array2 = %d\n', res_array2);
  fprintf(1,'res_array3 = %d\n', res_array3);
 end
%
% Instrument identity.
%
 instrument_name   = fread(lec_ptr, 16, 'char');
 instrument_number = longread( lec_ptr, swapflag);
 trace_label       = fread(lec_ptr, 16, 'char');
 reserved1         = wordread( lec_ptr, swapflag);
 reserved2         = wordread( lec_ptr, swapflag);

 if verbose > 1
  fprintf(1, 'Instrument name: %s\n', ...
   instrument_name( find(instrument_name ~= 0)));
  fprintf(1, 'Instrument number: %d\n', instrument_number);
  fprintf(1, 'trace_label: %s\n', ...
   trace_label( find(trace_label ~= 0)));
 end
%
% Waveform information.
%
 wave_array_count = longread( lec_ptr, swapflag);

 fftflag = 0;
 if wave_array_1 == 2 * wave_array_count
  fftflag = 1;
```

```
end

pnts_per_screen = longread( lec_ptr, swapflag);
first_valid_pnt = longread( lec_ptr, swapflag);
last_valid_pnt  = longread( lec_ptr, swapflag);
first_point     = longread( lec_ptr, swapflag);
sparsing_factor = longread( lec_ptr, swapflag);
segment_index   = longread( lec_ptr, swapflag);
subarray_count  = longread( lec_ptr, swapflag);
sweeps_per_acq  = longread( lec_ptr, swapflag);
obsolete1       = longread( lec_ptr, swapflag);

if verbose > 0
 fprintf(1, 'wave_array_count: %d\n', wave_array_count);
 if fftflag == 1
  fprintf(1,'FFT trace detected\n');
 end
end
if verbose > 1
 fprintf(1, 'pnts_per_screen: %d\n', pnts_per_screen);
 fprintf(1, 'first_valid_pnt: %d\n', first_valid_pnt);
 fprintf(1, 'last_valid_pnt: %d\n', last_valid_pnt);
 fprintf(1, 'first_point: %d\n', first_point);
 fprintf(1, 'sparsing_factor: %d\n', sparsing_factor);
 fprintf(1, 'segment_index: %d\n', segment_index);
end
if verbose > 0
 fprintf(1, 'subarray_count: %d\n', subarray_count);
 fprintf(1, 'sweeps_per_acq: %d\n', sweeps_per_acq);
end
%
% Vertical information.
%
 vertical_gain     = flotread(lec_ptr, swapflag);
 vertical_offset   = flotread(lec_ptr, swapflag);
 max_value         = flotread(lec_ptr, swapflag);
 min_value         = flotread(lec_ptr, swapflag);
 nominal_bits      = wordread(lec_ptr, swapflag);
 nom_subarray_count = wordread(lec_ptr, swapflag);

 if verbose > 1
  fprintf(1, 'vertical_gain = %f\n', vertical_gain);
  fprintf(1, 'vertical_offset = %f\n', vertical_offset);
  fprintf(1, 'max_value = %f\n', max_value);
```

```
   fprintf(1, 'min_value = %f\n', min_value);
   fprintf(1, 'nominal_bits = %d\n', nominal_bits);
   fprintf(1, 'nom_subarray_count = %d\n', nom_subarray_count);
  end
%
% Horizontal information.
%
  horiz_interval = flotread( lec_ptr, swapflag);
  horiz_offset   = dbleread( lec_ptr, swapflag);
  pixel_offset   = dbleread( lec_ptr, swapflag);

  if verbose > 1
   fprintf(1, 'horiz_interval = %f\n', horiz_interval);
   fprintf(1, 'horiz_offset = %f\n', horiz_offset);
   fprintf(1, 'pixel_offset = %f\n', pixel_offset);
  end
%
% Unit names.
%
  vertunit = fread(lec_ptr, 48, 'char');
  horunit =  fread(lec_ptr, 48, 'char');

  if verbose > 0
   fprintf(1, 'vertunit = %s\n', ...
     vertunit( find(vertunit ~= 0)));
   fprintf(1, 'horunit = %s\n', ...
     horunit( find(horunit ~= 0)));
  end
%
% Reserved exansion; no apparent present use.
%
  reserved3 = wordread( lec_ptr, swapflag);
  reserved4 = wordread( lec_ptr, swapflag);
%
% Times; trigger timestamp presently unparsed.
%
  trigger_time_stamp = fread( lec_ptr, 16, 'uchar');
  acq_duration       = flotread( lec_ptr, swapflag);

  if verbose > 0
   fprintf(1, 'acq_duration = %f\n', acq_duration);
  end
%
%record and processing enums.
```

```
%
 record_type     = fread(lec_ptr, 2, 'char');
 processing_done = fread(lec_ptr, 2, 'char');
 reserved5       = wordread( lec_ptr, swapflag);
 ris_sweeps      = wordread( lec_ptr, swapflag);
 timebase        = fread(lec_ptr, 2, 'char');
 vert_coupling   = fread(lec_ptr, 2, 'char');
 probe_att       = flotread( lec_ptr, swapflag );
 fixed_vert_gain = fread(lec_ptr, 2, 'char');
 bandwidth_limit = fread(lec_ptr, 2, 'char');
 vertical_vernier = flotread( lec_ptr, swapflag);
 acq_vert_offset = flotread( lec_ptr, swapflag);
 wave_source     = fread(lec_ptr, 2, 'char');

 if verbose > 1
  fprintf(1, 'record_type: %d\n', record_type(1));
  fprintf(1, 'processing_done: %d\n', processing_done(1));
  fprintf(1, 'ris_sweeps = %d\n', ris_sweeps);
  fprintf(1, 'timebase: %d\n', timebase(1));
  fprintf(1, 'vert_coupling: %d\n', vert_coupling(1));
  fprintf(1, 'probe_att = %f\n', probe_att);
  fprintf(1, 'fixed_vert_gain: %d\n', fixed_vert_gain(1));
  fprintf(1, 'bandwidth_limit: %d\n', bandwidth_limit(1));
  fprintf(1, 'vertical_vernier = %f\n', vertical_vernier);
  fprintf(1, 'acq_vert_offset = %f\n', acq_vert_offset);
  fprintf(1, 'wave_source: %d\n', wave_source(1));
 end
%
% Read user text block if present.
%
 if user_text > 0
  user_text_str = fread(lec_ptr, user_text, 'char');
  if verbose > 0
   fprintf(1, '%s\n', user_text_str);
  end
 end
%
% Read trigger time array block if present.
% Presence is (apparently? [S.H.C.]) specified by nom_subarray_count > 1.
% NEEDS VECTORIZING
 if nom_subarray_count > 1
  trigger_time = zeros([1,nom_subarray_count]);
  trigger_offset = zeros([1,nom_subarray_count]);
  for i = 1:nom_subarray_count
```

```
    trigger_time(i) = dbleread( lec_ptr, swapflag );
    trigger_offset(i) = dbleread( lec_ptr, swapflag );
    if verbose > 1
     fprintf(1, 'trigger_time(%d) = %f\n', i, trigger_time(i) );
     fprintf(1, 'trigger_offset(%d) = %f\n', i, trigger_offset(i) );
    end
   end
  end
%
% Read RIS offset time array block if present.
% Presence is specified by ris_time_array > 0.
% NEEDS VECTORIZING
  if ris_sweeps > 1
   ris_offset = zeros([1,ris_sweeps]); % Allocate memory.
   for i = 1:ris_sweeps
    ris_offset(i) = dbleread( lec_ptr, swapflag );
    if verbose > 1
     fprintf(1, 'ris_offset(%i) = %f\n', i, ris_offset(i) );
    end
   end
  end
%
% Assign pointers to the various parameters.
%
% For single sweeps, return a vector voltage and vector time.
%
% For segmented records, return matrix voltage and matrix time.
%
% For Fourier transform records, return complex vector and vector time.
%
  ncolumns = subarray_count;
  nrows = wave_array_count / subarray_count;
%
% volts_out needs to be complex for fft traces.
%
% Allocate memory.
%
  volts_out = ones([nrows, ncolumns]) + sqrt(-1) * fftflag;
%
% Read data.
%
  if wave_array_count > 0
   for i = 1:ncolumns
    bdata = fread(lec_ptr, nrows, 'int8');
```

```
    volts_out(:,i) = ...
     (vertical_gain * bdata - vertical_offset) / probe_att;
    if fftflag == 1
     bdata = fread(lec_ptr, nrows, 'uint8');
      volts_out(:,i) = volts_out(:,i) + ...
       sqrt(-1)*(vertical_gain * bdata - vertical_offset) / probe_att;
    end
   end
  end
%
% Create time vector or array.  NEEDS VECTORIZING.
%
 time_out = zeros(nrows, ncolumns);
 if ncolumns > 1
%   for i = 1:ncolumns
%     time_out(:,i) = ...
%       trigger_time(i) + trigger_offset(i) + ...
%         horiz_interval * [0:(nrows-1)]';
%   end
   time_out = kron( (trigger_time+trigger_offset), ones(nrows,1) ) + ...
    kron(ones(1,ncolumns), (horiz_interval * [0:(nrows-1)])' );
 else
  time_out = horiz_interval * [0:(nrows-1)]' + pixel_offset;
 end
%
% Close file.
%
 fclose(lec_ptr);
end

% Used to read in and sort double-precision variables into
% readlec.  NEEDS VECTORIZING.
%
function [retval,flag] = dbleread( ptr, swapflag )
%
% Function to read LeCroy 64 bit floating-point values.
%
[temp,flag] = fread( ptr, 64, 'uint1');
if swapflag == 1
%
% This swaps BYTE, not BIT, order.  1:8 -> 8:1.
%
 temp = [temp(57:64)',temp(49:56)',temp(41:48)',temp(33:40)',...
       temp(25:32)',temp(17:24)',temp(9:16)',temp(1:8)'];
```

```
end
s = temp(1);
e = sum( temp(2:12)' .* 2 .^[10:-1:0]);
f = sum( temp(13:64)' .* 2 .^[-1:-1:-52]);
retval = (-1)^s * 2 .^ (e-1023) * (1+f);

% Used to read in and sort double-precision variables into
% readlec.
%
function [retval,flag] = flotread( ptr, swapflag )
%
% Function to read LeCroy 32 bit floating-point values.
%
[temp,flag] = fread( ptr, 32, 'uint1');
if swapflag == 1
%
% This swaps BYTE, not BIT, order.  1:4 -> 4:1.
%
 temp = [temp(25:32)',temp(17:24)',temp(9:16)',temp(1:8)']';
end
s = temp(1);
e = sum( temp(2:9)' .* 2 .^[7:-1:0]);
f = sum( temp(10:32)' .* 2 .^[-1:-1:-23]);
retval = (-1)^s * 2 .^ (e-127) * (1+f);

% Function to read LeCroy 4-byte integer variables into readlec.
%
function [retval, flag] = longread( ptr, swapflag )
[temp,flag] = fread( ptr, 32, 'uint1');
if swapflag == 1
 temp = [temp(25:32)',temp(17:24)',temp(9:16)',temp(1:8)']';
end
retval = sum(temp' .* 2 .^[31:-1:0]);

% Function to read LeCroy 2-byte integer variables into readlec.
%
function [retval, flag] = wordread( ptr, swapflag )
[temp,flag] = fread( ptr, 16, 'uint1');
if swapflag == 1
 temp = [temp(9:16)',temp(1:8)']';
end
retval = sum(temp' .* 2 .^[15:-1:0]);

********************************
```

SMOOTH.M

```
**********
% function to smooth data
function [avg,time]=smooth(vl,t,num)
for i=1:length(vl)/num
avg(i)=mean(vl((i-1)*num+1:(i-1)*num+num));
time(i)=t(i*num-round(num/2));
end
**********
```

TEMP.M

```
**********
% This .m file should take raw lecroy data and calculate noise levels
% of each quasi-steady pressure part separately
%  This program requires dcname, rmsname, knum be declared before the program is
%called
%dcname is the file name of the dc signal
%rmsname is the file name of the ac signal

[vtot,ttot]=readlec(dcname);
[vrms,trms]=readlec(rmsname);
%[vnoise,tnoise]=readlec(nname);
%knum is the Kulite identifier, last two digits of serial number
%m is the slope of the calibration
%y is the offset*m
if knum==14;
 m=1/0.431
 y=0.0396/m
end;
if knum==16;
 m=1/0.485
 y=-0.437/m
end;
if knum==20;
 m=1/0.395
 y=0.0959/m
end;
if knum==21;
 m=1/0.465
 y=-0.153/m
end;
if knum==18;
 m=2.11;
 y=-0.587;
```

```
end;


%vm=mean(vrms);
%vrms=vrms-vm;
tpr=find(trms < -0.020);
yms=vrms(tpr)-mean(vrms);
noiv=(mean((yms).^2))^0.5;
noivp=noiv*m/100;

%converts voltage to pressure
ptot=m.*vtot+y;
prms=m.*vrms+y;
prms=prms./100;
%pnoise=vnoise*m/100.;
%pnm=mean(pnoise);
%pnoise=pnoise-pnm;
pm=mean(prms);
prms=prms-pm;
%noise=mean(pnoise.^2);
prat=prms./ptot;
rmss=prms.^2;
%%%
%Noise set to zero for now
noise=0.0;

%%%%%%%%%%%%%%%%%%%%%%%%%%%%%%%%%%%%5
% Attempt to evaluate the pressure inside each quasi-steady pressure
% chunk separated by the passing of the expansion wave


num=50;
[pp2,tt2]=smooth(ptot,ttot,num);
gg=1;
hhb=find(tt2 > 0.0);
hh=hhb(1);
while gg
hh=hh+1;
% Picks off expansion wave reflection, numbers work well for a 250 kHz sample rate

mpl=mean(pp2(hh+55:hh+70));
mmi=mean(pp2(hh-70:hh-55));
[pol,s]=polyfit(tt2(hh-65:hh-15),pp2(hh-65:hh-15),1);
[polp,s]=polyfit(tt2(hh+15:hh+65),pp2(hh+15:hh+65),1);
```

```
if abs(polp(1)) < 2
if polp(1)*pol(1) > 0.0
 if abs(polp(1)-pol(1)) < 1.05
%if abs(mpl-mmi)/mpl < 0.003;
 gg=0;
 truna=tt2(hh:length(tt2));
end;
end;
end;
end;
pp=pp2(hh:length(tt2));
tt=truna;
maxdev=0.008;
%maxdev=0.006+(mean(pp(50:80))-2.23)*0.002


ii=1;

te=0;
aa=200;
aast=1;
kk=1;
meanp=mean(pp(100:200));

if flag2==1;
  ff=find(tt>0.1);

  meanp=mean(pp(ff(1)+100:ff(1)+200));
end;
clear ff;

while kk;
 ii=1;
  if aa> length(pp)-501;
      ii=0;
      kk=0;
    end;

 meanp=mean(pp(aa:aa+100));
% if aa > 200;
%  aa=aa+100;
% end;
 if aa> length(pp)-501;
      ii=0;
```

```
    kk=0;
  end;
while ii
 aa=aa+1;
if aa> length(pp)-501;
    ii=0;
    kk=0;
  end;

dev=abs(mean(pp(aa-10:aa+10))-meanp)/meanp;
 if dev > maxdev;
  te=te+1;
  texp(te)=tt(aa);
   qq(te)=2.2;
  ii=0;
 if te > 7;
    ii=0;
    kk=0;
    te

  end;

%   meanp=mean(pp(aa:aa+200));
 end;
% aa=aa+500;
 end;
 aa=aa+400;
 if aa> length(pp)-501;
    ii=0;
    kk=0;
  end;

end;
%%%%%%%%%%%%%%%%%
for u=1:te;
tee(u)=find(ttot == texp(u));
end;
tstep=ttot(2)-ttot(1);

steppms=0.001/tstep;
fstep=20.0*steppms;
smstep=80.0*steppms;
tstep=ttot(2)-ttot(1);
vrms2=(vrms-mean(vrms)).^2;
```

```
%nl1 estimate of noise vs. p from pumpdown of tunnel, 2 pts.
nl1=0.0020*(mean(ptot(tee(1)+fstep:tee(1)+fstep+smstep)))+0.0310;
%nl2 estimation of noise vs. p from pre-run data

nl2=0.0031*(mean(ptot(tee(1)+fstep:tee(1)+fstep+smstep)))+0.0097;
nl1p=nl1*m/100;
nl2p=nl2*m/100;

% Calculates the mean values fore each segment here
for j=1:te;
% Several different rms calculations are performed, each with different noise
%approximations
  avg(j)=mean(rmss(tee(j)+fstep:tee(j)+fstep+smstep));
 avg1(j)=mean(rmss(tee(j)+fstep:tee(j)+fstep+smstep)-noivp^2);
 avg2(j)=mean(rmss(tee(j)+fstep:tee(j)+fstep+smstep)-nl1p^2);
 avg3(j)=mean(rmss(tee(j)+fstep:tee(j)+fstep+smstep)-nl2p^2);
  pta(j)=mean(ptot(tee(j)+fstep:tee(j)+fstep+smstep));
  vavg(j)=mean(vrms2(tee(j)+fstep:tee(j)+fstep+smstep));
% tav(j)=mean(ttot(tee(j)+fstep:tee(j)+fstep+smstep));
end;
avg=avg-noise;
%avg1=avg-noivp^2;
%nl1 estimate of noise vs. p from pumpdown of tunnel, 2 pts.
%nl1=0.0020*pta(1)+0.0310;
%nl2 estimation of noise vs. p from pre-run data

%nl2=0.0031*pta(1)+0.0097;
%nl1p=nl1*m/100;
%nl2p=nl2*m/100;
%avg2=avg-nl1p^2;
%avg3=avg-nl2p^2;

vavg=vavg.^0.5;
sqravg=avg.^0.5;
sqravg1=avg1.^0.5;
sqravg2=avg2.^0.5;
sqravg3=avg3.^0.5;

avrat=sqravg./pta;
avrat1=sqravg1./pta;
avrat2=sqravg2./pta;
avrat3=sqravg3./pta;
```

```
%%%%%%%%%%%%%%%%%%%%%%%%%%%%
% Now computing the time above 0.2%, 0.1% and 0.05% of the mean pressure
%%%%%%%%%%%%%%%%%%%%%%%%%%%5
%Doing it only for the parts in-between expansions
x=[0.005:0.01:5];
%using lower delta line of mean noise curve at correct psi

rmsa=(rmss-nl1p^2).^0.5;
for j=1:te;
p2pc=0.002*pta(j);
num=find(rmsa(tee(j)+fstep:tee(j)+fstep+smstep) > p2pc);
nnum=length(num);
total=smstep;
percent2(j)=nnum/total*100;
clear nnum num total

p2pc=0.001*pta(j);
num=find(rmsa(tee(j)+fstep:tee(j)+fstep+smstep) > p2pc);
nnum=length(num);
total=smstep;
percent1(j)=nnum/total*100;
clear nnum num total


p2pc=0.0005*pta(j);

num=find(rmsa(tee(j)+fstep:tee(j)+fstep+smstep) > p2pc);
nnum=length(num);
total=smstep;
percent05(j)=nnum/total*100;
clear nnum num total

%%%%%%%Making a histogram
hvec=rmsa(tee(j)+fstep:tee(j)+fstep+smstep)/pta(j)*100;
[hhh,x]=hist(hvec,x);
hs(:,j)=hhh';

end;
hs=hs./smstep*100;


pta=pta./.1388;
```

```
%Butterworth filter to try to eliminate noise from a signal, but not used, only
%here for reference at this point.

%[b,a]=butter(5,0.5);
%y=filter(b,a,pcrun2);

% Temperature analysis,
% tname is the temperature signal file name
% flag is set to 1 if there is temperature data
if flag == 1;
[vr,tr]=readlec(tname);
[v,t]=smooth(vr,tr,500);

l=length(v);
maxv=max(v);
% alpha is the resistivity coeff., rc is the reference resistance, tc is the reference
% temperature, vc, is the reference voltage, all must be set before calling the program
for i=1:1:l;
 if maxv==v(i);
   maxi=i;
 end;
end;
tinf2=(v-vc)./(0.25*alpha*rc)+tc;
tk2=tinf2+273.0;
tar2=tk2/0.98;
tinfc2=tar2-273.0;
tcel=tinfc2(maxi);
end;

%Theoretical Temperature and Pressure ratios

diam=1;  % LT dia. in feet
len=68; % LT driver tube len in feet
vol=pi*diam*diam*len/4; % volume of air
astar=1.369/144;  % throat area in sq. feet

r=53.35; % Univ. gas constant -  ft-lbf/R-lbm
gam=1.4; % ratio of specific heats

po=pd*144;
td=tcel*9/5+32;
to=td+460;
time=tts;
```

```
pn=(1+(gam-1)*astar*sqrt(32.2*r*to*gam*(2/(gam+1))^((gam+1)/(gam-
1))).*time./(2*vol)).^(2*gam/(1-gam));
tempn=pn.^((gam-1)/gam);
end;
thep=pd.*pn;
ppr=pp/pd;
if flag==1
va=vr;
ta=tr;
clear v t tinfc2 tk2 tar tinf2
[v,t]=smooth(va,ta,100);

% If there is no temperature data it is estimated using the theory
if flag==0;
 tinfc2=tempn;
end;

%plot(tt,ppr)
%Reynolds number calculations
%psi = pressure in Pa
% rho = density in nozzle
% mu= viscosity
% uinf = velocity in nozzle
% rel= unit Reynolds number (/cm)

pta=pta./.1388;
psi=pta.*(1e5/(14.7*0.9869));
rho=psi./(287.0.*(ttcel))./36.15;
uinf=4*(1.4*287.*(ttcel)/4.2).^0.5;
% Sutherland's law S=111
mu=1.716e-5.*(((ttcel)/4.2)/273).^1.5.*384./((ttcel)/4.2+111);
%re/cm
rel=rho.*uinf./mu/100;
**********************
```

Appendix C Data Lists

Chronological listing of Data, with certain parameters listed

Base Name	Date	Pressure, ps	Avg. RMS	Scope 1, kHz	Ch. 1	Ch. 2	Ch 3	Ch 4	Scope 2	Ch 1	Ch 2	Ch 3
jn0501	6/5/96	14.47	0.0013	500	dc, press	ac, press	N/A	N/A	250	dc, press	ac, press	N/A
jn0502	6/5/96	7.84	0.0011	500	dc, press	ac, press	N/A	N/A	250	dc, press	ac, press	N/A
jn0503	6/5/96	17.86		500	dc, press	ac, press	N/A	N/A	250	dc, press	ac, press	N/A
jn0504	6/5/96	10.50	0.00049	500	dc, press	ac, press	N/A	N/A	250	dc, press	ac, press	N/A
jn0505	6/5/96	16.00	0.0025	500	dc, press	ac, press	N/A	N/A	250	dc, press	ac, press	N/A
jn0506	6/5/96	15.27	0.002	500	dc, press	ac, press	N/A	N/A	250	dc, press	ac, press	N/A
jn0507	6/5/96	17.07	0.0035	500	dc, press	ac, press	N/A	N/A	250	dc, press	ac, press	N/A
jn0508	6/5/96	11.85	0.0009	500	dc, press	ac, press	N/A	N/A	250	dc, press	ac, press	N/A
jn0509	6/5/96	13.02	0.0011	500	dc, press	ac, press	N/A	N/A	250	dc, press	ac, press	N/A
jn0601	6/6/96	12.95	0.0011	500	dc, press	ac, press	low hot films		250	dc, press	ac, press	N/A
jn0602	6/6/96	16.13	0.0026	500	Filmes, dc, ac	J.D., Steve Norris			250	dc, press	ac, press	N/A
jn1101	6/11/96	14.30	0.00054	500	dc, press	ac, press	CW, dc	N/A	250	dc, press	ac, press	CW, dc
jn1102	6/11/96	16.24	0.00077	500	dc, press	ac, press	CW, dc	N/A	250	dc, press	ac, press	CW, dc
jn1103	6/11/96	12.50	0.00032	500	dc, press	ac, press	CW, dc	N/A	250	dc, press	ac, press	CW, dc
jn1104	6/11/96	18.00	0.0022	500	dc, press	ac, press	CW, dc	N/A	250	dc, press	ac, press	CW, dc
jn1105	6/11/96	20.00	0.0027	50	dc, press	ac, press	CW, dc	N/A	250	dc, press	ac, press	CW, dc
jn1201	6/12/96											
jn1202	6/12/96											
jn1203	6/12/96	13.08	0.00091	50	dc, press	ac, press	CW, dc	N/A	250	dc, press	ac, press	CW, dc
jn1204	6/12/96	19.00		50	dc, press	ac, press	CW, dc	N/A	250	dc, press	ac, press	CW, dc
jn1205	6/12/96	14.49	0.0011	50	dc, press	ac, press	CW, dc	N/A	250	dc, press	ac, press	CW, dc
jn1206	6/12/96	16.10	0.0019	50	dc, press	ac, press	CW, dc	N/A	250	dc, press	ac, press	CW, dc
jn1207	6/12/96	12.57	0.0011	50	dc, press	ac, press	CW, dc	N/A	250	dc, press	ac, press	CW, dc

Ch 4	TC temp	St. 1	St. 2	St 3	St 4	St 5	wire	Nozzle
N/A	71.4	N/A	N/A	N/A	N/A	N/A	N/A	N/A
N/A	69.3	N/A	N/A	N/A	N/A	N/A	N/A	N/A
N/A	73.3	N/A	N/A	N/A	N/A	N/A	N/A	N/A
N/A	72.4	N/A	N/A	N/A	N/A	N/A	N/A	N/A
N/A	74.6	N/A	N/A	N/A	N/A	N/A	N/A	N/A
N/A	75.5	N/A	N/A	N/A	N/A	N/A	N/A	N/A
N/A	76	N/A	N/A	N/A	N/A	N/A	N/A	N/A
N/A	74.9	N/A	N/A	N/A	N/A	N/A	N/A	N/A
N/A	75.7	N/A	N/A	N/A	N/A	N/A	N/A	N/A
N/A	72.9	N/A	N/A	N/A	N/A	N/A	N/A	N/A
N/A	75.1	N/A	N/A	N/A	N/A	N/A	N/A	N/A
N/A		105	103	98			113	39
N/A		105	102	97			118	43
N/A		104	103	97			121	36
N/A		105	104	99			XX	36
N/A		104	105	99			119	43
N/A		120	105	97			117	45
N/A		120	105	96			124	48
N/A		130	130	119	115		119	35
N/A		130	120	114	109		109	47
N/A		133	131	121	118		155	47

Base Name	Date	Pressure, ps	Avg. RMS	Scope 1, kHz	Ch. 1	Ch. 2	Ch 3	Ch 4	Scope 2	Ch 1	Ch 2	Ch 3
jn1208	6/12/96	17.48	0.0021	50	dc, press	ac, press	CW, dc	N/A	250	dc, press	ac, press	CW, dc
jn1209	6/12/96	19.50		50	dc, press	ac, press	CW, dc	N/A	250	dc, press	ac, press	CW, dc
jn1210	6/12/96	15.43	0.0017	50	dc, press	ac, press	CW, dc	N/A	250	dc, press	ac, press	CW, dc
jn1301	6/13/96	14.30	0.0022	50	dc, press	ac, press	CW, dc	N/A	250	dc, press	ac, press	CW, dc
jn1302	6/13/96	14.38	0.0026	50	dc, press	ac, press	CW, dc	N/A	250	dc, press	ac, press	CW, dc
Tunnel Cleaned												
jn1303	6/13/96	14.39	0.0022	50	dc, press	ac, press	CW, dc	N/A	250	dc, press	ac, press	CW, dc
Tunnel Cleaned												
jn1304	6/13/96	14.39	0.0024	50	dc, press	ac, press	CW, dc	N/A	250	dc, press	ac, press	CW, dc
Tunnel Cleaned												
jn1305	6/13/96	14.39	0.0021	50	dc, press	ac, press	CW, dc	N/A	250	dc, press	ac, press	CW, dc
Tunnel Cleaned, Contraction Removed												
jn1401	6/14/96	14.40	0.002	50	dc, press	ac, press	CW, dc	N/A	250	dc, press	ac, press	CW, dc
Tunnel Cleaned												
jn1402	6/14/96	14.38	0.0017	50	dc, press	ac, press	CW, dc	N/A	250	dc, press	ac, press	CW, dc
Tunnel Cleaned												
jn1403	6/14/96	14.38	0.0018	50	dc, press	ac, press	CW, dc	N/A	250	dc, press	ac, press	CW, dc
jn1501	6/15/96	14.31	0.0003	50	dc, press	ac, press	CW, dc	N/A	250	dc, press	ac, press	CW, dc
jn1502	6/15/96	18.99	0.0021	50	dc, press	ac, press	CW, dc	N/A	250	dc, press	ac, press	CW, dc
jn1503	6/15/96	16.14	0.00062	50	dc, press	ac, press	CW, dc	N/A	250	dc, press	ac, press	CW, dc
jn1504	6/15/96	17.96	0.0013	50	dc, press	ac, press	CW, dc	N/A	250	dc, press	ac, press	CW, dc
jn1505	6/15/96	15.20	0.00032	50	dc, press	ac, press	CW, dc	N/A	250	dc, press	ac, press	CW, dc
jn1506	6/15/96	17.02	0.0011	50	dc, press	ac, press	CW, dc	N/A	250	dc, press	ac, press	CW, dc

Ch 4	TC temp	St. 1	St. 2	St 3	St 4	St 5	wire	Nozzle
N/A		135	132	121	118		147	49
N/A		133	130	122	120		125	50
N/A		132	130	121	118		150	50
N/A		50	50	49	48		50	31
N/A		41	41	40	39		42	26
N/A		35	33	33	33		35	29
N/A		33	31	31	31		33	28
N/A		31	30	30	30		32	31
N/A		25	26	25	26		27	25
N/A		26	26	26	26		28	25
N/A		26	27	27	27		28	26
N/A		149	158	149	145		170	XX
N/A		153	158	148	144		180	XX
N/A		151	159	148	144		176	XX
N/A		153	158	148	144		182	XX
N/A		154	159	149	145		178	61
N/A		156	159	148	145		176	59

Base Name	Date	Pressure, psi		Scope 1, kHz	Ch. 1	Ch. 2	Ch 3	Ch 4	Scope 2	Ch 1	Ch 2	Ch 3
jn1507	6/15/96	12.79	0.0038	50	dc, press	ac, press	CW, dc	N/A	250	dc, press	ac, press	CW, dc
jn1601	6/16/96	14.42	0.0014	50	dc, press	ac, press	CW, dc	N/A	250	dc, press	ac, press	CW, dc
jn1602	6/16/96	14.44	0.0013	50	dc, press	ac, press	CW, dc	N/A	250	dc, press	ac, press	CW, dc
Tunnel Cleaned												
jy0801	7/8/96	14.25	0.00049	50	dc, press	ac, press	CW, dc	N/A	250	dc, press	ac, press	CW, dc
jy0802	7/8/96	19.60	0.0011	50	dc, press	ac, press	CW, dc	N/A	250	dc, press	ac, press	CW, dc
jy0803	7/8/96	16.17	0.00037	50	dc, press	ac, press	CW, dc	N/A	250	dc, press	ac, press	CW, dc
jy0804	7/8/96	18.98	0.00067	50	dc, press	ac, press	CW, dc	N/A	250	dc, press	ac, press	CW, dc
jy0805	7/8/96	15.29	0.0005	50	dc, press	ac, press	CW, dc	N/A	250	dc, press	ac, press	CW, dc
jy0806	7/8/96	14.40	0.00045	50	dc, press	ac, press	CW, dc	N/A	250	dc, press	ac, press	CW, dc
jy0807	7/8/96	20.75	0.0011	50	dc, press	ac, press	CW, dc	N/A	250	dc, press	ac, press	CW, dc
jy0808	7/8/96	17.90	0.00048	50	dc, press	ac, press	CW, dc	N/A	250	dc, press	ac, press	CW, dc
jy0809	7/8/96	16.97	0.00055	50	dc, press	ac, press	CW, dc	N/A	250	dc, press	ac, press	CW, dc
Tunnel Cleaned, Contraction Removed, Kulite determined to be failing												

Ch 4	TC temp	St. 1	St. 2	St 3	St 4	St 5	wire	Nozzle
N/A		154	160	148	145		179	60
N/A		38	38	36	35		38	27
N/A		38	37	36	35		37	29
N/A		214	200	178	170	184	207	50
N/A		225	199	179	175	184	207	60
N/A		228	200	178	173	185	215	77
N/A		227	200	179	172	185	207	68
N/A		228	201	177	173	184	208	75
N/A		230	201	176	172	185	211	82
N/A		231	202	177	171	185	207	80
N/A		233	201	177	171	185	212	82
N/A		233	201	177	170	185	211	82

List of Data used in Figures

Figure	Data	a typical file name is coded by:
36		ex. jn050312.bin....
37	jn1401	jn=month, June;
38	jn1401, jn1402, jn1403	05=day,
39	jn1401, jn1402, jn1403	03=run number;
40	a3001, ja3002, fb0701 fb0702	1=scope 1;
41	All runs jn11	2= channel 2.
42	N/A	
43	kcal603, kcal605	
44	jn0504	
45	jn0504	
46	jn0504	
47	jn0504	
48	jn0504	
49	jn0504	
50	All runs jn05	
51	jn0502	
52	N/A	
53	N/A	
54	jn1401	
55	jn1401, jn1402, jn1403	
56	jn1401	
57	jn1401, jn1402, jn1403	
58	jn11, All	
59	jn11, all	
60	jn1204-10	
61	jn1204-10	
62	jn15, all	
63	jn15, all	
64	jy08, all	
65	jy08, all	
66	N/A	
67	N/A	
68	jn0504	
69	jn0504	
70	jn0504	
71	jn0506	
72	jn0504	

Figure	Data
73	All, jn05, pre-run only
74	All, jn05
75	jn0504
76	jn0509
77	jn0504
78	jn0504
79	jn0504
80	jn0509
81	jn0509
82	jn0509
83	jn0509
84	jn0509
85	jn0509
86	jn0508
87	jn0508
88	jn0508
89	jn0501
90	jn0501
91	jn0501
92	jn0507
93	jn0507
94	jn0507
95	All, jn05
96	All, jn05
97	All, jn11
98	jn12-4-10
99	All, jn15
100	All, jy08
101	jn1101
102	jn1105
103	All, jn05, jn11, jn15, jy08
104	All, pre-run only
105	All, jn05, jn11, jn15, jy08
106	All, jn11, jn12
107	All, jn05, jn11, jn15, jy08
108	All, jn05, jn11, jn15, jy08
109	All, jn05, jn11, jn15, jy08
110	:wo segments, all, jn05, jn11, jn15
111	l605, kcal603, kcal713, kcal713u